NOTICE

The quality of this microform is heavily dependent upon the quality of the original thesis submitted for microfilming. Every effort has been made to ensure the highest quality of reproduction possible.

If pages are missing, contact the university which granted the degree.

Some pages may have indistinct print especially if the original pages were typed with a poor typewriter ribbon or if the university sent us an inferior photocopy.

Reproduction in full or in part of this microform is governed by the Canadian Copyright Act, R.S.C. 1970, c. C-30, and subsequent amendments.

AVIS

La qualité de cette microforme dépend grandement de la qualité de la thèse soumise au microfilmage. Nous avons tout fait pour assurer une qualité supérieure de reproduction.

S'il manque des pages, veuillez communiquer avec l'université qui a conféré le grade.

La qualité d'impression de certaines pages peut laisser à désirer, surtout si les pages originales ont été dactylographiées à l'aide d'un ruban usé ou si l'université nous a fait parvenir une photocopie de qualité inférieure.

La reproduction, même partielle, de cette microforme est soumise à la Loi canadienne sur le droit d'auteur, SRC 1970, c. C-30, et ses amendements subséquents.

Experimental Investigation on the Feasibility of Shock Wave Application as a Hydrogen Ignition Source in Diesel Engines

Carmine Lisio

A Thesis

in the Department of

Mechanical Engineering

Presented in Partial Fulfillment
of the Requirements
for the Degree of Master of
Engineering at Concordia University
Montréal, Québec, Canada

August 1990

ISBN 0-315-64747-7

ABSTRACT

Experimental Investigation on the Feasibility of Shock Wave Application as a Hydrogen Ignition Source in Diesel Engines

Carmine Lisio

This research was conducted to study the feasibility of utilizing a fluidic igniter called a resonance tube to ignite a hydrogen gas jet injected into a reciprocating piston engine. Gas heating occurs due to resonating shock waves which are formed in a tube facing a gas jet. To this end a test bench was designed and built to create the desired conditions and a gaseous fuel injection system was developed to deliver the required fuel. The fuel control system consisted of an electronically actuated and controlled injector with a manually operated metering valve at the injector inlet. The test rig consisted of a single cylinder reciprocating piston engine driven by a variable speed electric motor. The cylinder head of the engine was redesigned to accommodate the fuel injector, the resonance tube, a specially designed safety pressure relief valve and instrumentation to record the injection and resonance processes. The test rig was also equipped with rotational speed and piston position sensors to deliver signals to the electronic controller. Resonance tube tests were performed in three stages; under atmospheric conditions, inside the engine combustion chamber at constant elevated pressures,

and finally with the piston reciprocating and injections occurring during the compression stroke. Test results showed that the resonating shock wave/expansion wave cycles were easy to obtain at atmospheric conditions except when a peculiar phenomenon which we called a "saddle effect" occured. This saddle effect was eliminated with throttling of the gas inflow to the injector. At higher pressures it was found that the axial gap between the injector nozzle and the mouth of the resonance tube, would have to be reduced to obtain well developed resonating waves in the tube. However, the higher the back pressure the more difficult is was to create the shock waves. Similar trends were observed with the reciprocating piston, i.e. when injection occurred early in the compression stroke, the tube could be placed farther away from the injector and the resonating waves were easier to produce. However, the increased turbulence of the air in the chamber further hindered the formation of the pressure waves. Heating of the resonance tube was observed qualitatively however no ignition of the gas jet was obtained under the described.

ACKNOWLEDGEMENTS

The author wishes to express his gratitude to his supervisors Dr. T.Krepec and Dr. R. Neemeh. Special thanks to Dr. Krepec for his constant enthusiasm and patience throughout the course of this project.

Thanks are also directed to all the members of the Fuel Control Systems Laboratory at Concordia University; Domenico P. Miele, Antonios I. Georgantas, Gino Carrese, and Daniel Quinz for their help and advice on the project. Also thanks to Frank Joo, John Zalass, Tom Montor and Stuart Cassoff for their friendship and support.

The author would also like to thank all the technical staff of the Mechanical Engineering Department, especially the gentlemen in the machine shop who constructed much of the equipment required for the test rigs and the technicians at the Center for Industrial Control.

The author also thanks his family for their encouragement and understanding.

This work was supported financially by the Natural Science and Engineering Research Council Postgraduate Scholarship, by Fonds pour la Formation de Chercheurs et l'Aide à la Recherche du Québec, by Concordia University Graduate Teaching Fellowship, by Bendix Avelex Inc. and by the Department of Supply and Services Canada.

TABLE OF CONTENTS

page

LIST OF FIGURES x

NOMENCLATURE xvii

CHAPTER 1

1.0 THESIS OBJECTIVES AND JUSTIFICATION 1

CHAPTER 2

2.0 HYDROGEN AND RESONANCE TUBES LITERATURE SURVEY .. 6

CHAPTER 3

3.0 THESIS CONCEPT, DISCUSSION, DEFINITION AND METHODOLOGY 17

CHAPTER 4

4.0 SIMPLIFIED THEORY OF RESONANCE TUBES 26

4.1 Flow Field of a Resonance Tube 28

4.2 Pressure History in a Resonance Tube 32

4.2.1 Continuity Equation 32

4.2.2 The Momentum Equation 35

4.2.3 Derivation of Characteristic Relations..... 36

4.2.4 Analysis of Unsteady One Dimensional Flow in a Simple Resonance Tube..... 38

CHAPTER 5

5.0 EXPERIMENTAL APPARATUSES AND CONTROL SYSTEM 45

5.1 Introduction 45

5.2 Engine Simulation Test Rig 49

5.3 Electronically Actuated Injector and Nozzles 54

5.4 Electronic Hardware 57

5.5 Electronic Software 69

5.6 Safety Relief Check Valve 75

5.6.1 Computer Simulation of the Safety Valve 78

5.6.1.1 Determination of the Thermodynamic Properties in the Combustion Chamber 80

5.6.1.2 Determination of Forces and the Force Balance on Poppet Valve 82

5.6.1.3 Determining the Cracking Pressure of the Valve 86

5.6.1.4 Determining Flow Areas Through the Valve Orifices 88

5.6.1.5 Mass Flow Continuity Equations 91

5.6.2 Analysis of Valve Simulation 93

CHAPTER 6

6.0 EXPERIMENTAL INVESTIGATIONS OF SHOCK WAVES AT AMBIENT CONDITIONS 96

6.1 Teat Apparatus for Resonance Tubes at Ambient Conditions 97

6.2 Test Proceedures and Objectives 104

6.3 Test Results and Discussion 107

6.3.1 Initial Familiarization Tests 107

6.3.2 Gas Dose Calibration Tests 116

6.3.3 Initial Resonance Tube Sizing 123

6.3.4 Shock Wave Development for Short Gas Injection Duration 124

6.3.5 Gas Inflow Rate Tests 125

CHAPTER 7

7.0 EXPERIMENTAL INVESTIGATIONS OF RESONANCE TUBES AT ELEVATED BACK PRESSURE 128

7.1 Test Methodology 129

7.2 Test Apparatus for Investigation of Shock Waves in a Resonance Tube at High Ambient Pressure 131

7.3 Test Results and Discussion 132

CHAPTER 8

8.0 EXPERIMENTAL INVESTIGATION OF RESONANCE TUBES IN A RECIPROCATING ENGINE 149

8.1 Test Methodology 150

8.2 Apparatus for Tests in a Reciprocating Piston Engine 152

8.3 Test Results and Discussion 153

CHAPTER 9

9.0 SUMMARY, CONCLUSIONS and RECOMMENDATIONS 167

9.1 Summary of Work and Conclusions 167

9.2 Reccomendations for Future Work 174

REFERENCES 178

APPENDIX A

Control Software A1

APPENDIX B

Instrument Calibration..... A8

APPENDIX C

Derivation of Metering Valve Flow Area A20

APPENDIX D

Cylinder Head Redesign Drawings and Photos of
the Main test Rig A25

LIST OF FIGURES

		page
Figure 4.1	Schematic of Simplified Resonance Tube...	27
Figure 4.2	Stagnation Pressure History Along the Core of an Underexpanded Jet	29
Figure 4.3a	Incident Shock wave in a Resonance Tube..	31
Figure 4.3b	Reflected Shock Wave in a Resonance Tube.	31
Figure 4.3c	Incident Expansion Wave in a Resonance Tube	31
Figure 4.3d	Reflected Expansion Wave in a Resonance Tube	31
Figure 4.4a	Volume Element in a Pipe for Derivation of Continuity	33
Figure 4.4b	Force Diagram on a Volume Element in a Pipe	33
Figure 4.5	Simplified Wave Diagram in a Resonance Tube	40
Figure 5.1	Schematic of a Gaseous Fuel System	46
Figure 5.2	Schematic of the Primary Test Set-up for Resonance Tube Testing in a Reciprocating Piston Engine	48
Figure 5.3	Cylinder Head Cross Section	52
Figure 5.4	Cross Section of the Injector Unit	55
Figure 5.5	Fuel Injector Nozzle Modifications	58
Figure 5.6	Electrical Schematic of LAB MASTER Data Acquisition and Control System	60
Figure 5.7	Piston Position Interrupt Circuit	63
Figure 5.8	Rotational Speed Circuit	65
Figure 5.9	Injector Control Circuit	66
Figure 5.10	Solenoid Rectifier Switching Circuit	67

Figure 5.11	Current and Lift vs. Time Oscillogram ...	70
Figure 5.12	Flow Chart of "SOLENOID" Control Program for Static Tests	71
Figure 5.13	Flow Chart of "INJECT3T" Control Program for Reciprocating Piston Tests	74
Figure 5.14	Flow Chart for Interrupt Service Routine	76
Figure 5.15	Cross Section of Safety Relief Valve	77
Figure 5.16	Free Body Diagram on Poppet	83
Figure 5.17	Safety Valve Internal Dimensions	87
Figure 5.18	Volume Diagram in Safety Valve Simulation	89
Figure 5.19	Schematic for Determination of Flow Areas in the Safety Valve	90
Figure 5.20	Valve Lift vs. Crank Angle (simulation) .	94
Figure 5.21	Combustion Chamber Pressure History with Valve Opening and Not Opening Cases	95
igure 6.1	Ambient Conditions Test Set-Up	98
Figure 6.2	Injector on Axial Displacement Unit	100
Figure 6.3	Long Tube Test Set-Up	102
Figure 6.4	Gaseous Fuel Dose Calibration Set-Up	103
Figure 6.5a	Typical Pressure History in a Resonance Tube of 20mm.	108
Figure 6.5b	Single Wave Record of Figure 6.5a	108
Figure 6.6a	Typical Pressure History in a Resonance Tube of 60mm.	110
Figure 6.6b	Single Wave Record of Figure 6.6a	110
Figure 6.7	Pressure History in a 20 mm. Tube for 2 second injection	112
Figure 6.8	Pressure History at End Wall Showing the "Saddle Effect"	113

Figure 6.9 Pressure History Without "Saddle Effect" due to Metering Valve Throttling 115

Figure 6.10 Injector Lift and Injector Pressure During Hydrogen Injection Process 119

Figure 6.11 Hydrogen Dose Variations Due to the Duration of Injection and Metering Valve Opening 122

Figure 6.12 Hydrogen Pressure Record in the Long Tube Showing the "Saddle Effect" 127

Figure 6.13 Hydrogen Pressure Record in the Long Tube without the "Saddle Effect" due to Inlet Flow Throttling with the Metering Valve 127

Figure 7.1 Typical Pressure and Nozzle Lift Record for Injection in a Closed Chamber at Atmospheric Conditions at Δx = 8 mm 133

Figure 7.2 Pressure Record at 170 kPa gauge Back Pressure and Δx = 8 mm. 133

Figure 7.3 Pressure Record at 345 kPa gauge Back Pressure and Δx = 8 mm. 135

Figure 7.4 Pressure Record at 690 kPa gauge Back Pressure and Δx = 8 mm. 135

Figure 7.5 Typical Pressure and Nozzle Lift Record for Injection in a Closed Chamber at Atmospheric Conditions at Δx = 6 mm 136

Figure 7.6 Pressure Record at 170 kPa gauge Back Pressure and Δx = 6 mm. 136

Figure 7.7 Pressure Record at 345 kPa gauge Back Pressure and Δx = 6 mm. 138

Figure 7.8 Pressure Record at 690 kPa gauge Back Pressure and Δx = 6 mm. 138

Figure 7.9 Typical Pressure and Nozzle Lift Record for Injection in a Closed Chamber at Atmospheric Conditions at Δx = 4 mm 140

Figure 7.10 Pressure Record at 170 kPa gauge Back Pressure and Δx = 4 mm. 140

Figure 7.11 Pressure Record at 345 kPa gauge Back Pressure and Δx = 4 mm. 141

Figure 7.12 Pressure Record at 690 kPa gauge Back Pressure and Δx = 4 mm. 141

Figure 7.13 Typical Pressure and Nozzle Lift Record for Injection in a Closed Chamber at Atmospheric Conditions at Δx = 2 mm 142

Figure 7.14 Pressure Record at 170 kPa gauge Back Pressure and Δx = 2 mm. 142

Figure 7.15 Pressure Record at 345 kPa gauge Back Pressure and Δx = 2 mm. 143

Figure 7.16 Pressure Record at 690 kPa gauge Back Pressure and Δx = 2 mm. 143

Figure 7.17 Typical Pressure and Nozzle Lift Record for Injection in a Closed Chamber at Atmospheric Conditions at Δx = 1 mm 144

Figure 7.18 Pressure Record at 170 kPa gauge Back Pressure and Δx = 1 mm. 144

Figure 7.19 Pressure Record at 345 kPa gauge Back Pressure and Δx = 1 mm. 145

Figure 7.20 Pressure Record at 690 kPa gauge Back Pressure and Δx = 1 mm. 145

Figure 7.21 Pressure Record at 1035 kPa gauge Back Pressure and Δx = 1 mm. 146

Figure 7.22 Pressure Record at 1380 kPa gauge Back Pressure and Δx = 1 mm. 146

Figure 7.23 Pressure Record at 1725 kPa gauge Back Pressure and Δx = 1 mm. 147

Figure 7.24 Pressure Record at 2070 kPa gauge Back Pressure and Δx = 1 mm. 147

Figure 8.1 Pressure Record of Injection into the Reciprocating Piston Chamber (early injection, Δx = 8 mm, supercharge = 0 kPa gauge) 155

Figure 8.2 Pressure Record of Injection into the Reciprocating Piston Chamber (early injection, Δx = 4 mm, supercharge = 0 kPa gauge) 155

Figure 8.3 Pressure Record of Injection into the Reciprocating Piston Chamber (early injection, Δx = 2 mm, supercharge = 0 kPa gauge) 156

Figure 8.4 Pressure Record of Injection into the Reciprocating Piston Chamber (injection 45^{0} BTDC, Δx = 8 mm, supercharge = 0 kPa gauge) 158

Figure 8.5 Pressure Record of Injection into the Reciprocating Piston Chamber (injection 45^{0} BTDC, Δx = 2 mm, supercharge = 0 kPa gauge) 158

Figure 8.6 Pressure Record of Injection into the Reciprocating Piston Chamber (injection 45^{0} BTDC, Δx = 4 mm, supercharge = 0 kPa gauge) 159

Figure 8.7 Pressure Record of Injection into the Reciprocating Piston Chamber (injection 15^{0} BTDC, Δx = 8 mm, supercharge = 0 kPa gauge) 160

Figure 8.8 Pressure Record of Injection into the Reciprocating Piston Chamber (injection 15^{0} BTDC, Δx = 4 mm, supercharge = 0 kPa gauge) 160

Figure 8.9 Pressure Record of Injection into the Reciprocating Piston Chamber (injection 15^{0} BTDC, Δx = 2 mm, supercharge = 0 kPa gauge) 161

Figure 8.10 Pressure Record of Injection into the Reciprocating Piston Chamber (early injection , Δx = 2 mm, supercharge = 100 kPa gauge) 163

Figure 8.11 Pressure Record of Injection into the Reciprocating Piston Chamber (early injection, Δx = 1 mm, supercharge = 100 kPa gauge) 163

Figure 8.12 Pressure Record of Injection into the Reciprocating Piston Chamber (injection 45° BTDC, Δx = 2 mm, supercharge = 100 kPa gauge) 164

Figure 8.13 Pressure Record of Injection into the Reciprocating Piston Chamber (injection 45° BTDC, Δx = 1 mm, supercharge = 100 kPa gauge) 164

Figure 8.14 Pressure Record of Injection into the Reciprocating Piston Chamber (injection 15° BTDC, Δx = 2 mm, supercharge = 100 kPa gauge) 165

Figure 8.15 Pressure Record of Injection into the Reciprocating Piston Chamber (injection 15° BTDC, Δx = 1 mm, supercharge = 100 kPa gauge) 165

Figure A.1 LVDT Calibration Curve A.10

Figure A.2 Sample Lift vs. Time Curve A.11

Figure A.3 Combustion Chamber Pressure Transducer Calibration A.13

Figure A.4 Injector Pressure Transducer Calibration A.14

Figure A.5 Long Tube Test Pressure Transducer Calibration PCB 105A03 .....A.16

Figure A.6 Resonance Tube Test Pressure Transducer Calibration PCB 105A13 .....A.17

Figure A.7 Frequency to Voltage Converter Calibration A.19

Figure A.8 Metering Valve Flow Area Derivation Schematic A.23

Figure A.9 Metering Valve Flow Area vs. Turns Calibration A.24

Figure A.10 Cylinder Head Main Design Drawing A.27

Figure A.11 Cylinder Head Bolt Hole Location Drawing A.28

Figure A.12 Test Rig Photograph #1 .....A.29

Figure A.13 Test Rig Photograph #2 .....A.29

NOMENCLATURE

a	local velocity of sound [m/s]
A	area [m^2]
A_{12}	flow area from the combustion chamber into the relief valve [m^2].
A_{23}	flow area from the relief valve into the atmosphere [m^2]
C_{ave}	average circumference of centroid of flow area between the combustion chamber and the valve [m]
C_d	discharge coefficient
D	generalized diameter of pipe [m]
d	bore of clinder [m]
d_{cyl}	diameter of calibration cylinders [m]
F_d	damping force [N]
F_{dn}	pneumatic downward force on body [N]
F_f	Coulomb friction force [N]
F_l	inertial force [N]
F_{prel}	spring preload force [N]

F_s summation of spring forces [N]

F_{up} pneumatic upward force on body [N]

f frequency of oscillations of the pressure waves [Hz]

f body forces on fluid [N]

Δh poppet lift [m]

h_2 interface between poppet and valve body before outflow from the valve begins [m]

k_s spring constant [N/m]

L interface length between the entire poppet and the valve body [m]

l depth of cavity in resonance tube [m]

l length of connecting rod of engine [m]

ℓ length of flow element in valve [m]

M flow Mach number

M_s shock Mach number

Δm mass dose of gas injected [kg]

m_{tot} total mass of moving parts in the safety valve [kg]

m_p mass of poppet in safety valve [kg]

m_s mass of spring in safety valve [kg]

$\dot{m}_{12}$ mass flow from the combustion chamber into the valve chamber [kg / m^3]

$\dot{m}_{23}$ mass flow from the valve chamber into the atmosphere [kg / m^3]

n polytropic exponent of compression

n number of injections usedd in calibration

P $\left(\frac{2}{\gamma - 1} \right)$ a + u, Riemann P wave variable

p static pressure [N/m^2]

p_{atm} atmospheric pressure [N/m^2]

p_b back pressure keeping the valve closed [N/m^2]

p_c combustion chamber pressure [N/m^2]

p_d downstream pressure [N/m^2]

p_u upstream pressure [N/m^2]

p_2 pressure in the valve chamber [N/m^2]

Δp pressure amplitude [N/m^2]

Q $\left(\frac{2}{\gamma - 1} \right) a - u$, Riemann Q wave variable

R gas constant [kJ/kg K]

R_u universal gas constant [kJ/kg K]

r stroke length og the engine [m]

s entropy [kJ/kg K]

T absolute temperature [K]

t time [s]

t_p period of resonance [s]

u velocity of gas along x axis [m/s]

V, V_1 volume in the combustion chamber for flow derivation [m^3]

V_2 volume in the safety valve chamber for flow derivation [m^3]

V_3 volume of atmosphere for flow derivation [m^3]

V_c clearance volume of the combustion chamber (volume at TDC) [m^3]

ΔV volume of water displaced in calibration cylinders [m^3]

Δx axial gap between the injector nozzle and the mouth of the resonance tube [m]

GREEK SYMBOLS

ϕ diameter of the resonance tube cavity [m]

ρ density of fluid [kg/m^3]

ψ mass flow through the side walls per unit lenght [kg/m]

γ ratio of specific heats of a gas

$\bar{\gamma}$ specific weight of water [kg/m^3]

θ engine crank angle with respect to the TDC position of the piston [deg]

δ gap between the poppet & the valve body [m]

μ viscosity of air [Pa s]

CHAPTER 1

1.0 THESIS OBJECTIVES AND JUSTIFICATION

There will soon be a need to totally replace today's current fossil fuel resources with alternative fuels. With a potentially volatile political situation in major petroleum producing nations and the forecast for reduced supply of petroleum during the next century, a viable alternative fuel must be found. Another growing concern with society today, is the detrimental effect that exhaust from burning of carbon based fuels has on the environment. Global warming, acid rain, and smog are reducing the standard of the environment in which we must live. A need also arises for a clean burning and abundantly available fuel to replace present petroleum-based fuels. Hydrogen is a fuel that meets these requirements.

Hydrogen, though not readily available, can easily be manufactured. There are many processes which can be used to produce hydrogen such as steam reforming of natural gas, coal gasification, and electrolysis just to name a few examples. In Québec it is expected that most of the hydrogen would be produced by using electrolysis. This process is also beneficial because it is not contributing to global pollution if the electrical energy comes from

hydroelectric power stations.

Replacement of conventional liquid fuels in the automotive industry is extremely difficult because the alternative fuel must be easily transportable in a vehicle, should not create a large weight penalty and should be easily acceptable by the users. The most thermodynamically efficient power plant used in automobiles today is the "Diesel Engine". The direct injection of hydrogen gas into the compression ignition engine would deliver the best results in terms of thermal efficiency and power output. However, one of the obstacles in using hydrogen gas as a fuel in a "diesel engine" is the difficulty of igniting hydrogen with high compression. In this thesis an investigation was conducted on the feasibility of assisting the ignition of hydrogen in a compression ignition engine with a fluidic igniter called a "Resonance Tube" or a "Hartmann-Sprenger Tube".

A simple resonance tube consists of a cylindrical cavity closed at one end, with the open end facing an underexpanded jet directed axially into the mouth of the tube. The tube must be placed at certain axial distances from the jet nozzle where the gas jet is in an area known as the region of jet instability. In such zones the pressure of the jet is lower than that in the tube; this allows the gas, which penetrates the tube, to exit. When

the gas penetrates into the tube and compression waves form and then coalesce into shock waves. These shock waves penetrate into the tube and reflect off the back wall. The reflected wave exits the tube and an expansion wave forms and propagates towards the closed end of the tube, this expansion wave then reflects off the end wall and travels towards the mouth of the tube and then exits the tube. The cycle then repeats. The gas that penetrated into the tube, exits the tube and a different mass of the gas from the injector enters the tube in the next cycle (extraneous fluid). During each cycle, which occurs at close to the acoustic frequency, the shock wave irreversibilities, as well as frictional energy dissipation, increase the temperature of the gas which remains in the tube (indigenous fluid). The highest temperature occurs at the end wall of the tube, behind the reflected shock wave. It has been found, that the end wall temperature in a resonance tube can easily exceed the stagnation temperature of the gas jet by a considerable amount. This thesis will investigate the feasibility of using shock wave heating ability to ignite hydrogen gas jets in a reciprocating piston engine, more specifically in a diesel engine.

The above described objective of this investigation is justified as follows:

1- resonance tubes have been tested successfully in

---

*Numbers in square brackets designate references listed at the end of the thesis

the ignition of hydrogen-oxygen mixture jets used in rocket engines [1]*; however in rocket engines the time constraints for ignition of the jet are more relaxed, that is, there is much more time available to ignite the fuel and also the size of the ignition units, i.e. nozzle and tube diameters, could be made larger. The time required to ignite the jet in a diesel engine cycle is in the order of 1 to 3 milliseconds, and the injector nozzle and, consequently, the resonance tube cavity diameters, are in the range of 1 to 3 millimeters. Therefore, there might not be enough time to ignite the hydrogen jet in a diesel engine using this type of ignition supporting device.

2- In a diesel engine, at the time of ignition, the air temperature in the combustion chamber is already elevated due to the adiabatic compression of the air in the cylinder. Therefore, the heat required to increase the temperature of the gas jet to create ignition of the fuel is lower in the case of a diesel engine, than in a rocket engine igniter. However, the pressure in the combustion chamber of a diesel engine is much higher at the point of ignition, than the pressure found in a rocket engine. How this high back pressure

affects the creation of high amplitude resonating shock waves, has to be studied.

3- There is a large amount of energy available in compressed hydrogen fuel to produce the shock wave by the gas jet during the injection process; part of this fuel can be injected into the resonance tube.

Another aspect of direct hydrogen gas injection into a diesel engine is the task of controlling the gas discharge process in order to deliver the required dose of fuel and at the proper time. The injection process in a diesel engine is a highly transient one. Fuel must be injected during the compression stroke of every cycle. The duration of the injection process and the timing of injection point are critical for the efficient heat to work conversion process. The use of modern microprocessor controls with electronic actuators is considered the best way to manage the injection process. This technology allows for easy corrections and flexibility in shaping of the injection and ignition processes. Consequently, the test rigs used in this investigation, will also be designed to use microprocessor controls to perform the tests required in this research.

CHAPTER 2

2.0 HYDROGEN AND RESONANCE TUBES LITERATURE SURVEY

The idea of using hydrogen as fuel is not a new one, it has its roots in the mid-nineteenth century. Hydrogen which is considered by many to be the ultimate fuel of the future was first mentioned in 1870 by the futurist and writer Jules Verne. In his story "The Mysterious Island", he describes how hydrogen and oxygen are produced from water and then the hydrogen is used as fuel. Verne foresaw that the fossil fuel resources will not be infinite and a more permanent fuel source will be needed.

Hydrogen has several benefits over other fuels. The most important of these benefits is that hydrogen is a very clean burning fuel. The main product of a stoichiometric combustion process between hydrogen and oxygen is water. If hydrogen is produced by electrolysis of water, it then becomes a renewable fuel source. Another benefit of hydrogen is that it has a very broad flammability range so the fuel delivery system can tolerate some inaccuracy in the injected dose of fuel and still maintain a fuel to air ratio in which combustion can occur.

In the transportation industry, fuel has to be carried on board of the vehicle and, therefore, it should have a high energy to weight ratio. Hydrogen meets this

requirement. However, there are several barriers preventing hydrogen from quickly becoming a usable transportation fuel. First, hydrogen is not readily available in its pure state, and it has to be manufactured. As mentioned in the previous chapter, this can be done by electrolysis of water, by steam reformation of hydrocarbons such as methane etc. However, the production of hydrogen is costly, largely due to inefficient energy conversion techniques. Secondly, there are huge technical problems which must be solved in the distribution and storage of hydrogen due to its high specific volume when stored as a gas. Thirdly, hydrogen can presently be used as an effective upgrader of fuels such as "Tar Sands" products and in the manufacture of synthetic fuels at a lower cost [2].

Hydrogen can be used in all the transportation fields. It is the best rocket fuel which was used in the Saturn V rockets, and is presently being used in the Space Shuttle. Hydrogen, in a liquid state, has a very promising future in the aviation industry due to its exceptionally high energy density which is attractive to the aircraft industry and to the next generation supersonic transport aircraft which are projected to be in use in the twenty-first century. There are several examples of hydrogen-powered gas turbine engines used to propel experimental aircraft. The first such case was the conversion of one engine on an USAF aircraft to hydrogen, which occurred in the mid 1950's [3], another more

recent example was the conversion of one engine on a Soviet Tupolev aircraft in 1988.

The history of using hydrogen as a fuel in automotive engines dates from the 1920's. Ricardo used hydrogen as a fuel for research with spark ignition engines in 1923 [4]. Other early research work performed in Canada was by R.O. King [3]. He engaged in extensive research between 1948 and 1955 on hydrogen-fueled internal combustion engines at the University of Toronto. Presently, the research on hydrogen-fueled automotive vehicles cover a wide range of areas like hydrogen storage, hydrogen delivery and control, and also hydrogen ignition and combustion.

Hydrogen storage is difficult because it is a gas at standard atmospheric conditions, and obtaining a high enough energy per unit volume of hydrogen storage is a problem. There are several storage modes which can be used; the hydrogen can be stored as a high pressure gas, as a liquid under cryogenic conditions, in metal hydrides or in a "semi-cryogenic" state.

The use of conventional high pressure gas bottles for hydrogen storage is not very attractive. This storage mode does not provide a high enough energy density level and this severely limits the operational range of a vehicle. Also, the gas storage bottles made of steel are very bulky and heavy which reduces the vehicles' payload.

Metal hydrides store hydrogen in a chemical bond with

certain metals. The hydrogen is then released by the addition of heat to the hydride. This mode can provide a satisfactory range for a vehicle, but there is a very large weight increase with the addition of heavy metal hydride tanks. Research on this type of fuel storage system has been limited to fleet vehicles, such as buses. Hama et al. have used hydride storage on a bus [5], and Davidson et al. used hydride storage on a farm tractor [6].

The most weight effective method of hydrogen storage for automotive use has been as a liquid in a cryogenic tank. However, the boiling point of hydrogen at standard atmospheric pressure is only 20.4 K and the cooling of hydrogen to this temperature increases the costs. Special cryogenic tanks must also be used to maintain the low temperature required to keep hydrogen as a liquid. Furuhama et al. used a liquid hydrogen storage system and developed a special liquid hydrogen pump to deliver the fuel from the tank to the engine. The hydrogen was then injected into the combustion chamber as a cold gas [7]. Strobl and Peschka also used a cryogenic tank in a modified BMW car. In their work with the German Aerospace Research Establishment (DFVLR) and Bavarian Motor Works (BMW) they developed both a cryogenic pump and cryogenic injectors. They tested the engine with both: port injection into the manifold and direct injection into the combustion chamber [8].

A semi-cryogenic hydrogen storage method has been

proposed by Krepec et al. [9,10]. This method stores hydrogen as a cold gas at 100 K and at high pressure. This eliminates the need for special and difficult to produce equipment to pump cold liquid hydrogen to high pressures required for direct injection. The hydrogen energy density using this method is 2.8 times higher than that of high pressure gas storage in cylinders, and only 1.8 times lower than the density in cryogenic tank.

There are also several methods of delivery of hydrogen to the combustion chamber of an engine. Usually hydrogen is induced and mixed with air in the engine intake manifold. Ricardo [4] experienced violent pre-ignition and flashback phenomena in the manifold when the equivalence fuel to air ratio exceeded unity. Other researchers experienced similar problems and tried to reduce these effects. Schoeppel [4], Furuhama et al. [11] and Strobl and Peschka [8] developed methods such as water induction and cooling of the intake charge which met with some limited success. These researchers finally abandoned the induction of hydrogen through the manifold and switched to direct hydrogen injection into the combustion chamber.

Direct injection of hydrogen was originally reported to have been tested by Rudolf Erren in Germany before World War II [4]. However, much of the information about his work did not survive the war but it has been reported, by one of his aides, that his engines had no problems with knock

phenomenon.

In combustion engines, compression ignition of hydrogen has been found to be particularly difficult. Therefore, several methods have been used to ignite the hydrogen. Ikegami et al. [4] reported that they were able to achieve compression ignition with a compression ratio of 18.6 : 1. However Homan et al. [4] disputed these results as he and his team were not able to achieve compression ignition with compression ratios up to 29:1. Homan suggests that Ikegami's good results were due to some minute quantities of hydrogen leaking from the injector or to the presence of hot spots on the combustion chamber walls. Ikegami et al. [12], in later work, confirmed Homans' suspicions by obtaining smooth sparkless ignition of hydrogen by introducing a pilot injection and also by purposely allowing some leakage of hydrogen from the injector before the injection process. Giannacopolous [13] was also unable to obtain regular compression ignition during his tests.

Hot surface ignition with glow plugs has been used by Furuhama and Kobayashi [14]. They obtained "smooth diesel ignition by blowing hydrogen gas onto a heated platinum wire at 1000^{0}C from a close location", mainly due to the catalytic effect of platinum.

It seems that the use of spark plugs allows for the best control of the ignition point. Many researchers have used spark ignition of hydrogen in engines which inject the

fuel directly into the combustion chamber. Varde and Frame [14] used a hydraulically actuated injector with the support of spark ignition. Giannacopolous [13] also used spark ignition with an electronically actuated injector. He found that the spark seriously interfered with his electronic control system. This can be explained by the fact that the voltage required to create a spark in the diesel engine must be quite high because the pressure in the combustion chamber is much higher than the pressure found in a gasoline engine.

A method that can be used to support hydrogen ignition avoiding electronic interference, is to employ a passive igniter such as a resonance tube, also called a "Hartmann-Sprenger" (H-S) or "Resonance" tube. Hartmann [15] in 1919, was the first to notice the acoustic and pressure amplification which occurred when placing a shallow circular-cylindrical tube of uniform cross-section in the axial path of a sonic air jet. The sound amplification of the Hartmann whistle, as it was called at that time, has been known to exceed 120 dB.

Sprenger [16] in 1954, observed that along with the loud noise created by the H-S tubes, there is a significant increase in the average air temperature in the tube. He recorded an end wall temperature of 450^{o}C.

Thompson [17] was one of the first investigators who studied the boundary conditions at the open end of the tube and then he was able to describe the fluid flow in the tube

using wave diagrams. The gas in the tube is either indigenous (permanently remaining in the tube) or extraneous (fluid from the nozzle remaining in the tube for only one cycle). There are also two flow phases involved; the inflow or penetration of the jet into the tube, and the outflow or evacuation of the tube. Thompson and Kang [18] did some research on trying to theoretically predict and analyze the heating effects of a resonance tube. Brocher [19] tried to predict the maximum attainable temperature in the tube given that the tube is a perfect insulator and all the heat energy from the shock wave irreversibilities and from the frictional heating is transferred to the gas in the tube. He noted that as the temperature of the gas increased, the shock strength would decrease and, therefore, the heating effect would decrease. His predicted temperature values (3200 K) far exceeded his experimental data (1570 K). This discrepancy was attributed to the fact that the tube could not be considered as a perfect insulator, and some heat must have been lost through the tube material.

The use of H-S tubes as igniters has been shown by Conrad and Pavli [20] and Phillips and Pavli [1]. They tested the use of resonance tubes for igniting hydrogen-oxygen mixtures in rocket engines. Other researchers who did work on resonance tube igniters for rockets were Marchese, Rakowsky and Bement [21]. Their work investigated the effects of initial supply pressure and

axial distance on resonance tube thermal heating.

Conrad and Pavli conducted a test. demonstrating the heating effect of a resonance tube by placing a block of wood, with a cylindrical cavity, facing an air jet flowing out of a sonic nozzle of similar diameter as the cavity in the wood. By optimizing the axial distance to fall within one of the unstable zones of the jet, a resonating shock wave condition was established. Within a few seconds smoke began to issue from the block of wood. The area around the bottom of the hole had become deeply charred.

Ignition times achieved for the rocket igniter tests were in the order of .1 to .2 seconds. This ignition time is acceptable for rocket ignition and possibly for aircraft igniters, but for diesel engines an ignition delay in the order of 1 ms. would be required. Also the igniter for a diesel engine would have to ignite the fuel repeatedly several thousand times in a minute for extended periods of time. However, there is an aiding factor regarding a diesel engine combustion chamber in which the air charge is already preheated by the compression stroke. This should improve the prospects of the shock wave igniter for a diesel engine.

The parameters which affect the heating effects of a H-S tube are the frequency of oscillations, the jet stagnation pressure, and the tube geometry. Brocher [19] showed that monotonic gases are able to reach higher temperatures and Wu et al. [22] showed that the end wall

temperatures for a light gas, helium, reached 1200 ^{0}C, and for a heavier gas, such as nitrogen, reached only 400 ^{0}C. Molar mass and ratio of specific heats of the gas also affect the frequency of the shock wave resonance.

The tube geometry is also an important factor. A reduction in the area for a shock wave will increase the shock strength, which increases the energy released by the shock wave in the reversible process. McAlevy and Pavlak [23] found that using tapered tubes increases the acoustic noise production and also increases the frequency of oscillations by 50% over a cylindrical tube of equal length. As a result, the end wall temperature increased by over 100^{0}C when compared to a simple H-S tube. Similarly, Brocher and Kawahashi [24] also studied the thermal effects of a stepped H-S tube. They noted that the angle of the step and the shock wave frequency mode affect the temperature distribution. Neemeh et al. [25] concluded that a tube with a logarithmic spiral profile achieved higher temperatures than tapered and cylindrical cavities.

Ignition of unsteady hydrogen jets has already been achieved in a period as short as 0.5 ms [26]. To produce this result the hydrogen jet was injected into an oxidizer at high temperature created by the reflection of a shock wave in a shock tube. Sakurai was able to obtain ignition of hydrogen in about 1 ms. with the oxidizer temperature at 1100^{0}C. As the oxidizer temperature was increased, the

ignition delay was reduced. Ishii et al. [27] obtained similar results and they also noted that the ignition delay was longer when only hydrogen was injected, as compared to the injection of a hydrogen-air mixture.

Summarizing the published research results it can be concluded that hydrogen can be ignited within the time that is required in a diesel engine, and that H-S tubes can be considered as passive heating devices which can be used as igniters. However, still many questions remain:

1-can the resonance tube filled with compressed air heat the hydrogen jet fast enough to cause the ignition in the combustion chamber of a diesel engine,

2-what are the effects of the high gas pressure and temperature found in a diesel combustion chamber on the development of the shock wave,

3-how does the short unsteady injection process affect the shock wave development.

These are some of the subjects that have to be studied before H-S tube igniters can be proposed in a diesel engine.

CHAPTER 3

3.0 THESIS CONCEPT, DISCUSSION, DEFINITION AND METHODOLOGY

The main objective of this thesis is to study the feasibility of using resonance tubes to ignite a jet of gaseous fuel, hydrogen, under conditions existing in a diesel engine combustion chamber. This can be justified by the fact that a significant amount of research work has been done on the subject of hydrogen-fueled engines for transportation vehicles. This is despite the fact that the prospects of hydrogen, becoming a widely used fuel in the near future, are not sure. Other alternative fuels such as methane (natural gas), propane and most recently, methanol, are more easily available and less expensive at the present time. However, from the point of view of environmental protection , hydrogen is the perfect fuel and many scientists devote their research to develop the hydrogen fueled engines with financial help from governments.

Hydrogen fuel has already been tested in many different types of power plants ranging from rocket motors to diesel engines. However, presently only rocket motors are using hydrogen as a fuel with oxygen as the oxidant. Resonance tubes have been tested as igniters in rocket motors.

Some gas turbine engines have also been converted

experimentally to operate on hydrogen fuel. The advantages of hydrogen as aviation fuel is fully recognized and the aircraft industry is expected to be the next customer to utilize hydrogen as a fuel on a wide basis. The use of resonance tube for ignition of the hydrogen fuel in aircraft engines is, therefore, a good possibility. There are many similarities between a rocket fuel delivery system and that of an aircraft engine, the most important of which is that the fuel delivery is at steady flow rate and that the ignition delay time is not such a critical factor as it would be in a diesel engine. The major difference between the rocket engine and a gas turbine engine is that the temperature and pressure when ignition must occur is higher for the gas turbine engine because of the compression of the air before it reaches the combustion chamber.

Hydrogen as a fuel for engines in the automotive field has been studied since the early 1920s. The common trend has been to rely on hydrogen-air mixture induction into the combustion chamber through the intake manifold. However, problems such as knock, backfiring and preignition are difficult to avoid which limit the performance of the engine relying on this type of fuel supply. Injection of gaseous fuel into the cylinder during the intake stroke reduces some of the problems mentioned above, but still the hydrogen gas charge takes up a large volume of the cylinder

capacity, thereby reducing the amount of air being introduced. This in turn, reduces the net work of the cycle and the engine specific power. Direct injection of liquid hydrogen would have the disadvantage that cold hydrogen is very difficult to ignite and it has to absorb some amount of heat from the compressed air to vaporize, hence reducing the thermal efficiency of the cycle. It can be, therefore, concluded that direct injection of gaseous hydrogen into the combustion chamber of a diesel engine, at close to the TDC position of the piston ,has the potential to obtain the best possible work output by letting only air enter through the intake manifold. Also, the direct injection of gas allows the use of higher compression ratio which produces a higher thermal efficiency. Presently, the electronic controls technology which has allowed the automotive industry to improve the engine performance through fuel injection can be also used for the direct injection of high pressure hydrogen to the engine and allows, due to its flexibility, to meet all fuel delivery requirements for the engine.

In the development of hydrogen fueled diesel engines, ignition of gaseous hydrogen has been a difficult problem to overcome. The traditional compression ignition is almost not possible to obtain. Hot surface ignition using glow plugs does not give a precise control of the time of

ignition ,with respect to the angular crankshaft position, and it also needs a substantial electric power source. Spark ignition gives much better control of the ignition timing. However, a much higher electrical potential difference is required to bridge the spark plug gap in a diesel engine than in spark ignition gasoline engines because of the higher density of air which is compressed in the combustion chamber. This is also known to interfere with the engine's electronic controls. A passive ignition system such as resonance tubes would, therefore, be advantageous.

The use of resonance tube for the ignition of hydrogen jets under diesel engine conditions is much more complicated than in rocket engines. First, in a diesel engine, the pressure and temperature of air in the combustion chamber are much higher at the moment of injection; second the physical space available is severely limited; third, fuel is injected during a very short period of time and hence the fuel flow is a highly transient process. Also, because of the short time available for injection, of a few milliseconds duration only, the ignition delay period must be very short.

It has to be acknowledged that the ignition of a hydrogen jet within the time limits desired for a diesel engine has already been achieved. Tests performed by

injecting hydrogen gas into a high temperature oxidizer have yielded ignition delay times as low as half of a millisecond during experiments [24]. To obtain such short ignition delay period, a temperature of at least 1000 K is required. Whether the heating effect from the resonating shock waves in a resonance tube is fast enough to provide these temperature, and what will be the optimum conditions to achieve this goal, has yet to be studied.

The initial high temperature of air compressed in the combustion chamber should have a beneficial effect in reducing the ignition delay. However, the effects of high air density on the formation of the shock waves and on gas jet penetration towards the tube are not known, and have to be studied. Tube geometry such as internal diameter, cavity length, and axial distance between the injector nozzle and the tube entry have to be the subject of studies as well.

The space inside a diesel engine combustion chamber is small and therefore the axial distance between the injector and the resonance tube is limited, and so is the tube length. The dimensional requirements of the gas injector also affect the resonance tube dimensions. A typical injector orifice diameter (for a single hole pintle type nozzle) is between 1mm and 2mm. The tube diameter should be of similar size, and hence the boundary layer effect in

such a tube will be greater than in a larger diameter tube, the shock wave development and amplitude can be affected.

The fuel injection time period in a diesel engine is very short. If a four stroke engine is running at 1000 rpm and the injection period to deliver the required fuel dose is 30 degrees of crankshaft angle, the injection period is only 5 milliseconds. During this period, the hydrogen gas flow rate must first increase to a very high flow rate and then decrease to no flow. This causes the hydrogen gas flow rate into the resonance tube to become a highly transient process, which is very different from the case of constant flow rate of a much longer duration found in rocket fuel injection systems. Therefore, the unsteady boundary conditions at the tube inlet are much more difficult to predict, as compared with the steady flow case. Diesel engines, unlike rocket motors or gas turbine engines, require repeating of the ignition process at a high frequency. There has been no previous studies on the repeatability of resonance tube ignitions at a high frequency. The resonance tube must be able to survive the high number of ignitions and must be made from a material with low heat conductivity to reduce the heat transfer to the combustion chamber and to restrict the heat release from the resonating shock waves in order to ignite the gas in the tube.

These are just some of the problems which must be investigated and overcome before resonance tubes could be used in the manner desired in a diesel engine. Some of these aspects will be investigated in this thesis.

To test some of the characteristics of resonance tubes, when applied as ignition support in a diesel engine, a test device which simulates the diesel engine conditions must be used. To obtain the proper air to fuel ratio and the correct gaseous fuel dose, a controllable injector must be used and the air in the test chamber must also be exchanged for each injection. The best method to obtain all the desired conditions is to use an existing engine modified according to the requirements ; with small modifications, this engine can also be used for some static high pressure tests. Chapter 5 describes the test bench developed for this purpose; the solenoid actuated injector as well as the electrical hardware and software are also described in that chapter. Included in Chapter 5 is the design of a safety relief valve and a simulation to test the design of this valve. The valve has been designed to open, and release the gases if a large pressure increased in the combustion chamber occurs.

Chapter 6 describes and shows results of initial tests which were performed under atmospheric conditions to study the feasibility of resonance tube ignition in a diesel

engine. In this chapter the fuel injection system was calibrated. Also initial optimization of H-S tube parameters such as hole depth and diameter was initially performed under atmospheric conditions. Because the gas injection period is short, the development of constant tube inlet boundary conditions typical for other tests is not possible. For this reason, a test to qualitatively assess instantaneous gas inflow measurement was developed. This was done by using the pressure wave propagation record in a long tube to qualitatively determine the gas mass flow rate.

The acquisition of the test data was difficult due to the short duration of the processes; therefore, a properly developed and organized testing procedure was followed, in which a computer-based data acquisition and control system was used to control the injection process. However, recording of the shock wave characteristics required faster equipment, therefore,a high speed digital storage oscilloscope interfaced with a plotter to record and get hard copies of data became an essential tool in these investigations.

Final tuning and proper gas penetration tests were done at higher pressures. Chapter 7 describes the tests which were performed at high air pressure, closer to the pressures found in the diesel engine combustion chamber.

High pressure air from gas bottles was induced into the chamber and gas injections followed into the resonance tube. During these tests the gap between the injector nozzle and the mouth of the resonance tube was varied together with the pressure in the chamber, as well as injection parameters such as injection duration and metering valve opening.

For final tests ,the pressure and temperature of the air, as well as the correct fuel dose, were used. Chapter 8 utilized the apparatus to simulate conditions found in a combustion chamber of a reciprocating engine. Injections of hydrogen were done under these conditions with varying amounts of air charge, initial point of injection, as well as various doses of fuel and different gap between the injector nozzle and the tube.

CHAPTER 4

4.0 SIMPLIFIED THEORY OF RESONANCE TUBES

As discussed in an earlier chapter, Hartmann discovered that a strong repetitive pressure and acoustic amplification occurred when a sonic air jet was sent axially into a cylindrical cavity. Sprenger later discovered that there is a significant increase in temperature of the air in one of these tubes. He was able to record a temperature of 450^{0}C at the end of the tube. To give credit to these early scientists' work studying this phenomena, the system was called a "Hartmann-Sprenger Tube" also known as a "Resonance Tube" because of the resonating pressure wave which occur inside the cavity of the tube. Later Conrad and Pavli were able to create ignition of a hydrogen/oxygen gas mixture driven into one of these resonance tubes.

A simple H-S tube consists of a cylindrical cavity, closed at one end, and a sharp edged open end facing an underexpanded gas jet (Figure 4.1). The heating effect of a resonance tube has been attributed to the internal travelling shock waves, and friction of the air flowing against the walls. The heating rate can be made larger by increasing the shock strength. One method of doing this is by reducing the flow area of the travelling shock wave.

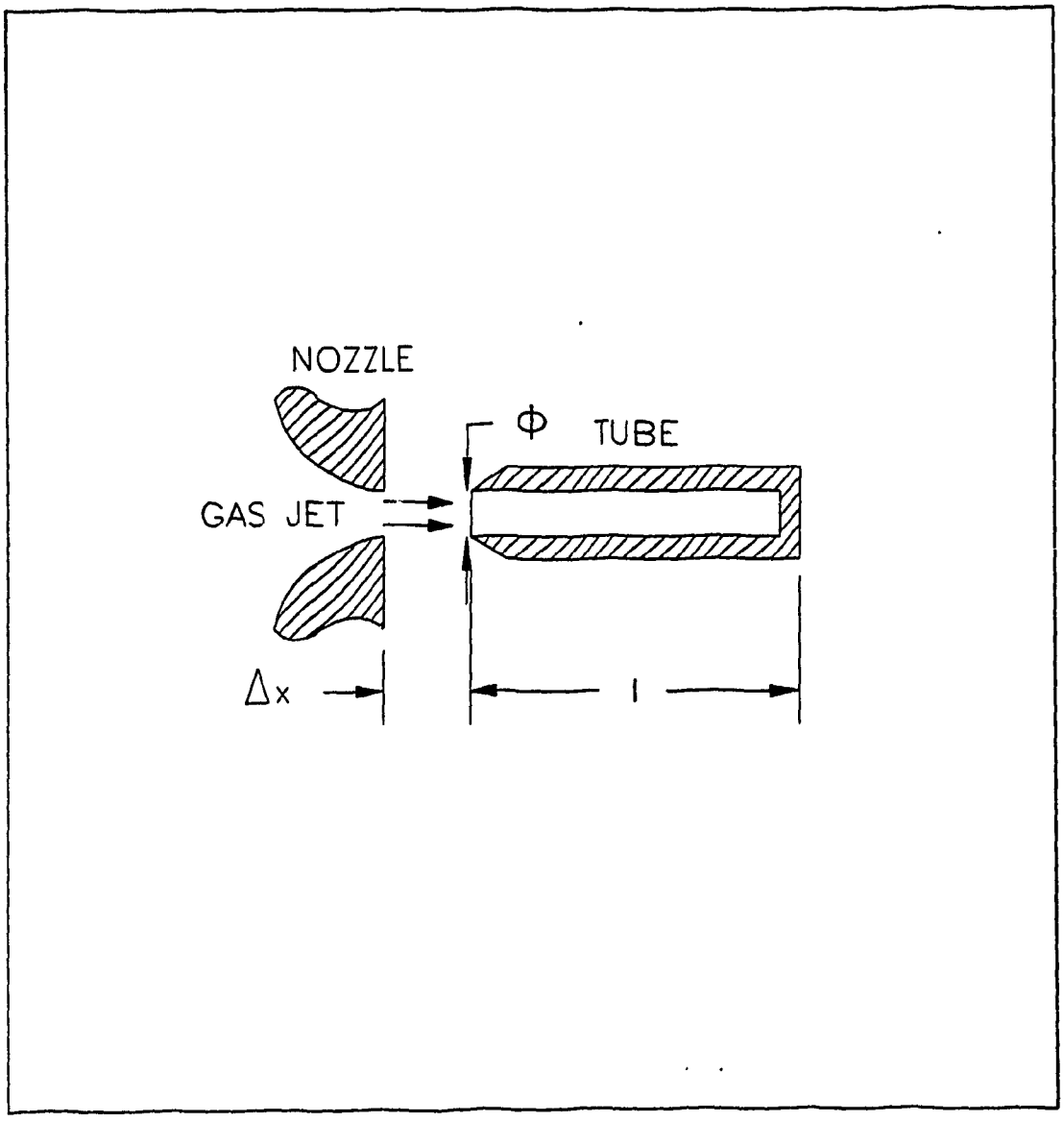

Figure 4.1 Schematic of Simplified Resonance Tube.

Many researchers have discovered this fact experimentally using tapered resonance tubes, however, Neemeh, Ostrowski, and Wu determined that a tube with a logarithmic spiral cross section performed better, in terms of end wall temperature than both simple or tapered H-S tubes.

4.1 Flow Field of a Resonance Tube

Resonating pressure waves can occur in a H-S tube when the open end of the tube is aligned axially with an underexpanded jet; however there are only certain axial distances in which this phenomenon occurs. Figure 4.2 shows a typical stagnation pressure record for the center line of an underexpanded jet. As can be seen, there is a cyclic rise and fall of the stagnation pressure with increasing axial displacement, with a tendency of reduced amplitude with increased displacement. The H-S tube must be placed within the areas where the pressure is rising, so that the shock wave which develops at the mouth of the tube, can be swallowed by the tube and then be able to return upstream and out of the tube. The lower pressure regions allow for easy upstream flow of the gas in the tube. To further decrease the core pressure of the jet, a wire is usually placed along the axis of the nozzle or along the center axis of the nozzle.

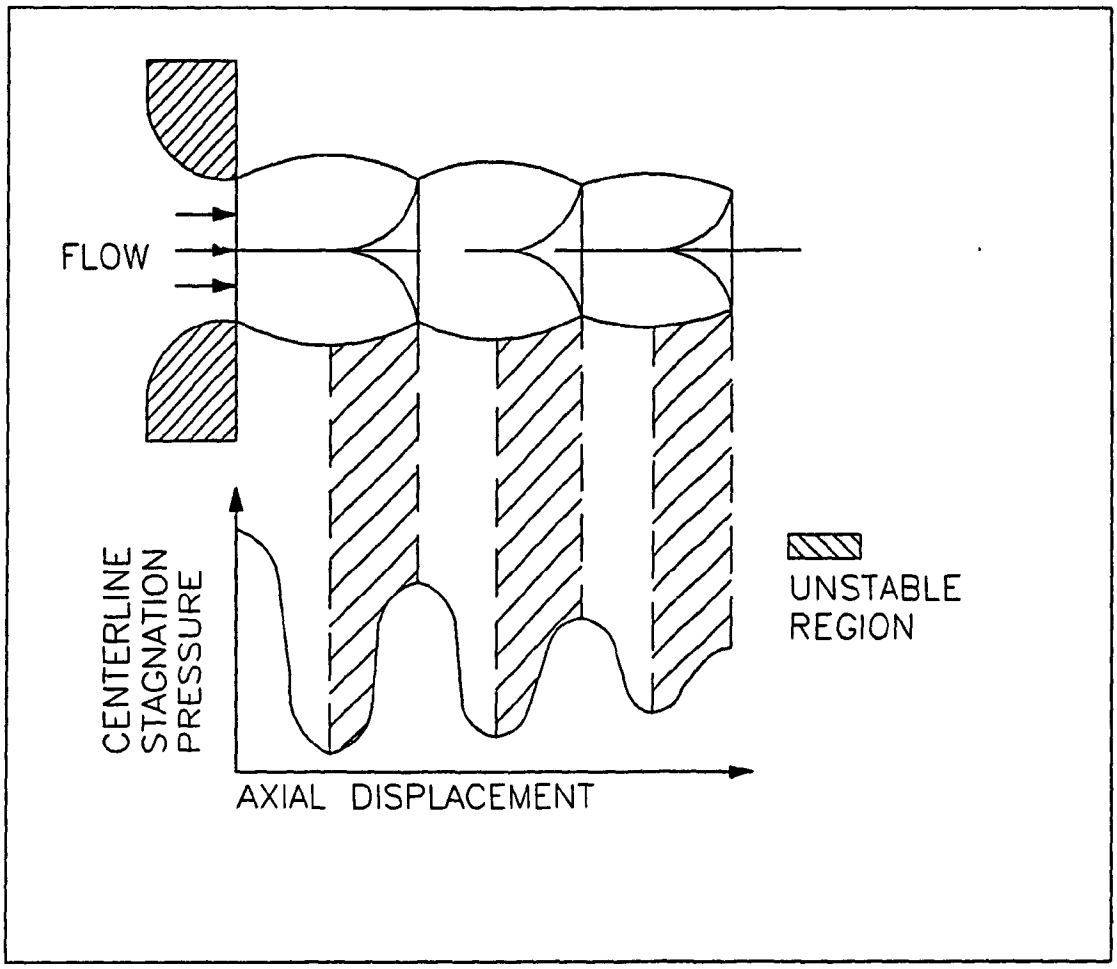

Figure 4.2 Stagnation Pressure History Along the Core of an Underexpanded Jet

The flow field of the cycle can be separated into four distinct phases:

1) temporary steady inflow,

2) sudden transition from inflow to outflow,

3) outflow, and

4) relative slow transition from outflow to inflow.

Because the stagnation pressure of the jet is greater than the pressure in the tube, an incident shock wave develops at the mouth of the tube. This shock wave is swallowed into the tube and travels downstream the tube (Figure 4.3a). The wave reflects off the back wall and travels upstream the jet direction. The fluid in the tube is at rest until the shock wave passes and returns to rest after the shock wave has passed in the opposite direction as seen in Figure 4.3b. The temperature and the pressure of the gas behind the reflected shock wave is higher that the initial gas properties because of the reflected shock wave. Inflow at the mouth of the tube begins as the shock wave enters the tube and ends only when the shock wave exits the tube. The transition from inflow to outflow occurs suddenly when the shock wave exits the tube; a centered expansion wave then propagates into the tube (Figure 4.3c). Outflow continues until the reflected expansion wave reaches the open end (Figure 4.3d). The gas in the tube is now at a reduced pressure and temperature and is again at

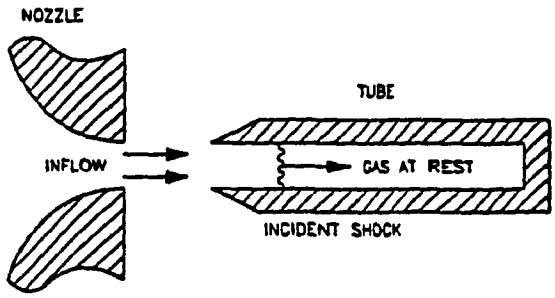

Figure 4.3a Incident Shock wave in a Resonance Tube.

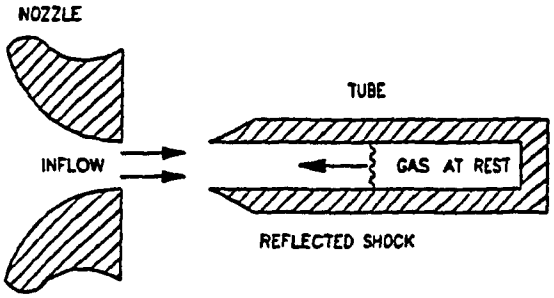

Figure 4.3b Reflected Shock Wave in a Resonance Tube.

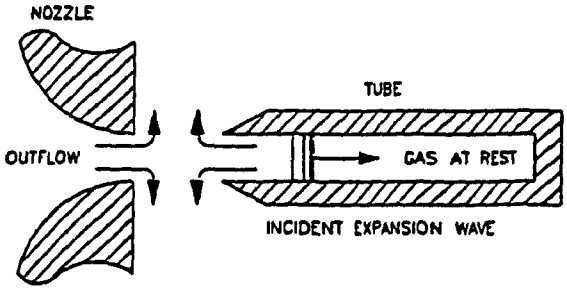

Figure 4.3c Incident Expansion Wave in a Resonance Tube.

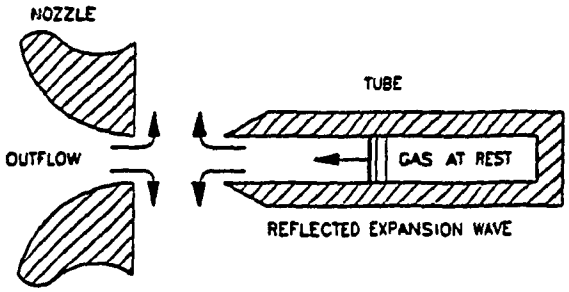

Figure 4.3d Reflected Expansion Wave in a Resonance Tube

rest.

Transition from outflow to inflow is much more gradual than the inflow to outflow transition. The outflow velocity gradually decreases until the impulse of the excitation jet exceeds that of the H-S tube outflow impulse. Then the jet enters the tube creating a shock wave and the cycle repeats itself.

The ideal resonance tube flow has two distinct sections of gases in the tube. A portion of the gas always remains in the tube (indigenous fluid) and a portion of gas which changes with every cycle (extraneous fluid).

4.2 Pressure History in a Resonance Tube

As is the case for any flow of fluids, the governing equations for the flow of gas in the resonance tube can be derived from the continuity and momentum equations. The nature of the differential equations after several simplifying assumption, are allowing for the solution using the method of characteristics [28].

4.2.1 Continuity Equation

The continuity equation expresses the property of conservation of mass. Using Figure 4.4a, consider a volume

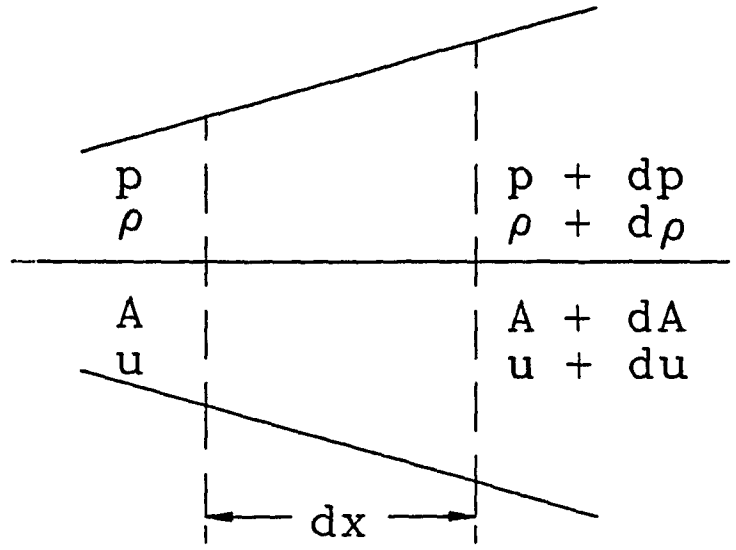

Figure 4.4a Volume Element in a Pipe for Derivation of Continuity.

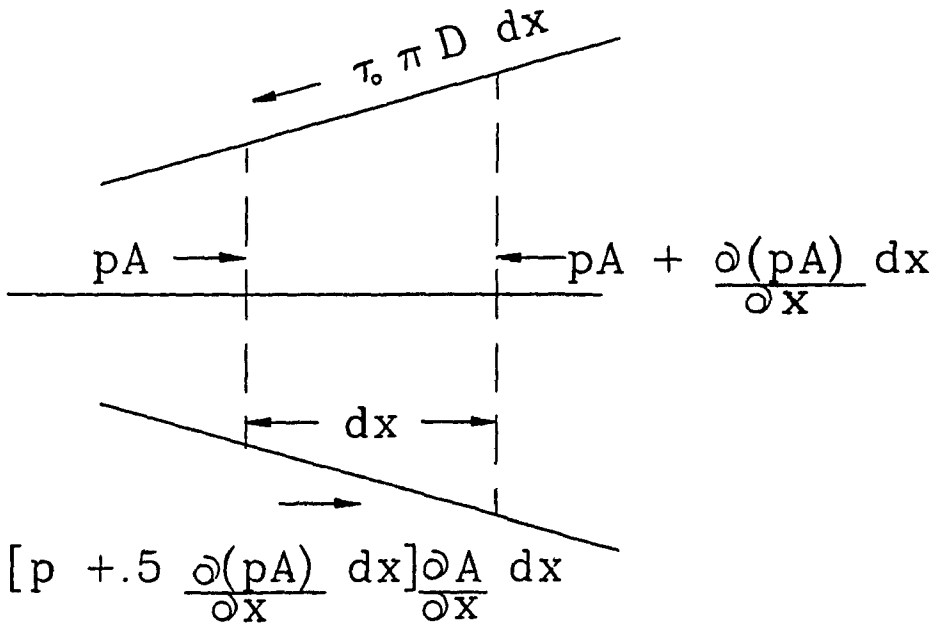

Figure 4.4b Force Diagram on a Volume Element in a Pipe.

element of a duct, A dx. The mass influx entering the volume for a time period of dt is denoted by:

$$\rho \, u \, A$$

The mass efflux along the duct and through the walls is given by:

$$\left(\rho + \Delta\rho \right) \left(u + \Delta u \right) \left(A + \Delta A \right) + \psi \, \Delta x$$

At the same time the mass contained in the element changes from

$$\rho \, A \, dx$$

to

$$\rho \, A \, dx + \frac{\delta(\rho \, A)}{\delta t} \, dt \, dx$$

The continuity equation states that the change in efflux must equal the change in mass contained in the element. After neglecting higher order derivative terms the continuity equation then becomes:

$$\frac{\delta(\rho \, A)}{\delta t} + \frac{\delta(\rho \, u \, A)}{\delta x} + \psi = 0$$

4.2.2 The Momentum Equation

The momentum equation is Newton's Second Law applied to fluids. Consider the fluid element shown in Figure 4.4b. The mass of the fluid in this element is:

$$\rho \, A \, dx$$

The forces acting on the element are also shown in this figure. Newton's second law states that the sum of all the effective forces on a body is equal to the rate of change of momentum of the body. The forces acting on the elements are given by:

$$\Sigma F = P A - (p + dp)(A + dA) + \left(p + \frac{\Delta p}{2} \right) dA - f_0 \rho A \, dx$$

The rate of change in momentum is:

$$\frac{\delta (m u)}{\delta t} = \frac{\delta (\rho A \, dx \, u)}{\delta t}$$

Applying these equations to the fluid element and simplifying, the momentum can be given as:

$$-\frac{1}{\rho} \frac{\delta p}{\delta x} + f = u \frac{\delta u}{\delta x} + \frac{\delta u}{\delta t}$$

4.2.3 Derivation of the Characteristic Relations

Continuity and momentum equations can be rewritten as:

$$\frac{\delta(\ln \rho)}{\delta t} + \frac{\delta u}{\delta x} + u\frac{\delta(\ln \rho)}{\delta x} = -\frac{\delta(\ln A)}{\delta t} - u\frac{\delta(\ln A)}{\delta x} - \frac{a^2\psi}{\gamma p A}$$

$$\frac{\delta u}{\delta t} + u\frac{\delta u}{\delta x} = -\frac{a^2}{\gamma}\frac{\delta(\ln p)}{\delta x} + f$$

Expressing the derivative terms of pressure, p, and density, ρ, in terms of the derivatives of the velocity of sound, a, and entropy, s, as so:

$$d(\ln \rho) = \frac{2}{\gamma - 1}\frac{da}{a} - \frac{ds}{R}$$

$$d(\ln p) = \frac{2\gamma}{\gamma - 1}\frac{da}{a} - \frac{ds}{R}$$

These two equations can be substituted into the continuity and momentum equations to obtain:

$$\frac{2}{\gamma - 1}\frac{\delta a}{\delta t} + \frac{2}{\gamma - 1}u\frac{\delta a}{\delta t} + a\frac{\delta u}{\delta x} = -a\,u\frac{\delta(\ln A)}{\delta x} - a\frac{\delta(\ln A)}{\delta t} - \frac{a}{R}\frac{DS}{Dt} - \frac{a^3\psi}{\gamma p A}$$

and

$$\frac{\delta u}{\delta t} + u\frac{\delta u}{\delta x} + \frac{2\,a}{\gamma - 1}\frac{\delta a}{\delta x} = \frac{a^2}{\gamma\,R}\frac{\delta s}{\delta x} + f$$

When the above two equations are added to each other, and also subtracted from each other this general expression is obtained:

$$\frac{\delta}{\delta t}\left(\frac{2}{\gamma - 1}\,a \pm u\right) + (u \pm a)\frac{\delta}{\delta x}\left(\frac{2}{\gamma - 1}\,a \pm u\right) =$$

$$-a\,u\frac{\delta(\ln A)}{\delta x} - a\frac{\delta(\ln A)}{\delta x} + \frac{a}{R}\left(\frac{DS}{Dt} \pm \frac{a}{\gamma}\frac{\delta s}{\delta t}\right) \pm f - \frac{a^3\,\psi}{\gamma\,p\,A}$$

Defining

$$P = \left(\frac{2}{\gamma - 1}\right) a + u$$

and

$$Q = \left(\frac{2}{\gamma - 1}\right) a - u$$

the left hand side of these equations become:

$$\frac{\delta P}{\delta x} + (u + a)\frac{\delta P}{\delta x} = \text{LHS}$$

$$\frac{\delta Q}{\delta x} + (u - a)\frac{\delta Q}{\delta x} = \text{LHS}$$

The right hand side of the equations can be simplified with some assumptions. For a simple H-S tube the area is constant, therefore $dA/dx = 0$. Also the tube is not porous so there can be no flow through the tube walls so $\psi = 0$ and assuming that the body forces are negligible then $f = 0$. Assuming also that the flow is isentropic, because the shock strength is small, then the two equations become:

$$\frac{\delta P}{\delta t} + (u + a) \frac{\delta P}{\delta x} = 0$$

$$\frac{\delta Q}{\delta t} + (u - a) \frac{\delta Q}{\delta x} = 0$$

These two equations can be solved using the method of characteristics by defining the curves:

for P waves $\quad \frac{dx}{dt} = u + a$

for Q waves $\quad \frac{dx}{dt} = u - a$

4.2.4 Analysis of Unsteady One Dimensional Flow in a Simple Resonance Tube

For analysis of the pressure history in a simple H-S tube, some simplifying assumptions must be made, these

assumptions are:

1 - motion in the tube is one dimensional,

2 - the viscous forces are negligible,

3 - the flow is isentropic,

4 - the internal shock (Ms < 2) is replaced by compression wave,

5 - the central expansion wave is replaced by a single expansion wave.

Figure 4.5 shows a simplified wave diagram in a resonance tube obtained by using the above mentioned assumptions. The P characteristic waves are defined as the waves with a positive x vs. t slope. The Q characteristic waves are defined as the waves with a negative x vs. t slope. The values of P and Q are constant along their respective characteristic lines. Using these characteristics we can solve the wave diagram for each of the regions in the figure.

REGION 1 and REGION 2

$$P_1 = P_2$$

with $u_1 = u_{jet}$

and $a_1 = a_{jet}$

and $u_2 = 0$ (gas at rest behind reflected wave)

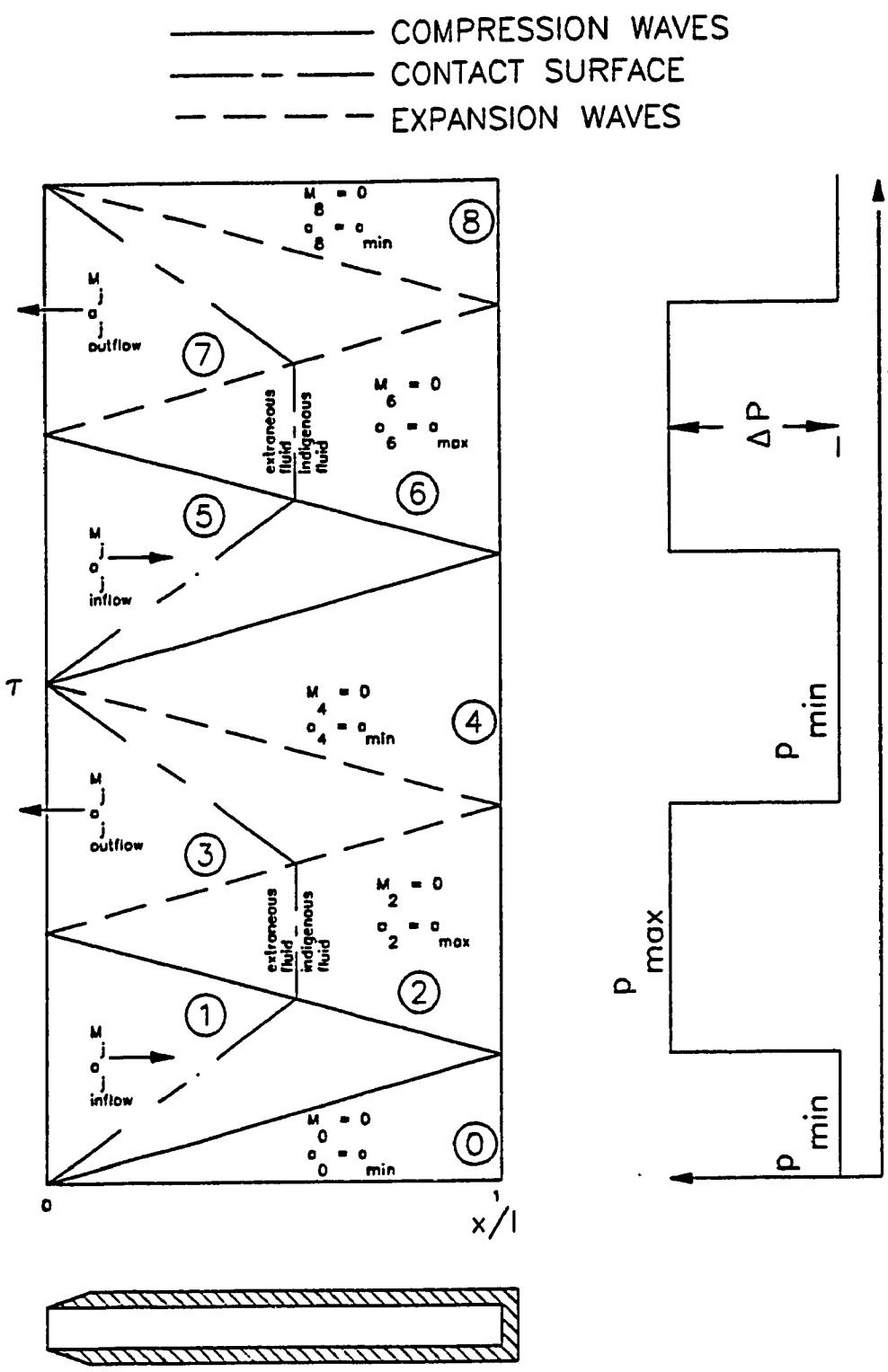

Figure 4.5 Simplified Wave Diagram in a Resonance Tube.

we get $\frac{a_2}{a_{jet}} = 1 + \frac{\gamma - 1}{2} M_{jet}$

and $\frac{p_2}{p_{jet}} = \left(1 + \frac{\gamma - 1}{2} M_{jet} \right)^{\frac{2\gamma}{\gamma - 1}}$

REGION 2 and REGION 3

$$Q_2 = Q_3$$

with $p_a = p_{jet}$ (assuming a fully expanded wave

$a_3 = a_{jet}$

and $u_2 = 0$ (gas at rest)

we get $u_3 = -u_{jet}$

REGION 3 and REGION 4

$$P_3 = P_4$$

with $u_4 = 0$ (gas at rest)

we get $\frac{a_4}{a_{jet}} = 1 - \frac{\gamma - 1}{2} M_{jet}$

and $\frac{p_4}{p_{jet}} = \left(1 - \frac{\gamma - 1}{2} M_{jet} \right)^{\frac{2\gamma}{\gamma - 1}}$

The pressure amplitude for the simplified wave diagram can

now be determined by:

$$\frac{\Delta p}{p_{jet}} = \frac{p_{max} - p_{min}}{p_{jet}} = \frac{p_2 - p_4}{p_{jet}} =$$

$$\left(1 + \frac{\gamma - 1}{2} M_{jet} \right)^{\frac{2\gamma}{\gamma - 1}} - \left(1 - \frac{\gamma - 1}{2} M_{jet} \right)^{\frac{2\gamma}{\gamma - 1}}$$

The wave will resonate at a frequency close to the acoustic frequency. Taking the average wave velocities the frequency of the cycles can be determined.

Region 0	$a_0 = a_{min}$
Region 1	$a_1 = a_{jet} + u_{jet}$
	$= a_{jet} (1 + M_{jet})$
Region 2	$a_2 = a_{max}$
Region 3	$a_3 = a_{jet} - u_{jet}$
	$= a_{jet} (1 - M_{jet})$

where $$a_{min} = \left(1 - \frac{\gamma - 1}{2} M_{jet} \right) a_{jet}$$

$$a_{max} = \left(1 + \frac{\gamma - 1}{2} M_{jet} \right) a_{jet}$$

Now defining the average velocity of the wave as the sum of the sound velocities across the wave divided by two,

we get:

$$\overline{u_{01}} = \overline{u_{34}} = \frac{a_{jet}\ (\ 1 + M_{jet})}{2} + \frac{a_{min}}{2}$$

$$\overline{u_{12}} = \overline{u_{23}} = \frac{a_{jet}\ (\ 1 - M_{jet})}{2} + \frac{a_{max}}{2}$$

A complete cycle requires four traverses of the tube by the waves and the time period to accomplish this is:

$$t_p = \frac{\ell}{\overline{u_{01}}} + \frac{\ell}{\overline{u_{12}}} + \frac{\ell}{\overline{u_{23}}} + \frac{\ell}{\overline{u_{34}}}$$

$$= \frac{4\ \ell}{\left[\ 1 - \left(\frac{3 - \gamma}{4}\right)^2 M_{jet}^2\ \right] a_{jet}}$$

Taking the inverse of the period solves for the frequency of the resonating waves and this is given by:

$$f = \frac{1}{t_p} = \frac{\left[\ 1 - \left(\frac{3 - \gamma}{4}\right)^2 M_{jet}^2\ \right] a_{jet}}{4\ \ell}$$

The simplified wave analysis overestimates both the shock wave pressure amplitude as well as the frequency.

The frequency is overestimated by approximately 10 % and the pressure amplitude overestimation diverges with increasing jet mach number and can this can be as much as 25% at a jet mach number of 1 [29].

CHAPTER 5

5.0 EXPERIMENTAL APPARATUSES AND CONTROL SYSTEM

5.1 Introduction

For all experimental investigations, there must be special apparatus which can be used to perform the test in such a manner as to simulate the real working conditions at which the system being tested, will be used. The test set-up must also have the data recording capabilities to analyze the results. In this thesis the real working conditions that the test rig must simulate, are that of a diesel engine. The control system must deliver the correct dose of fuel into a variable volume combustion chamber at the right instant during the compression stroke. Figure 5.1 is a schematic of a gaseous fuel system proposed for our research in the Fuel Control Systems Laboratory at Concordia University. The major parts of this fuel storage and delivery control system consist of a semi-cryogenic fuel tank, a fuel metering and delivery system, the Engine Electronic Fuel Control (EEFC) unit, and all relative sensors to provide information to the EEFC.

The fuel metering and delivery system consists of a metering valve actuated by a digital stepper motor and, a

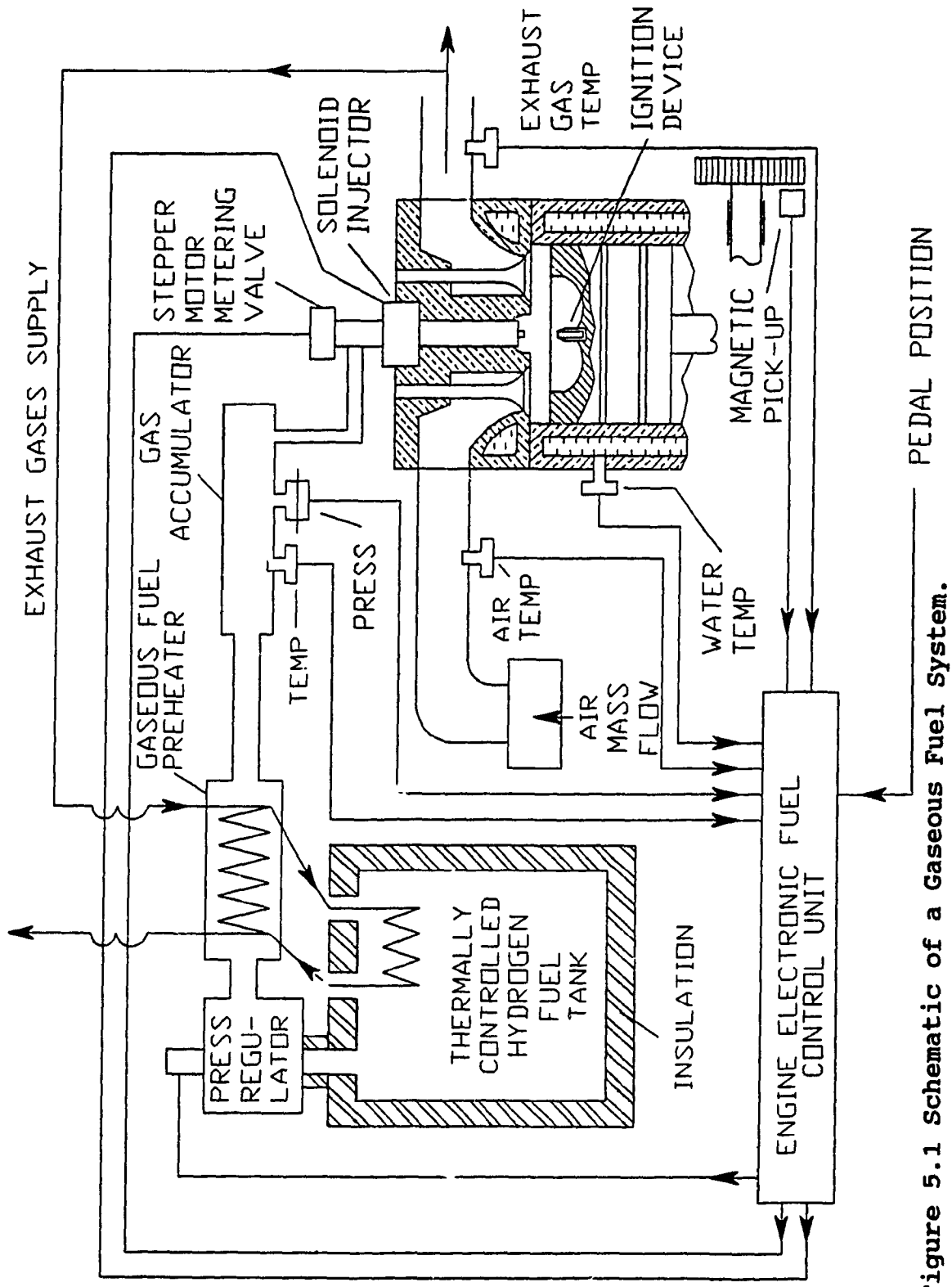

Figure 5.1 Schematic of a Gaseous Fuel System.

solenoid actuated fuel injector. These components are the muscles of the fuel control, the brain of the system is the EEFC. For future engines using gaseous fuels and electronic actuators only an electrically controlled fuel system can provide the flexibility of operation required. From the schematic in Figure 5.1 it can be seen that the EEFC is receiving data from the many sensors installed on the engine. Information such as engine speed, piston position, intake air flow rate and temperature, exhaust gas temperature, cooling water temperature, fuel pressure and temperature and throttle position, are the required data for the EEFC. The EEFC receives this information and determines the correct fuel dose that is required and then outputs signals to the actuators to vary the opening of the metering valve and to open the injector for a certain amount of time to deliver the required fuel. The control system loop is closed through the engine response to the fuel input.

The final test rig in this thesis will be part of the system described above. Figure 5.2 shows the test rig used for the tests in this research. It consists of a modified single-cylinder, side valve gasoline engine, an electronically actuated fuel injector, a manually actuated metering valve, gaseous fuel tanks, air supply with supercharging ability, an electric variable speed motor to

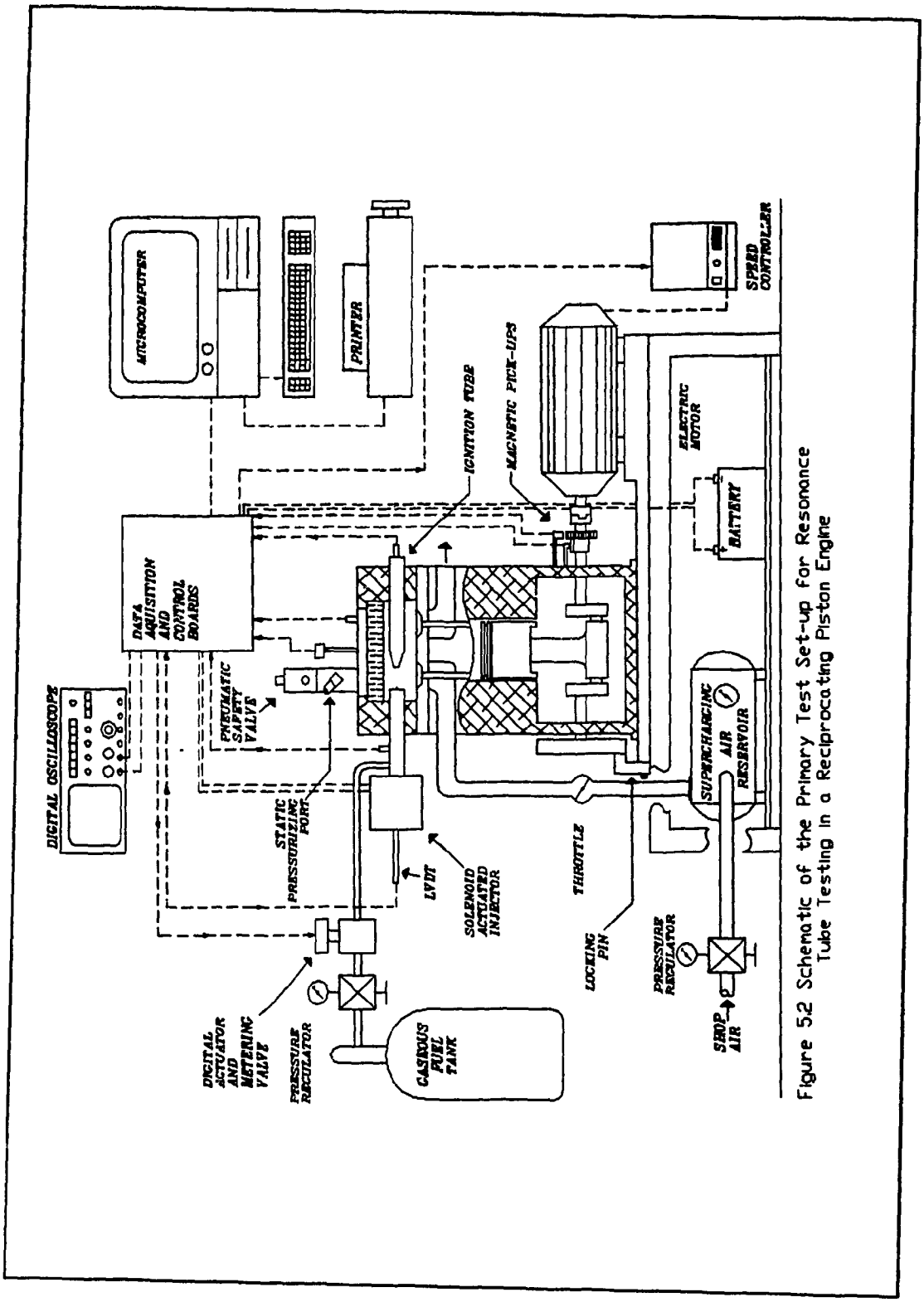

Figure 5.2 Schematic of the Primary Test Set-up for Resonance Tube Testing in a Reciprocating Piston Engine

drive the engine, an electronic control unit and a data acquisition equipment. This chapter will describe the mechanical components of this test rig, the electronic control system, the software controlling the unit and the test procedures which will be followed.

5.2 Engine Simulation Test Rig

Figure 5.2 shows the schematic of the engine simulation test rig. The engine used is a modified Briggs and Stratton, one cylinder, four-stroke engine. This engine has a bore of 76.2 mm. (3.00 in.) and a stroke of 70.0 mm. (2.756 in.). The intake and exhaust valves are situated at the side of the cylinder, which allowed for easy modification of the cylinder head of the engine to incorporate the injector, resonance tube, a transparent quartz glass window, a safety check valve, a static supercharging port, pressure transducer and thermocouple. The port for the safety check valve can accommodate a spark plug in its place for further ignition development work. The magneto ignition unit has been removed, however the carburetor is maintained to have some control of the inlet air using the throttle butterfly valve. A 30 tooth gear is placed on the output shaft for rotational speed sensing with a magnetic pick-up. An optical sensor is also placed

on the output shaft to send a piston position signal to the control unit. The engine's crankshaft is rotated by a 5 HP electric motor with a speed controller. Since the principal aim of this research is to study ignition, then the engine need not turn under its own power.

To closer simulate the conditions found in a diesel engine, the possibility of supercharging the engine intake air, with high pressure shop air, has been added. In this way, the effective compression ratio of the engine can be increased to as high as 20:1 from the present value of 6:1. A large reservoir is added in the supply line to reduce the fluctuations in air supply pressure. It must be noted that only partial simulation of diesel engine conditions are accommodated because the temperature compensation is not installed; to reach typical diesel engine temperatures, the supply air would have to be preheated.

The hydrogen fuel supply is taken from high pressure gas bottles and a pressure regulator is placed in the supply line to set the gas pressure to the desired value.

The fuel injection unit consists of two parts; a metering valve and a solenoid actuated fuel injector. The injector solenoid is under computer control and the metering valve can also be under computer control, as Miele has done [30] by coupling it with a digital stepper motor to turn the valve stem; this type of control was not

required in this research.

The engine is equipped with a safety check valve. The important purpose of this valve is to open and release gases if the combustion chamber pressure exceeds the cracking pressure set on the valve. Because the engine was originally a low compression gasoline engine with an aluminum block, it might not be able to withstand the pressures that can occur if the hydrogen ignites and burns in the restricted combustion chamber. Therefore, the valve has to open fast to relieve the pressure in the combustion chamber in case of excess pressure created by ignition.

The cylinder head was machined from a two inch thick slab of aluminum. Figure 5.3 shows a cross section of the cylinder head incorporating the fuel injector entering from one side, the resonance tube ignition unit facing this injector protruding from the opposite face, a hole for the static pressure charging port and the check valve, as well as a pressure transducer and a thermocouple. The machine drawings for this cylinder head can be found in Appendix D. This cylinder head is fastened with special reenforcement brackets and high strength bolts. These brackets were required because during cylinder head redesign two of the bolt holes were omitted to accommodate the injector and the ignition unit.

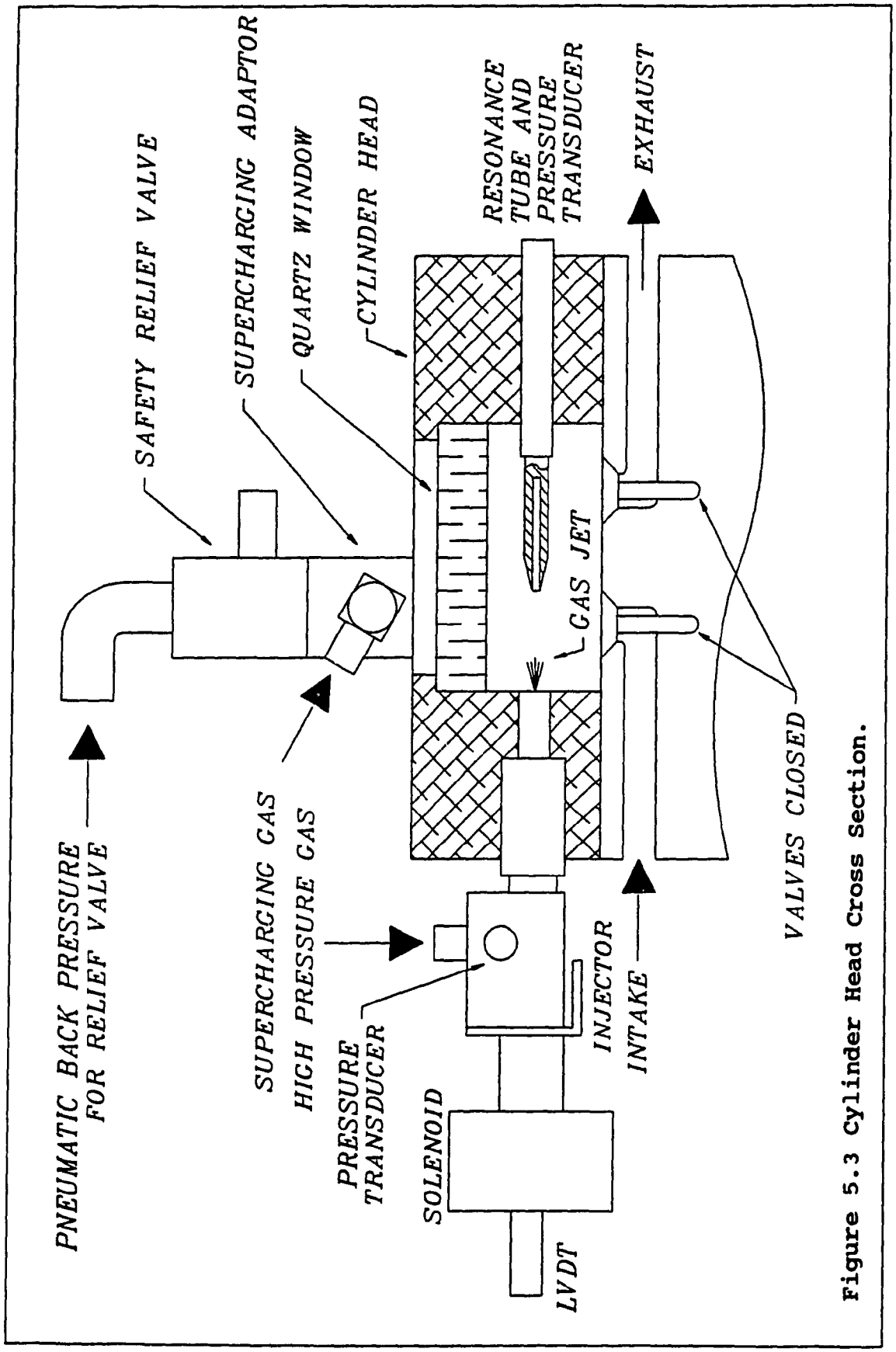

Figure 5.3 Cylinder Head Cross Section.

The final major component of the test rig is the engine electronic fuel control unit. This black box consists of the electronic circuitry to control the injection process.

This test set-up will be used for two different types of tests:

1- high pressure constant volume chamber injections

2- injections with reciprocating piston.

The first set of tests use the engine as a "bomb" chamber. The piston is locked into place with the valves closed at TDC. Compressed air is then added through the static pressure charging port to create a high air pressure for static tests. Hydrogen is then injected into the chamber.

The second set of tests have the piston reciprocating and hydrogen injections will occur during the compression stroke of the engine. The intake air can be supercharged through the air supply reservoir. These tests will closer simulate true engine conditions with air exchange and adiabatic heating and cooling as well as compression and expansion of the air.

The following sections will more closely describe the major components of the engine simulation test rig.

5.3 Electronically Actuated Injector and Nozzles

Gaseous fuel systems differ greatly from typical liquid diesel fuel systems. The most important factor contributing to these differences is that diesel fuel, as any other liquid fuels, are almost incompressible, while gaseous fuels, such as hydrogen or natural gas, are compressible. Therefore, a different type of fuel delivery and metering system must be used and one of these systems has been shown in Figure 5.1.

The fuel metering system controls the dose of fuel by varying the time period when the needle is lifted off the seat of the injector by the solenoid and by modulating the pressure in the injector by throttling the gas flow into the injector by the metering valve. The use of the metering valve adds the benefit of lowering the leakage through the injector by reducing the pressure in the injector during the injection cycle. It also causes faster closing and better sealing of the needle because the gas force helping to keep the needle open during the injection period, is lower at the end of injection due to the throttling of the gas flow at the metering valve during the injection period.

The injectors used in this research were developed by Giannacopoulos [13]. Figure 5.4 shows a schematic of the

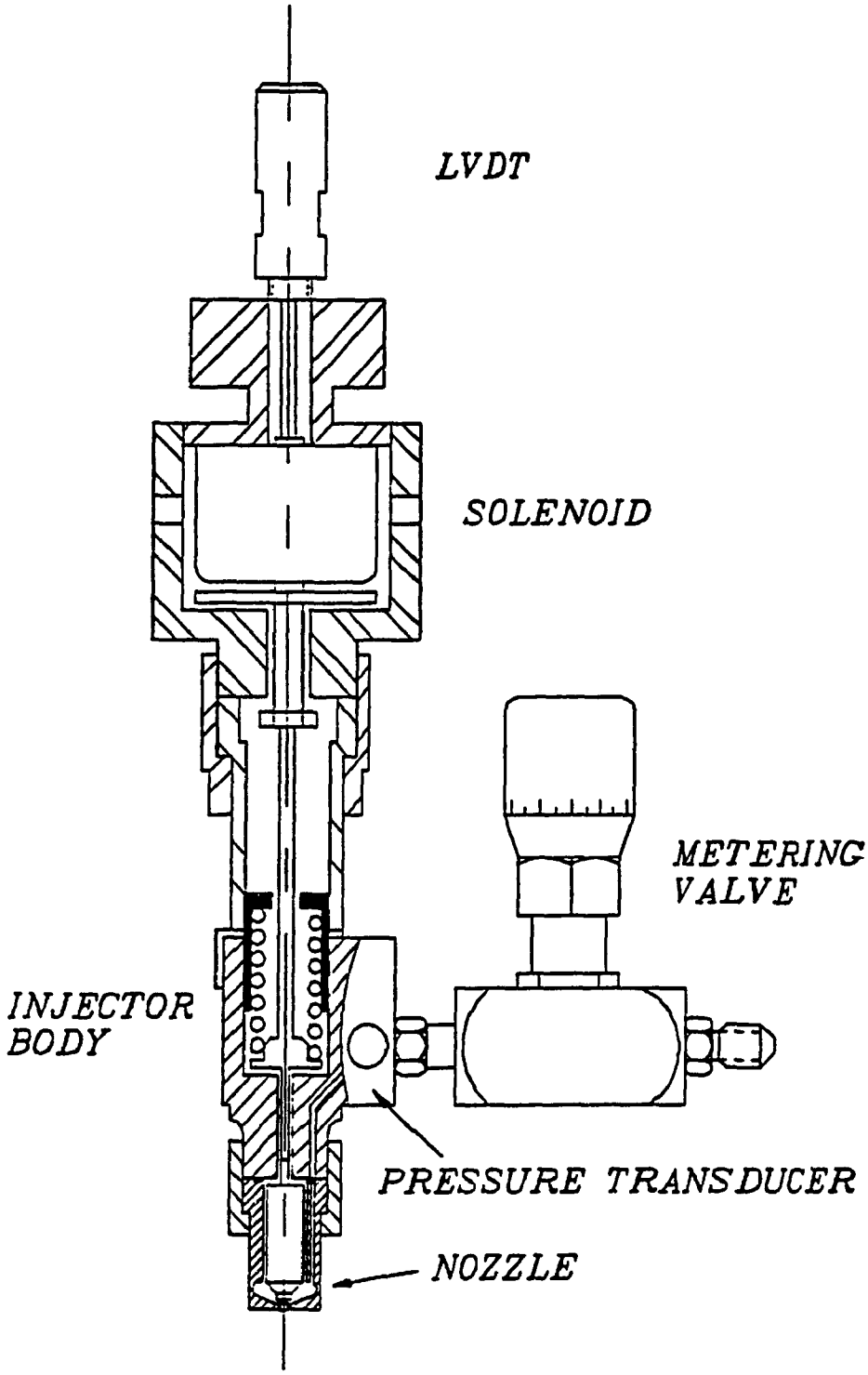

Figure 5.4 Cross Section of the Injector Unit.

injector unit with a metering valve at the inlet. It is a modified CAV KBK 40S546V injector housing with a CAV BDN45D508W nozzle. The nozzles were modified to allow the development of the "jet cells" required for shock wave creation, as was described earlier. This was done by reducing the pintle diameter to 0.15 mm. in order to reduce the pressure at the core of the jet. A linear solenoid actuator manufactured by LENDEX INC. was adapted to the injector housing and connected to the push rod of the injector . The actuator is a Model 5-SF, PUSH/PULL type and is controlled by the actuating circuit which will be described later in this chapter. The original spring has been replaced by a stiffer spring with a constant of 321 kN/mm. The metering valve is a HOKE 316SST tapered valve with an orifice of 1.59 mm. diameter, and the stem has a 1 degree taper.

The injector is instrumented with a linear variable differential transducer (LVDT) manufactured by AVL INC. (Model AVL 421103). The LVDT has a range of travel of 1 mm. to either side of the datum. The signal of the LVDT is amplified with an AVL carrier amplifier Model 3075-A02. The injector is also instrumented with a Kistler Model 603B2 piezoelectric pressure transducer to measure the pressure of the gaseous fuel in the injector. This pressure signal is amplified with a Kistler Model 504E dual

mode amplifier.

Several nozzle configurations were tested for delivering the correct fuel dose and creation of a weak core of the gas jet out of the injector. The three nozzles that were tested are shown in Figure 5.5. The third nozzle configuration was chosen because it provided enough fuel flow and also promoted high amplitude resonating shock waves in the H-S tube.

5.4 Electronic Hardware

As stated earlier, with the added complexity of a hydrogen control system, the best results can be obtained with electronic controls. From Figure 5.2, it can be seen that the test rig is controlled with an electronic control unit. The electronic control allows for the correct dose of fuel to be delivered by the injector/metering valve unit at a specified crank angle position, and at particular engine's rotational speed, piston position and other engine operating parameters.

The inputs to the EEFC are: engine rotational speed, and piston position. The engine rotational speed is obtained from a magnetic pick-up. This sensor detects magnetic pulses from a 30 tooth gear placed on the engine shaft. The piston position is sensed using an optical

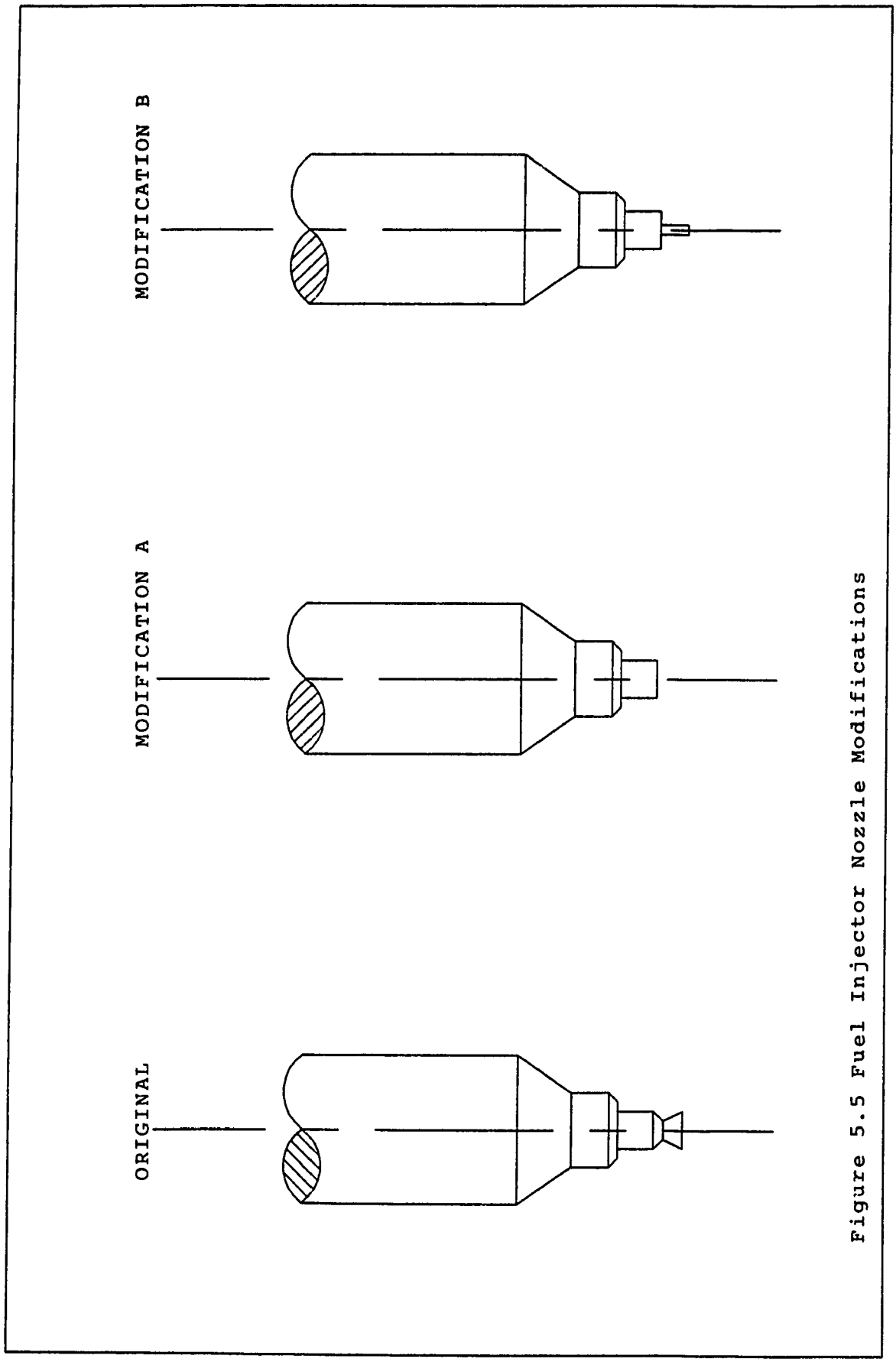

Figure 5.5 Fuel Injector Nozzle Modifications

sensor receiving a signal from a reflective strip placed on the flywheel 180 degrees before the top dead center position of the piston. The outputs from the EEFC are the start of injection point and the duration of the injection.

The computer and electronic controls for this set-up consist of an IBM XT personal computer with a LAB MASTER data acquisition and control board installed, and electronic circuits designed and made especially for this EEFC.

The computer is an IBM XT with 640 kilobytes of memory, and a 20 Megabyte hard disk. The CPU is an Intel 8088 coupled with a Intel 8087 math co-processor operating at 4.7 MHz.

The Lab Master Data Acquisition and Control board is manufactured by Scientific Solutions Inc. This board interfaces the computer with the actuation circuit and sensors. The data acquisition and control unit consists of a mother board installed in the computer through a 62 pin bus and a daughter board, external to the computer, connected to the mother board through a 50 pin cable. A block diagram of this Lab Master system is shown in Figure 5.6. The system features 4 basic I/O ports:

- parallel port
- timer port
- analog to digital (A/D) port

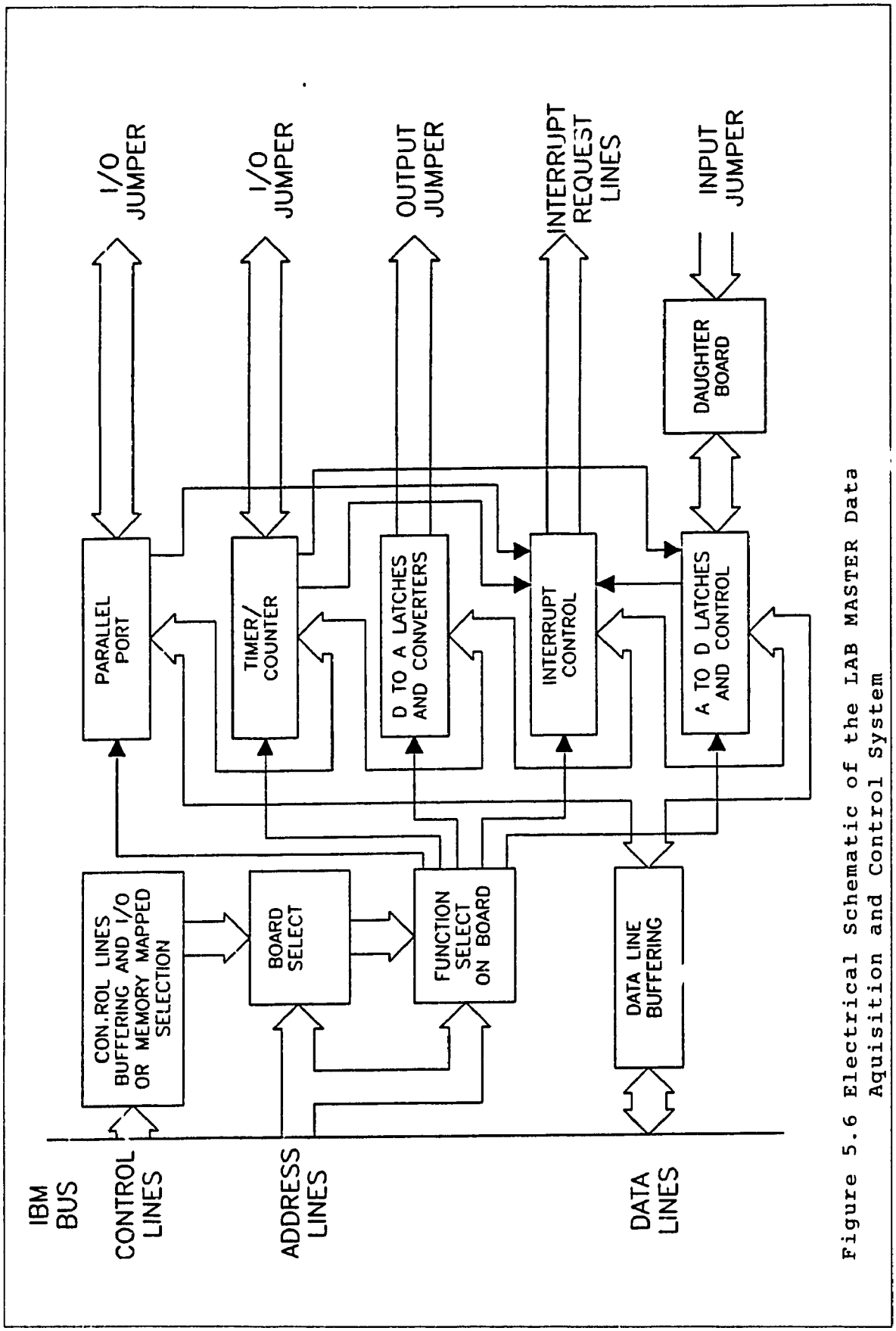

Figure 5.6 Electrical Schematic of the LAB MASTER Data Aquisition and Control System

- digital to analog (D/A) port

There are 24 parallel I/O lines which are programmable as two 12 bit lines or as three 8 bit lines. It can be programmed as bi-directional I/O ports with handshaking and it originates from the INTEL 8255 chip situated on the mother board.

The system also includes five 16 bit timer/counters using AMD 9513 timer chips also located on the mother board and are cascadable. The count can be in hexadecimal or in binary coded decimal form, and has the ability to count up or to count down. The source of the count can be from an external source or an internal source accurate to 1 microsecond. The IC can output a terminal count signal when the counting is completed; in this way this signal can be used for interrupts.

The A/D module is situated on the daughter board. It has 12 bit resolution at a 30 kHz. conversion rate. The A/D can accommodate 16 single-ended signals or 8 true differential inputs. The A/D board can be multiplexed to 256 single-ended signals or 128 true differential signals.

The D/A has 12 bit resolution on two independent digital to analog converters. The ranges of the outputs can easily be varied using jumpers.

The circuits developed for this EEFC can be listed

as:

1 - position interrupt circuit

2 - rotational speed circuit

3 - injector control circuit

4 - injector actuating circuit

Figure 5.7 shows the schematic of the position interrupt circuit. It uses an optical sensor with a built in LED with a photo NPN transistor to send the position signal. The LED constantly sends out a light on to the engine shaft. A reflective strip is placed on the shaft at the 180 degrees BTDC, the light reflects off this strip and the light signal is received by the photo transistor. This voltage signal is then amplified to a useful level using an operational amplifier, and next conditioned to a square shaped pulse using two Schmitt Hex Inverters.

The engine is working in a four stroke cycle, that is the fuel must be injected every second revolution, during each compression stroke. Since the interrupt signal occurs every revolution, the signal from the position interrupt is divided by two with a D-type flip-flop circuit.

This signal is sent to the mother board of the data acquisition and control unit, triggering the IRQ2 timer interrupt on the board.

The speed sensor is a magnetic pick-up sensing the

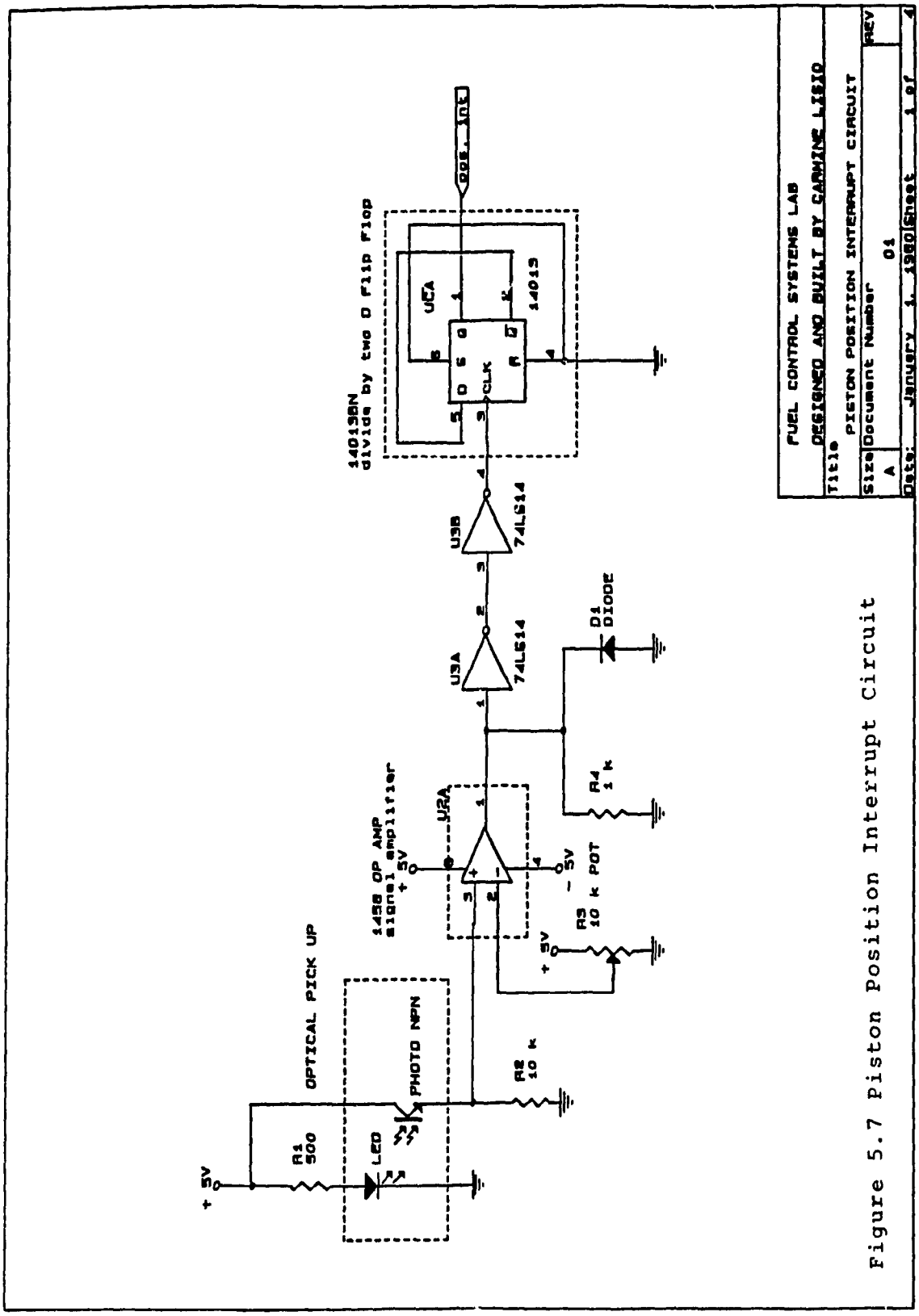

Figure 5.7 Piston Position Interrupt Circuit

magnetic field created by metal teeth from a 30 tooth gear, placed on the engine output shaft, passing over the sensor. The IC used is a National Semiconductor LM2907N frequency to voltage converter. Figure 5.8 shows the circuit which acts as a tachometer to convert the rotational speed to an analog voltage. The tachometer is referenced to ground to easily interface with a magnetic pick-up. The analog output is sent to the daughter board for digital conversion.

Previous trial of a TELEDYNE 9400CJ frequency to voltage converter was unsuccessful because this IC would saturate when the electric motor was turned on; the chip seems not to be as well protected against electromagnetic interference as the National Semiconductor IC.

The injector control circuit is shown in Figure 5.9 and the solenoid switching circuit is shown in Figure 5.10. The switching circuit is identical to that used by Giannacopoulos [13]. The parallel ports of the data acquisition and control unit transmit the signal to energize and de-energize the solenoid injector.

The input signals Q0 and Q1 are sent and latched, by a TTL 7475 bistable latch, when E01 is set to the high state. These signals are then processed through the other components of the logic circuit to form four different output data signals:

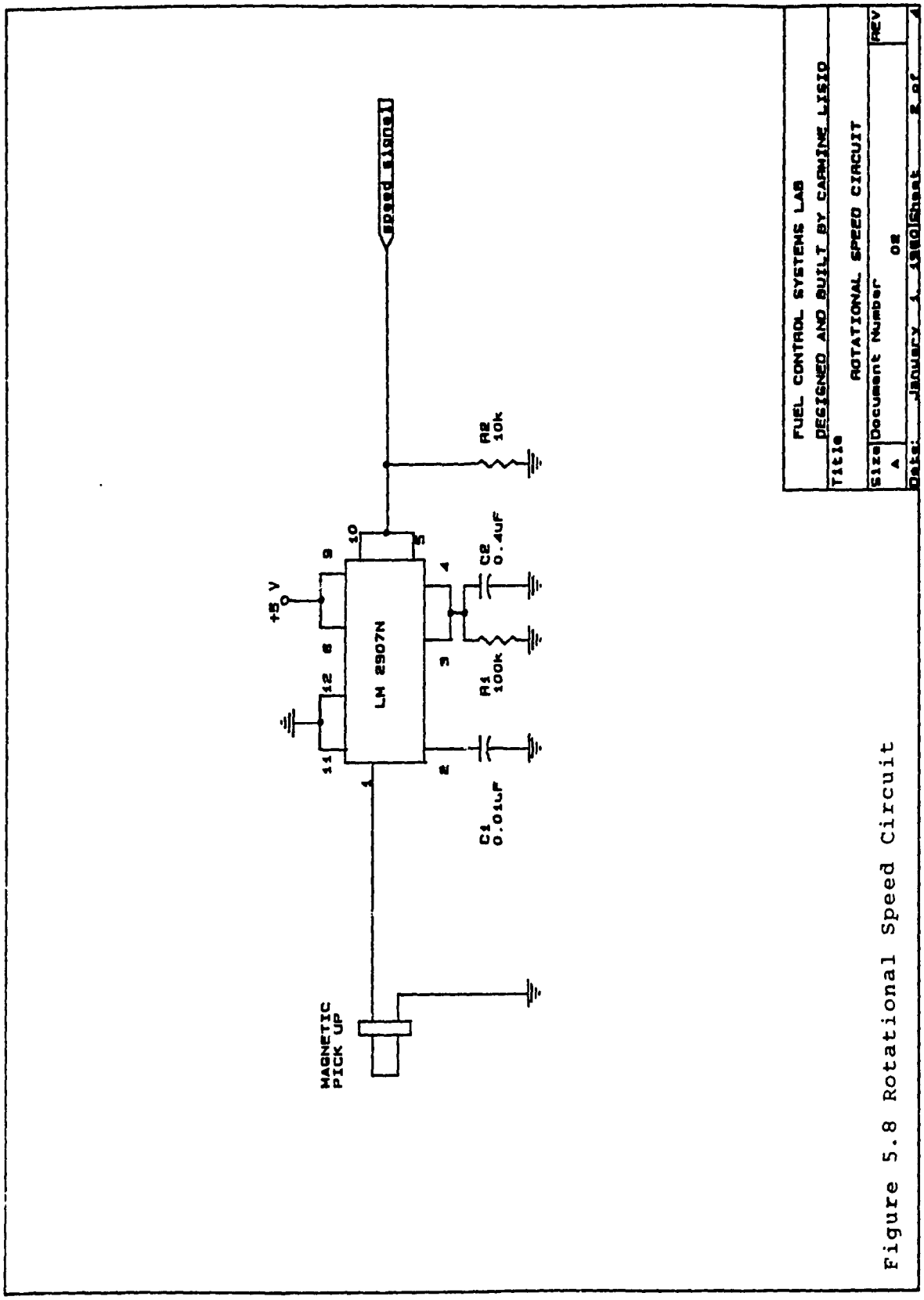

Figure 5.8 Rotational Speed Circuit

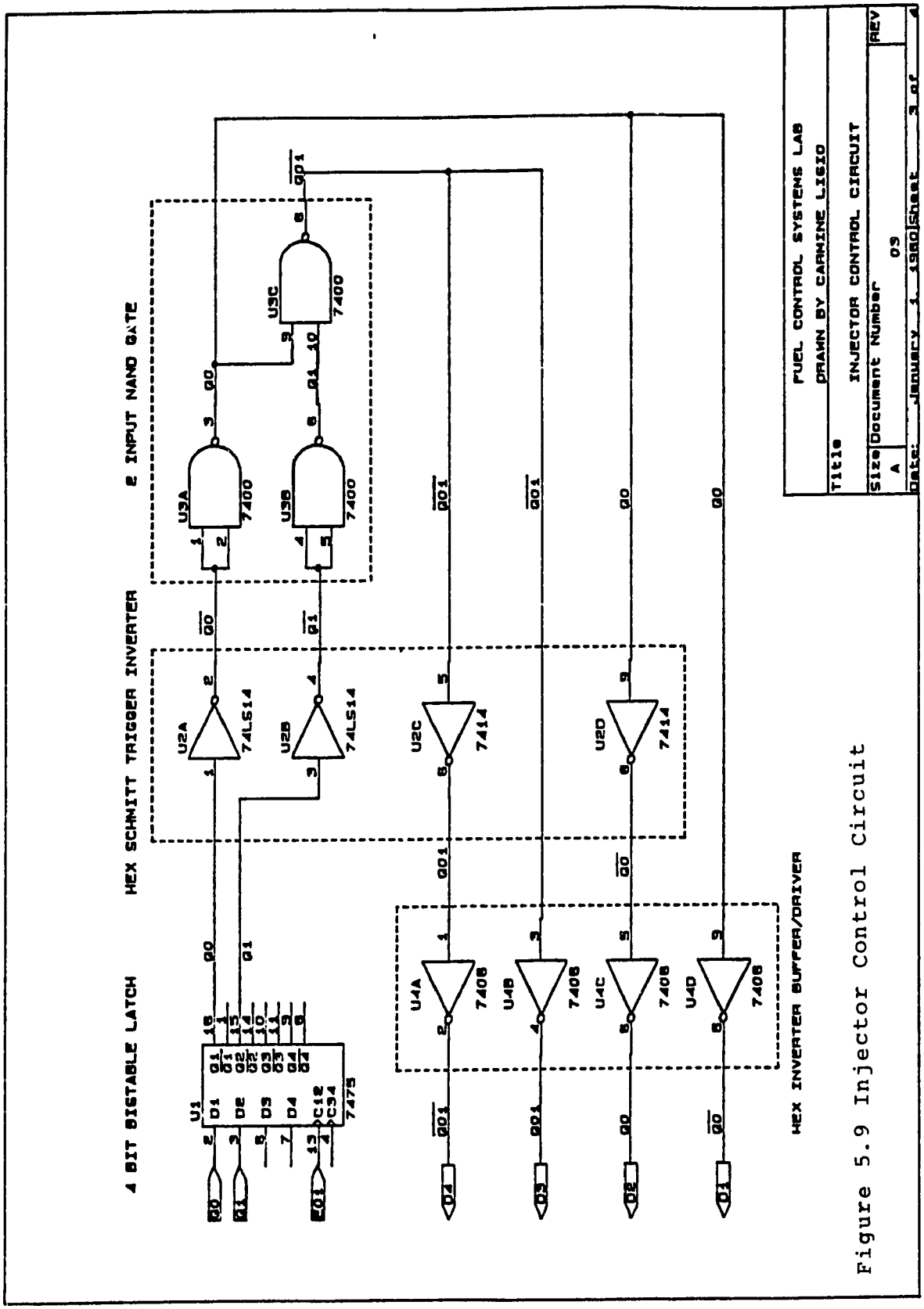

Figure 5.9 Injector Control Circuit

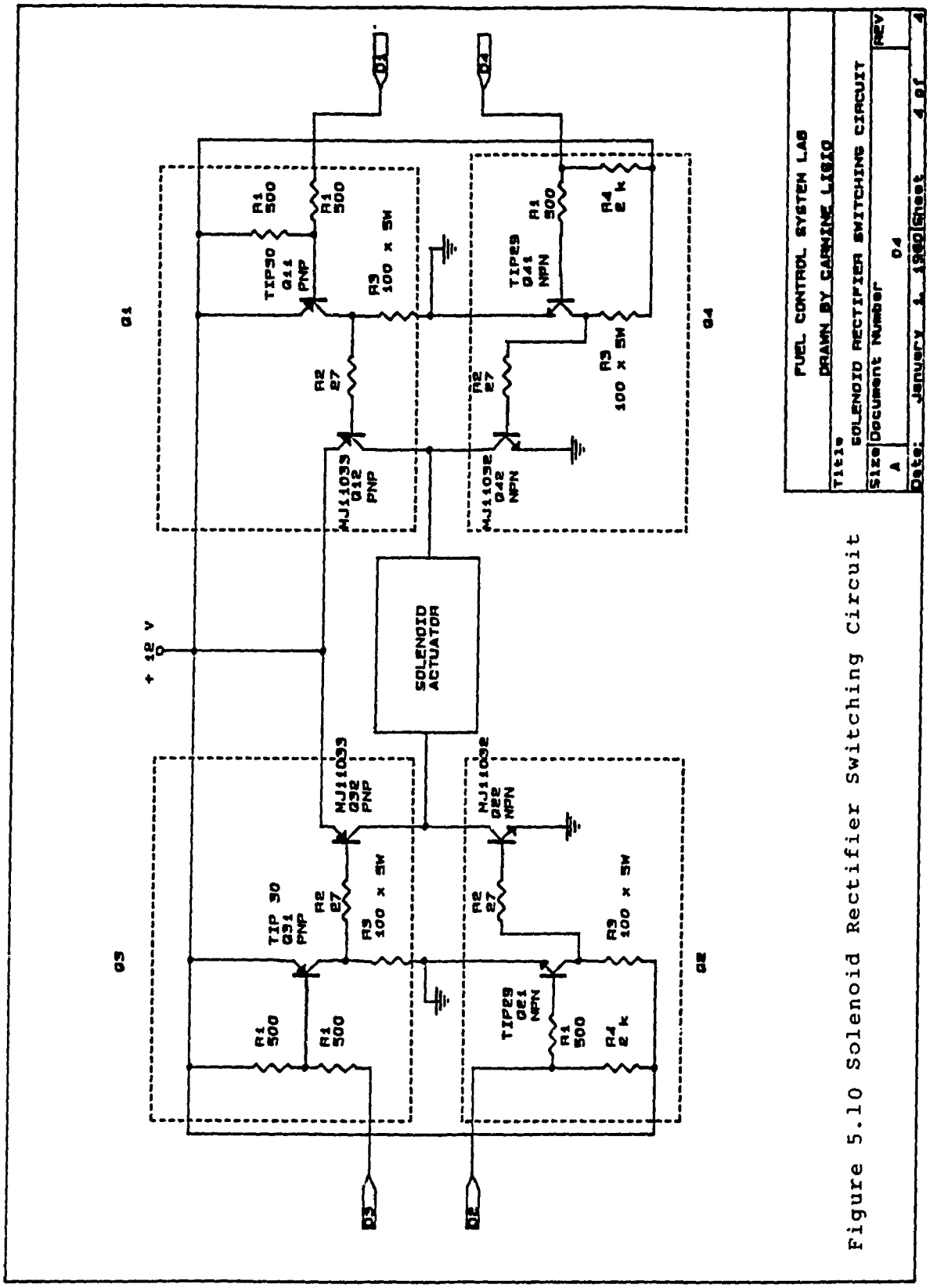

Figure 5.10 Solenoid Rectifier Switching Circuit

$$D_1 = Q_0$$

$$D_2 = \overline{Q_0}$$

$$D_3 = Q_{01}$$

$$D_4 = \overline{Q_{01}}$$

It was found that due to the large force required to open the injector a strong and massive solenoid is required to overcome this force; then a conventional charging circuit would require a large time delay of 7 ms. to 8 ms. to saturate the power transistors to charge and discharge the solenoid. The delay during charging portion for the solenoid can be accommodated by synchronizing the transmission of the charging signal to be sent earlier in the cycle; however during the closing process, this delay would keep the solenoid charged. This would prevent the injector needle from rapidly closing , as it is required for proper end of injection. The switching circuit acts as a rectifying circuit. Two transistors, Q_1 and Q_2, are turned on to allow current to charge the solenoid. When these transistors are turned off, then the other two, Q_3 and Q_4, are turned on to reverse the current flow to quickly discharge the solenoid. The charging delay still remains, however the discharge time is significantly reduced. This reduced discharge time and the large spring force, as well as the lower gas pressure under the needle at the end of injection, cause the needle to close very

rapidly. Figure 5.11, extracted from Giannacopoulos' work [13] shows the advantages of this switching circuit. The solenoid is charged using two 12 Volt car batteries in parallel through high power transistors (MJ11032 and MJ11033).

5.5 Electronic Software

There are two distinctive types of tests to be performed which require a computer control program. The first set of tests is injection of the fuel into air under a constant pressure. The second set of tests has injections occurring into the engine combustion chamber with the piston reciprocating.

The first type of test require a rather simple control code that will activate the control circuit to charge the solenoid and after a certain opening period enable the circuit to discharge the solenoid and close the injector. The flow chart of this program is shown in Figure 5.12 and the computer code for this program called "SOLENOID" can be found in the Appendix A. After the program begins, the solenoid is charged when the CPU outputs the control word NOPEN11 through the PIO of the control board. Using the computers' timer, the injector is kept open for the specified length of time. After the injection time has

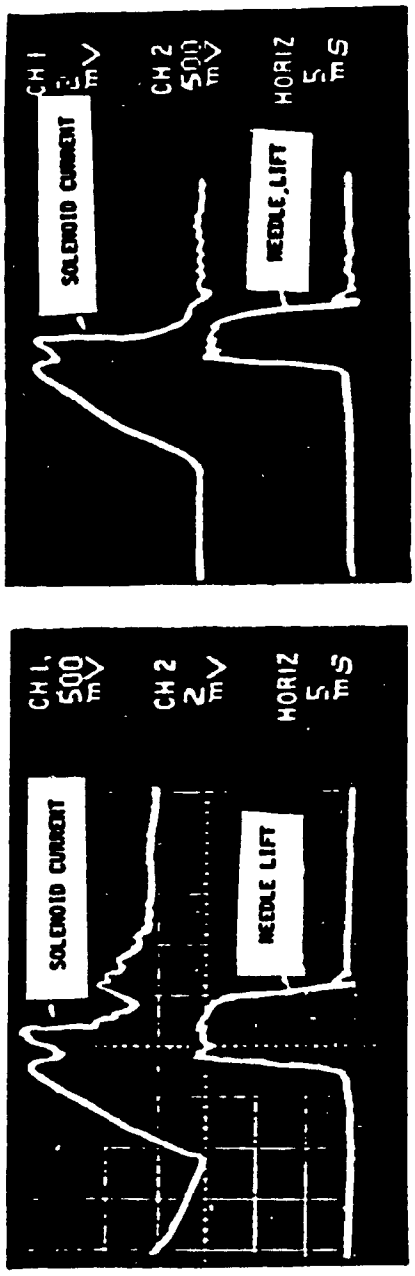

Figure 5.11 Current and Lift vs. time Oscillograms[13]

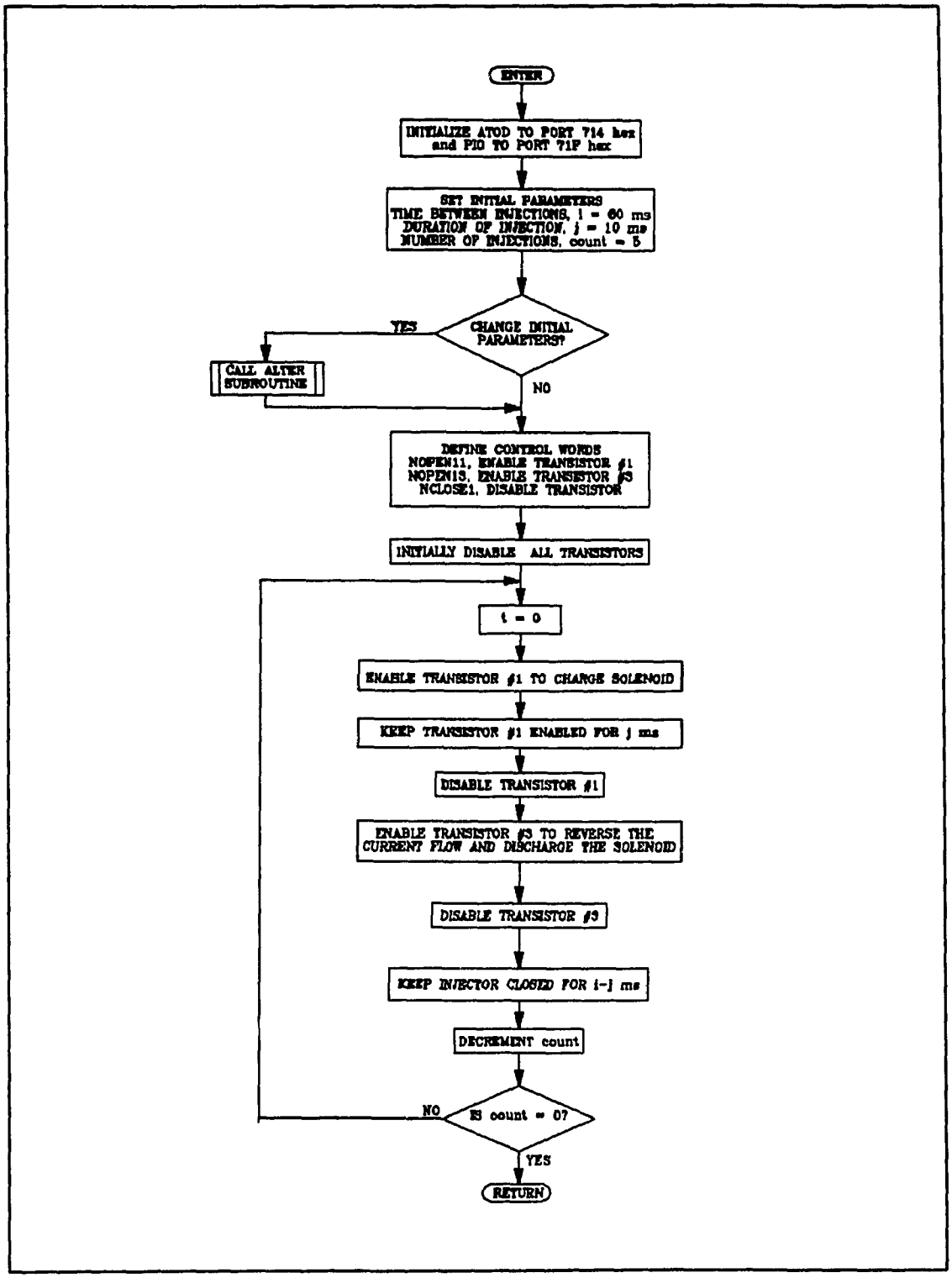

Figure 5.12 Flow Chart of "SOLENOID" Control Program for Static Tests

elapsed, the computer outputs the control word NCLOSE1 to disable transistor #1 and then immediately outputs the control word NOPEN13 to reverse the current flow in the solenoid by enabling the reverse flow transistor #3. Transistor #3 is then disabled and the controller then waits until the next cycle is commenced. When the number of injections specified have been completed, the program returns to the beginning.

The program allows the operator to vary the injection period, the time between injections and also the number of injections. It also provides a signal a few seconds after the operator presses any key to commence the program to turn on the power switch to the circuit board.

The control code was written in the 'C' programming language using 'Turbo C' version 1.5 by Boreland.

The second control program is more complex in that it must receive information from the control board, perform some calculations and then operate the injector at the proper time. Some difficulty arose initially when the standard interrupt service routine (ISR) from the IBM computer interfered with the closing of the injector due to higher priority interrupts in the IBM. To resolve this problem, a new interrupt service routine was written to run instead of the standard ISR when this code was running.

The control code named "INJECT3C" can be found in the

Appendix A, the flowchart is shown in Figure 5.13. It begins by defining the control words NOPEN11, NOPEN13, and NCLOSE1 as well as the interrupt cycle skip count CYCLES as well as the new ISR pointer. The hardware is then initiated, first the Analog to Digital (A/D) converter is set at address 714 hex., then the Parallel Input/Output I.C. is initiated to address 71f hex.

The old ISR is stored in a save location in memory and the new ISR ,IRQ2 is activated.

The main code is now in use. The speed signal is received by the CPU as a 12 bit word and then converted to a value in revolutions per minute. This signal is range checked, if the speed does not fall within the limits of 400 rpm and 2000 rpm, the control program returns to the top of the program. . If the range check criteria is passed, then the speed signal is converted into a time period between injections (injection delay), TIME2, and an injection period, TIME3. These variables are constant in this program but should be variable with data retrieved from engine maps on a dedicated engine controller. These maps would have to be developed with extensive research to obtain the best engine performance.

When the piston reaches TDC and interrupt signal from the optical interrupt circuit invokes the new IRS and changes the value of the variable FLAG. The flow chart of

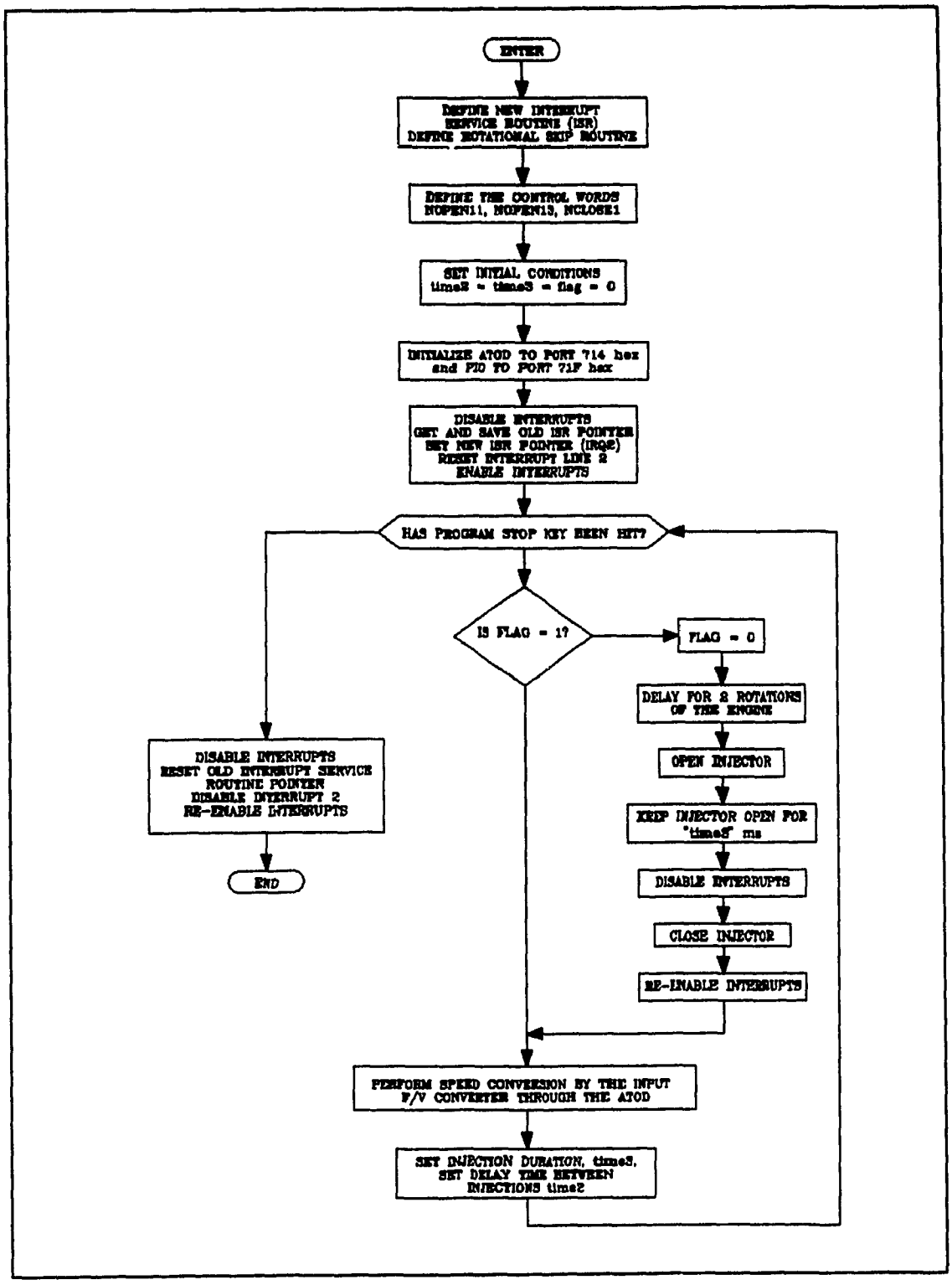

Figure 5.13 Flow Chart of "INJECT3T" Control Program for Reciprocating Piston Tests

the interrupt service routine is shown in Figure 5.14.

During the next pass in the control code the injection process is activated in the same fashion as described in the 'SOLENOID' control program. At TDC the variable FLAG is again changed and speed conversion is invoked.

Upon stopping the control program, the old ISR is enabled and all the computer function as it did before running this program.

The need to change the ISR would lead this researcher to believe that for further development a dedicated CPU to control the engine's functions would be required.

5.6 Safety Relief Check Valve

Since the engine chosen for this investigation, due to the good access to its combustion chamber, was initially designed to operate on gasoline, the compression ratio of the engine was low and the pressures experienced in the combustion chamber would be considerably lower than those in a diesel engine. A concern arose that with high supercharging and combustion of hydrogen the cylinder head would explode. To avoid this possibility, the engine was equipped with a safety check valve. Figure 5.15 shows a cross sectional drawing of this valve. It operates with a

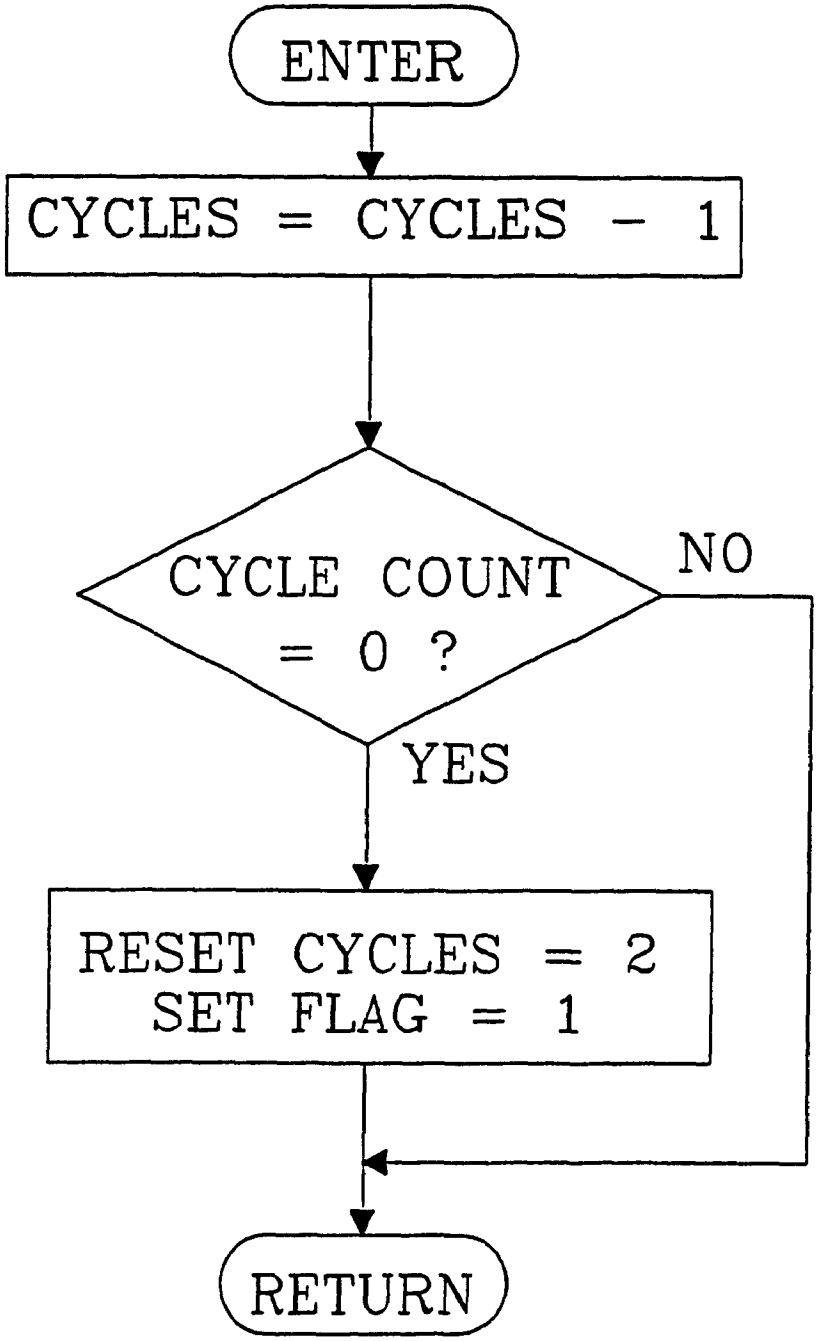

Figure 5.14 Flow Chart for Interrupt Service Routine.

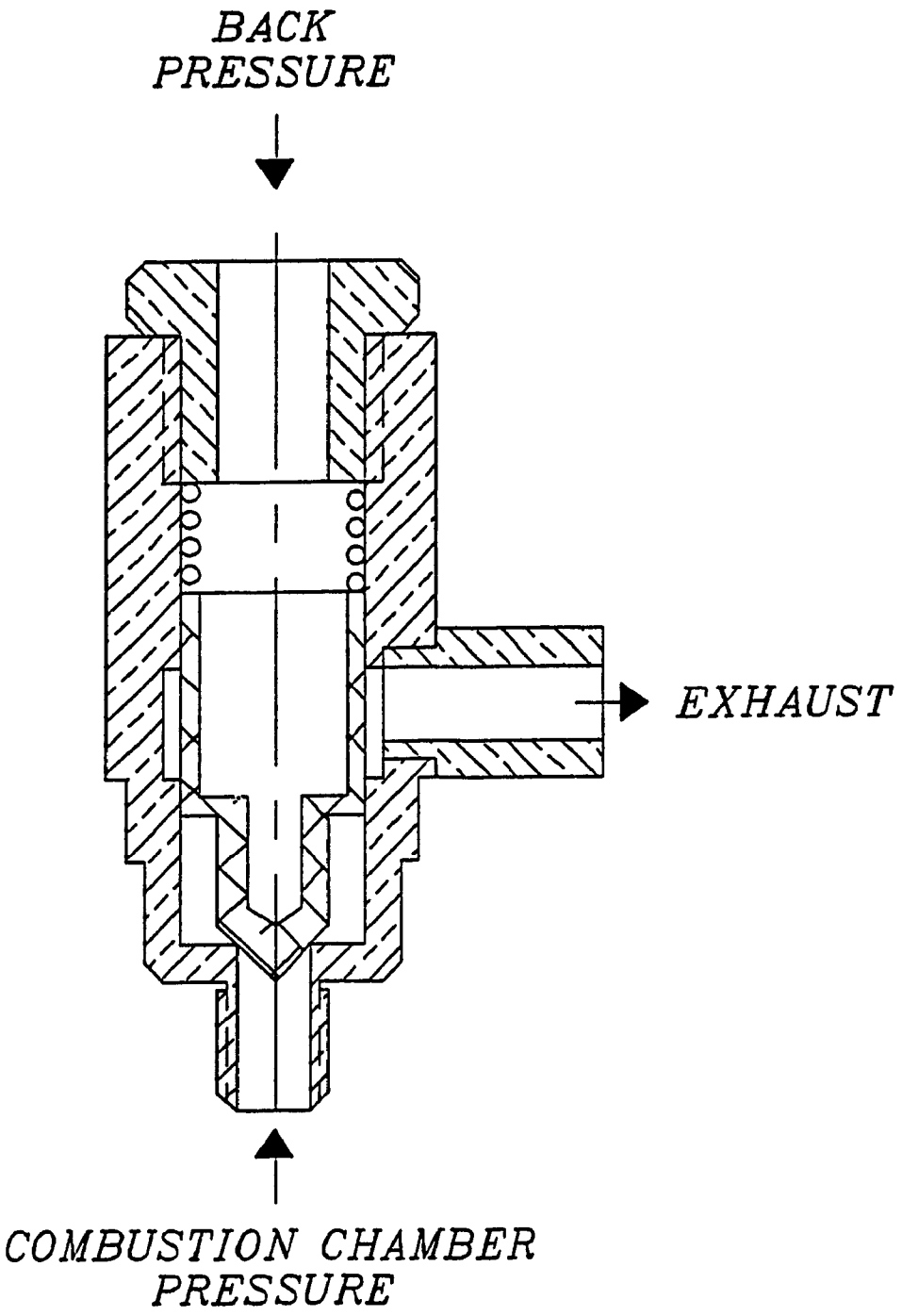

Figure 5.15 Cross Section of Safety Relief Valve.

pneumatic back pressure maintaining the plunger closed due to the differential area on which the pneumatic forces act between the bottom of the plunger and the top of the plunger. There is also a spring to keep the plunger closed in case of insufficient back pressure . The body of the valve is made of brass, and the plunger is of aluminum to reduce its inertia. The contact surfaces are lapped together to reduce leakage through the seat between the plunger and the valve body. The cylindrical surfaces are machined to provide a tight fit.

Once the plunger lifts off the seat, there is a sudden increase of the area onto which the higher combustion chamber pressure acts. The surface areas are then equal, the plunger opens very quickly.

5.6.1 Computer Simulation of the Safety Valve

As mentioned earlier the purpose of the safety relief valve is to prevent the consequences of too high pressure in the test engine. This is required because the test engine was originally designed for low compression ratios using gasoline as a fuel. If the tests require supercharging of the inlet air and an ignition occurs, then the pressure can rise to a point that the engine might fail in a catastrophic manner. The relief valve was designed to

open and discharge some of the gas from the combustion chamber, relieving the pressure in the chamber. The valve functions as a pneumatic poppet valve. When the pressure force from the combustion chamber gases exceeds the pressure force maintaining the valve closed, and the other smaller forces, then the valve will open.

The computer program that is used to model this valve consists of the following steps:

1- A simulation of a piston compressor cycle,

2- A force balance on the valve's conical poppet,

3- Calculation of the flow areas in the valve, and

4- Calculation of the mass flow rates of the combustion chamber gases through the valve orifices.

The compressor cycle simulation uses the engine parameters; bore, stroke, clearance volume and connecting rod length, to calculate the volume in the combustion chamber as a function of the engine crank angle. With the inlet conditions of the air, the thermodynamic properties of the air in the combustion chamber can be determined.

From the pressure in the combustion chamber, a force balance on the poppet is calculated. If the total force to open the valve is greater than the forces to keep the valve closed, then the valve will begin to open and the differential equation describing the force on the poppet is

solved using a fourth-order Runge-Kutta algorithm..

Due to the lift of the valve and the differential pressure across the orifices of the valve, mass flows of air out of the chamber will commence reducing the pressure in the chamber. The lift of the poppet determines the flow areas, and the differential pressures determine whether the flow of gases is choked or unchoked. With this information the mass flow rates can be solved. Using the continuity equation in the combustion chamber volume and in the volume within the valve body, a new pressure and mass can be determined in each of these volumes.

5.6.1.1 Determination of the Thermodynamic Properties in the Combustion Chamber

The engine's combustion chamber can be modeled analytically by defining the model of a reciprocating piston and the applying fundamentals of mechanisms and thermodynamics to the model.

The volume in the combustion chamber can be defined by:

$$V = V_c + \frac{\pi d^2}{4}\left\{ r\,(1 - \cos\theta) + \ell \left[1 - \sqrt{1 - \left(\frac{r}{\ell}\sin\theta\right)^2} \right] \right\}$$

where V_c = clearance volume (volume at TDC) [m^3]

d = bore of the cylinder [m]

r = stroke length of the piston [m]

ℓ = length of the connecting rod [m]

θ = crank angle measured from TDC [deg]

The thermodynamic properties of the gas in the combustion chamber is calculated using the polytropic relation:

$$p_2 = p_1 \left(\frac{V_1}{V_2} \right)^n$$

$$T_2 = T_1 \left(\frac{p_2}{p_1} \right)^{\frac{n-1}{n}}$$

where p_i = Absolute pressure at time = i [N/m^2]

T_i = Absolute temperature at time = i [K]

n = polytropic exponent

The value of the polytropic exponent, n, has been determined for diesel engines by Heywood [31] as a function of engine speed and varies from between 1.3 and 1.35 for engine speeds of 500 rpm to 2500 rpm .

5.6.1.2 Derivation of Forces and the Force Balance on the Poppet Valvee Poppet Valve

The main objective of the poppet is to open and relieve the pressure in the combustion chamber if the pressure in the chamber exceeds the cracking pressure set on the valve.

Figure 5.16 shows a schematic of the free body diagram of the forces acting on the poppet. There are six forces acting on the body:

1- the inertia force,

2- spring force (preload and compression force),

3- fluid damping force,

4- coulomb friction force,

5- back pressure pneumatic force

6- combustion chamber pneumatic force.

The inertia force consists of the product of the total moving mass and the acceleration of this moving mass. The total moving mass, m_{tot}, is defined as:

$$m_{tot} = m_p + \frac{m_s}{3}$$

where m_p = mass of the poppet = 12.0 g

and m_s = mass of the spring = 1.8 g

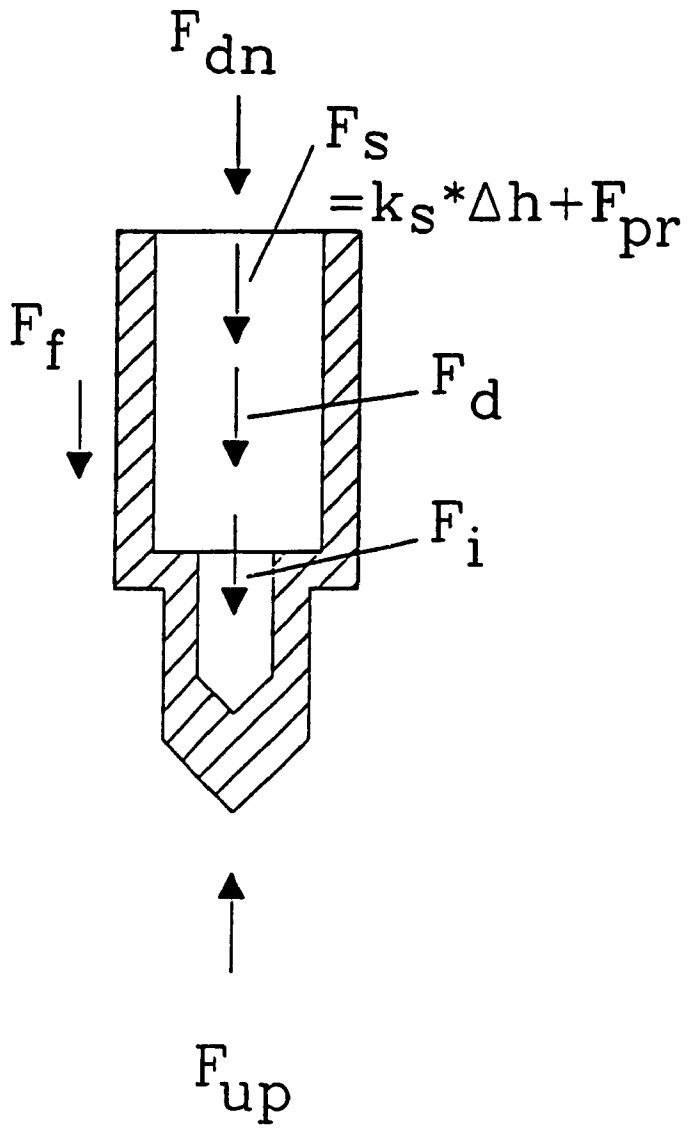

Figure 5.16 Free Body Diagram on Poppet.

The damping force is derived assuming laminar flow of a fluid between two plates. The derivation is based on COUETTE FLOW for fluids between two plates, with one plate held stationary (the valve body) and the other plate moving at some velocity (the poppet)and also a differential pressure from one end to the other. The damping force consists of 2 parts; the first is a function of the velocity of the valve and the second part is a function of the differential pressure. The damping force is described as:

$$F_d = C_1 \frac{dh}{dt} + C_2$$

where $$C_1 = \frac{- \pi \, d_1 \, \mu \, L}{\delta}$$

$$C_2 = \frac{\pi \, d_1 \, \delta}{2} (p_o - p_L)$$

with d = the average diameter between the needle and the valve body [m],

μ = the viscosity of the fluid [Pa s},

L = the interface length between poppet and valve body [m],

δ = the clearance between poppet and the valve body [m], and

p_o, p_L = pressure at either end of the valve [N/m^2].

The spring force is the sum of the spring preload force, F_{prel}, and the product of the spring constant, k_s= 600 N / m, and the displacement of the valve, Δh.

$$F_s = F_{pr} + k_s \Delta h$$

The coulomb friction force acts against the motion of the poppet, however in this analysis it will be neglected.

The largest forces are the pneumatic pressure forces. The back pressure force is set manually using shop air supply through a pressure regulator. This pressure initially acts on an area much larger that the upward pressure from the combustion chamber. When the valve begins to open then the pressure in volume 2 increases and the upward force increases also very quickly due a larger area in which the higher pressure is acting upon. The pneumatic forces are defined as:

$$F_{dn} = p_b A_{dn}$$

$$F_{up} = p_c A1_{up} + p_2 A2_{up}$$

where p_b = pressure keeping the valve closed [N/m^2]

p_c = pressure from the combustion chamber [N/m^2]

p_2 = pressure in the valve body [N/m^2]

Figure 5.17 shows the basic dimension of the valve and from this diagram the areas mentioned above can be derived as:

$$A_{dn} = \frac{\pi}{4} d_{so}^2$$

$$A1_{up} = \frac{\pi}{4} d_{hi}^2$$

$$A2_{up} = \frac{\pi}{4} (d_{so}^2 - d_{hi}^2)$$

Using d'Alembert's Principle the differential equation describing the movement of the poppet is:

$$m_{tot} \frac{d^2h}{dt^2} + C_1 \frac{dh}{dt} + k_s \Delta h + F_{pr} + C_2 + F_{dn} - F_{up} = 0$$

5.6.1.3 Determining the Cracking Pressure of the Valve

To determine the cracking pressure of the valve, the forces due to transients must be set at zero, and a static force analysis must be taken. Using some sample inputs which will be used in the sample simulations, the back pressure is set at 175000 Pa and the spring is compressed 10mm for preload. The static equation is:

$$F_{up} - F_{dn} - k_s x_0 - C_2 (p_o - p_L) = 0$$

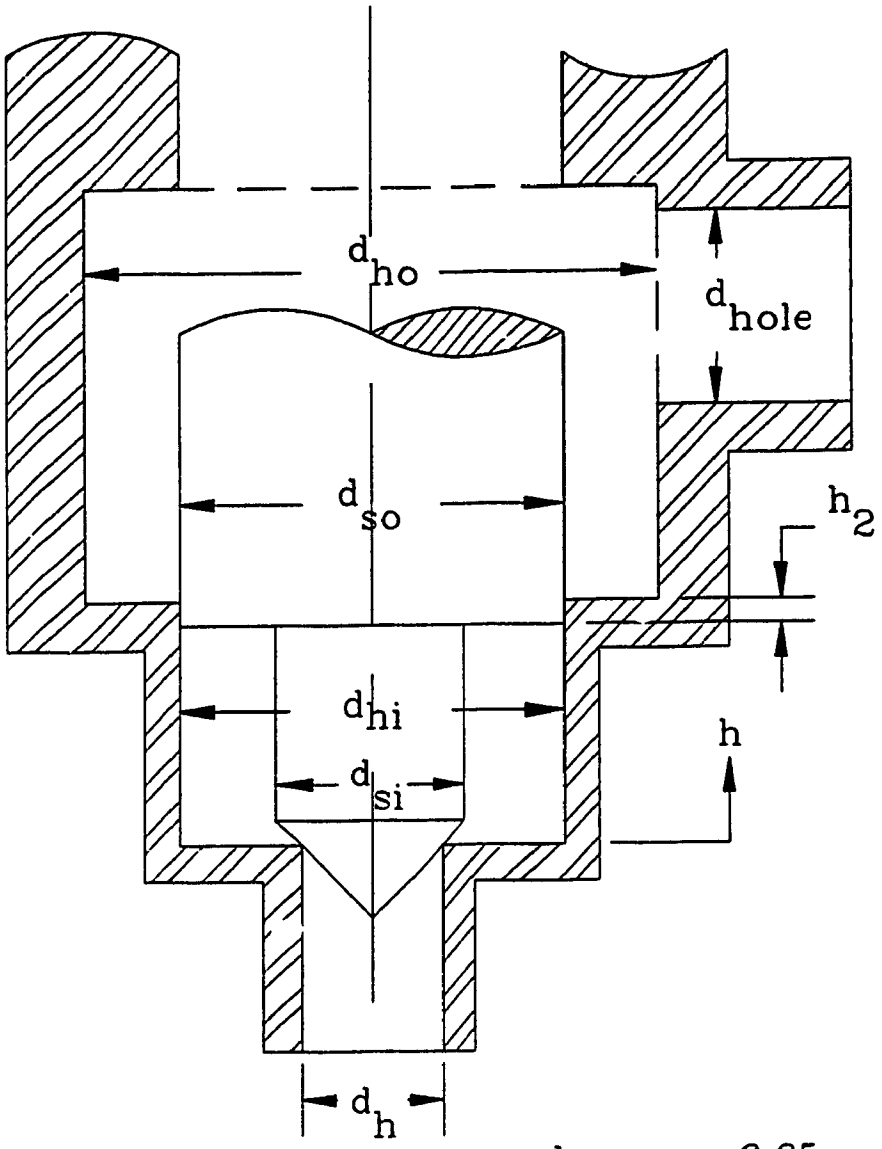

d_h = 6.35 mm
d_{si} = 9.525 mm
d_{hi} = 14.2875 mm
d_{so} = 14.2875 mm
d_{ho} = 19.05 mm
d_{hole} = 9.525 mm
h_2 = 1.98 mm

Figure 5.17 Safety Valve Internal Dimensions.

Applying these numbers, the cracking pressure would be approximately 750000 Pa.

5.6.1.4 Determining the Flow Areas Through the Valve Orifices

The system can be modeled fluidically as shown in Figure 5.18. V_1 is the combustion chamber, $V_2$is the volume in the valve, and V_3 is the surroundings. The flow area from V_1 into V_2 can be described using Figure 5.19 a,b. The flow is through a conical poppet type valve which can be equated as a function of the lift of the valve.

The length of the element *l* is:

$$l = h \sin(\theta)$$

The average circumference of this element is given by:

$$C_{ave} = \pi \left(d_{h1} - h \cos(\theta) \sin(\theta) \right)$$

Using Guldin's rule, the flow area can be defined as:

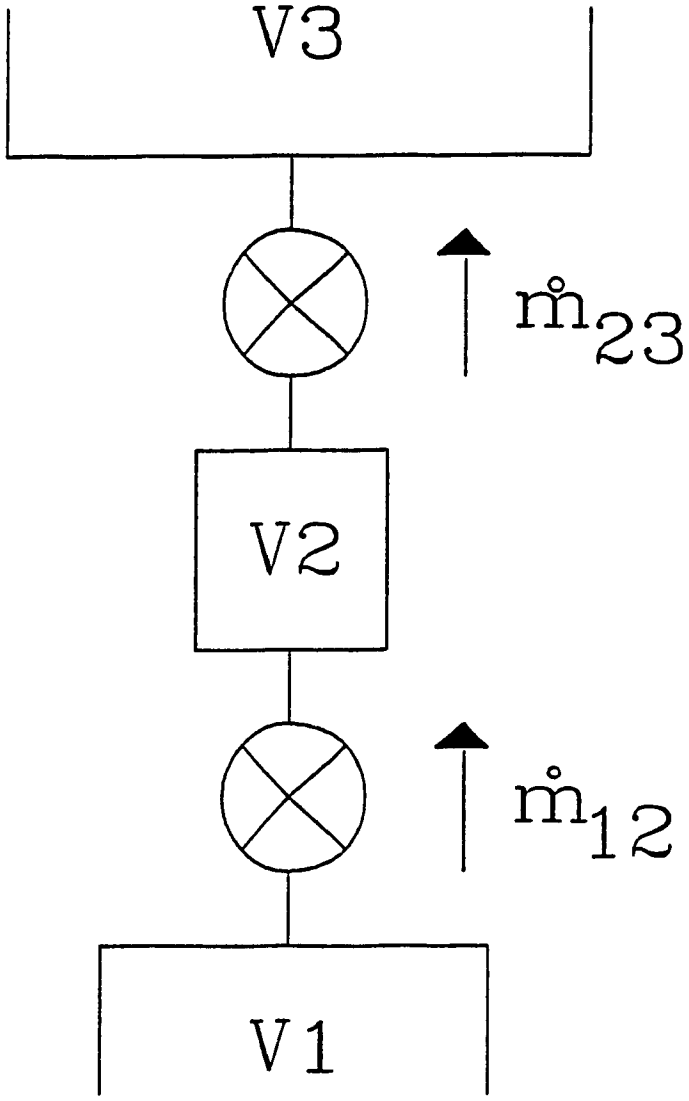

Figure 5.18 Volume Diagram in Safety Valve Simulation.

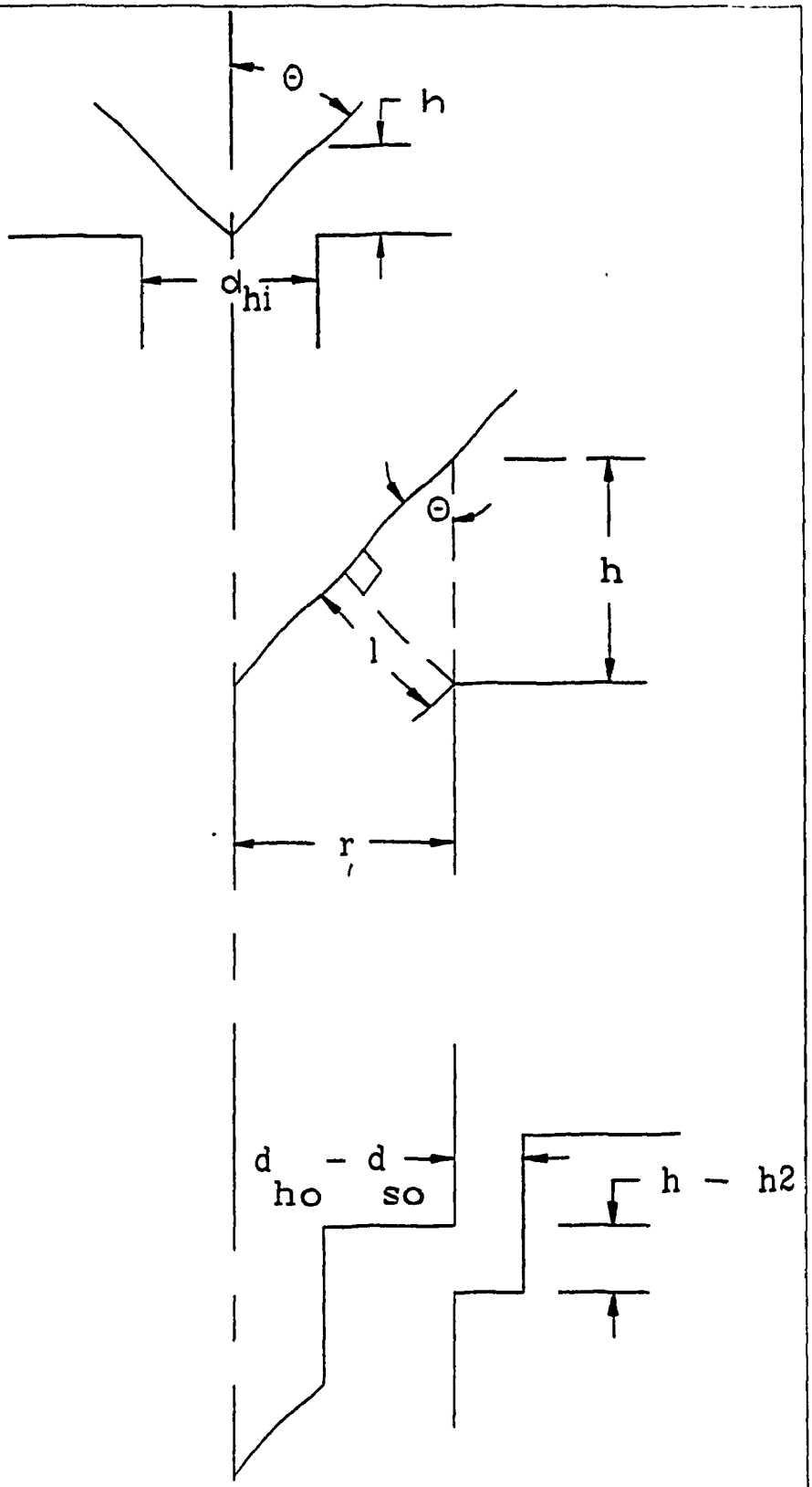

Figure 5.19 Schematic for Determination of Flow Areas in the Safety Valve.

$$A_{12} = l\ C_{ave} = \pi\ h\ \sin(\theta)\ [\ d_{hl} - h\ \sin(\theta)\ \cos(\theta)\ ]$$

The valve is considered fully open when

$$A_{12} = \frac{\pi}{4}\ d_{hl}^2 .$$

The flow area out of V_2 can also be determined using Figure 5.19 c. This flow area is the smallest of these three possible critical flow areas:

$$A_{23a} = \pi\ d_{so}\ (\ h - h_2)$$
$$A_{23b} = \frac{\pi}{4}\ (\ d_{ho}^2 - d_{so}^2\ )$$
$$A_{23c} = \frac{\pi}{4}\ d_{hole}^2$$

5.6.1.5 Mass Flow Continuity Equations

Referring back to Figure 5.18 the mass flow continuity equations can be described. Mass continuity for a volume is the rate of change of mass within the volume with respect to time plus the influx into the volume and is equal to the mass efflux out of the volume. For V_1 the continuity equation is:

$$\frac{dm_1}{dt} - \dot{m}_{12} = 0$$

For V_2 a similar equation can be written:

$$\frac{dm_2}{dt} + \dot{m}_{12} - \dot{m}_{23} = 0$$

where the mass in each volume is described by the equation of state for a fluid, by assuming the gas as a perfect gas.

To determine the gas flow rates through the orifices, it must first be determined whether the flow is choked or unchoked. The condition for choked flow exists when:

$$\frac{p_d}{p_u} \leq \left(\frac{2}{\gamma + 1} \right)^{\frac{\gamma}{\gamma + 1}}$$

where p_d = the downstream pressure $[N/m^2]$

p_u = the upstream pressure $[N/m^2]$

γ = the gas constant of the fluid

If the flow is choked then the mass flow equation is:

$$\dot{m} = C_d \, A \sqrt{\frac{2 \, \gamma \, p_u^2}{(\gamma + 1) \, R \, T} \left(\frac{2}{(\gamma + 1)} \right)^{\frac{2}{\gamma - 1}}}$$

where A = the critical flow area $[m^2]$

C_d = the discharge coefficient

R = the gas constant [kJ/kg K]

T = the absolute temperature of the gas [K]

If the flow is not choked then the governing equation can be expressed as:

$$\dot{m} = C_d A \sqrt{\frac{2 \gamma p_u^2}{(\gamma + 1) R T} \left[\left(\frac{p_d}{p_u} \right)^{\frac{2}{\gamma}} - \left(\frac{p_d}{p_u} \right)^{\frac{\gamma + 1}{\gamma}} \right]}$$

5.6.2 Analysis of Valve Simulation

The valve is very effective at relieving the pressure in the cylinder. Figure 5.20 and Figure 5.21 show the combustion chamber pressure for a case when the valve is closed and when the valve is opening. It can easily be seen that there is a sudden decrease in the pressure inside the combustion chamber. To ensure that the opening time of the valve and the pressure release is sufficient a computer model was developed for the valve and an analysis was conducted.

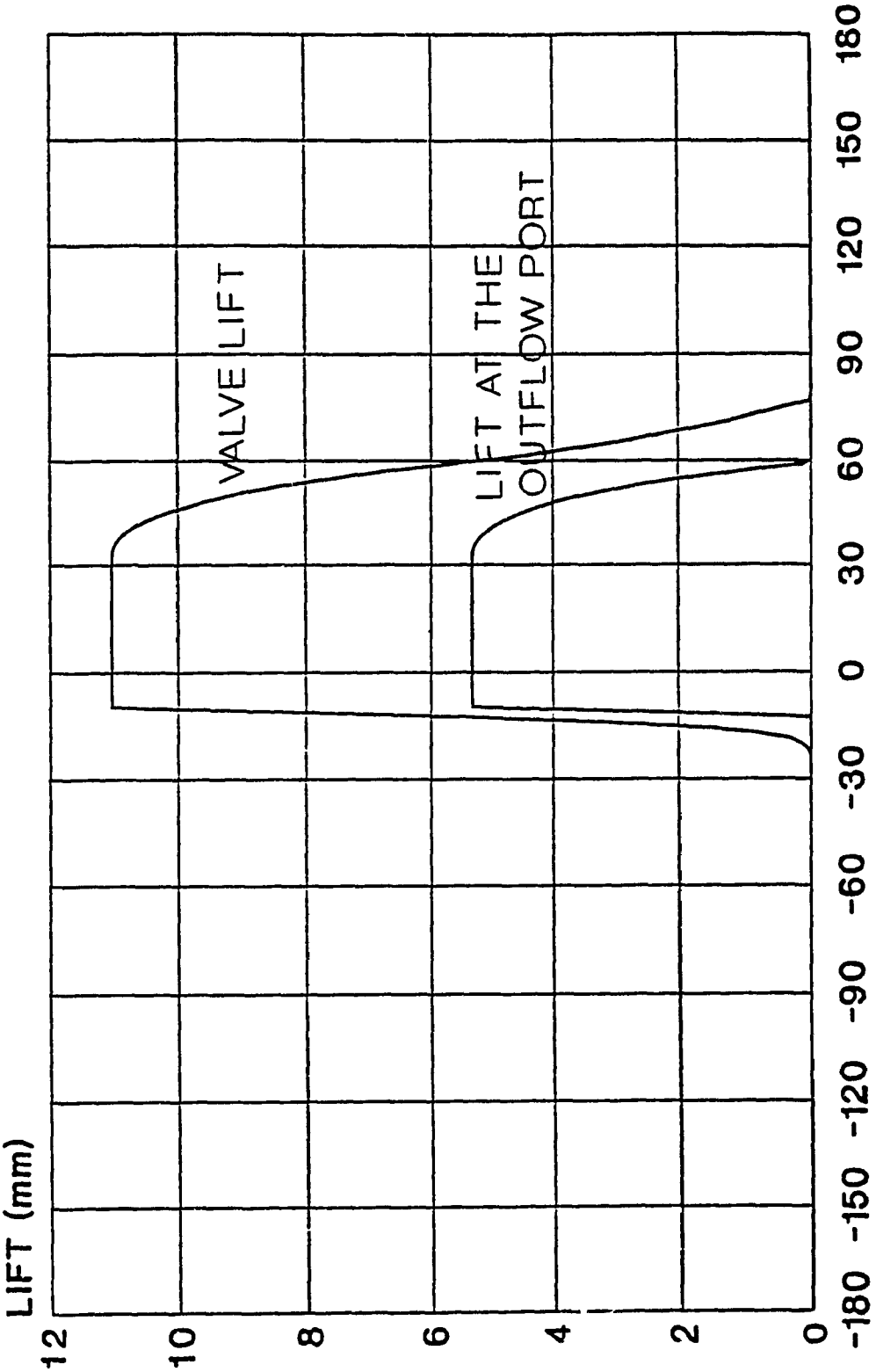

Fig. 5.19. Relief valve lift simulation during opening and closing

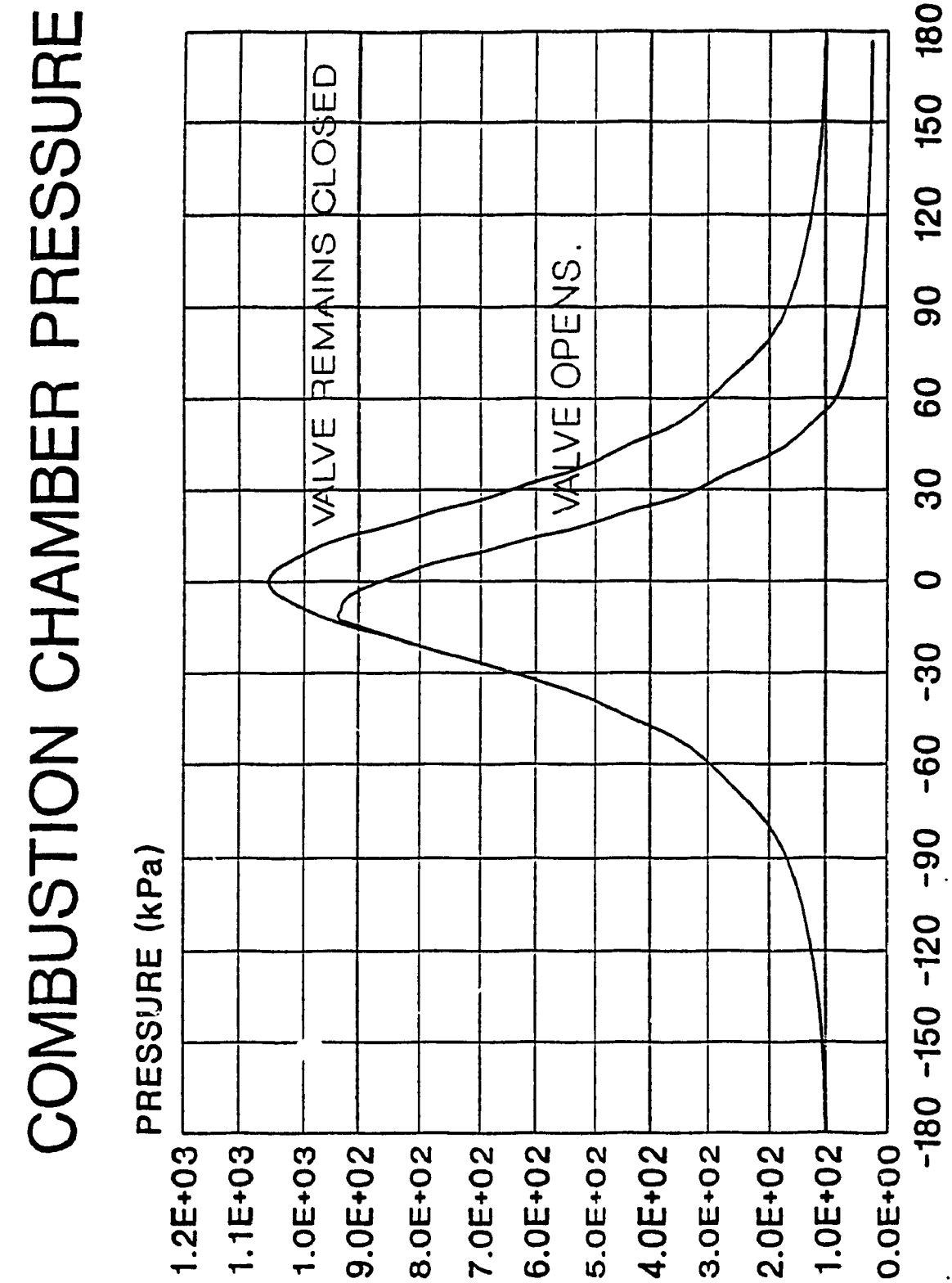

Fig. 5.20. Compression pressure history showing the impact of the relief valve opening

CHAPTER 6

6.0 EXPERIMENTAL INVESTIGATIONS OF SHOCK WAVES AT AMBIENT CONDITIONS

The purpose for these tests performed under ambient conditions, was to make a preliminary investigation of shock waves created in a resonance tube by short gas jets from the hydrogen injector set-up, as described in Chapter 5. The primary motive for these tests was to select the initial dimension for the resonance tube such as resonance tube diameter and depth, as well as the distance between the injector and the tube. Also included in these tests was the calibration of the injection system by using a special device to measure the injected gas dose and the measurement of the gas inflow using a special long tube with a pressure transducer.

Several interesting phenomena were found with these tests. The first of these was that the datum of the pressure readings obtained tended to decrease during the injection. This was attributed to heating of the quartz in the pressure transducer affecting the datum voltage. Another phenomenon observed was that a certain amount of time, in the order of 1 ms.,was required before resonating wave was created in the tube. The third and most interesting phenomenon which was observed was a "saddle" in the pressure record at the end of the tube during certain

injections. It occurred only under certain conditions and was eliminated by reducing the mass flow rate from the injector. Reduction of mass flow was accomplished by several means, the easiest being throttling of the inflow of gas into the injector by reducing the flow area in the metering valve. It was chosen as the best solution.

The calibration tests confirmed what was expected. With the time of injection increased as well as the metering valve opened the gas dose became larger. The injection unit could easily deliver between 3.5 mg to 5 mg of hydrogen for injection durations of 3ms to 6 ms. For a cylinder of the size found in our test engine, this fuel dose range was considered as quite good for all operating conditions.

It was found that well developed resonating waves were easy to create for most conditions, except for the conditions where the "saddle effect" occurred.

Initial sizing tests determined that a simple resonance tube of 2 mm in diameter and with a cavity of 20 mm. in depth would be used for further tests.

6.1 Test Apparatus for Resonance Tubes at Ambient Conditions

Figure 6.1 shows a schematic of the test set-up for the initial resonance tube sizing tests. The

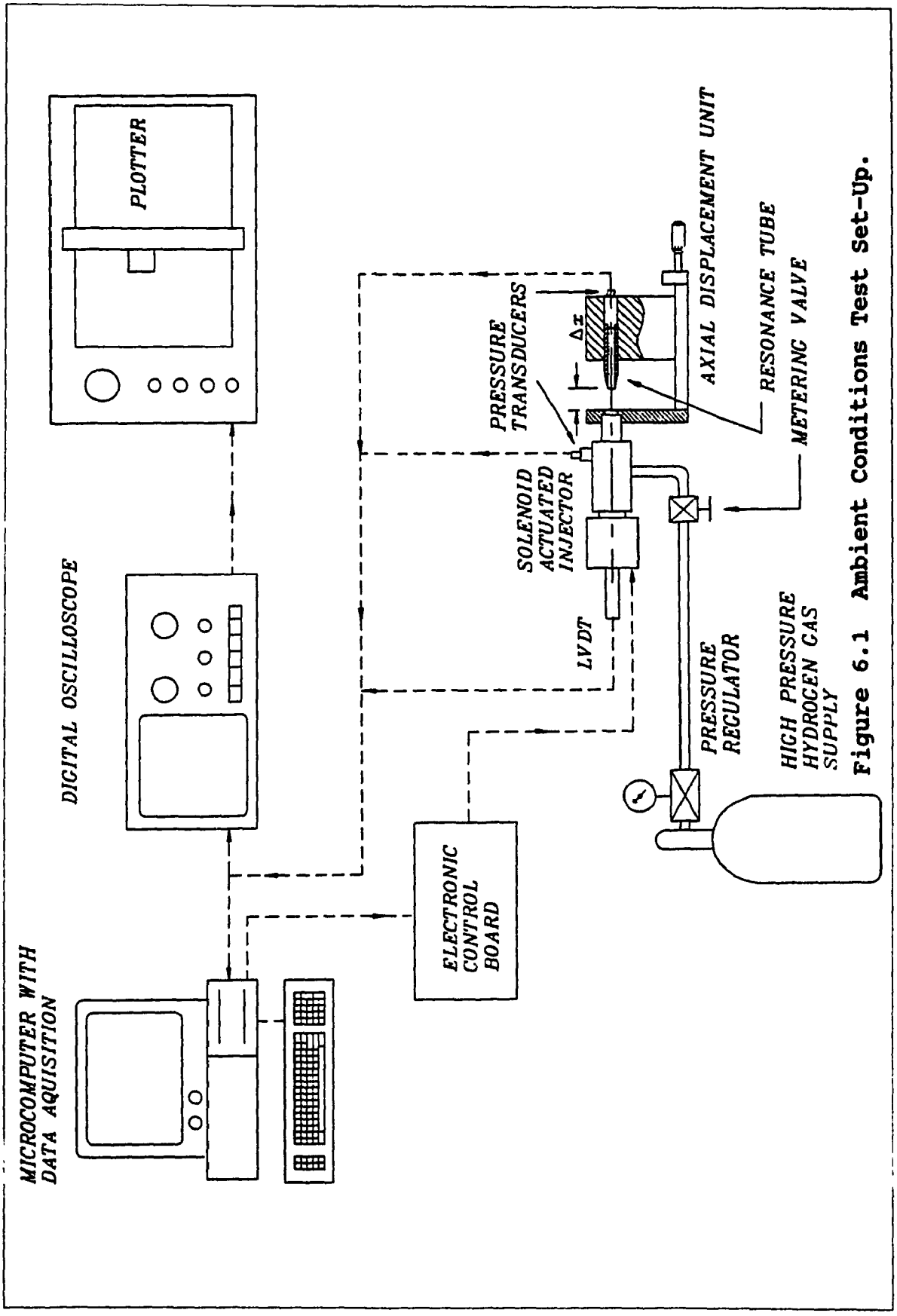

Figure 6.1 Ambient Conditions Test Set-Up.

electronically controlled fuel injector is placed on an Axial Displacement Unit (ADU) which also houses the resonance tube with a pressure transducer. The injector is connected to the electronic control board which is interfaced with a computer equipped with a data acquisition and control board. The gas supply is brought from a high pressure gas bottle and the gas pressure is lowered to the operating pressure through a pressure regulator.

The axial displacement unit is shown in a larger scale in Figure 6.2. It is designed to axially align the injector nozzle orifice with the mouth of the resonance tube. The resonance tube is installed in an adapter on the vertical column of the ADU, which is screwed onto a dovetail slider placed into a track milled in the base piece. The column is pushed forward by a linear displacement unit with a micrometer head and it is returned under spring load. The adapter has a modular design which allows for quick changing of resonance tubes with different design parameters (that is cavity depth and diameter). The resonance tube is positioned by a step in the adapter on one end, and is held in place flash with the pressure transducer on the other end ,fastened with the transducer nut.

The pressure transducer is manufactured by PCB Piezotronics and is of their 105A series. It has a flush

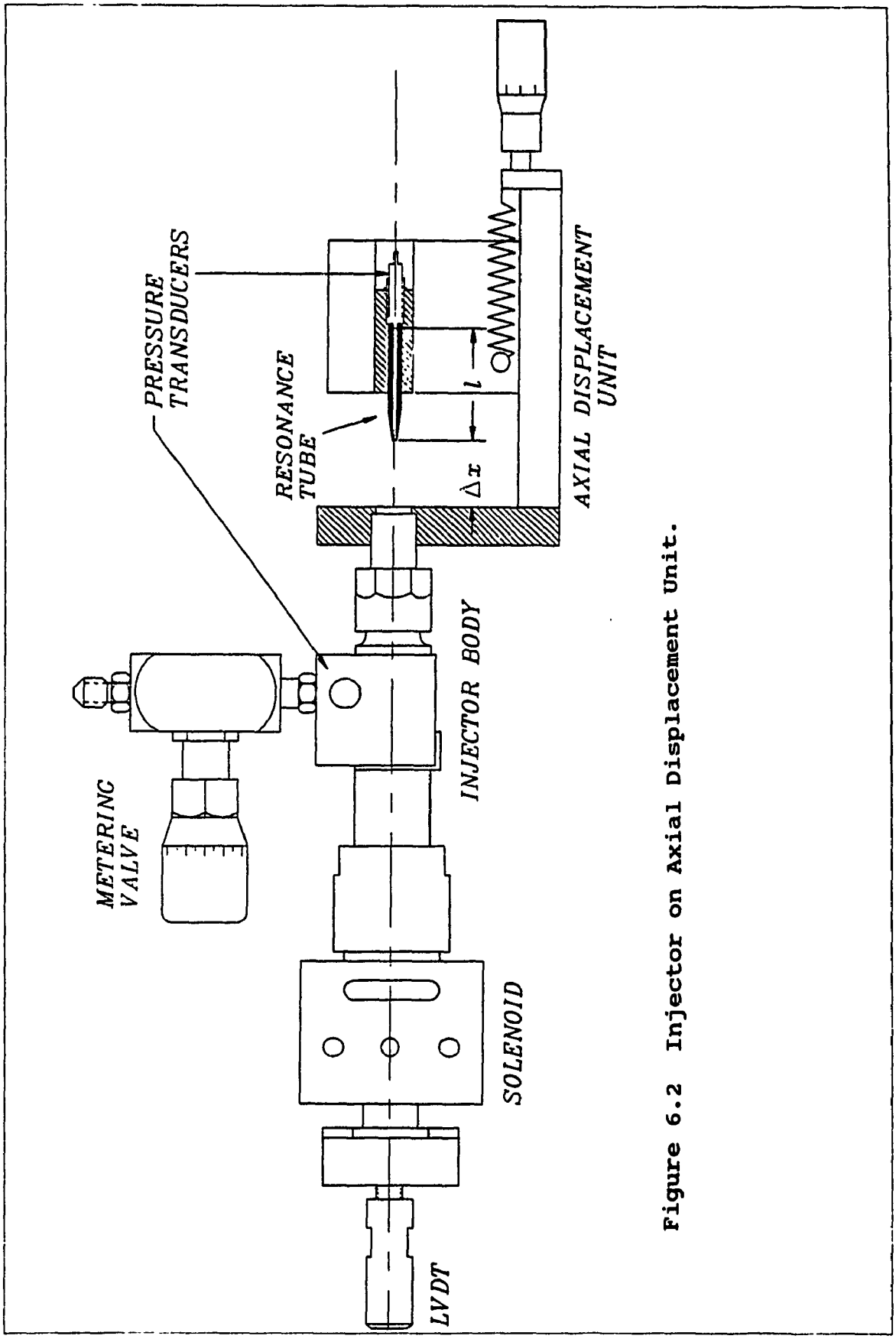

Figure 6.2 Injector on Axial Displacement Unit.

flat diaphragm which has only 2.54 mm. diameter and includes a rigid quartz element. An integrated unity gain amplifier is built into the transducer to enhance resolution, so no external amplifier is required for this transducer when connected to an oscilloscope. It's small frontal area fits well with the resonance tubes of this small size; the transducer actually forms the flat back face of the resonance tube cavity. The calibration curves for this transducer can be found in Appendix B.

Another test set-up for ambient condition tests is shown in Figure 6.3. In this test configuration the resonance tube is replaced by a long tube with a small internal diameter of 3 mm, kept at some axial distance from the nozzle. A similar pressure transducer is placed flush with the internal wall of the tube, just downstream of the tube mouth. The purpose of this test set-up is to qualitatively evaluate the mass inflow of gas into the tube. This is used to study the effect of gas inflow rate on shock wave development.

A third test set-up, shown in Figure 6.4, is used to calibrate the fuel dose delivered by the gas injection unit. The injector is clamped to a pair of vertical plexiglass cylinders filled with water via flexible tubing. The first cylinder is closed at both ends, except for connections to the long tube and gas release valve at the

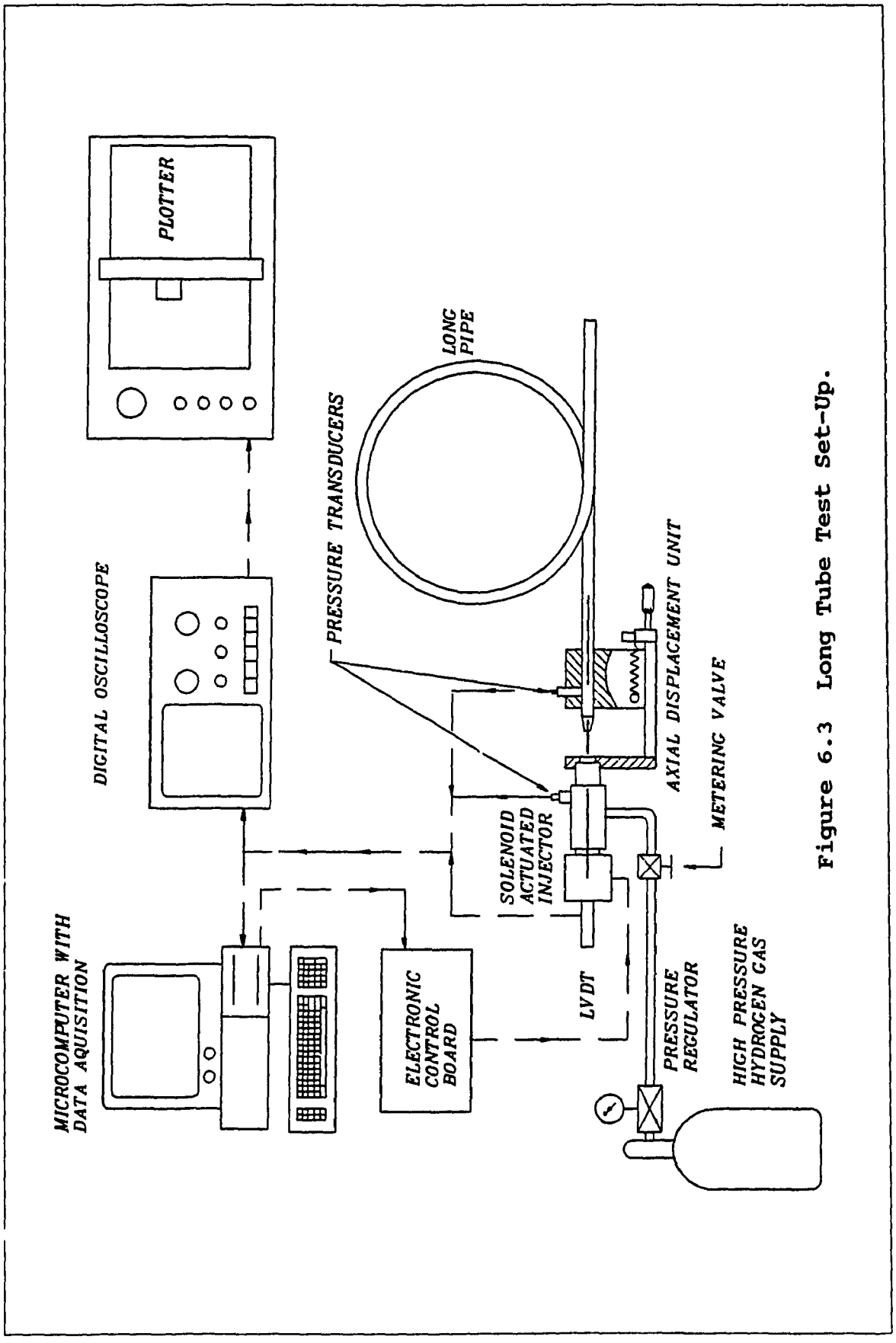

Figure 6.3 Long Tube Test Set-Up.

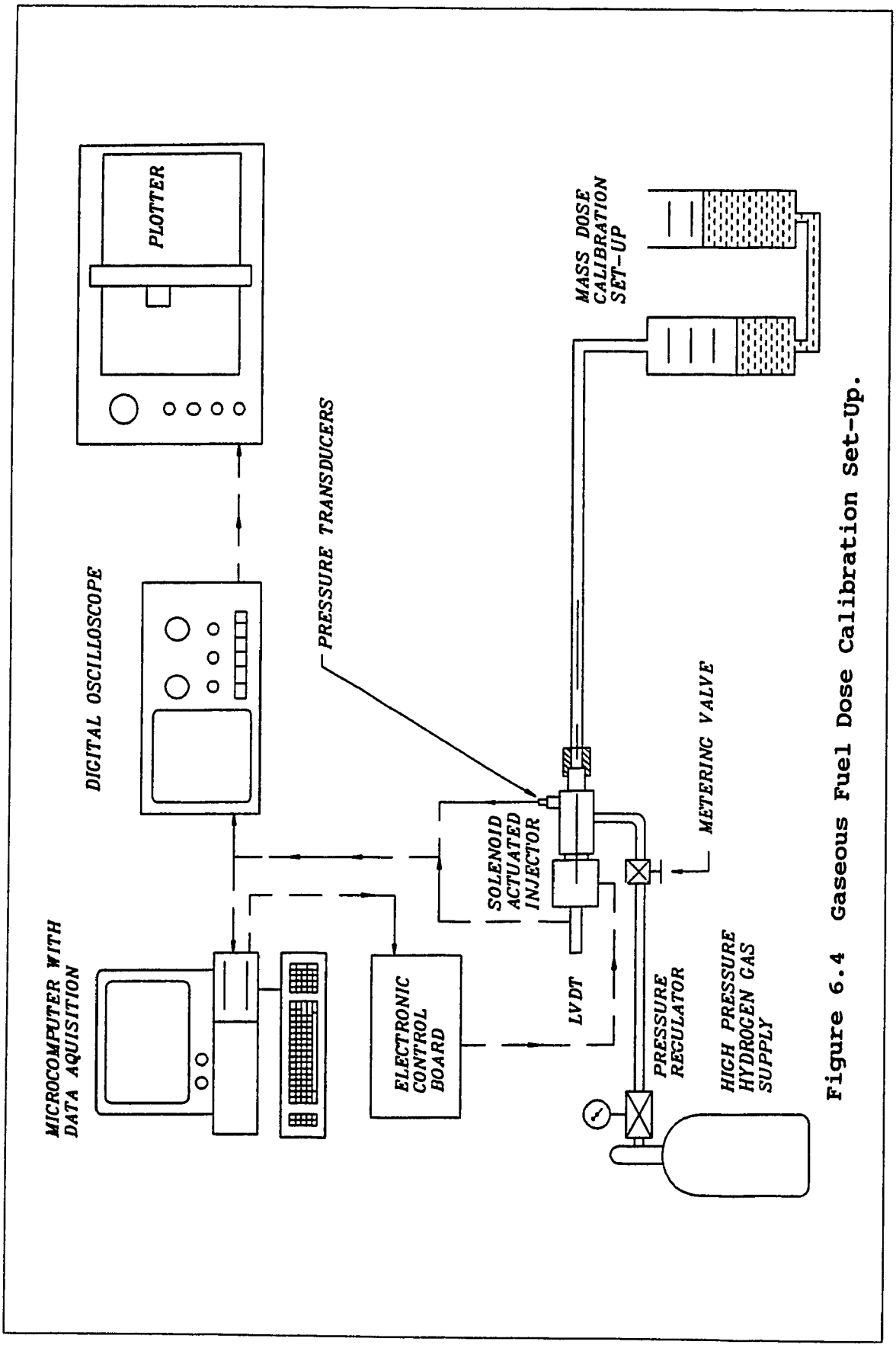

Figure 6.4 Gaseous Fuel Dose Calibration Set-Up.

top, as well as to the other cylinder at the bottom. The second cylinder is open to the atmosphere at the top. When hydrogen is injected, it displaces some volume of water. Using the equation of state, the hydrogen dose can be calculated by knowing the change in the water levels, as well as the number of injections.

6.2 Test Procedures and Objectives

There are several objectives for the tests performed at atmospheric conditions. These objectives can be listed as follows:

1 - to familiarize oneself with the equipment and with the processes involved at easier to operate ambient conditions
2 - to calibrate the injector unit,
3 - to select preliminary some initial design parameters of the resonance tube such, as hole diameter, depth and the distance from the injector to the resonance tube
4 - to study the development of the shock waves for short duration injections, and
5 - to study the effects of mass inflow into the resonance tube on shock wave development.

To confirm that all the equipment and control software is functioning properly and to master all the data collection techniques, some preliminary tests were performed. The equipment was first checked to ensure that the injector operated properly, that is that the nozzle opened fully and closed quickly and sealed well to reduce gas leakage. The electronic software and hardware was next checked to ascertain that the injection period is controllable, as well as to familiarize oneself with the data acquisition equipment including the digital oscilloscope. The first tests used nitrogen gas as a test fluid to eliminate any hazard which can occur when using hydrogen. Once the level of confidence in the equipment, as well as in the procedures, was considered satisfactory, the hydrogen was utilized.

The next set of tests was performed to calibrate the injection unit. These tests determined the gaseous fuel dose that the injector was delivering. If the fuel was a liquid, the measurement of the average dose would be straight forward, however with gases, the situation was not as simple. The calibration set-up used the displacement of water to determine the volume of the gas injected and then using the equation of state, calculated the mass of gas injected. There are several parameters which can be altered to vary the gaseous fuel dose such as; changing the time of

injection, the metering valve opening, the type of the nozzle orifice, and varying the injection pressure. The fuel dose requirements for an engine vary as well with the type and size of the engine and also with the engine speed and load requirements. In this thesis the aim was not to calibrate the injector for a specific engine but to show how certain variables affect the dose of hydrogen fuel injected.

Further tests at ambient conditions did determine some initial design parameters for the resonance tubes using hydrogen as the test gas. The hole diameter of the resonance tube must be best matched with the injector nozzle, the optimum distance from the injector to the resonance tube must be selected and the depth of the resonance tube hole must be chosen in order to produce high frequency resonating waves during the short injection period; then, it can produce more irreversibilities and consequently generate more heat during the short injection period. However, there is a limit to how short the cavity can be, because the shock wave requires some length to develop properly; also, the tube cannot be too long, otherwise the boundary layer will dissipate the shock strength. As stated before in this chapter, due to the modular design of the ADU, it was a simple task to replace one resonance tube with another one which had different

design parameters. Therefore, during investigations, the criteria for selecting the resonance tube and the injector nozzle will be based on the success in the shock wave development (largest pressure amplitude) with the axial distance being set at the optimum distance.

Since the gas injection period is so short, it is important that the shock wave begins to heat the gas immediately after the start of injection. So a study on how the wave is developing for the short injection duration has to be done. In previous studies cited in the literature review, there have been no such extreme time constraints in trying to ignite a gas jet, as they are required in a diesel engine. The ignition of hydrogen must occur within few milliseconds to obtain the highest work output from the engine, and consecutive ignitions must be repeatable in each engine working cycle.

6.3 Test Results and Discussion

6.3.1 Initial Familiarization Tests

From the first set of familiarization tests with the above mentioned equipment, some strange phenomena were noticed in the pressure history plot. Figure 6.5a shows the first phenomenon: the pressure waves maintain a fairly

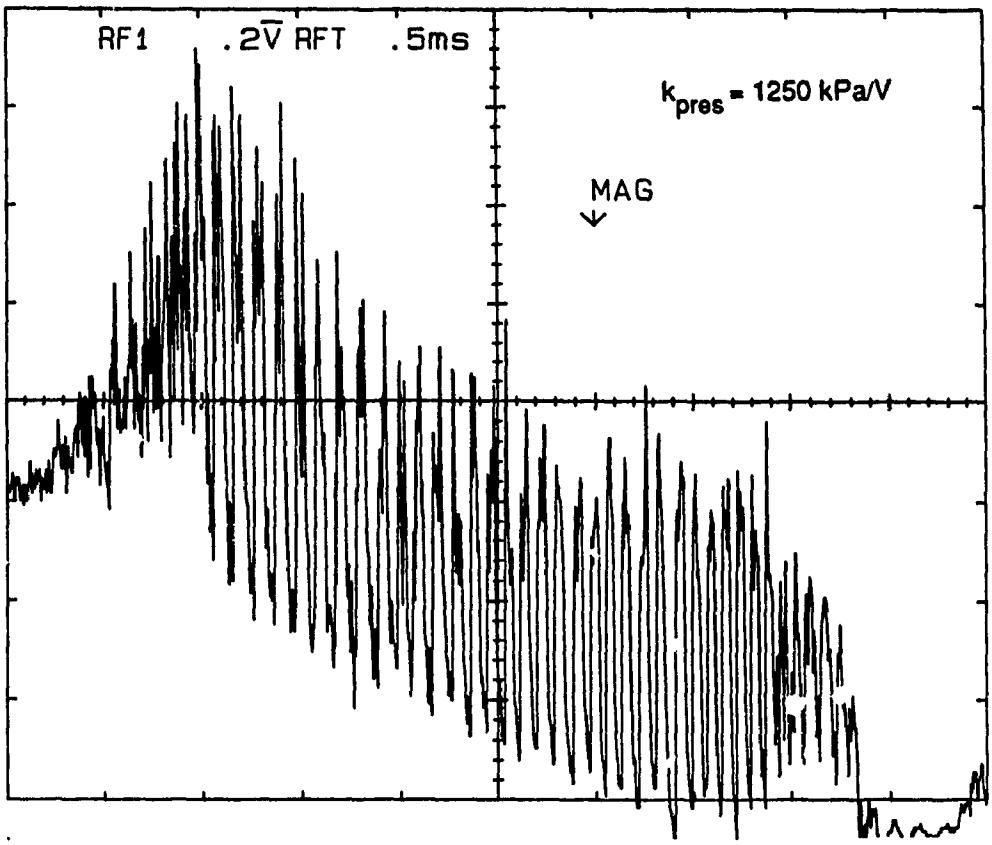

Figure 6.5a Typical Pressure History in a Resonance Tube of 20mm.

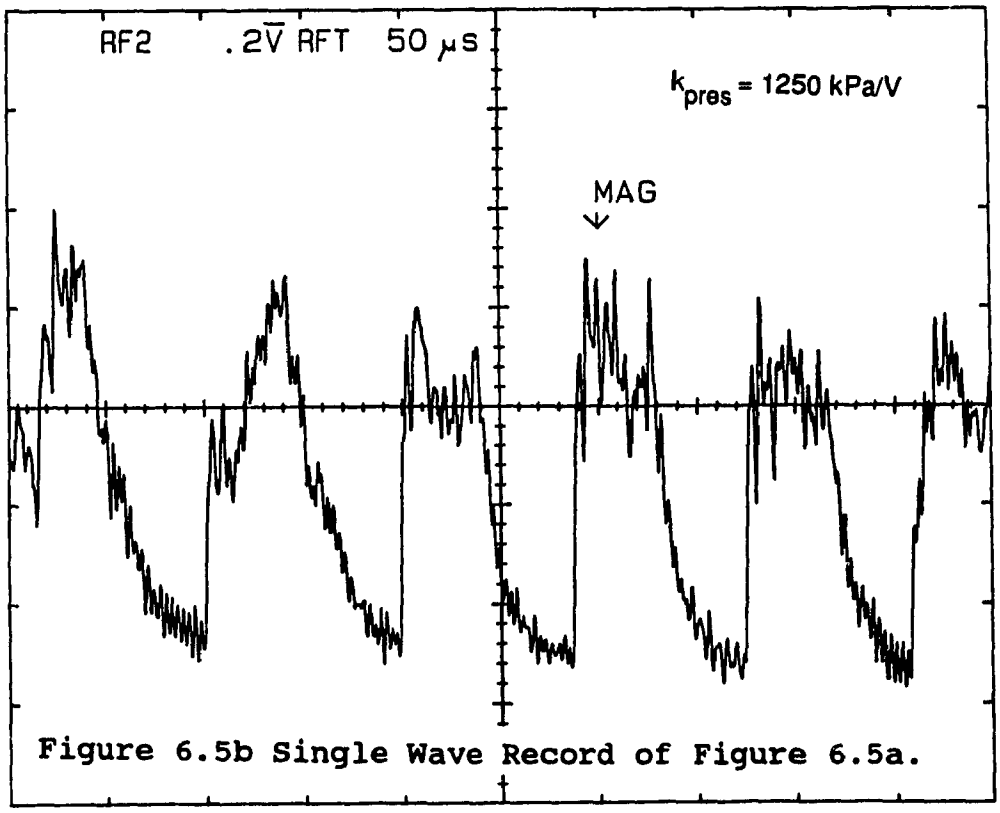

Figure 6.5b Single Wave Record of Figure 6.5a.

constant amplitude versus the injection time, however the absolute pressure level is dropping. In fact, the pressure wave value at the end of the injection period falls below absolute zero, what, of course, is not possible. In this Figure 6.5a the hydrogen injected into a resonance tube with a cavity depth of 20.0 mm, a hole diameter of 2 mm and the tube mouth situated 10 mm from the injector nozzle opening, resonated at a frequency of 10100 Hz with an average amplitude of 150 psi. Using the simplified wave diagram theory discussed in Chapter 4, the expected frequency should be 13800 Hz . Figure 6.5b shows an enlargement of the above record.

Figure 6.6a and Figure 6.6b shows injection into a resonance tube which has the same diameter but a cavity depth of 60.0 mm. The frequency of recorded pressure waves is 3175 Hz. Again, the theory over estimates the frequency by about 30%, however, the frequency was expected to decline by one third between the tests shown in Figure 6.5 and Figure 6.6 due to the increased length of the tube and this did occur. The pressure amplitude recorded during these two tests remained almost the same. The lower waves frequency can be attributed to the presence of air in the tube which was creating a mixture with injected hydrogen.

To investigate the indicated drop in the average pressure datum level, additional tests were carried out

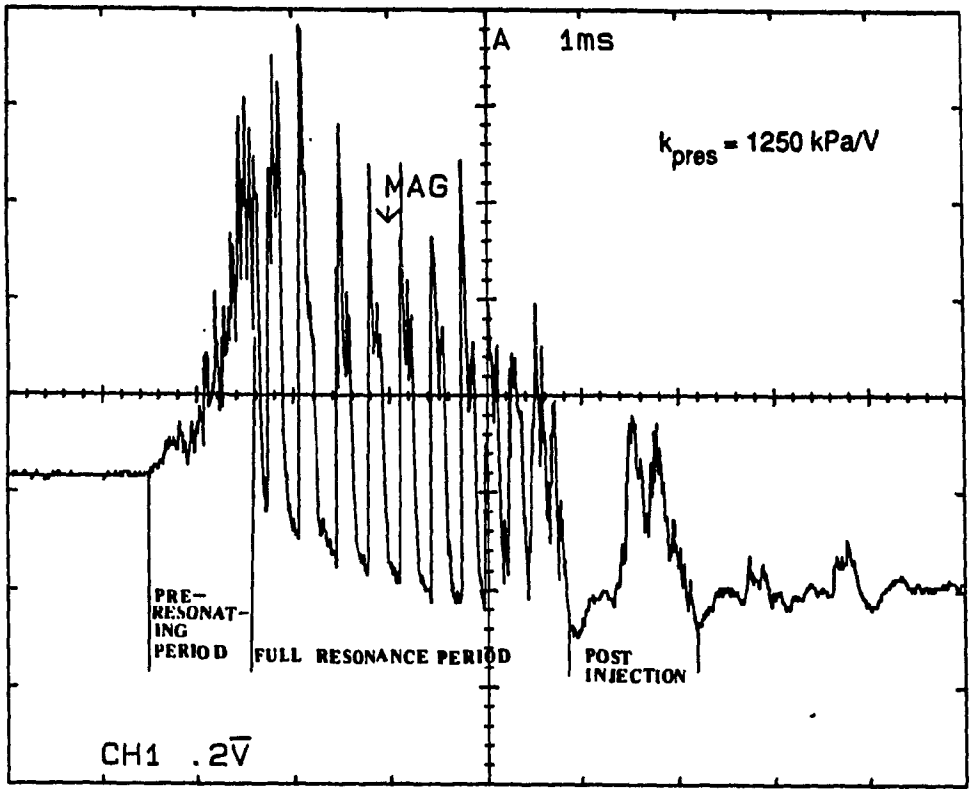

Figure 6.6a Typical Pressure History in a Resonance Tube of 60mm.

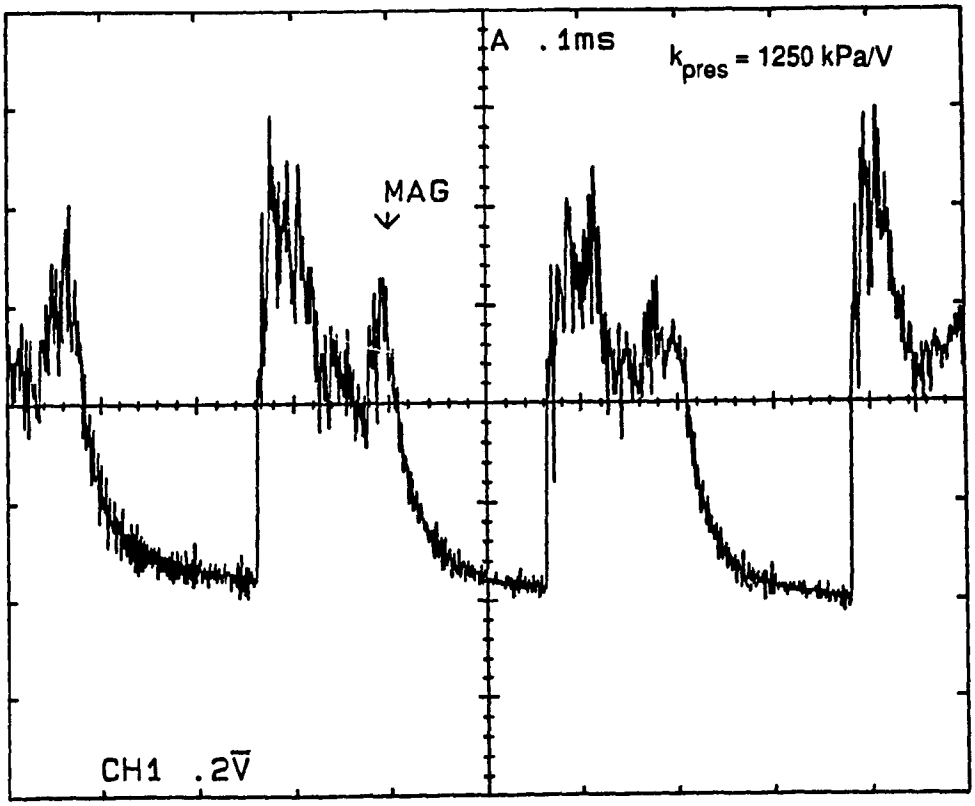

Figure 6.6b Single Wave Record of Figure 6.6b.

with a much longer injection period. Figure 6.7 shows the pressure history inside the resonance tube for an injection period lasting approximately 2 seconds. From this record it can be seen that the datum pressure initially drops dramatically, and then slowly rises to the initial datum value. The explanation for this phenomenon is leading to the change in temperature of the transducer, which affected the datum voltage created by the piezoelectric transducer. It eventually reached a steady value when the sensor reached a steady state condition as well. This effect, which would be difficult to compensate, will have to be accounted for when interpreting the pressure graph shown in Figure 6.5 and in other records.

A second strange phenomenon found during the initial tests can be seen in Figure 6.8. There is a distinct decrease in the pressure amplitude at the center portion of the shock wave record; the shape of the pressure record shows some kind of a "saddle" which will be referred to as the "saddle effect". This effect, which was not understood from the beginning, was finally related to the gas inflow rate into the tube. It can be explained as follows:

When the injector begins to open and also when it is closing, the gas flow through the injector is being throttled by the considerably small flow area of the needle seat in the nozzle, which results in a lower gas discharge

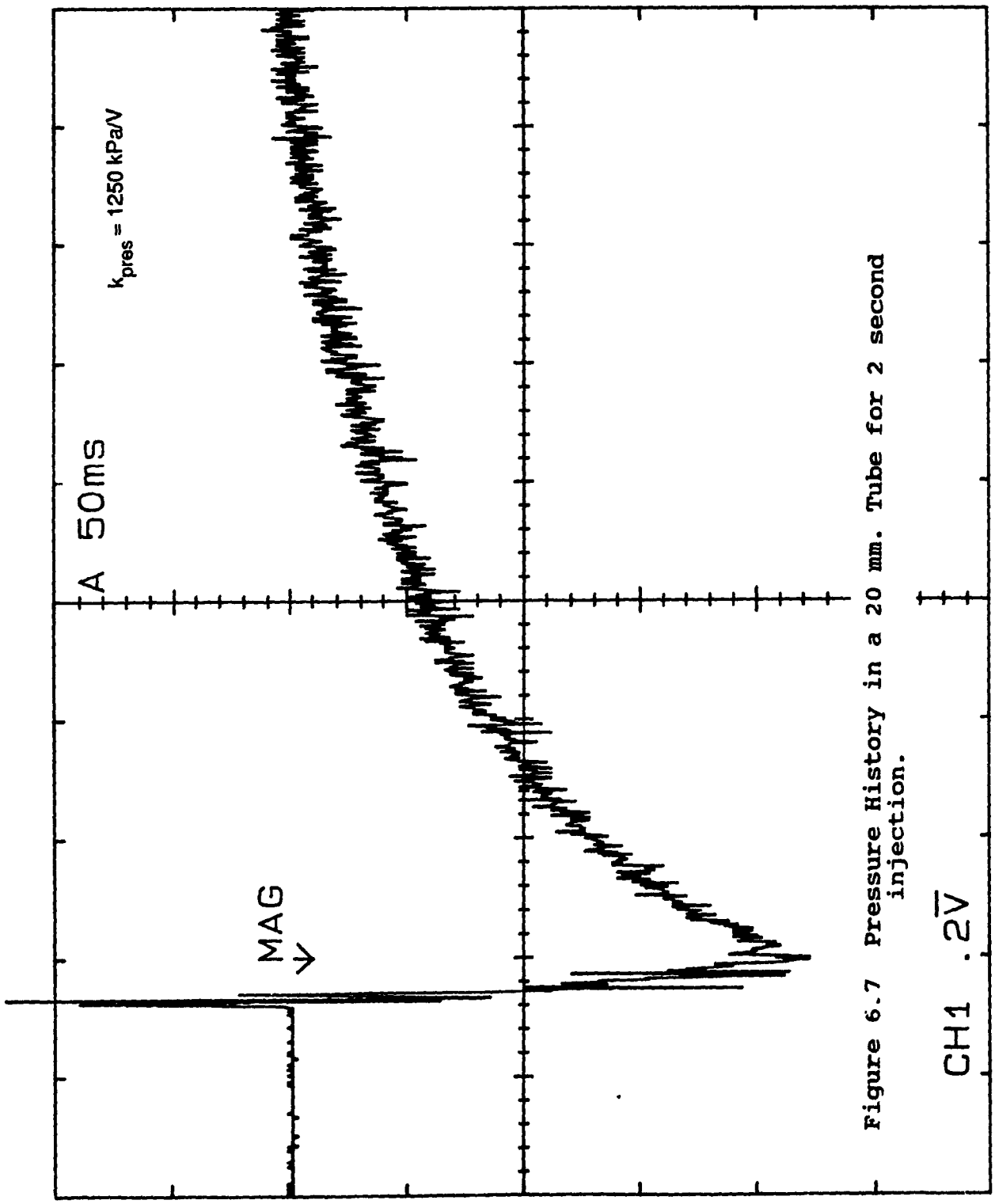

Figure 6.7 Pressure History in a 20 mm. Tube for 2 second injection.

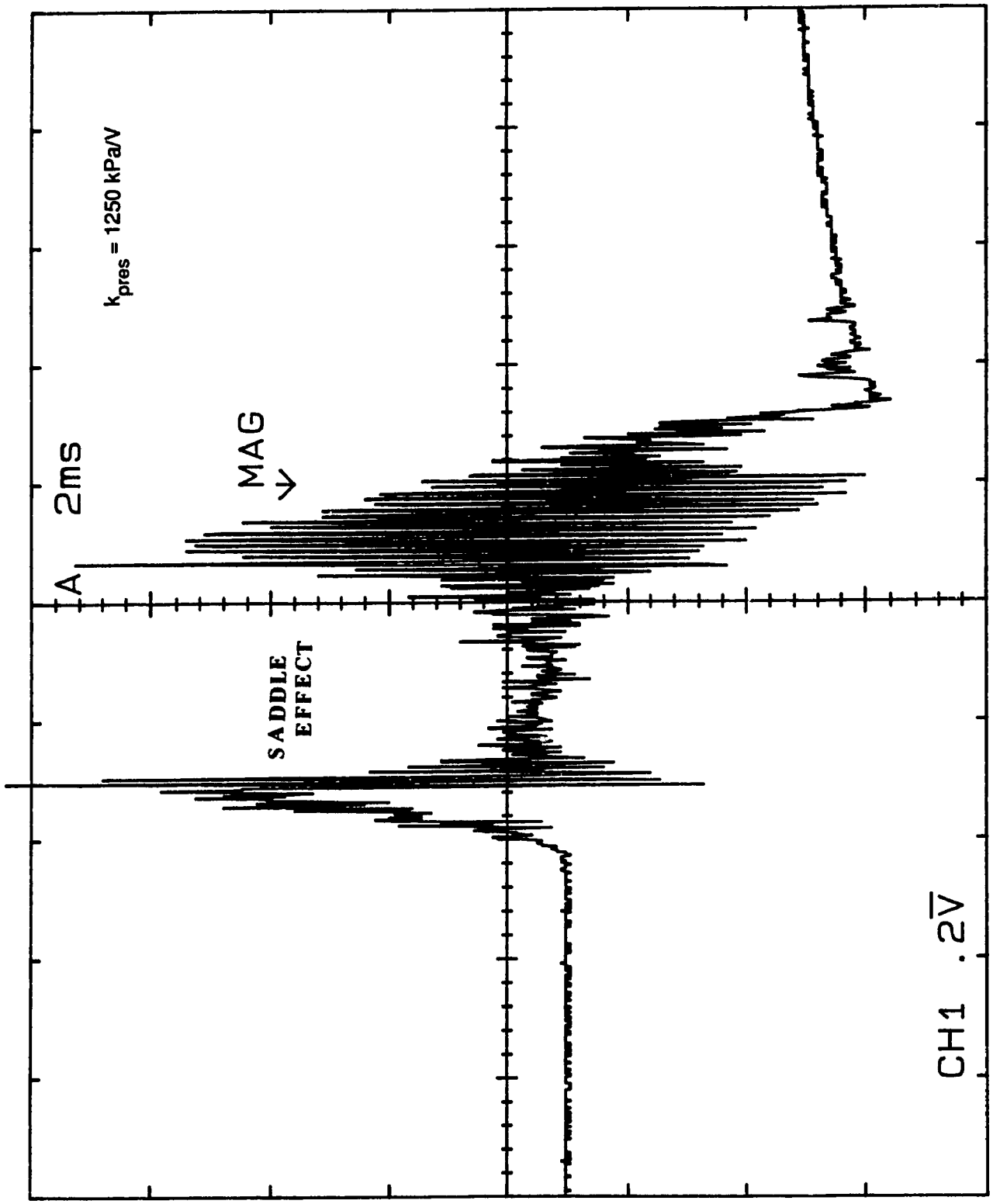

Figure 6.8 Pressure History at End Wall Showing the "Saddle Effect".

rate. When the injector nozzle is fully open, there is much less throttling of the gas flow, except at the nozzle exit orifice. However, at this maximum discharge conditions, the gas inflow into the resonance tube seems to be choked.

During investigations of this phenomenon it was found experimentally that there are three ways to eliminate the "saddle effect" in the resonance tube:

1 - by throttling the flow of gas into the injector using the metering valve,
2 - by moving the resonance tube farther away from the injector.
3 - by reducing the pressure of the gas supplied from the bottle to the injector.

The record of shock waves in the resonance tube without "saddle effect", due to gas inflow throttling in the metering valve, is shown in Fig. 6.9.

One can be convinced by these results that the "saddle effect" is strictly related to the inflow rate of hydrogen into the tube. Therefore, it was concluded that the "saddle effect" is the result of high gas discharge rate which contributes to the reduction of the gas inflow rate into the resonance tube.

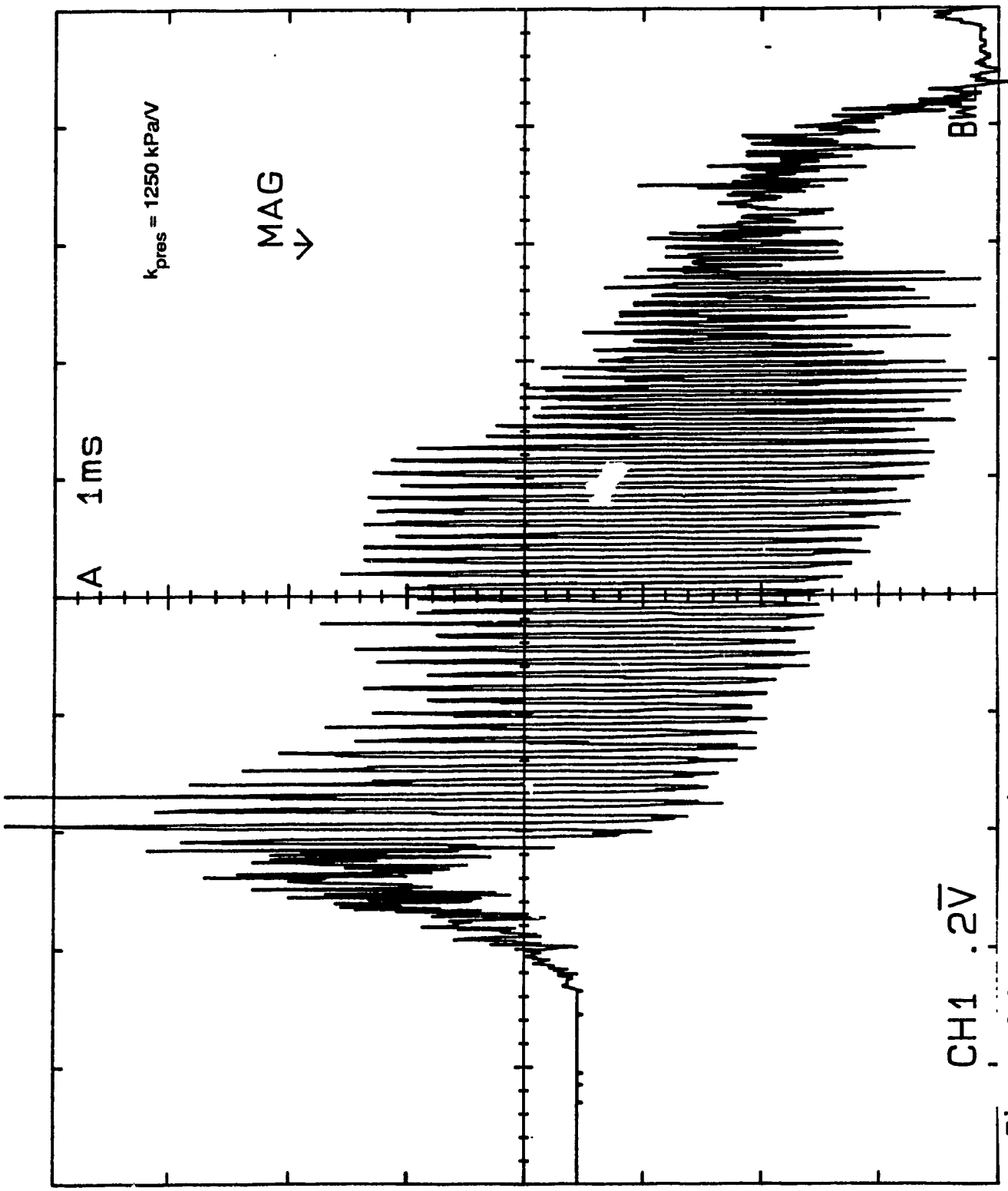

Figure 6.9 Pressure History Without "Saddle Effect" due to Metering Valve Throttling.

When comparing the Figure 6.8 with Figure 6.5 or Figure 6.9 without the saddle effect, it can be seen that due to the absence of the high amplitude shock waves in the "saddle part" of the pressure record in Fig. 6.8, the pressure datum line is becoming almost horizontal. This means that there is almost no heat release at the bottom of the resonance tube because the piezoelectric pressure transducer is not affected by the temperature change.

The nature of the "saddle effect" which has been so distinctly identified, is difficult to explain. The conclusion that it is caused by high gas inflow rate into the resonance tube, has its backing in the experiments described above, which show the means used to avoid this phenomenon. However, a more direct proof is required that at higher hydrogen jet velocity, the gas inflow rate into the tube is being reduced. Such proof will be given in the next part of this thesis.

6.3.2 Gas Dose Calibration Tests

Before selecting any initial design parameters for the resonance tube, some parameters had to be set regarding the injector. The gas mass dose discharged by the injection unit must produce the required power scheduled for a specific engine size. It must also be injected within a

certain injection time period. There are several variables which affect the injected gas dose:

1 - duration of the injection,

2 - metering valve opening,

3 - gas injection pressure,

4 - flow area through the nozzle.

The time allowed for gas injection will vary with the operating speed of the engine and with its load. This is also the simplest way of varying the fuel dose by changing the time of injector opening. However, there is a limit to how long the fuel injection process can last. If a typical diesel engine is operating at 1000 rpm, and the injection period is limited to 30 degrees of the crank angle, the injection period corresponds to 5 milliseconds. This time of 5 ms will be considered as an upper limit for the tests made in this study. There is also a lower limit which should be taken into consideration because of the shock wave creation period.

The metering valve flow area can be varied to change the dose of hydrogen to be injected in two ways. The first mode is by reducing the pressure during the injection period; however, the pressure at the beginning of the injection will be equal to the gas supply (bottle)

pressure. Figure 6.10 shows the injector lift and pressure in the injector during a typical 5 ms injection period with the inlet flow choked by the metering valve.

The second mode occurs by reducing the gas pressure also at the beginning of injection. This can happen if the pressure in the injector, following the previous injection, cannot reach the gas supply (bottle) pressure before the next injection, because there is not enough time to charge the injector volume at that particular metering valve opening; then, the mass of the gas dose will also be reduced.

The third method to vary the dose of gas being injected is to change the injection pressure by supplying gas at a higher or lower pressure from the storage tank. Since the outflow from the injector will remain choked, the driving pressure is the only pressure variable which determines the gas discharge rate.

Varying the flow area of the nozzle is another way of changing the gas dose. A throttling type pintle nozzle will reduce the gas flow versus the lift of the needle. If the end cone of the pintle is removed, then the gas flow will only be throttled by the needle seat for a short initial period of the needle lift, and the throttling will occur at the orifice of the nozzle. The considerations for the nozzle design was to create the best results in terms

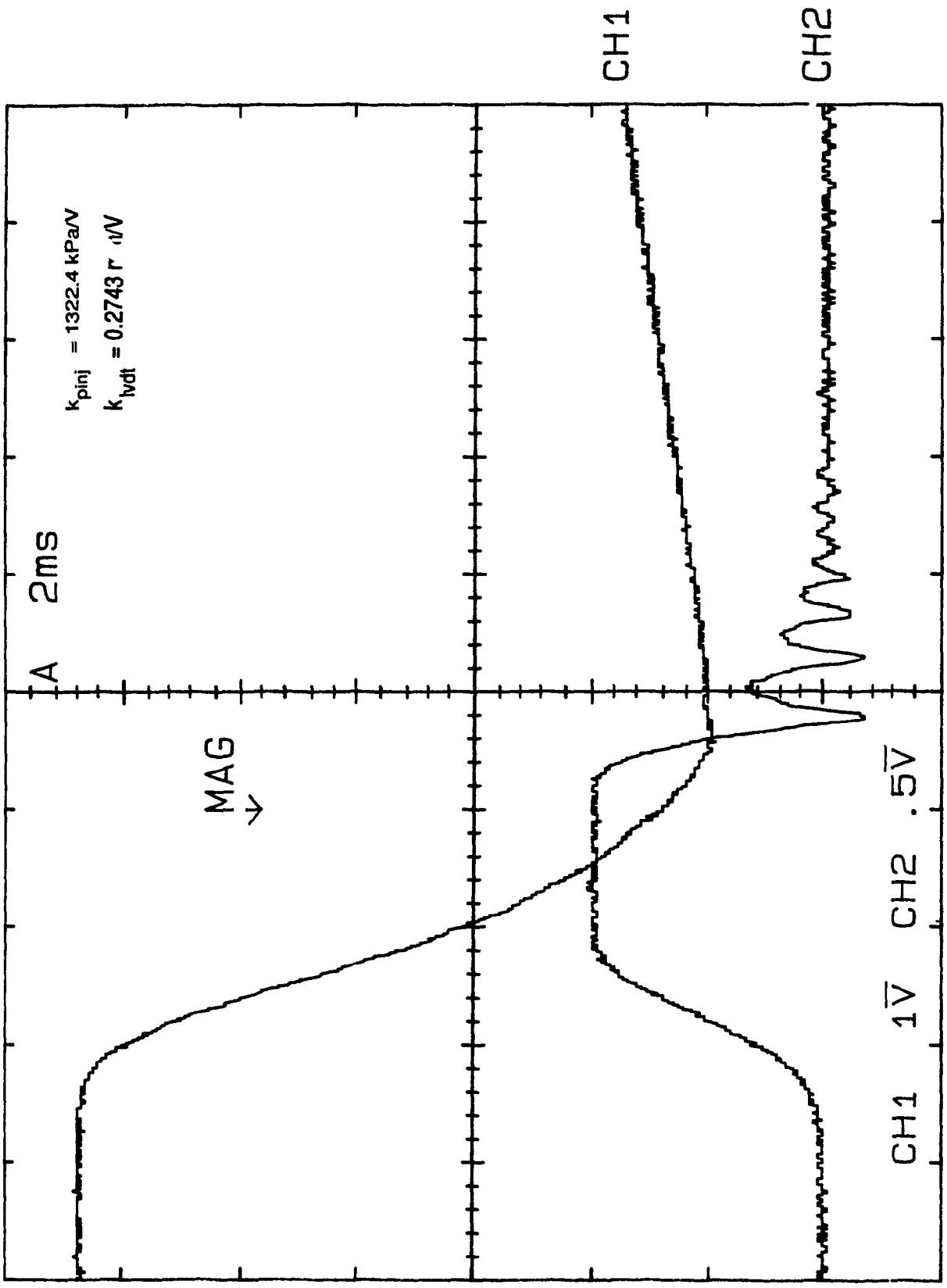

Figure 6.10 Injector Lift and Injector Pressure
During Hydrogen Injection Process.

of shock wave development. It was decided to use the 1.5 mm pintle nozzle among three sizes of 1 mm, 1.5 mm, and 2 mm. It was found from initial calculations, based on an engine with a displacement volume of about 350 cc. per cylinder, that the 1.5 mm pintle nozzle would be well suited, if the pintle end was removed.

Figure 6.4 shows the gas dose calibration set-up. The injected gas dose displaces a certain volume of water and using the equation of state, the dose can be calculated as:

$$\Delta m = \frac{p\ \Delta V}{n\ R\ T}$$

where: p = absolute pressure exerted on the gas [kPa]

ΔV = the volume of water displaced [m^3]

R = the gas constant for hydrogen [kJ/kg K]

T = the absolute temperature of hydrogen [K]

n = number of injections performed

Defining the absolute pressure exerted on the gas with respect to the vertical difference measured between the two water levels, Δh, we get:

$$p = p_{atm} + \overline{\gamma\ \Delta h}$$

where $\overline{\gamma}$ = the specific weight of water [kg/m^3]

The displaced volume can also be written as a function of the difference in water levels Δh:

$$\Delta V = \frac{\pi \, d_{cyl}^2}{4} * \left(\frac{\Delta h}{2} \right)$$

where d_{cyl} = the internal diameter of the cylinders

The average gas mass dose injected for '*n*' number of injections is given by:

$$\Delta m = \frac{\left[\left(p_{atm} + \overline{\gamma} \, \Delta h \right) \left(\frac{\pi}{4} \, d_{cyl}^2 \right) \left(\frac{\Delta h}{2} \right) \right]}{n \, R \, T}$$

The test procedure will consist of injecting gas consecutively several times. This will result in an average dose per injection, thereby reducing the effect of dose variations. Next, these tests will continue by varying the duration time of injection or the metering valve opening; then, the other variable will be changed. The needle has the pintle entirely removed, and the gas supply pressure is set at 8275 kPa (1200 psi). The result is shown in Figure 6.11.

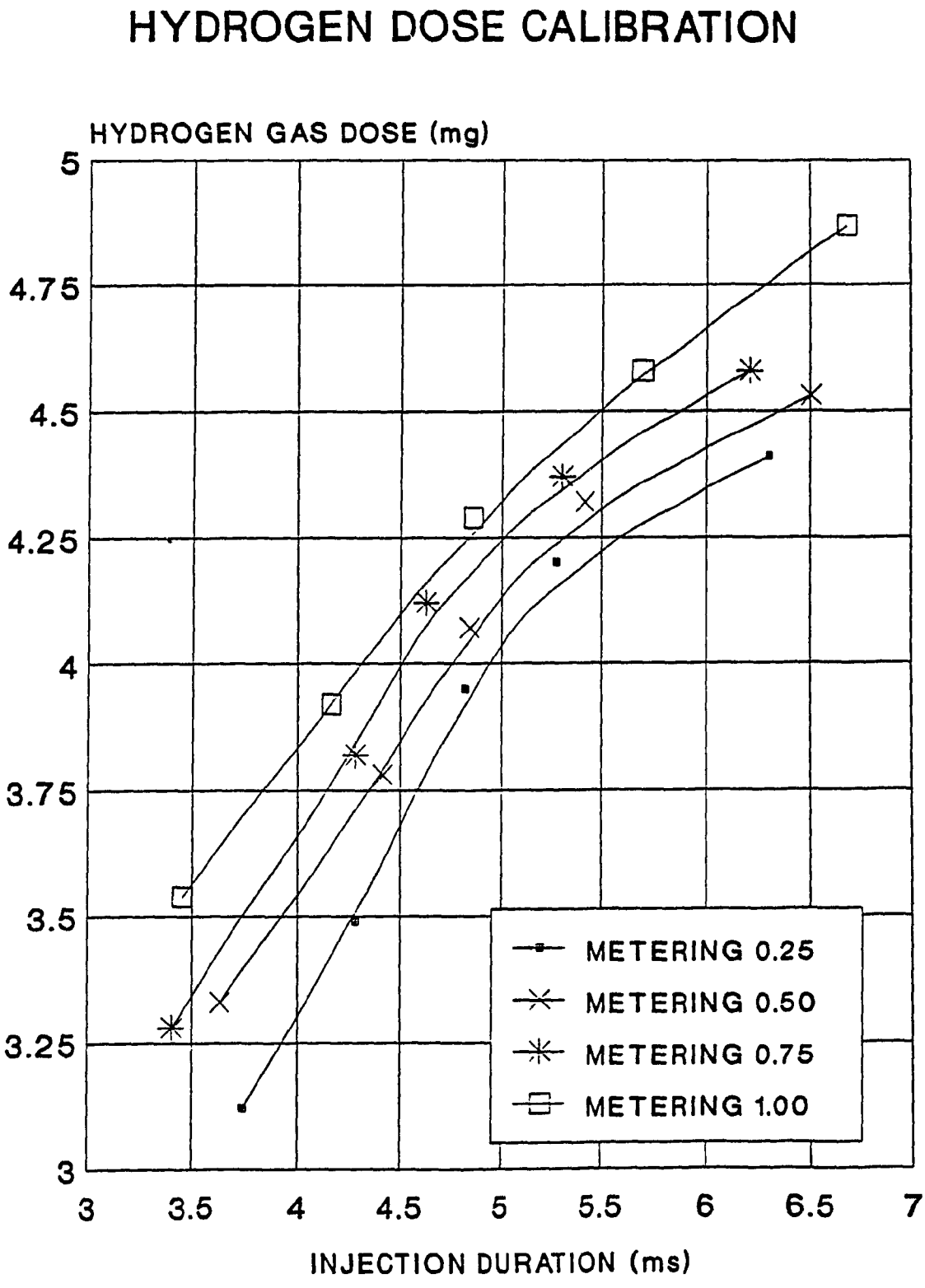

Figure 6.11 Hydrogen Dose Variations Due to the Duration of Injection and Metering Valve Opening.

6.3.3 Initial Resonance Tube Sizing

After selecting the best nozzle, the next task was to find the best resonance tube diameter which would match with this nozzle. Several resonance tubes were tested having all the same length to diameter (l/ϕ) ratio of 20. This l/ϕ ratio was initially chosen arbitrarily with optimization of this ratio to follow later, once the resonance tube diameter has been chosen.

The tube diameters which were tested were of 1 mm, 1.5 mm, 2 mm, and 2.5 mm. Each of these tubes had the pressure transducer installed at its end and forming, to some extent, the back wall of the tube cavity. The axial distance between the tube and nozzle was varied, to obtain the best results in terms of pressure wave amplitude. These best results were found for the 2 mm dia. tube hole for the 1.5 mm dia. nozzle orifice. This corresponds quite well to the literature data which recommend a nozzle orifice to tube hole diameter ratio of 1.25.

The tube length was next varied to get the best results. As stated earlier, to achieve the highest shock wave frequency and a little impact of the boundary layer build up, the tube length should be as short as possible, however long enough to form a one dimensional shock wave in the tube. After testing several tube lengths with a 2 mm

dia. resonance tube, an l/ϕ ratio of 10 was chosen, i.e. a tube with 20 mm cavity length.

6.3.4 Shock Wave Development for Short Gas Injection Duration

In studying a typical pressure record taken at the end wall of a resonance tube, the graph could be broken down into three parts, (Figure 6.6a):

1 - an initial pre-resonating period where the shock waves are starting to develop,
2 - a full wave resonating period, where the pressure waves are of similar amplitude, and
3 - post-resonating period, which is characterized by some pressure waves caused by the injector needle bouncing.

Improvements in the injector and nozzle design would be required to reduce the first and last parts of the pressure record. Some solutions to the needle bouncing problem have been proposed, but good matching of the injector spring can also have a beneficial effect in reducing the needle bouncing. Another solution would be to design the injector so that the gas force has no effect on the opening of the injector.

The first pre-resonating part of the pressure record is caused by two events. First, the injector requires some time to open fully and to create a quasi-steady discharge rate of fuel; this time should be reduced, as much as possible and this can be done by using a faster charging solenoid (that is a lighter yet stronger solenoid). Second cause is due to the time of development of the gas flow from the injector to create the resonating shock wave, and there is little that can be done, except trying to modify the gas jet from the nozzle. It is imperative that for a shock wave ignition to occur in a short time, it would be necessary to create as long duration period of steady resonating shock waves, as possible, so that the heating effect would be the greatest with respect to the available time.

6.3.5 Gas Inflow Rate Tests

In the thesis by Giannacopoulos, he described the highly transient one-dimensional unsteady gas discharge rate from an injector into a long tube of constant diameter and connected to the injector, as being proportional to the pressure wave in the tube. A qualitative evaluation of such inflow rate into a long tube, however placed at some axial distance from the nozzle, will be now discussed:

qualitative evaluation would not be possible, due to the gas dissipation at the tube entry.

Figure 6.12 shows a pressure record for the long tube tests. The saddle shape of the pressure curve is very noticeable, corresponding to the "saddle effect" observed previously (Figure 6.8) with gas injection into the resonance tube, when all the injected conditions for the two tests have been maintained the same. However, when the flow was throttled with the metering valve (Figure 6.13), the "saddle effect" was eliminated and the pressure wave generated by the gas flow rose up to a high quasi-steady value. The previous test with gas injection into a resonance tube, conducted under the same conditions, i.e. with metering valve throttling, showed no "saddle effect" either (Figure 6.9).

An important conclusion can be drawn from this experiment that the saddle effect is not only appearing in the resonance tube at high enough inflow rate, but also in a tube in which there are no conditions for the pressure wave reflection because of the big length of this tube. So, the conditions in which the "saddle effect" appears have been discovered, however the nature of this effect is not known and requires further investigations.

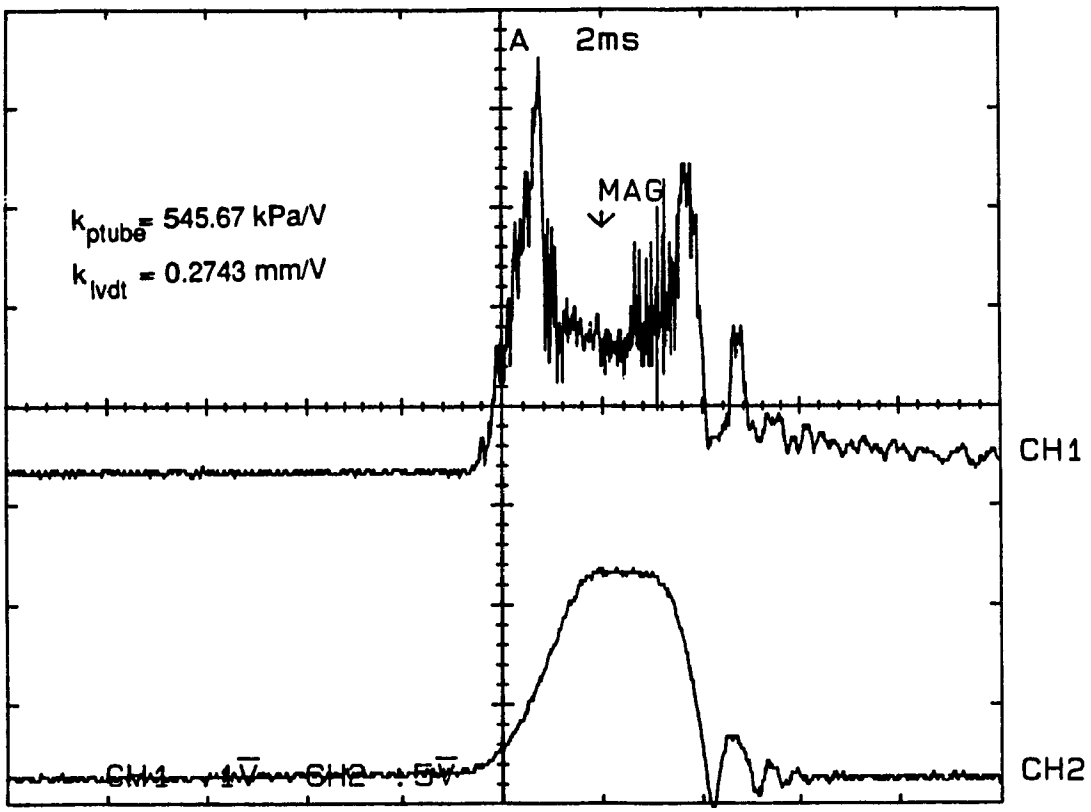

Figure 6.12 Hydrogen Pressure Record in the Long Tube Showing the "Saddle Effect".

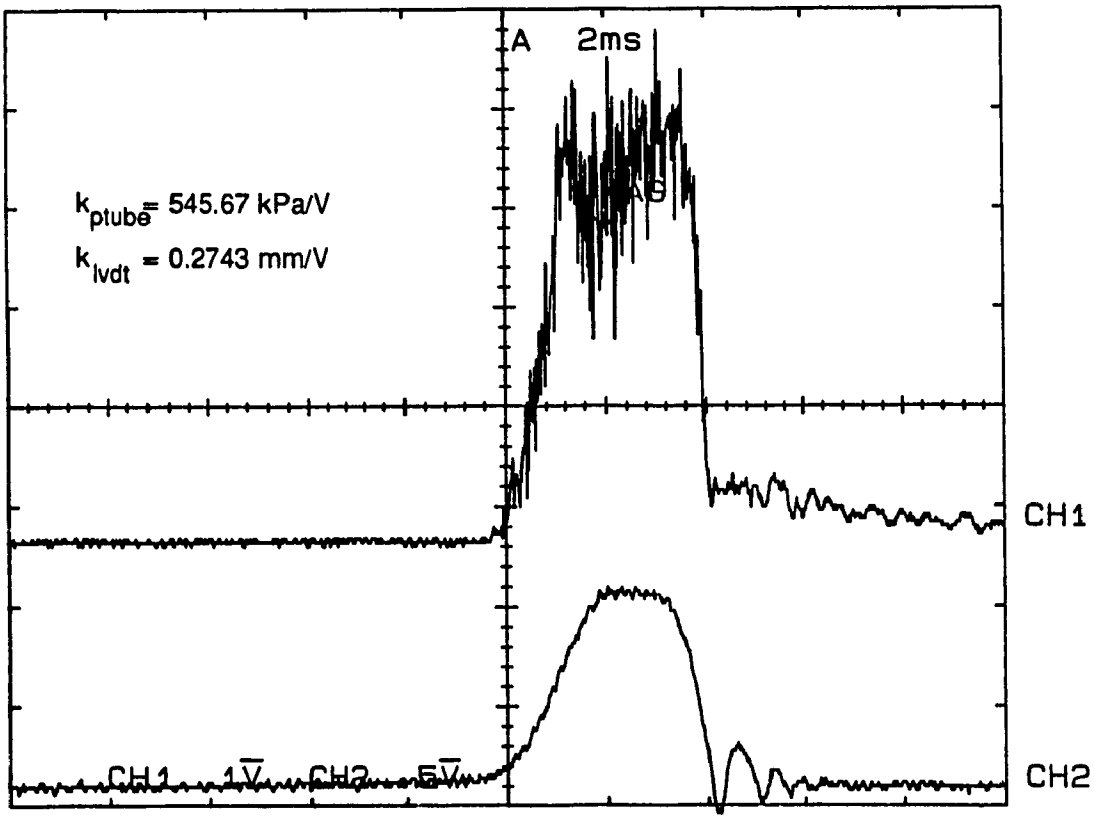

Figure 6.13 Hydrogen Pressure Record in the Long Tube without the "Saddle Effect" due to Inlet Flow Throttling with the Metering Valve.

CHAPTER 7

7.0 EXPERIMENTAL INVESTIGATIONS OF RESONANCE TUBES AT ELEVATED BACK PRESSURE

Following the initial familiarization and sizing tests, the next investigations were made under conditions which can be found in reciprocating internal combustion engines. The first step was to perform the tests to study how the injection system, as well as the resonance tubes, perform when the hydrogen gas is injected into air at elevated pressure. Specifically, it should be determined how higher ambient pressure affects the creation of resonating shock waves in the H-S tube, as well as to determine how variations in the axial distance between the mouth of the resonance tube and the injector nozzle, and the gas discharge rate from the injector, affect the shock wave creation and strength.

The results from this chapter show that, as the pressure of the air into which the gas is injected increases, it was more difficult to obtain fully developed resonating pressure waves in the resonance tube. One method of improving the wave development was to decrease the gap between the injector nozzle and the tube.

The testing procedure began with using the closed chamber, but keeping the pressure in the chamber close

to atmospheric and testing the resonance tube with decreasing axial gaps. The next step was to increase the pressure in the chamber and to repeat the tests. These tests continued until the gap was reduced to 1 mm and the pressure was set as high as 2070 kPa gauge (300 psig). The fully developed shock wave became more difficult to create at higher pressures. Also, the period of time during which the waves existed decreased with higher back pressure; it was no longer lasting for the full injection period.

7.1 Test Methodology

The testing methodology which followed, consisted of setting a fixed axial distance between the injector and the resonance tube and choosing the metering valve opening and then, recording the pressure at the closed end of the resonance tube, as well as the injector needle lift, while varying the air back pressure inside the chamber into which the gas was injected. The same procedure was repeated for other axial distances when moving the resonance tube closer or farther from the injector.

The next set of tests intended to determine how the variation of the hydrogen discharge rate from the injector affects the shock wave development. There are several ways of varying the gas discharge rate. The easiest is to change the opening of the metering valve by throttling the

gas flow into the injector. For these tests the axial distance between nozzle and the tube were fixed and the supply pressure was held constant while varying metering valve openings. The back pressure was then changed and the tests were repeated for the same metering valve position. Next, the system gas pressure supplied to the injector was also varied to study the effects of the gas discharge rate on the shock wave in the resonance tube. The benefit of varying the gas discharge rate was that a wide spectrum of driving pressures were present during each injection because the pressure in the injector dropped, as the injection occurred due to the choking of the gas flow into the injector.

The injector, nozzle and metering valve tested were the same, as described in Chapter 5, and the resonance tube had the previously selected cavity diameter of 2mm and the depth of 20mm. The injection process, i.e. the duration of gas injection and the needle lift, were maintained constant through the use of the proper control software and hardware.

7.2 Test Apparatus for Investigation of Shock Waves in Resonance Tube at High Ambient Pressure

The test rig used in these tests was the full engine set-up previously described in Chapter 5 and shown in Figure 5.2. However, the test engine's piston was held at the top dead center position with both the intake and exhaust valves closed, by placing a locking pin on the fan/flywheel assembly to prevent the rotation of the engine crank shaft. Compressed air was introduced into this chamber through the charging port placed below the safety valve. The safety valve's cracking pressure was set to a value approximately 50% above the charging pressure. The combustion chamber cross section is shown in Figure 5.3.

The injection unit and the cylinder head were instrumented, as described in Chapter 5 with pressure transducers to measure the gas pressure in the chamber, in the injector and an LVDT to measure the injector nozzle lift. Another pressure transducer was installed at the back wall of the resonance tube and was squeezed against the resonance tube securely with the pressure transducer nut on a holder. This holder was placed into an adapter which has an M10 x 1 metric thread so that the distance between the injector and the resonance tube could easily be varied by the known increments.

The control software was identical to the one in the experiments described used in Chapter 6 for the initial familiarization tests and which has been described in Chapter 5.

7.3 Test Results and Discussion

In the closed chamber conditions, the tests were performed with an axial distance between the injector end and the resonance tube, that proved to provide the best results under atmospheric conditions, that is at 8.0 mm. A metering valve position of .2 turns with flow area of 8.7 x 10^{-9} m^2 (determination of the flow area can be found in Appendix B) was set as nominal. Each record of test data occurred after a few consecutive injections resulting in the accumulation of hydrogen gas in the chamber which could affect the frequency of pressure oscillations in the resonance tube. However, the chamber had also a substantial leakage that helped to keep the concentration of hydrogen down.

Figure 7.1 shows the test records for Δx = 8mm and with no supercharge. As previously under atmospheric conditions, the well developed shock waves are shown. These waves have an amplitude of 1800 kPa (260 psi) and a frequency of approximately 10900 Hz. Figure 7.2 shows

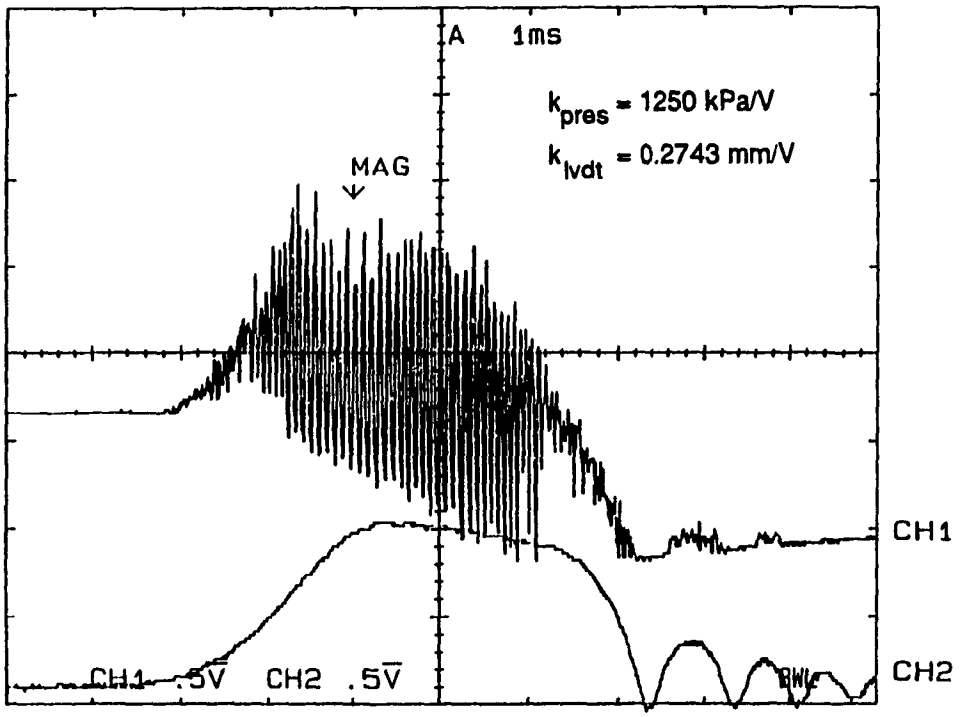

Figure 7.1 Typical Pressure and Nozzle Lift Record for Injection in a Closed Chamber at Atmospheric Conditions at Δx = 8 mm.

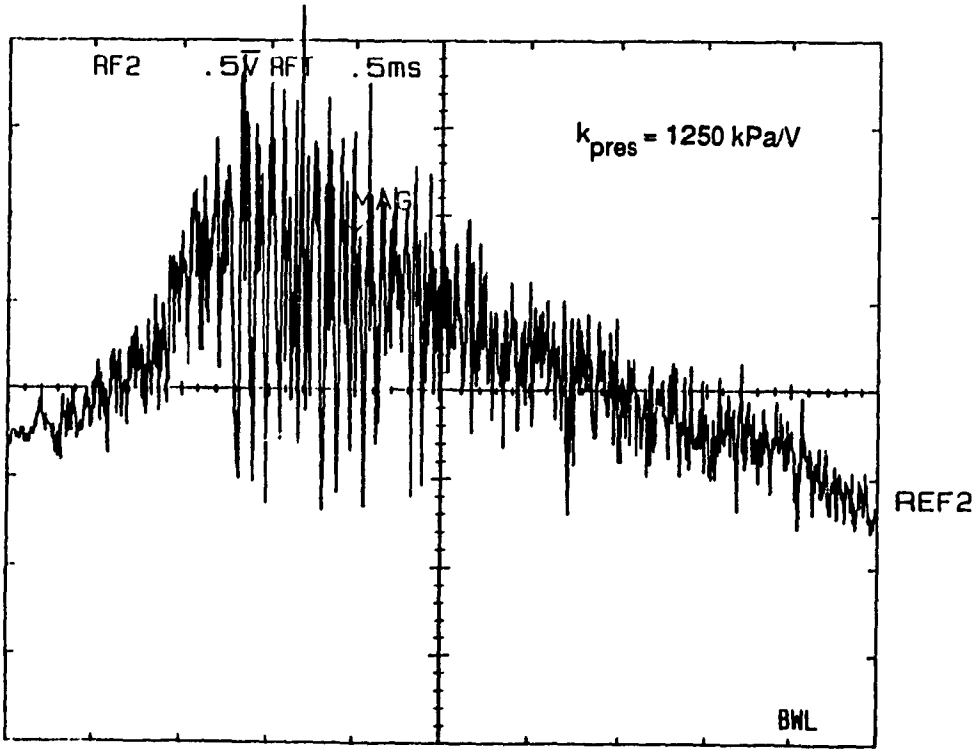

Figure 7.2 Pressure Record at 170 kPa gauge Back Pressure and Δx = 8 mm.

the results at an increased chamber pressure of 170 kPa gauge (25 psig) decreased the strength of the shock waves. The shock waves are still present, however, they are not as well developed and they are not of uniform amplitude; some of the waves are reaching much higher amplitude than the others. Further increase of the back pressure to 345 kPa gauge (50 psig) (Figure 7.3) and next to 690 kPa gauge (100 psig) (Figure 7.4) made the shock wave even weaker.

These results are not promising from the point of view of hydrogen ignition because much higher pressures are present in the combustion chamber of a diesel engine. The high back pressure seems to be affecting the penetration of the gaseous jet into the resonance tube as well as the cell length of the gas stream. Therefore, it was concluded that the resonance tube must be moved closer to the injector nozzle and for the next set of data, the axial distance was reduced to 6 mm

The results obtained from these tests at 6 mm distance were encouraging because the decrease in the axial distance did improve the resonance tube strength at elevated pressures. Figure 7.5 shows the pressure history in the resonance tube, as well as the injector needle lift, obtained with the atmospheric pressure. The pressure waves have a relatively constant average amplitude of 1600 kPa (230 psi) at a frequency of approximately 12000 Hz. There

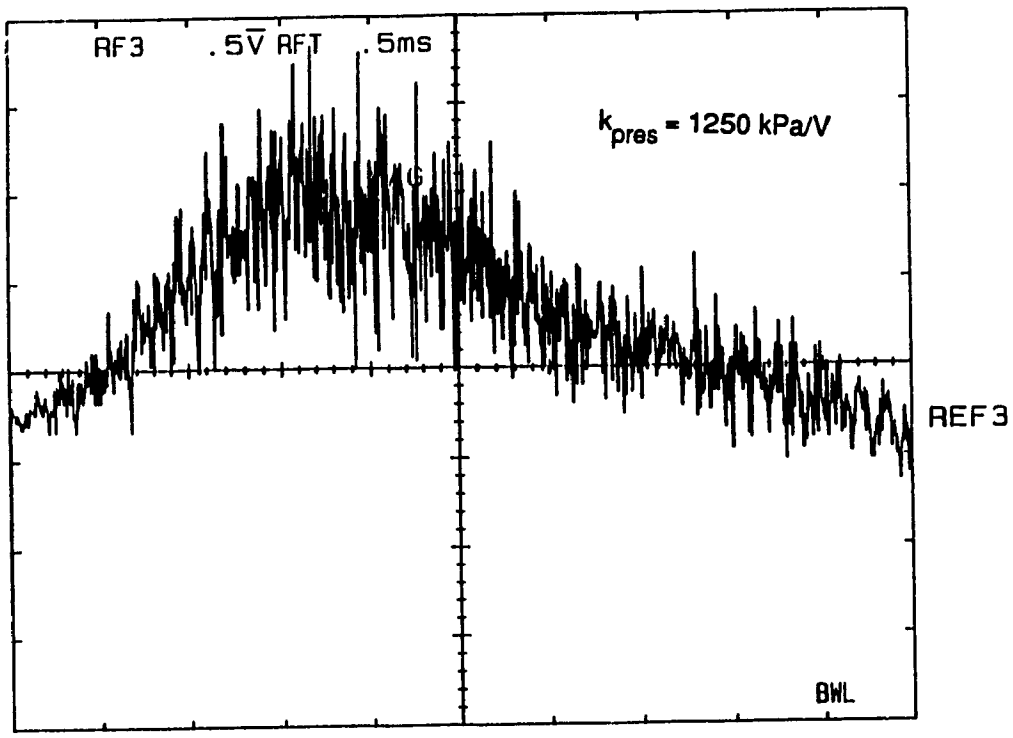

Figure 7.3 Pressure Record at 345 kPa gauge Back Pressure and Δx = 8 mm.

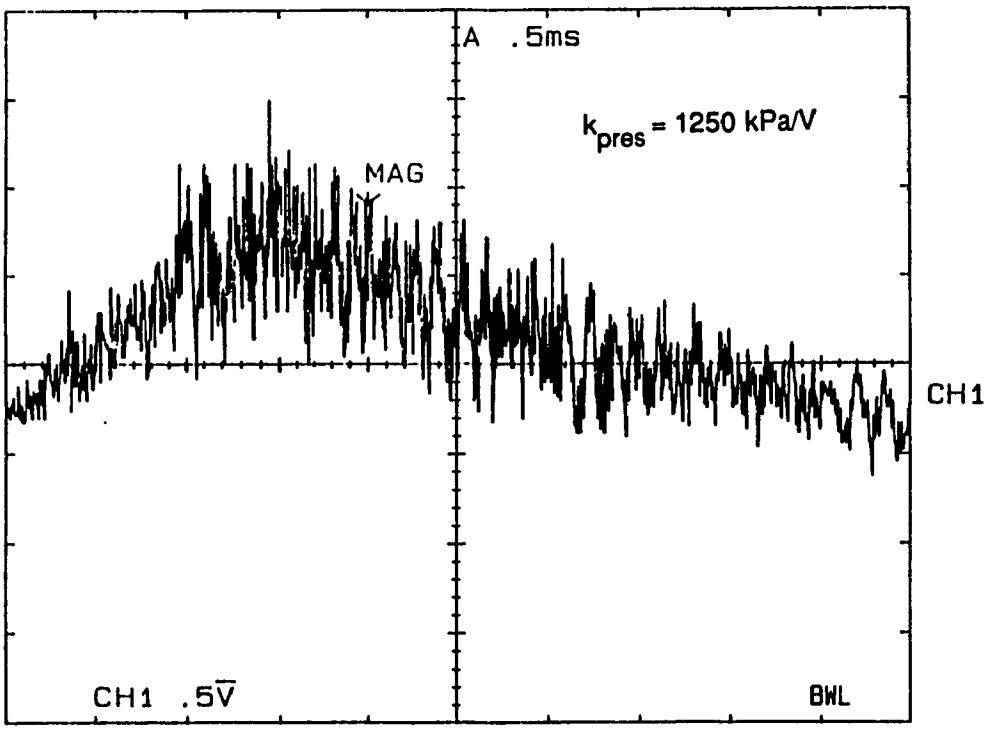

Figure 7.4 Pressure Record at 690 kPa gauge Back Pressure and Δx = 8 mm.

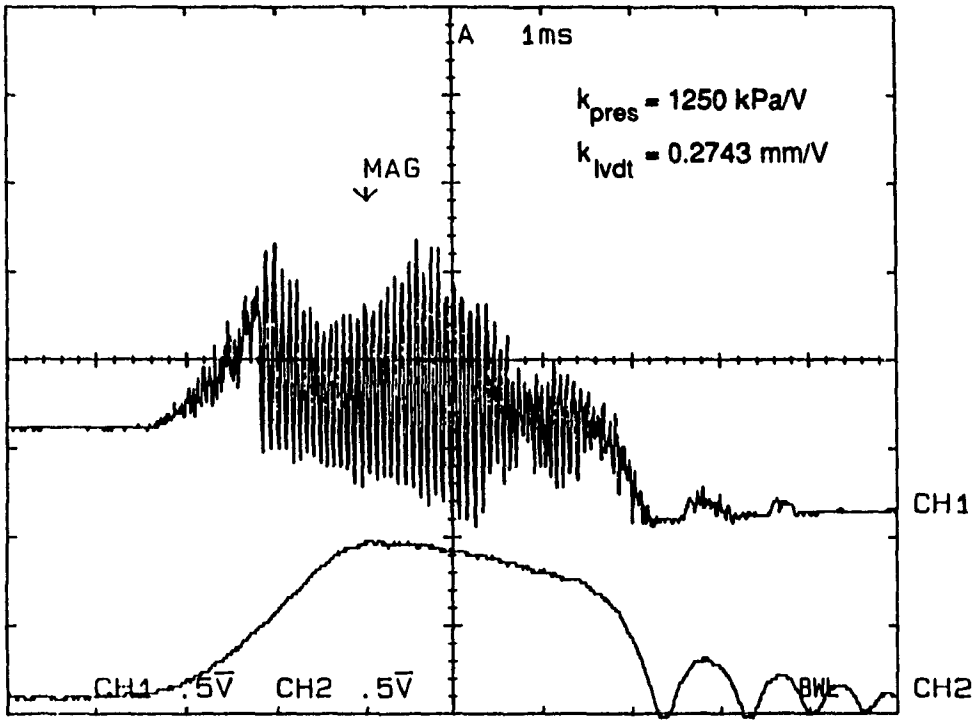

Figure 7.5 Typical Pressure and Nozzle Lift Record for Injection in a Closed Chamber at Atmospheric Conditions at Δx = 6 mm.

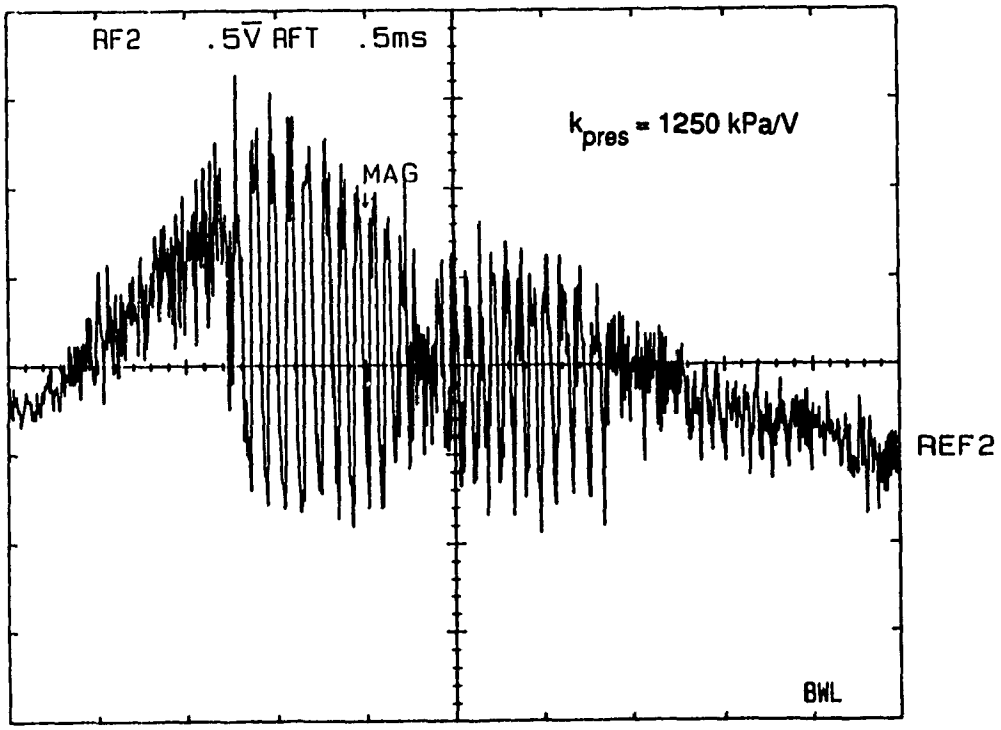

Figure 7.6 Pressure Record at 170 kPa gauge Back Pressure and Δx = 6 mm.

is also a small saddle effect. At 170 kPa gauge back pressure, Figure 7.6, the waves have a lower frequency of 10700 Hz, however the amplitude of the waves is much higher, at an average of 2900 kPa gauge (420 psi.) At 345 kPa gauge back pressure, the amplitude of the waves increases again to a maximum of 3300 kPa gauge (480 psi), however, this phenomenon lasts only few cycles at a lower frequency of approximately 11500 Hz (Fig. 7.7). This is an improvement, as compared with the tests at 8 mm axial distance and 345 kPa gauge supercharge. At 100 psig back pressure (Fig. 7.8) there are no more distinct waves with higher amplitude, however, if the trend continues, then moving the resonance tube closer to the injector nozzle should improve the situation.

There were two trends shown in shock waves development which are promising. The first is that the closer is the tube to the injector, the higher can be the back pressure and still the resonating shock waves could be created. Second, the higher is the back pressure at which the resonating waves are being formed, the higher wa,s the amplitude of the waves, and the larger the irreversible effect emitting heat to the gas. The frequency of the waves did vary and the most likely cause of this is that the recording was taken during some of the later injections of the test cycle, and therefore the concentration of

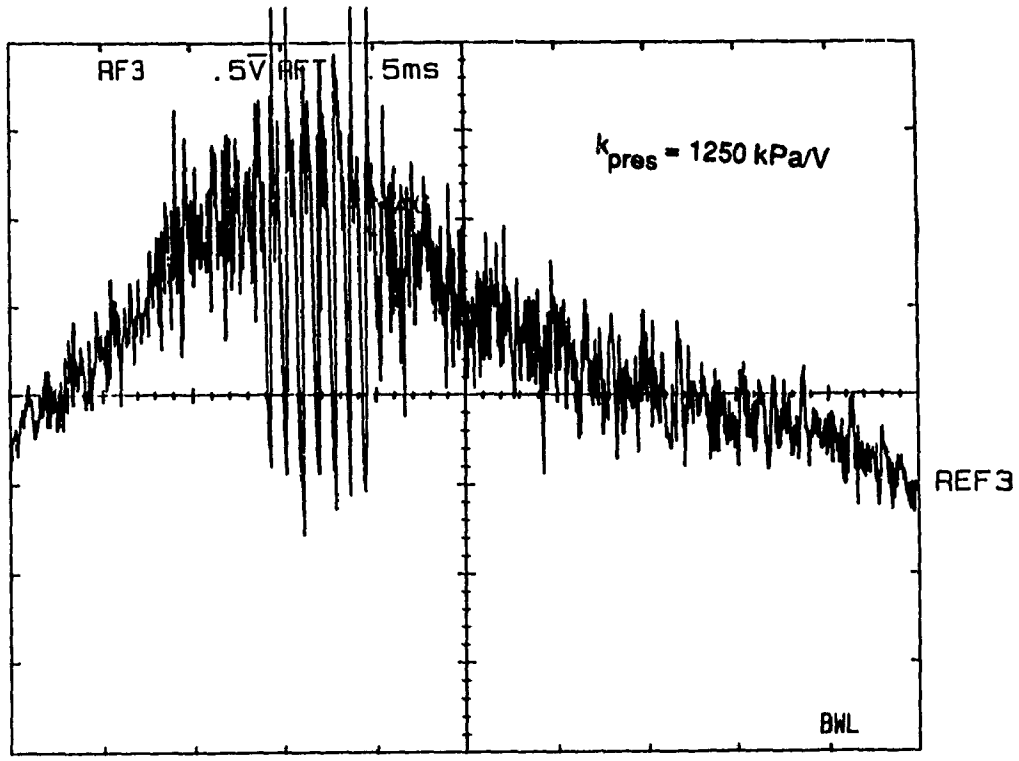

Figure 7.7 Pressure Record at 345 kPa gauge Back Pressure and Δx = 6 mm.

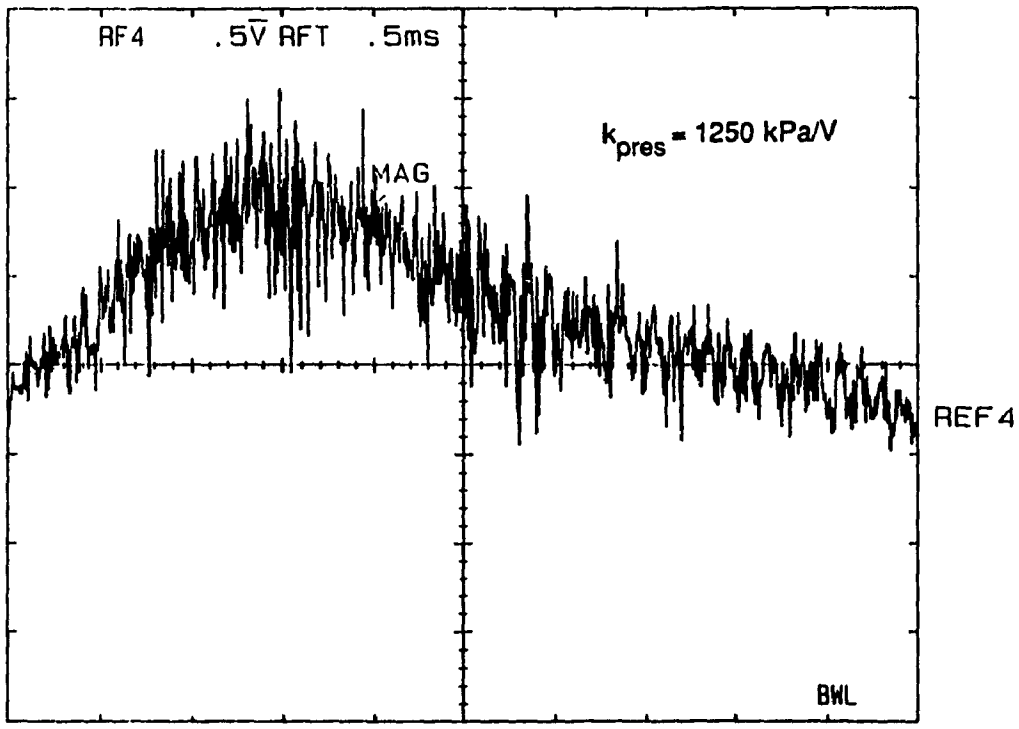

Figure 7.8 Pressure Record at 690 kPa gauge Back Pressure and Δx = 6 mm.

hydrogen was higher in the chamber, increasing the frequency.

Figures 7.9 to 7.12 show some sample results of shock waves when the axial distance was reduced to 4 mm. Similar comments as before can be made.

Reducing the axial distance to 2 mm showed some different results. At atmospheric pressure (Figure 7.13) there was no development of resonating waves until the injector began to close. At 345 kPa gauge (Figure 7.14) the shock waves did develop at an amplitude of 2700 kPa and a frequency of 10500 Hz. The next two oscillograms showed how the shock waves deteriorated with increasing back pressure. Figure 7.15 shows the record for the back pressure at 60 psig and Figure 7.16 for the back pressure of 520 kPa gauge. At 690 kPa gauge (not shown) the shock waves again were not developing. For an axial displacement of 1 mm, the shock waves are shown in Figures 7.17 to 7.24 , the waves were still noticeable even at 2100 kPa gauge back pressure (Figure 7.24). The next step would be to increase the pressure farther, as well as exchanging the air for each injection and increase the temperature in the hope of obtaining ignition, however the test set-up could only accomplish this when the piston is reciprocating. Such tests were made and will be described in the next chapter.

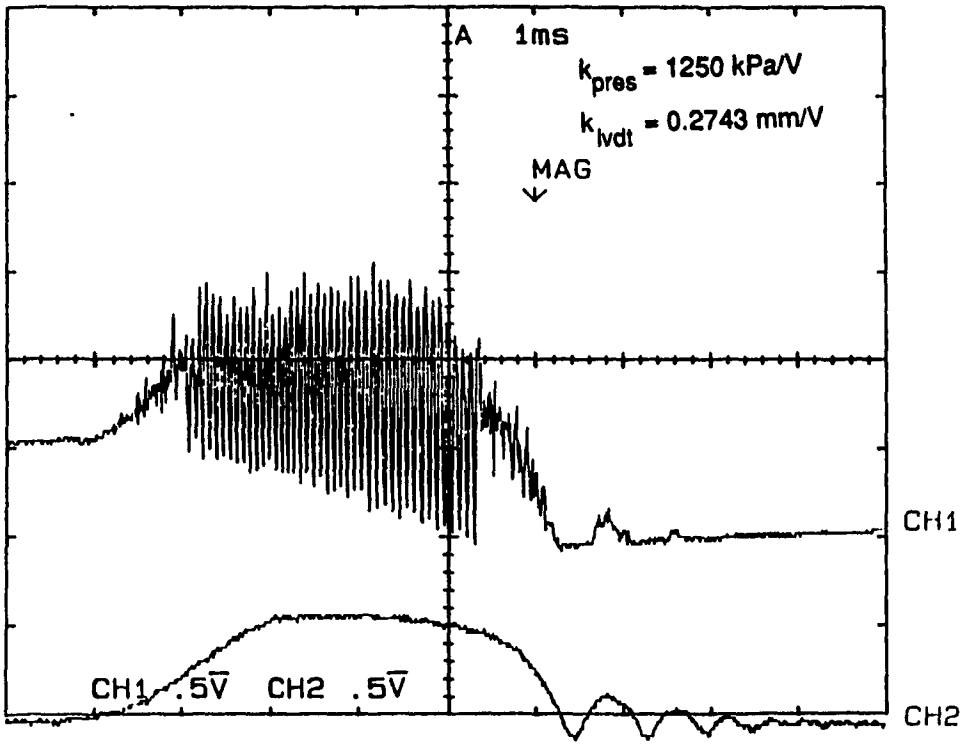

Figure 7.9 Typical Pressure and Nozzle Lift Record for Injection in a Closed Chamber at Atmospheric Conditions at Δx = 4 mm.

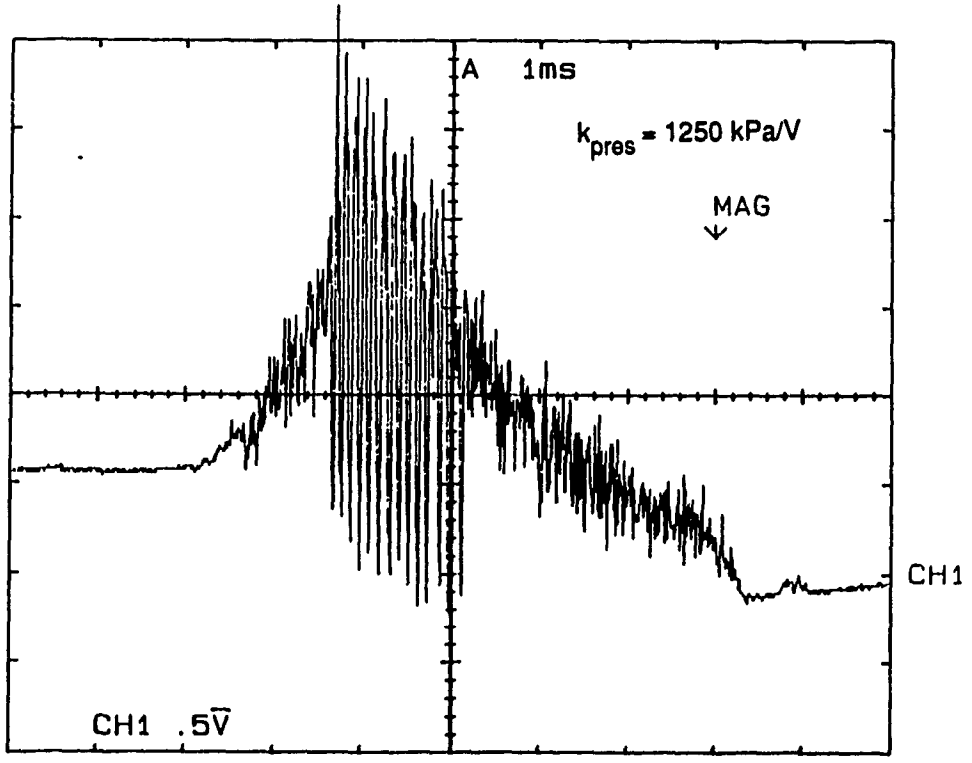

Figure 7.10 Pressure Record at 170 kPa gauge Back Pressure and Δx = 4 mm.

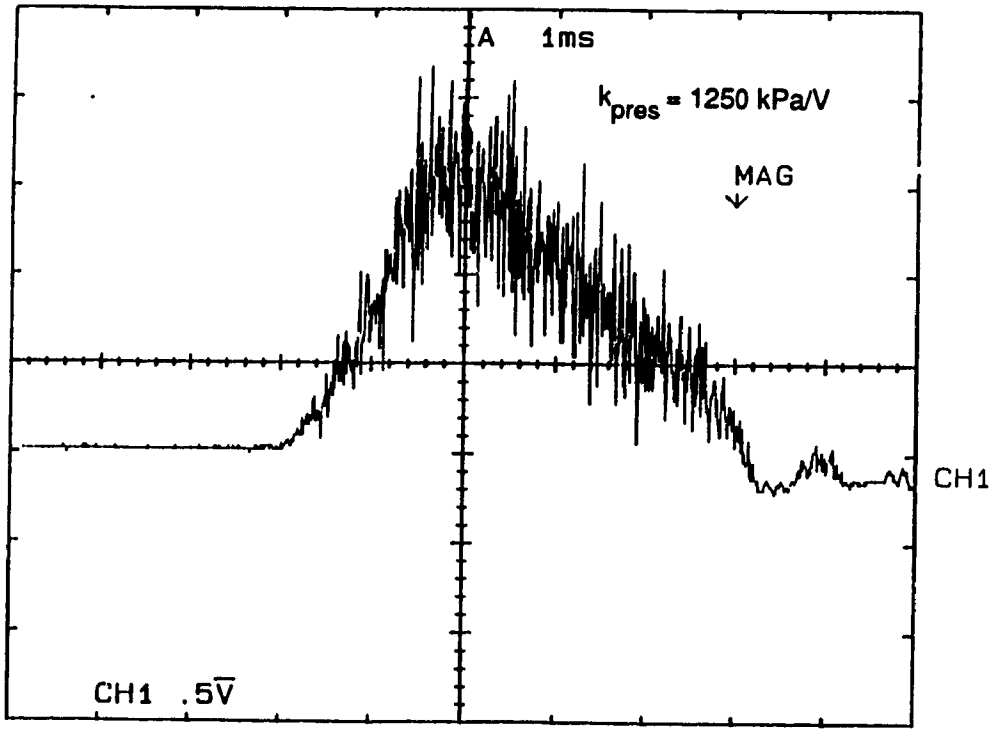

Figure 7.11 Pressure Record at 345 kPa gauge Back Pressure and Δx = 4 mm.

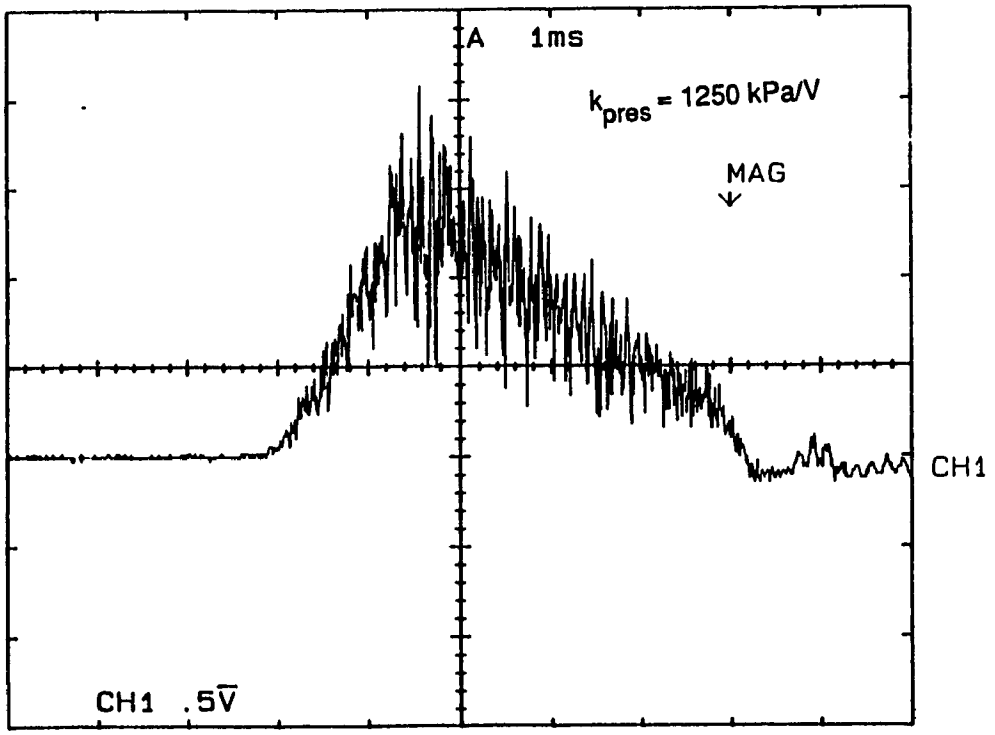

Figure 7.12 Pressure Record at 690 kPa gauge Back Pressure and Δx = 4 mm.

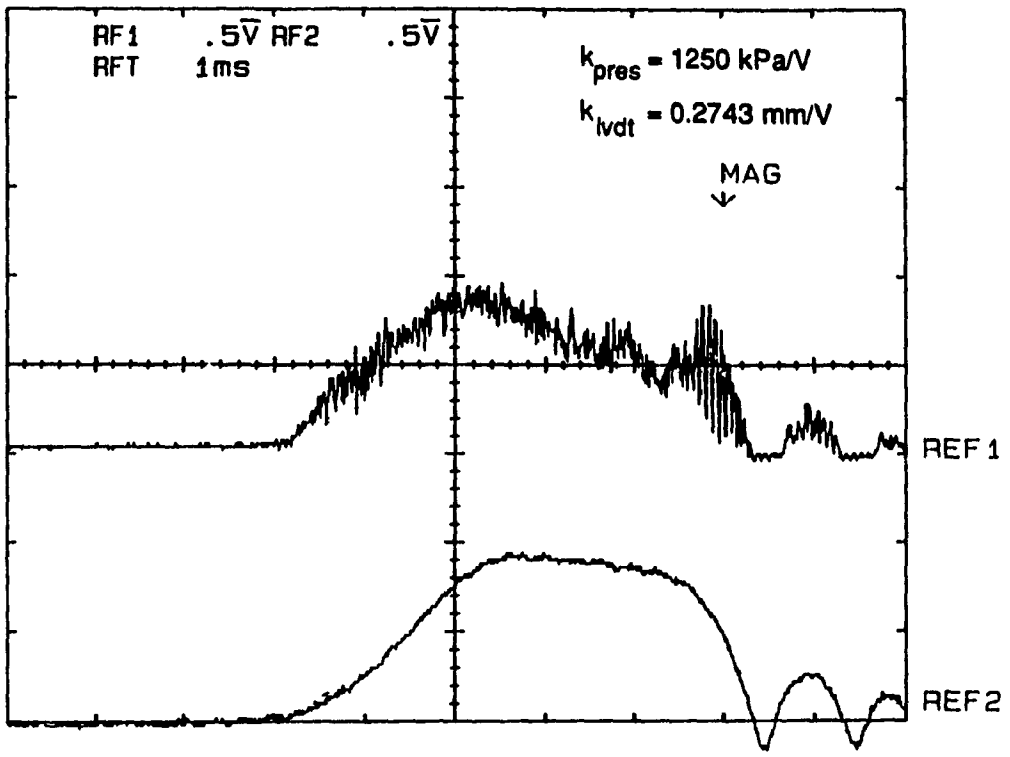

Figure 7.13 Typical Pressure and Nozzle Lift Record for Injection in a Closed Chamber at Atmospheric Conditions at Δx = 2 mm.

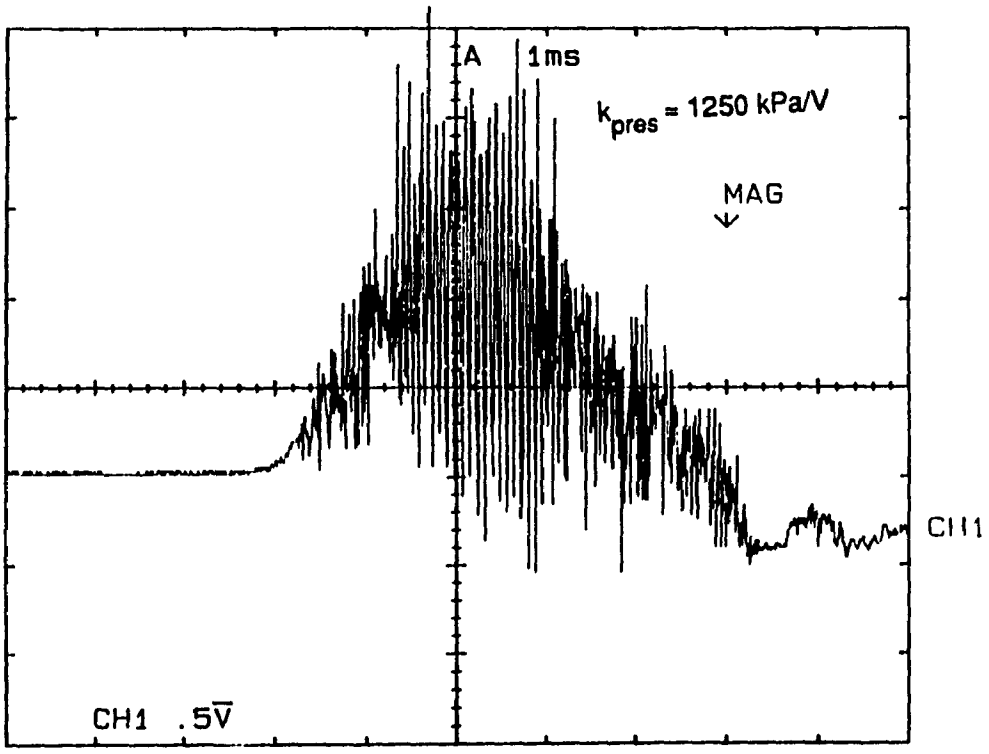

Figure 7.14 Pressure Record at 170 kPa gauge Back Pressure and Δx = 2 mm.

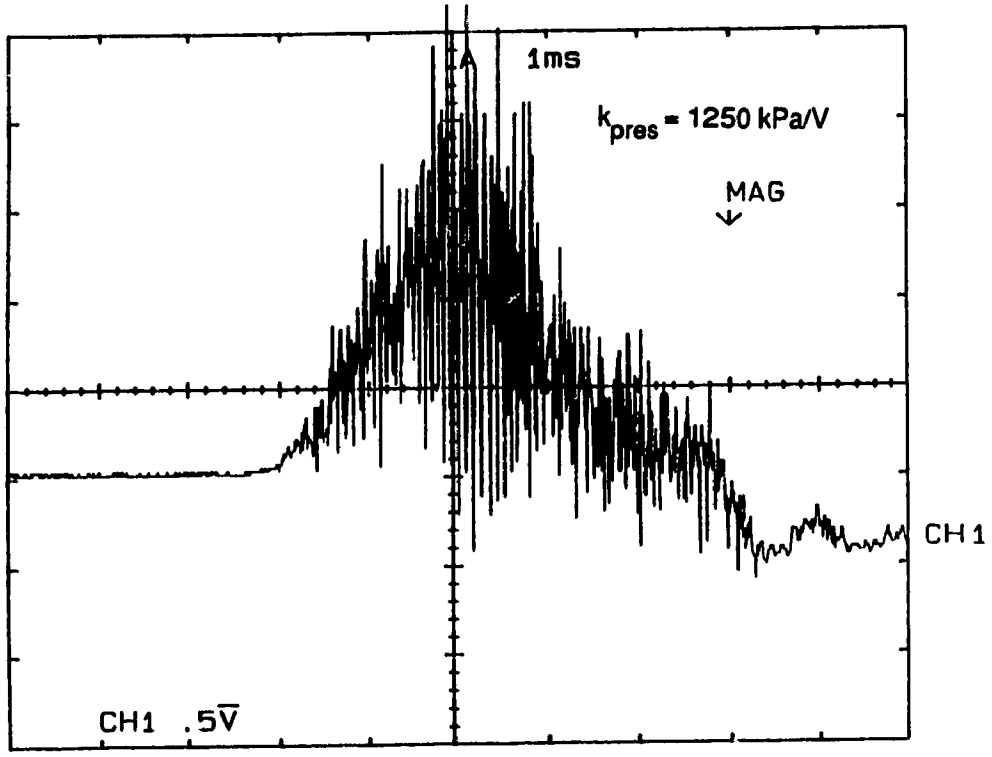

Figure 7.15 Pressure Record at 345 kPa gauge Back Pressure and Δx = 2 mm.

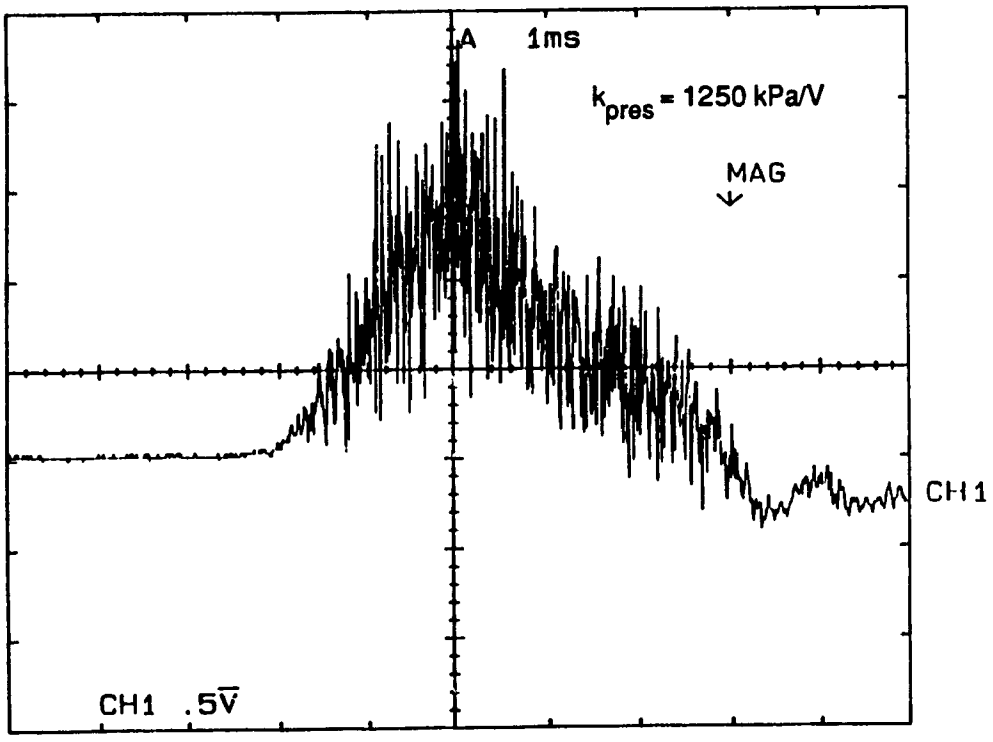

Figure 7.16 Pressure Record at 690 kPa gauge Back Pressure and Δx = 2 mm.

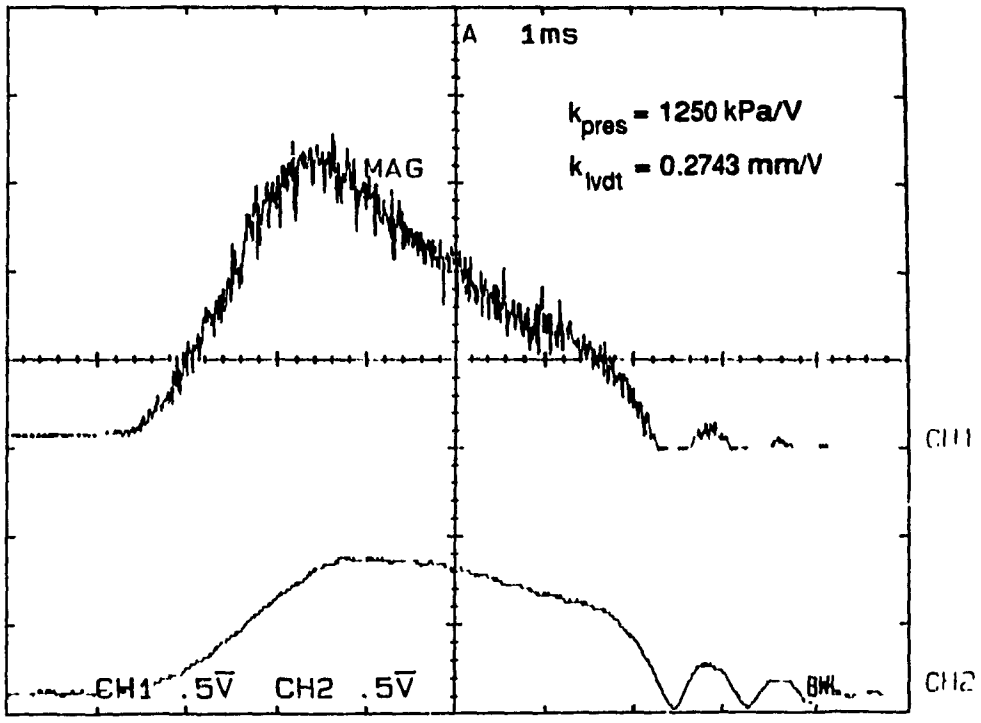

Figure 7.17 Typical Pressure and Nozzle Lift Record for Injection in a Closed Chamber at Atmospheric Conditions at Δx = 1 mm.

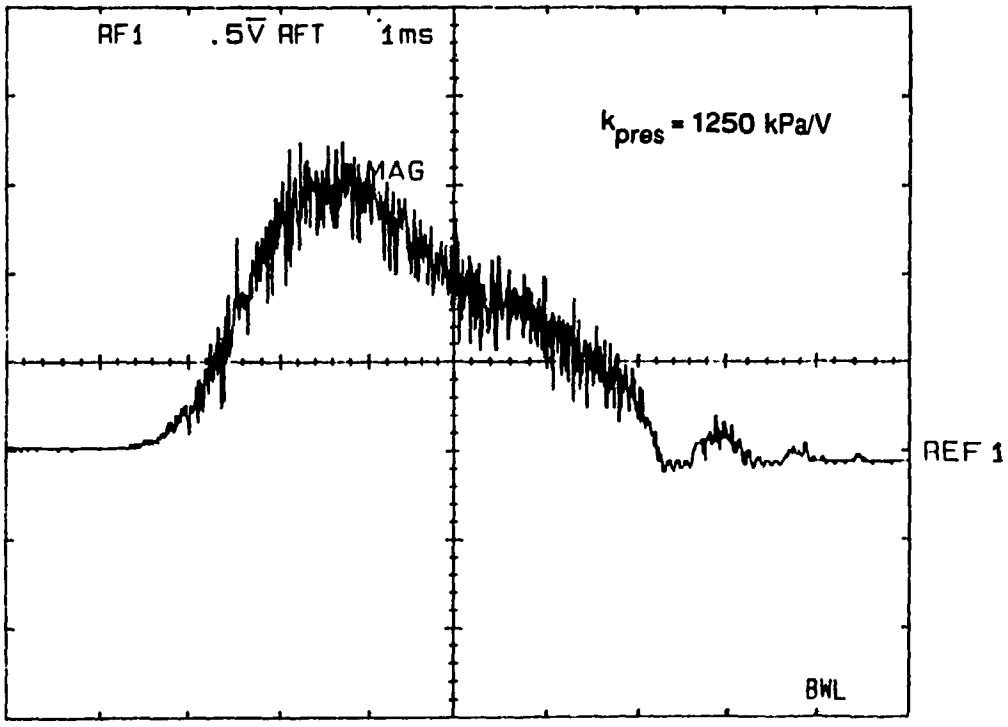

Figure 7.18 Pressure Record at 170 kPa gauge Back Pressure and Δx = 1 mm.

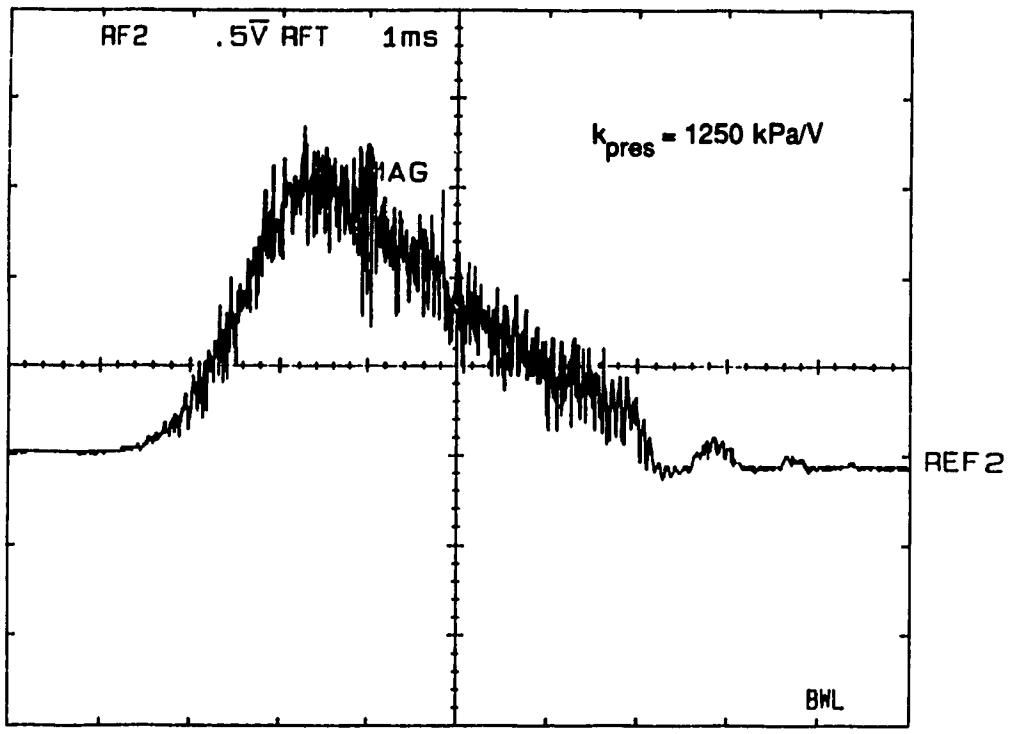

Figure 7.19 Pressure Record at 345 kPa gauge Back Pressure and Δx = 1 mm.

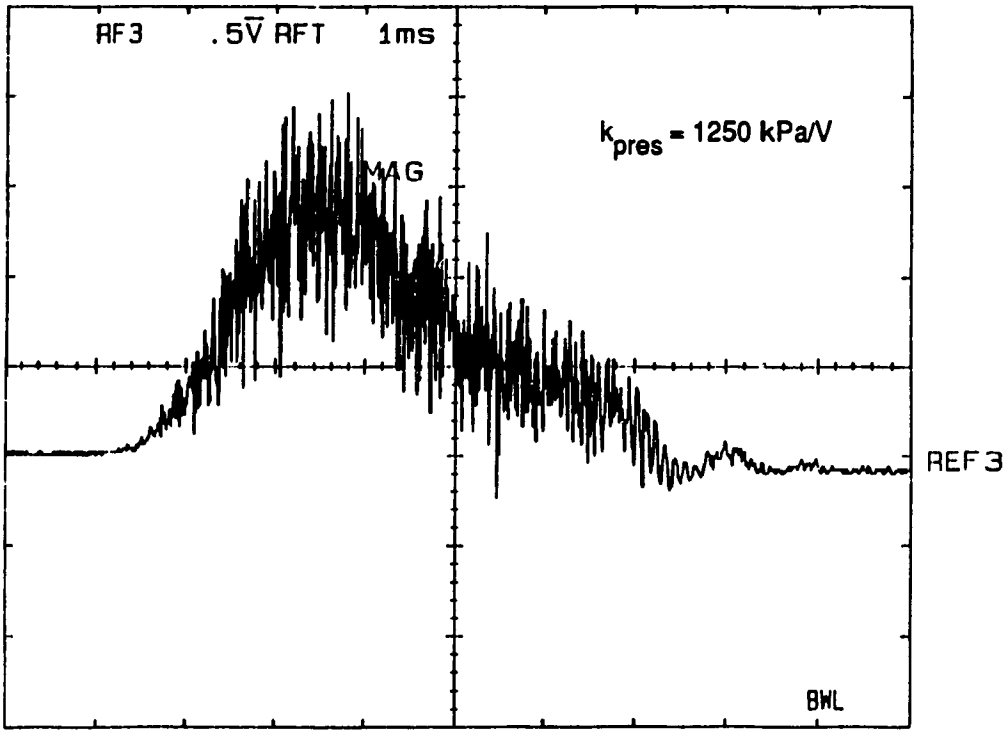

Figure 7.20 Pressure Record at 690 kPa gauge Back Pressure and Δx = 1 mm.

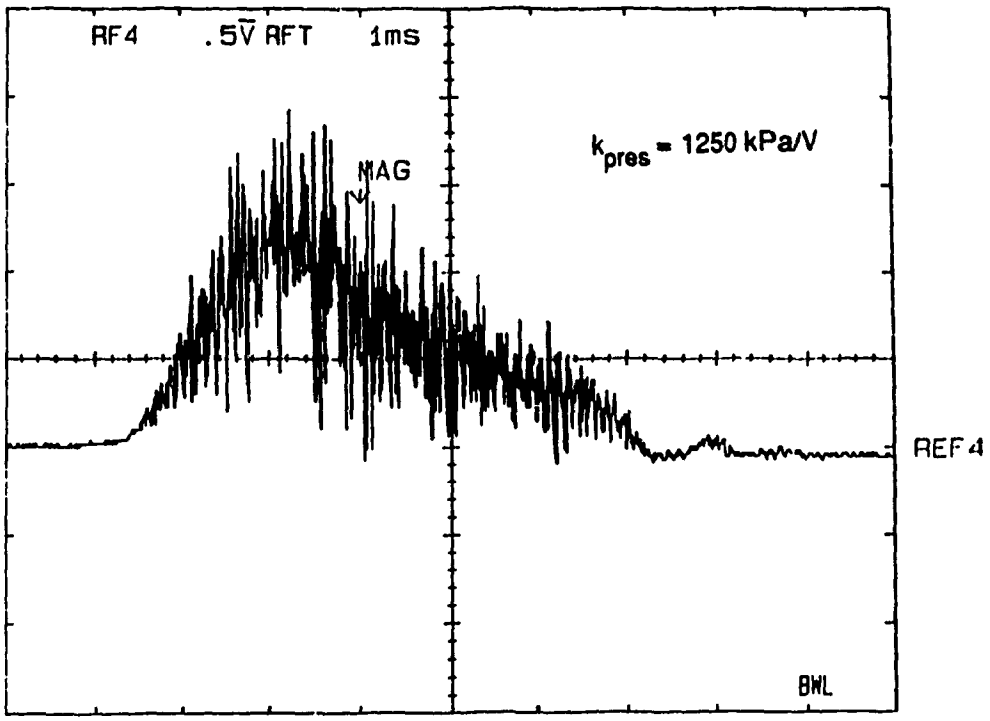

Figure 7.21 Pressure Record at 1035 kPa gauge Back Pressure and Δx = 1 mm.

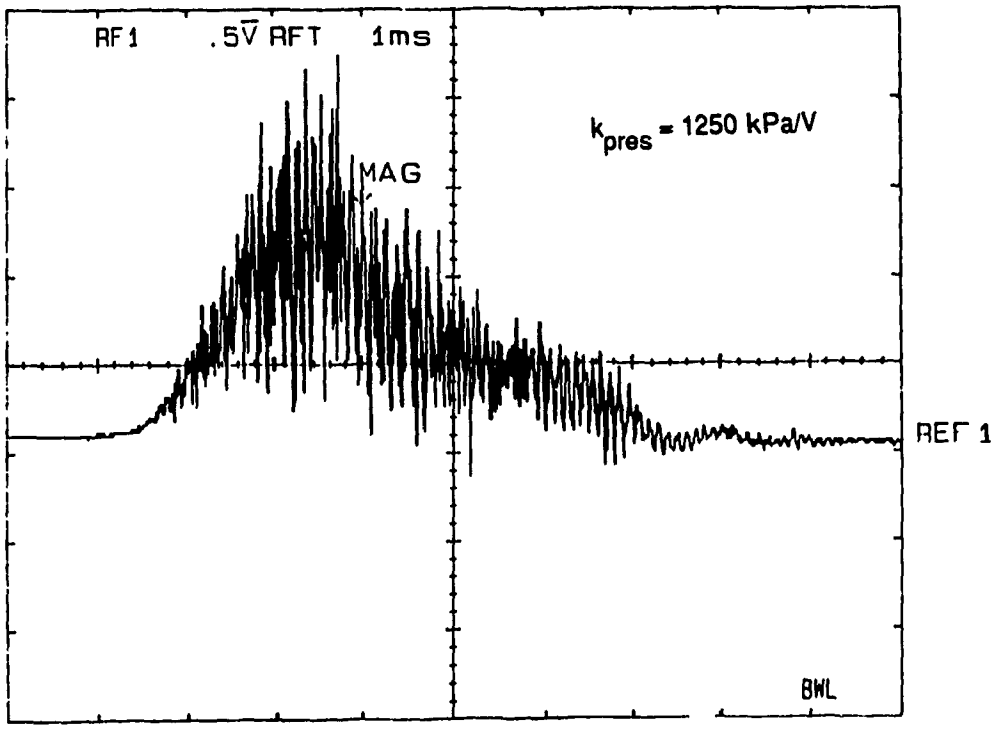

Figure 7.22 Pressure Record at 1380 kPa gauge Back Pressure and Δx = 1 mm.

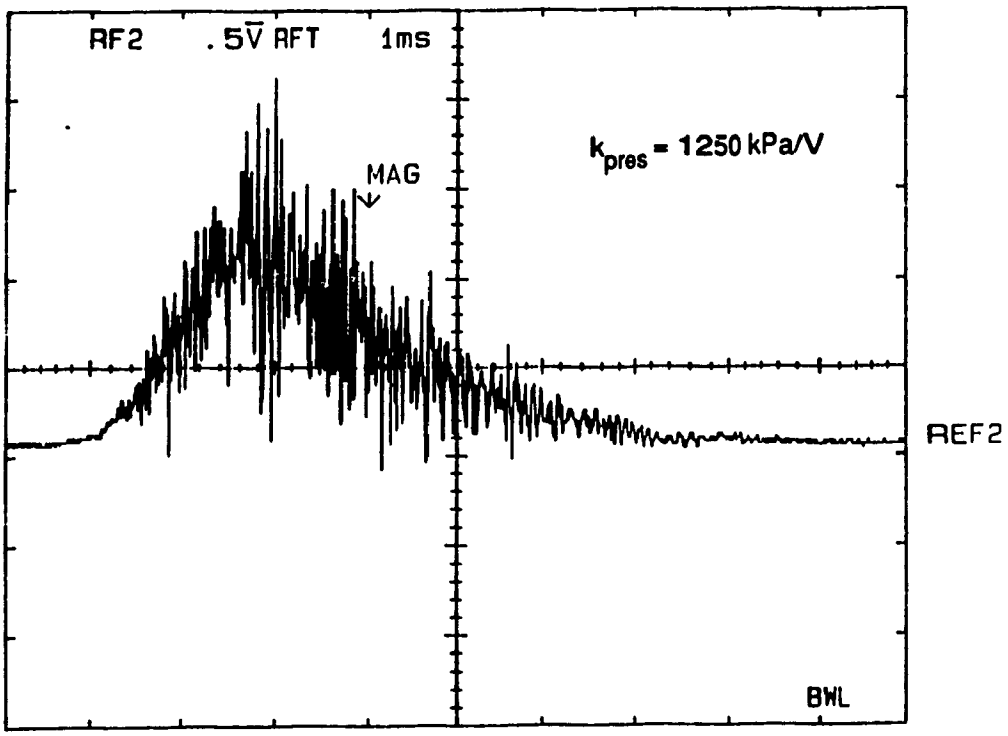

Figure 7.23 Pressure Record at 1725 kPa gauge Back Pressure and Δx = 1 mm.

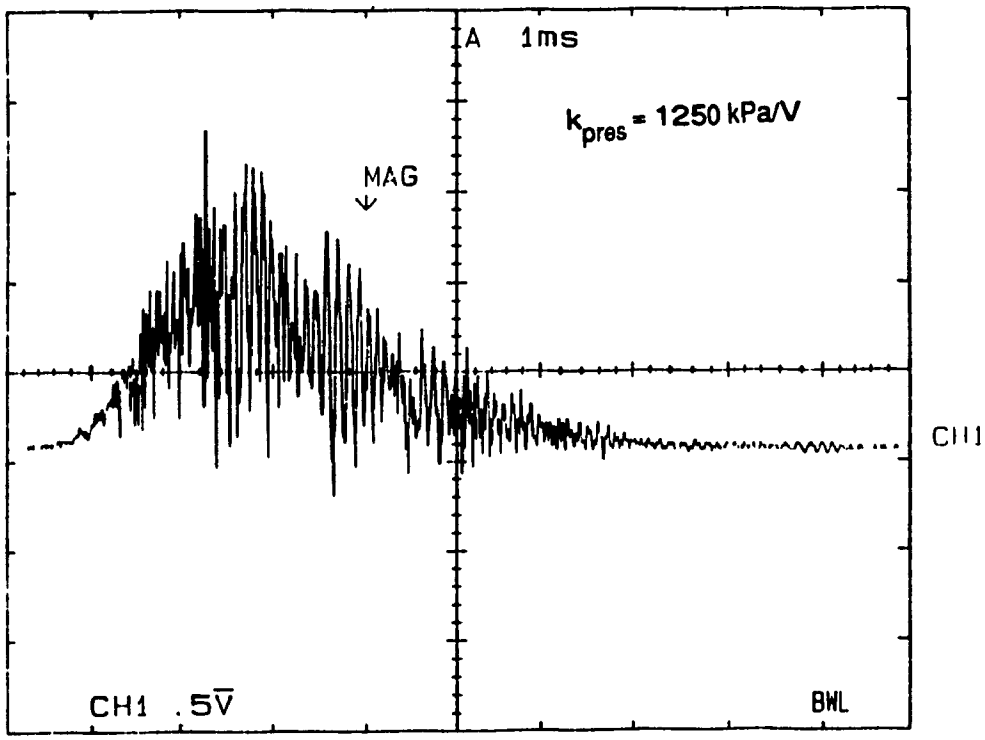

Figure 7.24 Pressure Record at 2070 kPa gauge Back Pressure and Δx = 1 mm.

To summarize the results described in this chapter, it was found that there is a difficulty in trying to create high amplitude resonating shock waves in the resonance tube when the pressure in the chamber is high. Reducing the gap between the nozzle and the resonance tube did help, however there seem to be a limitation to such action. There can be many reasons for this behavior, such as that there is too great dissipation of jet energy resulting in the reduction of the penetration of the gas flowing out of the injector,and therefore the flow cells described in Chapter 4 may be affected by the higher back pressure. Another possible reason is that the core pressure of the gas is too strong so that the waves cannot resonate out of the tube easily and commence another cycle. This set-up was not designed to study these effects, but it seems to be important to study these phenomena in future research.

CHAPTER 8

8. EXPERIMENTAL INVESTIGATION OF RESONANCE TUBES IN A RECIPROCATING ENGINE

The next step in the experiments was to test the performance of the resonance tubes in a chamber in which the volume is changing, the mass of air is exchanged between injections and the pressure and temperature are above ambient, that is in the conditions of a reciprocating engine's combustion chamber.

The conditions mentioned have been obtained using the test engine set-up described in Chapter 5. They more closely matched those existing in a diesel engine, however, the pressure and temperature levels were not reaching these of a diesel engine.

The test results from this chapter will show the same trends that were observed in the previous chapter. That is if the injection occurred into air at lower pressure, the tube would have to be located at a greater distance from the injector nozzle and it was also easier to develop the resonating waves. By varying the point of injection this trend was evident. Increasing the air inlet pressure had the same effect; a the higher pressures, it was also much more difficult to create the resonating waves.

Another phenomena was the non repeatability, from

injection to injection, of the resonating waves when operating with a supercharge and injecting hydrogen late in the compression cycle. The high pressure seemed to have a detrimental effect on development of the waves and this was compounded with several other factors cited in this chapter resulting in the increase of the non repeatability in creating the pressure waves.

No ignitions were observed in any of the tests performed, however heating of the resonance tube and its holder were well observed. After removal and disassembly of the unit from the cylinder head, the holder had undergone thermal expansion and was difficult to remove; it was also difficult to handle due to the high temperature. This heating was not observed when the engine was running without injections.

8.1 Test Methodology

The testing methodology consisted of setting an axial distance between the injector nozzle and the resonance tube which was selected according to the data obtained from the tests under higher pressure, as described in Chapter 7. The metering valve opening was also fixed. The variables for these tests were the gas doses injected, as well as the level of pressurizing the intake air.

The first two variables mentioned above were a function of the control code described in Chapter 5 and given in Appendix B. The third variable was obtained by bringing pressurized shop air into the engine; the factor limiting the supercharging pressure was the steady state mass flow rate which could be supplied for the particular engine speed.

During the tests, the beginning of injection was varied, while the injection duration was maintained constant. The pressure at the end wall of the resonance tube was recorded, as well as, either the engine chamber pressure, needle lift or the injector pressure. Varying of the beginning point of injection, also affected the pressure and temperature of the air into which the hydrogen was being injected.

The next step was to readjust the distance between the injector nozzle and the resonance tube and to repeat the above procedure. This was done because, as we saw in Chapter 7, the lower was the back pressure, the larger should be the axial distance from the nozzle to the mouth of the resonance tube, to obtain the best results in terms of wave pressure amplitude and development.

During these tests, the nozzle used was the one chosen in Chapter 5 with small pintle extension on the needle, as well as the resonance tube with a depth of 20 mm and a hole diameter of 2 mm.

8.2 Apparatus for Tests in a Reciprocating Piston Engine

The set up used for testing of shock waves in a reciprocating engine has been described in Chapter 5. During these tests, the engine was driven by the electric motor, thereby simulating the conditions in a reciprocating piston engine. The electric motor was a 5 HP, 3 phase, 60 HZ, 220 V motor built by G.E.C. Small Machines Ltd. The rotational speed of the motor was controlled by a variable electric motor controller A-C V*5 Drive Controller built by Reliance Electric Inc. The controller was set to manual operation and the engine rotational speed was varied by the operator. A speed potentiometer varied the frequency of revolution of the motor and the readings were displayed on a LED readout of the controller.

The control software required to be modified whenever one of the variables was changed. A fully developed controller would contain engine maps to obtain the values of the injection parameters under specific operating conditions. The control hardware would read the engine speed and piston position from the magnetic and optical pick ups placed on the engine shaft. For a multicylinder, 4-stroke, engine an extra input would be required to determine not only the piston position, but also whether the piston is in its compression stroke or exhaust stroke. The set up did not distinguish

between the two strokes and if injections were occurring during the exhaust stroke, then by passing an inverter on the control board after the divide-by-two flip flop circuit would correct the problem.

The injector was instrumented with an LVDT to measure nozzle lift and a piezoelectric pressure transducer to measure the pressure of hydrogen in the injector. The cylinder head was equipped with a pressure transducer as well as the safety valve. The resonance tube had a pressure transducer at the end wall and was placed in a holder which aligned the resonance tube axially with the injector nozzle and could vary the axial distance from the nozzle.

8.3 Test Results and Discussion

The first tests were performed with a reciprocating piston but with no intake air supercharging. The first variable was the beginning point of injection, which was varied from 90 degrees before TDC, when the pressure rise is minimal, to a point very close to TDC, when the ambient pressure is much higher than the initial inlet pressure. The second variable was the axial displacement between the nozzle and the mouth of the resonance tube, which was varied in values between 8mm and 1mm.

Based on the results obtained in Chapter 7, it could be

expected that the distance between the mouth of the resonance tube and the injector nozzle should somehow correspond to the pressure in the combustion chamber. However, this pressure varies with respect to time in the chamber due to the movement of the piston. This led to a situation that the distance which was set for the lower pressure at the beginning of the injection, was not the best position when injection occurred at close to the TDC piston position where the pressure in the chamber is much higher.

The results did meet the prediction with early injections; well developed resonating waves occurred at axial distance of 8 mm. (Figure 8.1) and at 4 mm. (Figure 8.2), however, at an axial distance of 2 mm. well developed waves did not materialize (Figure 8.3). Again the tube being too close to the nozzle did not create resonating pressure wave because the pressure of the gas entering the tube was too high so that it prevented the reflected wave to exit the tube and therefore the resonating cycle could not continue. The tube is situated on the first half of the jet cell as was described in Chapter 4.

Delaying the injection later in the compression stroke, that is at higher pressure, was expected to result in shock waves developing better with reduced axial

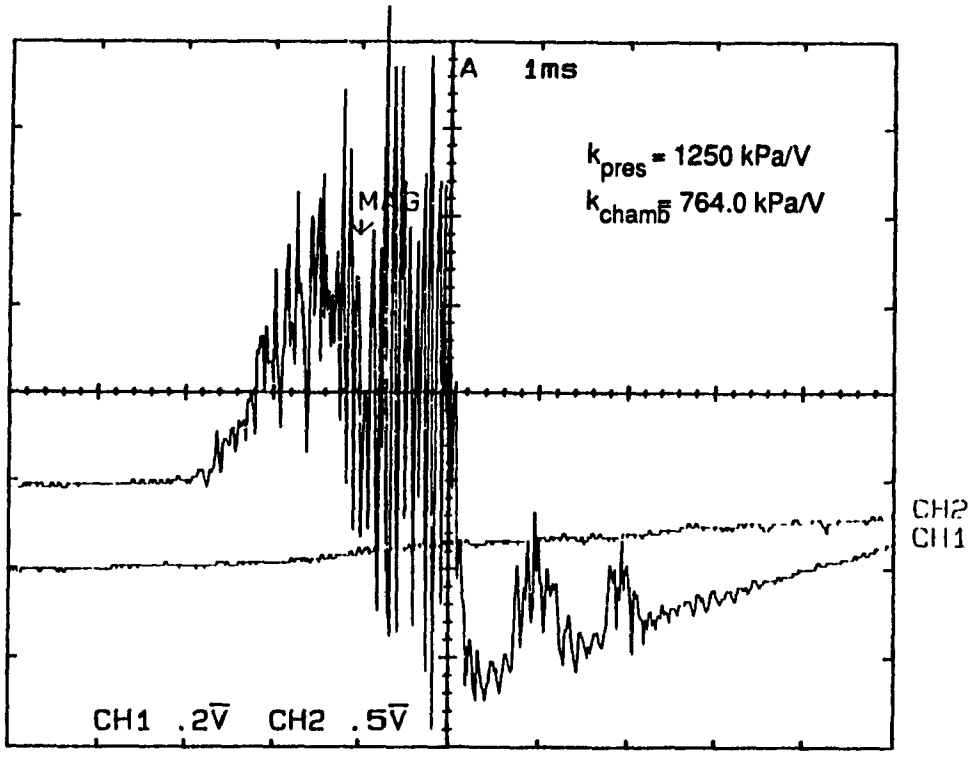

Figure 8.1 Pressure Record of Injection into the Reciprocating Piston Chamber (early injection, Δx = 8 mm, supercharge = 0 kPa gauge).

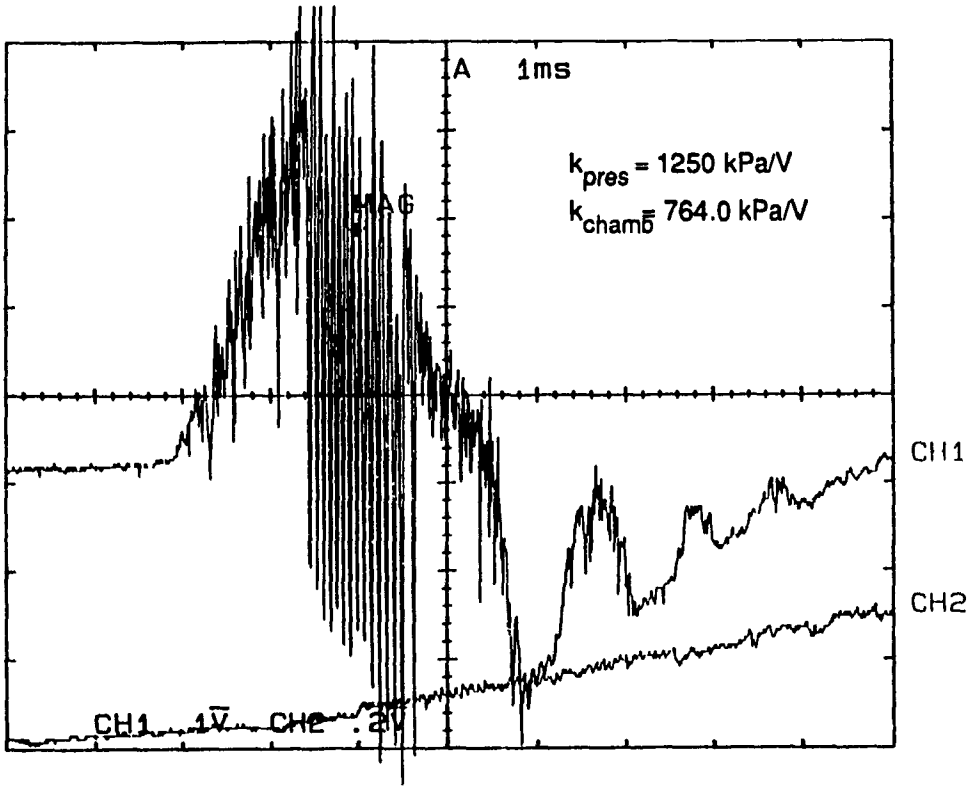

Figure 8.2 Pressure Record of Injection into the Reciprocating Piston Chamber (early injection, Δx = 4 mm, supercharge = 0 kPa gauge).

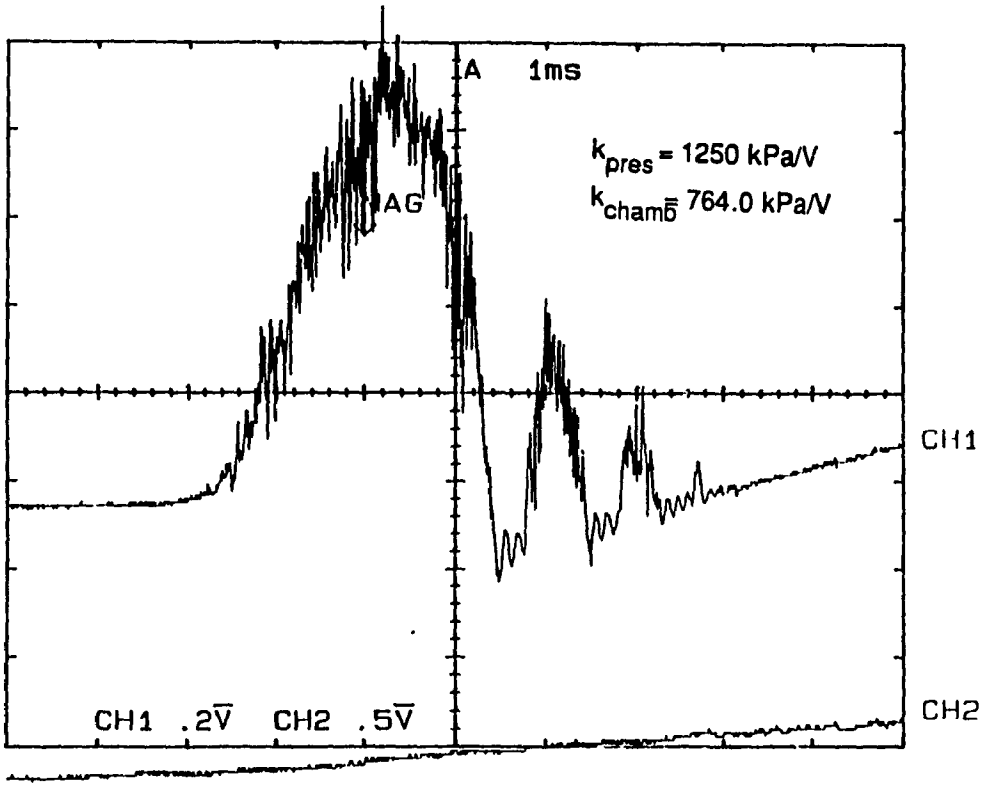

Figure 8.3 Pressure Record of Injection into the Reciprocating Piston Chamber (early injection, Δx = 2 mm, supercharge = 0 kPa gauge).

distance, and deteriorate with greater axial distance. This again occurred, and at axial displacement of 8 mm.(Figure 8.4) as well as at 2mm.(Figure 8.5) the waves did not develop as well, but at 4mm (Figure 8.6), the shock waves developed better and with a larger amplitude (N.B.different vertical scaling was used in Figure 8.4 and Figure 8.5). The same trend was expected with delaying the injection of hydrogen into the resonance tube until the piston was very close to the top dead center position. This can be seen in Figure 8.7 (8 mm), Figure 8.8 (4 mm) and Figure 8.9 (2 mm); the waves developed better for the case with the smaller axial distance than for the case with larger 4 mm. distance. The waves produced at the 2 mm distance, however were not as well developed and were of smaller amplitude than those obtained for the cases with earlier injection.

To study the resonance tube performance at increased chamber pressure by supercharging the intake air, was the next step to follow. From earlier results described in Chapter 7 and in the previous paragraphs, it was expected that the waves would not develop as well as at lower pressures, and that the axial distance must be reduced at the higher back pressures.

In the set of tests the same set up, as in the previous tests, was used, however, the intake air was

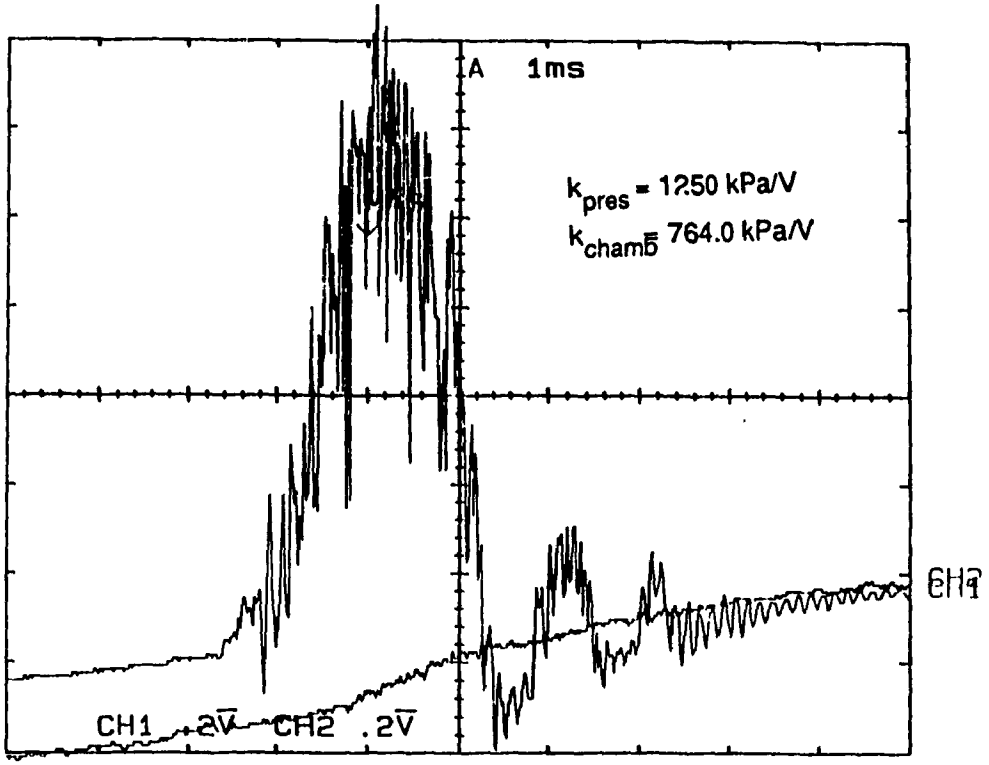

Figure 8.4 Pressure Record of Injection into the Reciprocating Piston Chamber (injection 45° BTDC, Δx = 8 mm, supercharge = 0 kPa gauge).

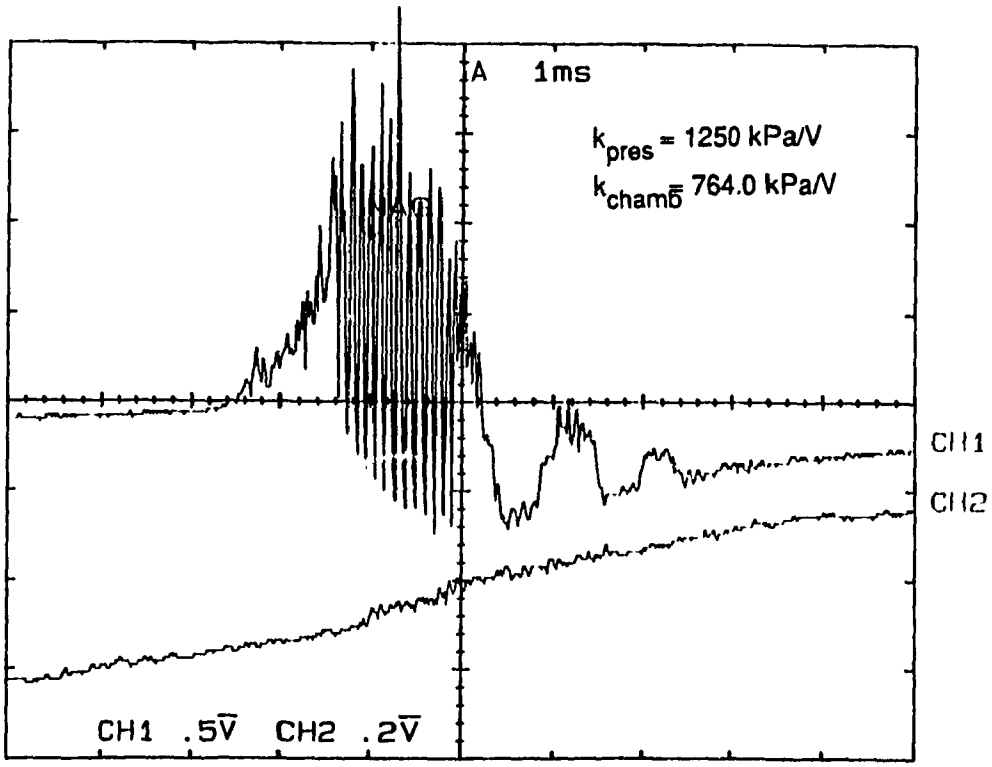

Figure 8.5 Pressure Record of Injection into the Reciprocating Piston Chamber (injection 45° BTDC, Δx = 2 mm, supercharge = 0 kPa gauge).

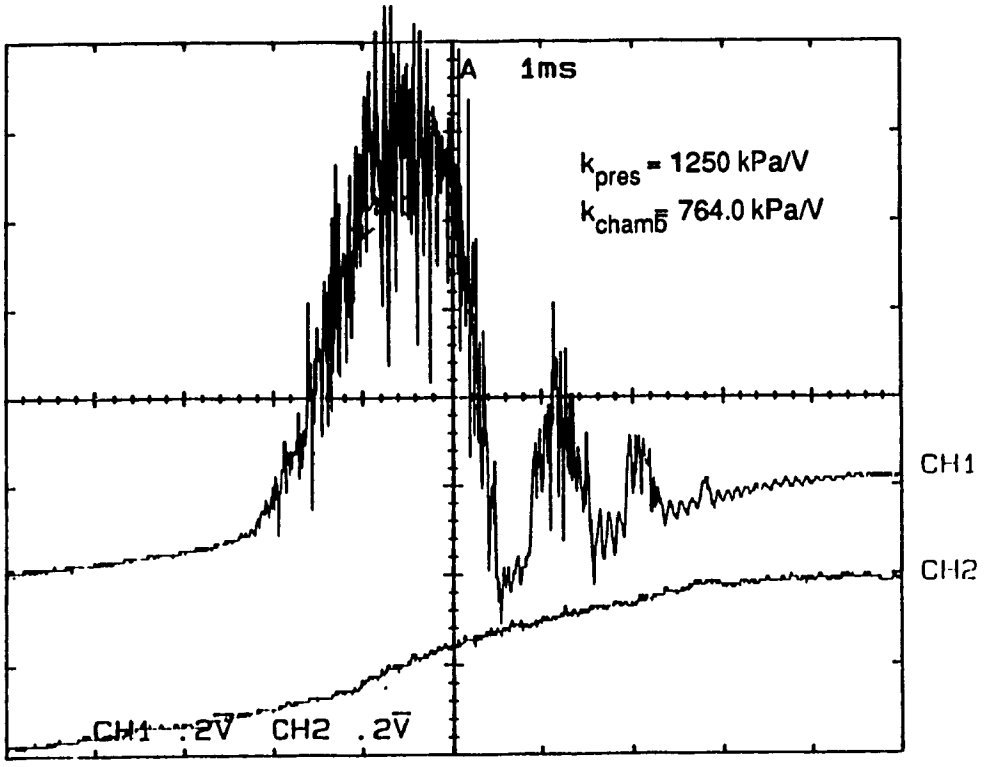

Figure 8.6 Pressure Record of Injection into the Reciprocating Piston Chamber (injection 45^{o} BTDC, Δx = 4 mm, supercharge = 0 kPa gauge).

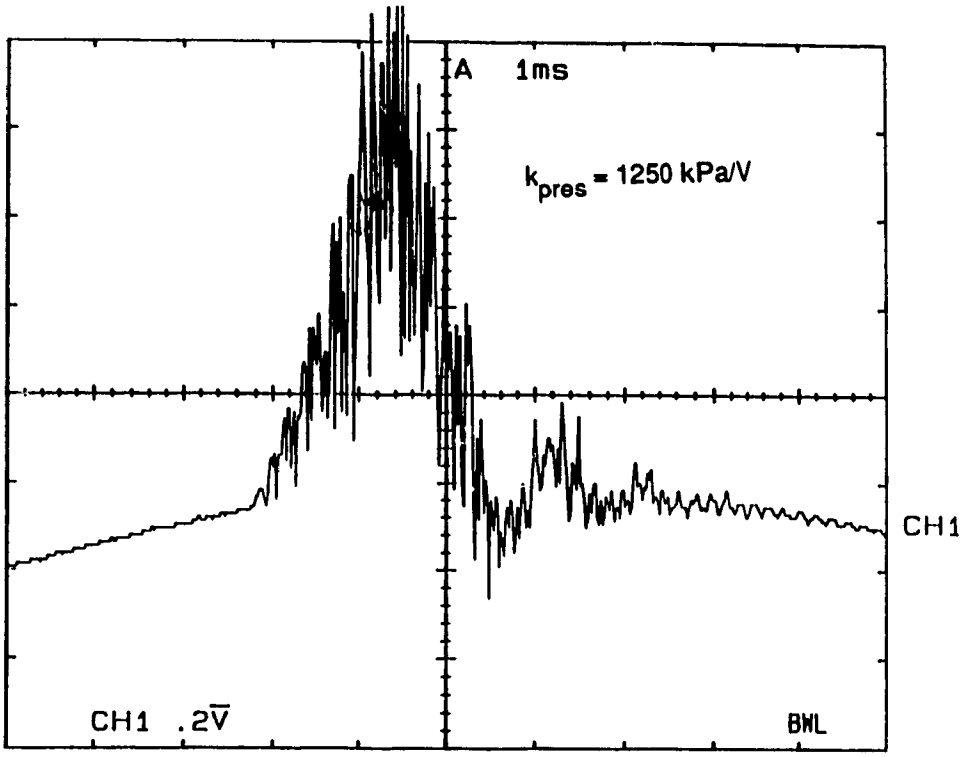

Figure 8.7 Pressure Record of Injection into the Reciprocating Piston Chamber (injection 15° BTDC, Δx = 8 mm, supercharge = 0 kPa gauge).

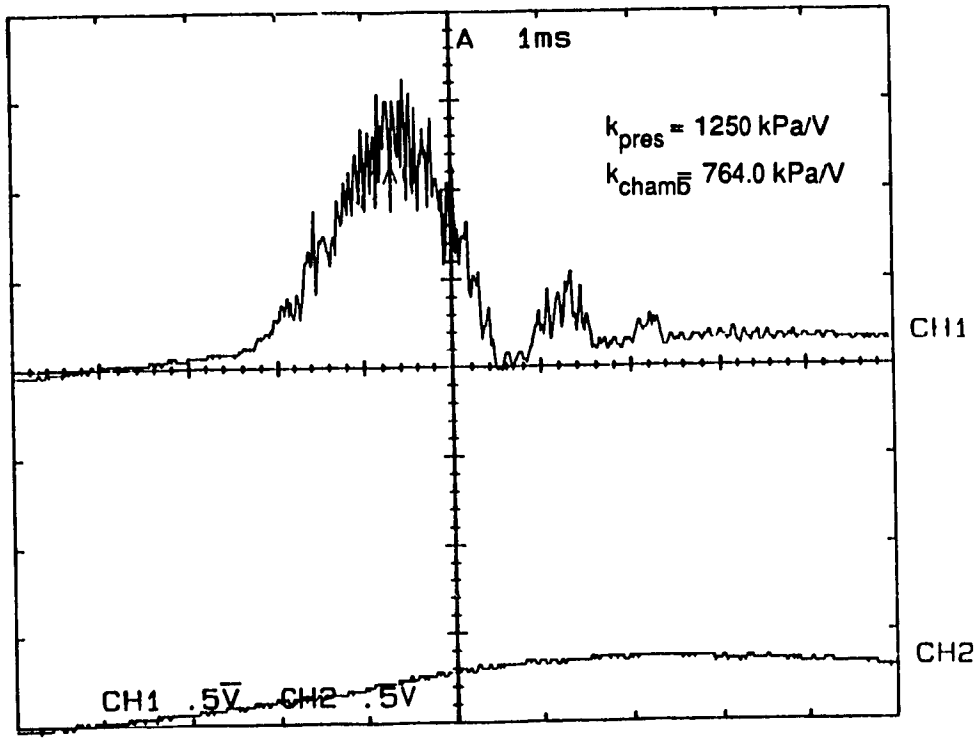

Figure 8.8 Pressure Record of Injection into the Reciprocating Piston Chamber (injection 15° BTDC, Δx = 4 mm, supercharge = 0 kPa gauge).

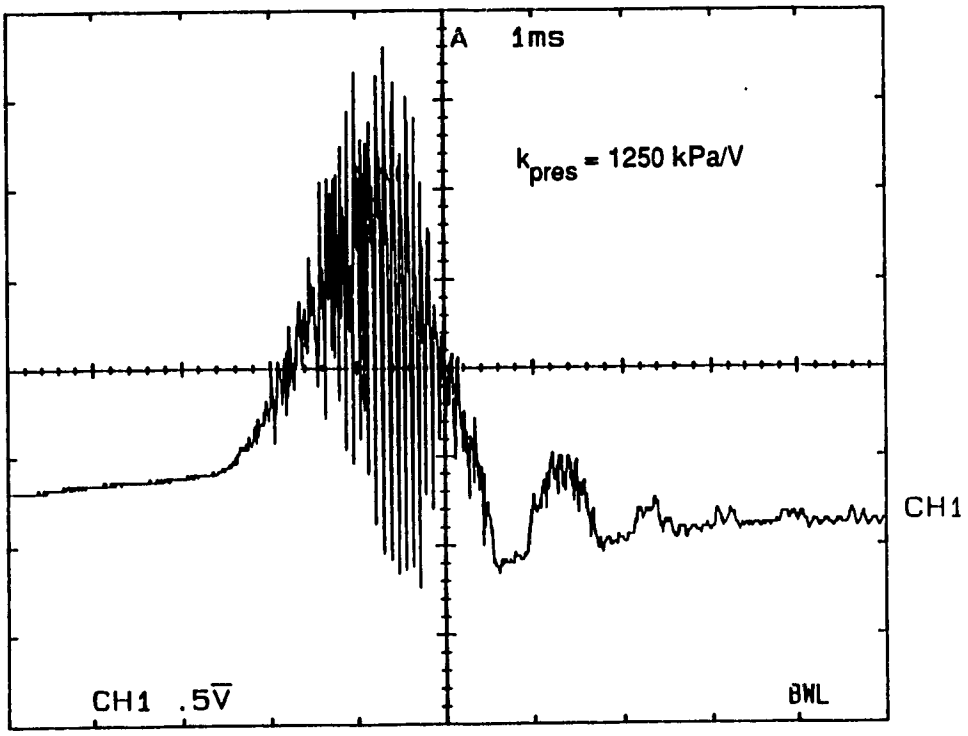

Figure 8.9 Pressure Record of Injection into the Reciprocating Piston Chamber (injection 15^{0} BTDC, Δx = 2 mm, supercharge = 0 kPa gauge).

supercharged to create higher pressure in the engine chamber. The supercharging pressure used for these tests was 100 kPa gauge (the intake pressure was then two times that of atmosphere). Again the axial distance and the point of injection were varied to see how resonance tubes would behave at higher pressure.

Figure 8.10 shows the shock waves for early injection test with the axial distance of 2 mm and with the air supercharge at 100 kPa gauge. It can be seen that the shock waves develop quite well however after moving the tube closer to the nozzle (1 mm), the shock waves were not developing, as shown in Figure 8.11.

Moving the ignition point closer to TDC suggested that the tube must be moved closer. Figure 8.12 shows the test at 2mm displacement, where the shock waves did not form, however, at 1 mm (Figure 8.13) the shock waves did develop, but at smaller amplitude than for the early injection case. The late injection case showed similar results. Figure 8.14 has an axial distance of 1 mm where Figure 8.15 has an axial distance of 2mm.

The trends that were discovered in Chapter 7, were again evident in this chapter. The shock waves did develop when hydrogen was injected into air at high pressures, however as the pressure of the air increased the axial displacement had to be reduced to create well defined high

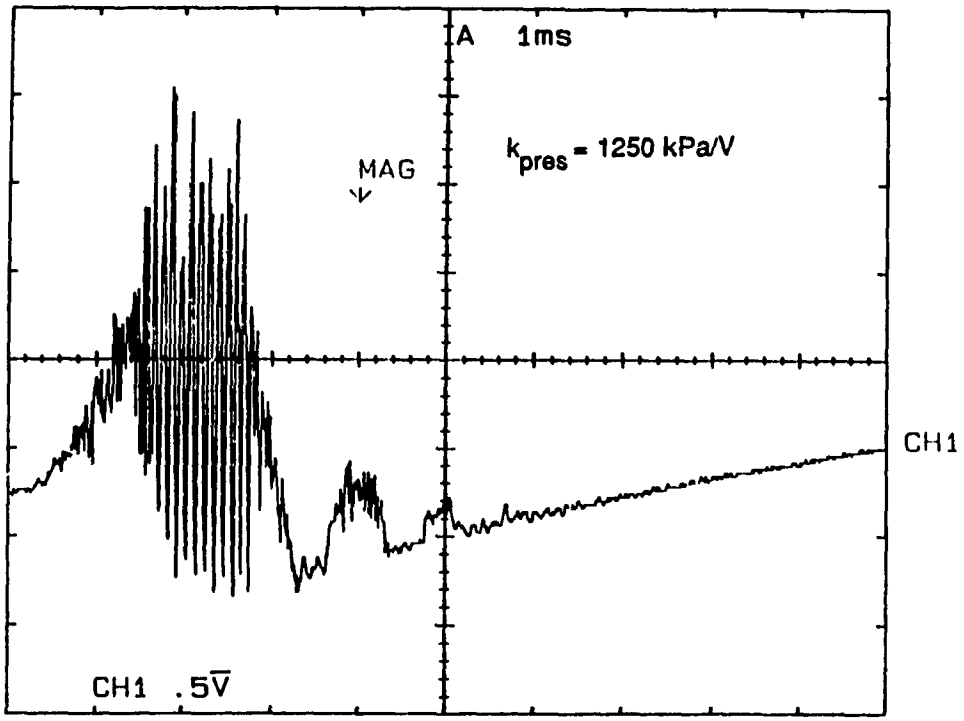

Figure 8.10 Pressure Record of Injection into the Reciprocating Piston Chamber (early injection, Δx = 2 mm, supercharge = 100 kPa gauge).

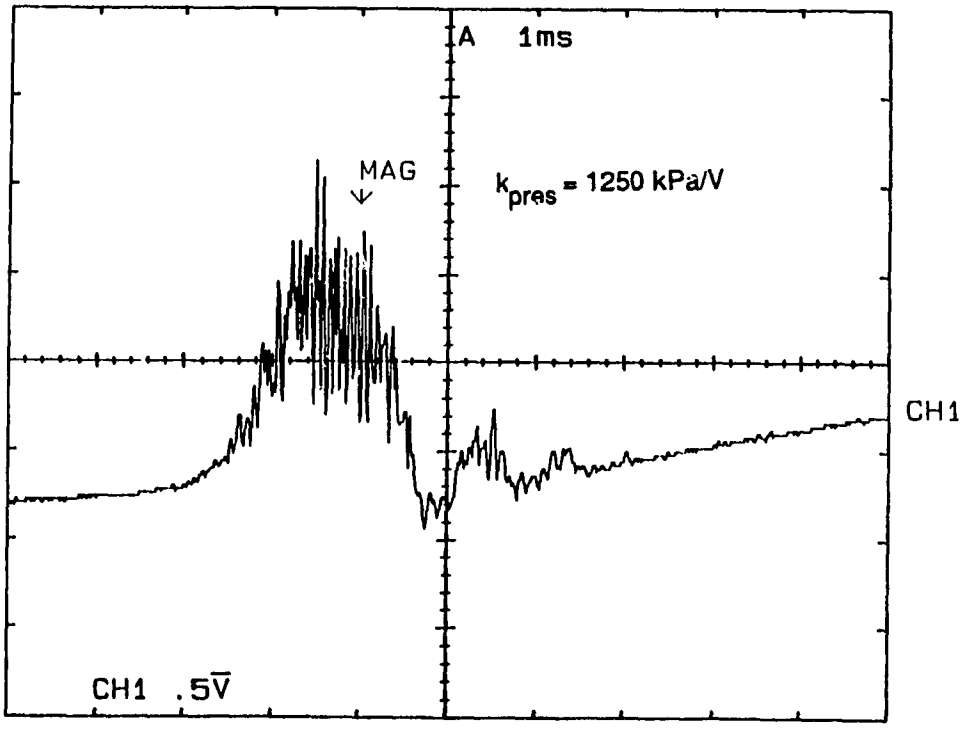

Figure 8.11 Pressure Record of Injection into the Reciprocating Piston Chamber (early injection, Δx = 1 mm, supercharge = 100 kPa gauge).

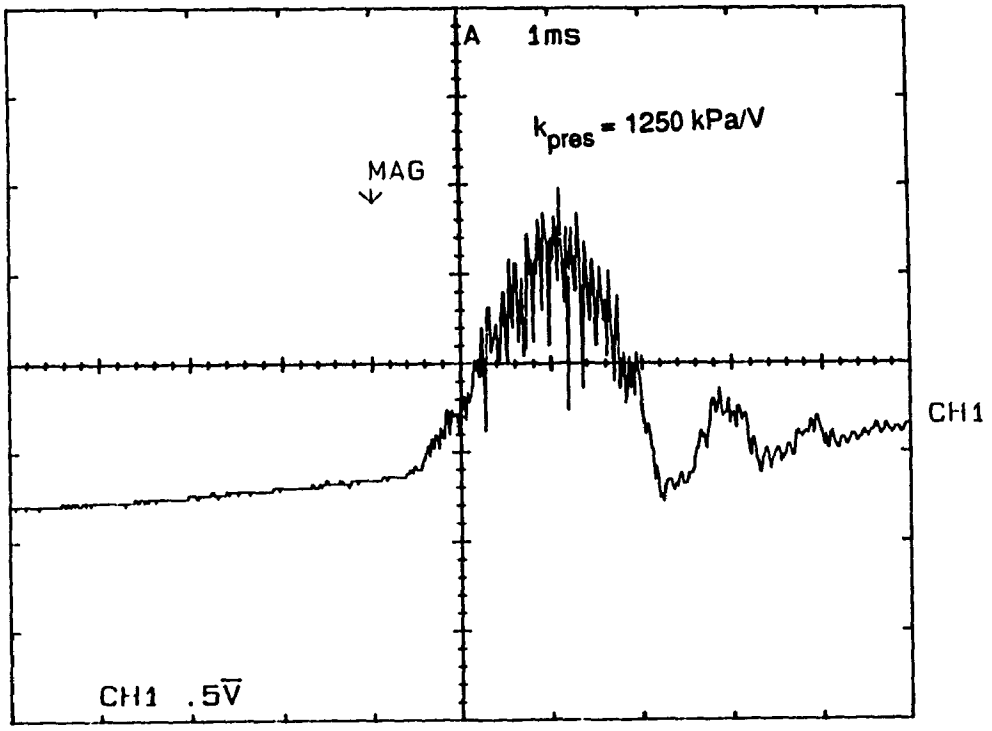

Figure 8.12 Pressure Record of Injection into the Reciprocating Piston Chamber (injection 45° BTDC, Δx = 2 mm, supercharge = 100 kPa gauge).

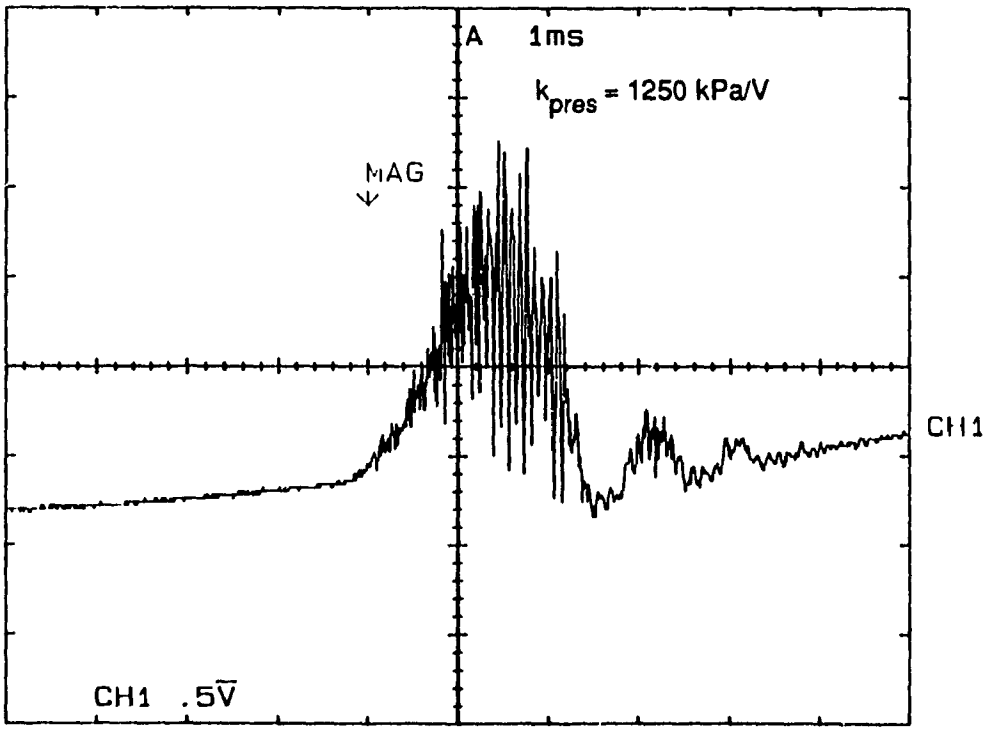

Figure 8.13 Pressure Record of Injection into the Reciprocating Piston Chamber (injection 45° BTDC, Δx = 1 mm, supercharge = 100 kPa gauge).

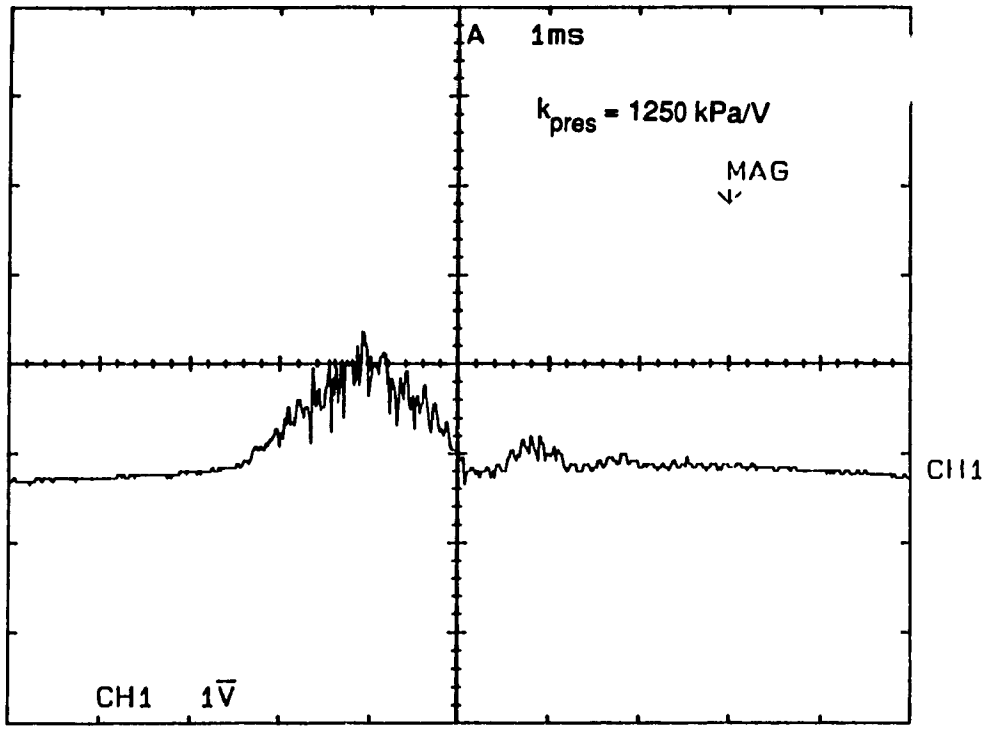

Figure 8.14 Pressure Record of Injection into the Reciprocating Piston Chamber (injection 15° BTDC, Δx = .2 mm, supercharge = 100 kPa gauge).

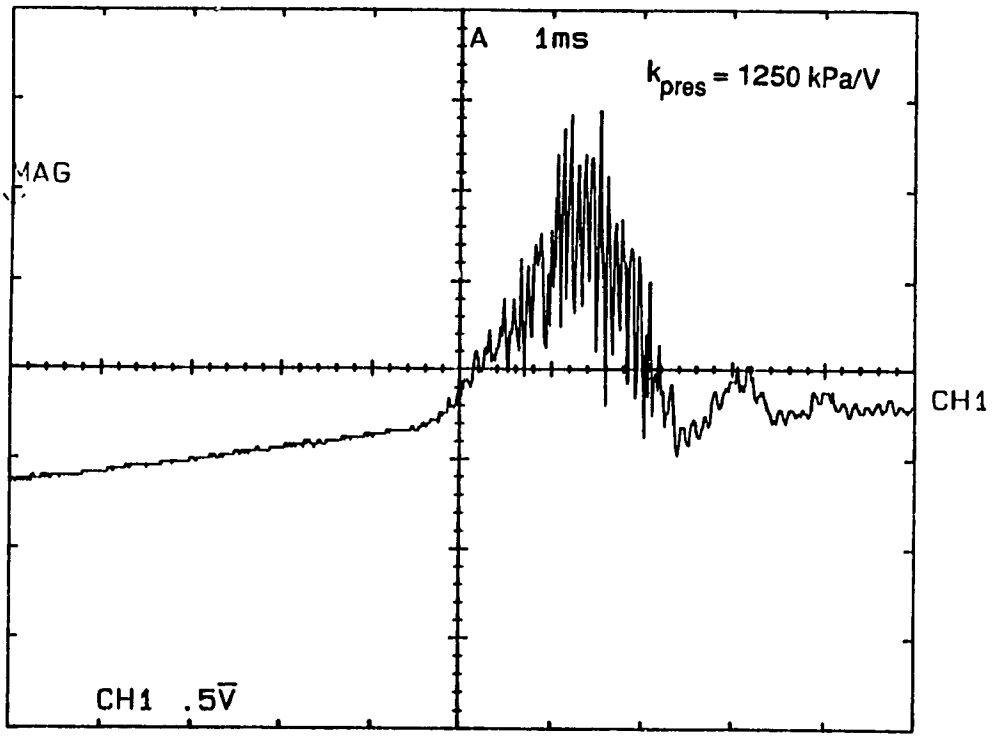

Figure 8.15 Pressure Record of Injection into the Reciprocating Piston Chamber (injection 15° BTDC, Δx = 1 mm, supercharge = 100 kPa gauge).

amplitude resonating pressure waves. Also, at a certain higher pressures, it was not possible to create high amplitude resonating waves and, at some point, to create the shock waves at all.

During the tests it was observed that the pressure records did not repeat well in the reciprocating engine. This can be attributed to the following factors; in a reciprocating single cylinder engine, the intake conditions are varying for particular cycles due to pressure waves created in the intake manifold by the opening and closing of the intake valve, second there are pressure waves present in the combustion chamber because of the movement of the piston, and third, vibration of the resonance tube with respect to the nozzle orifice can cause misalignment of the orifices.

To answer these result variations several records were taken for the same working conditions and typical pressure wave records were chosen for further analysis.

CHAPTER 9

9.0 SUMMARY,CONCLUSIONS, AND RECOMMENDATIONS

9.1 Summary of Work and Conclusions

The objective of this thesis was to study the feasibility of using a fluidic igniter called a "Resonance Tube" or a "Hartmann Sprenger (H-S) Tube" to ignite a hydrogen gas jet injected in reciprocating piston engine. Hydrogen was chosen as the fuel because of its potential of becoming the first non-polluting and renewable fuel.

To this end, a gaseous fuel injection system, a reciprocating piston test rig, the electronic circuitry and control software, as well as other miscellaneous test rigs, were designed for tests required to reach the objective of this thesis.

The electronic hardware supplied power to the solenoid actuator as well as received and conditioned electronic signals obtained from the test rig and sent these signals to the computer. The computer would use these signals in the control software and then sent a signal to the hardware to open and close the injector. The control software allowed for variations of the injector parameters to change the duration of injection, as well as the injection time

or advance. The test apparatuses were instrumented so that data could be recorded on a plotter.

The test rig consisted of a variable speed electric motor driving a modified single cylinder engine. The cylinder head was redesigned to include the fuel injector, the resonance tube, as well as sensors, to record the pressure in the combustion chamber and the pressure at the back wall of the resonance tube. A safety valve was also designed to relieve the pressure in the combustion chamber in case it would rise to an unsafe level.

Three different types of tests were performed during the course of this research:

1- injection of hydrogen into a H-S tube under atmospheric pressure

2- injection of hydrogen into a H-S tube under constant, above atmospheric pressure

3- injection of hydrogen into a H-S tube, in a reciprocating piston chamber with varying pressure.

The first set of tests allowed to select resonance tube dimensions, as related to the hydrogen injector dimensions. A simple resonance tube with a cavity of 2.0 mm diameter and a depth of 20 mm was chosen. The injector nozzle used had an orifice of 1.5 mm diameter and the nozzle needle had the pintle removed except for a small diameter extension through the nozzle orifice to reduce the

core pressure of the gas jets to allow for outflow of the extraneous gas from the tube.

Resonating pressure waves were easily created when the hydrogen was injected axially into the mouth of the resonance tube, at the low ambient pressure. As this back was pressure increased, the axial gap between the injector nozzle and the resonance tube would have to be reduced to obtain comparable results in terms of shock wave development and pressure amplitude in the tube. As the back pressure continued to rise, it became much more difficult to create these pressure waves and the axial gap was reduced to a minimum of 1 mm.

It was not possible to obtain ignition of the hydrogen at any of the conditions created during the tests with hydrogen gas injection into the resonance tube. There are several factors which limited the increase in the shock strength which was required required for large heat release from the shock wave energy dissipation. These are specifically:

1- The "Saddle Effect", this phenomenon did not allow for the utilization of the full energy of the gas jet in creating the shock waves. The discovery of the "saddle effect", as the result of high jet velocity, is not accompanied in this thesis by the explanation of the nature of this phenomenon.

2- The short duration of hydrogen injection required for diesel engine operation, limited the time of heat release from the shock wave which would increase the temperature of the gaseous mixture.

3- The shock wave formation delay period during the injection which was required tc initiate the resonating shock waves, farther reduced the already short period of time available for heat release.

4- The negative impact of high back pressure was detrimental on the development and amplitude of shock waves in the resonance tube.

5- The variations of the chamber pressure during the compression period available for hydrogen injection made difficult to optimize the resonance tube position for the best shock wave development.

This research has been initiated knowing of the time constraint. The concept was to produce stronger shock waves by using higher jet velocities resulting from higher driving pressure of the hydrogen available for injection. This assumption was hampered by the "saddle effect" which did not allow the development of the shock waves in the resonance tube at higher hydrogen jet velocities. The second major hampering effect was the impact of the higher back pressure, adversely affecting the strength of the shock waves. This is most likely due to the difficulties of

hydrogen gas to penetrate into the tube and to compress the indigenous gas inside the tube. This situation was even worse, due to the fact that the back pressure varied with the piston movement: optimization of the distance between the nozzle and the resonance tube was not possible .

This thesis does make some contributions to the engineering knowledge and gives some guide lines for future work.

It produced original records of a transient pressure waves phenomena in a resonance tube. By the nature of the injection process in a diesel engine, the gas jet is a highly transient event in which was discovered an initial delay in the creation of the shock waves in the resonance tube, as well as the existence of a "Saddle Effect" which occurred in the resonance tube under certain conditions. This "Saddle Effect" process was found to be related to the gas flow rate (or gas velocity) from the injector because it could be eliminated by either reducing the injector gas discharge rate, or by lowering the hydrogen driving pressure in the injector or finally by reducing the nozzle flow area. The next phenomenon discovered was the limitation in shock wave strength when hydrogen was injected into the resonance tube in the presence of high pressure air. This effect could be limited by reducing the

gap between the resonance tube and the injector nozzle; however, at higher pressures this remedy did not work.

9.2 Recommendations for Future Work

Future work can be carried out in several different ways on several topics. Recommended future work can be listed as:

1 - Study the "saddle effect" and the detrimental effects of high pressure in the creation of resonating shock waves in resonance tubes.

2 - Devise a system to instantaneously measure the temperature in the resonance tube.

3 - Improve the design of the gaseous fuel injector so that the initial delay period of charging the solenoid can be reduced.

4 - Develop a dedicated controller for the control of the fuel injector.

The nature of these phenomena can be studied in future works. However, the study of the resonance tube behavior at higher pressures should take a more basic scientific approach and not such an application oriented approach, as taken by this researcher. In other words study the fluid mechanics of producing high amplitude shock waves into a higher pressure medium. This can be done with several

methods such as using flow visualization techniques to study the gas jet from the injector into the resonance tube at higher pressure using high speed photography or using hot wire anemometer techniques. With this the injector nozzle can be redesigned to help in creation of the shock waves.

Then new methods of measuring fast temperature transient should be developed. In this way temperature measurements can be taken and shape optimization for the resonance tube can be done.

The basic work should avoid the complexity of a reciprocating piston and first study the shock wave development in a "bomb" chamber in which higher pressure and temperature air could be used to charge the device and then inject hydrogen into a resonance tube of the test rig or a "shock tube" test rig can be developed as was suggested by Awad to create the high temperatures and pressures which are found in a diesel engine [32]. Then when all these problems are overcome then move to tests in the more complex fluid environment of a diesel engine combustion chamber.

In terms of the gas injection system, improvements can be made in redesigning the injector so that smaller solenoids could be used by having the gas pressure equalizes at both ends of the nozzle, thereby reducing the

spring force required to keep the injector closed and eliminating the gas pressure force from the dynamics of the nozzle opening. The smaller solenoid will reduce the problem of the large initial charge time of the solenoid and allow for better control of the opening of the injector. an added benefit is in the reduction problem of the needle seizure in the nozzle body caused in the present system because of the small clearances between the two surfaces required to reduce leakage and the poor lubricating properties of gases.

A dedicated controller is recommended to reduce the limitations of a personal computer. Triggering and latency problems which were encountered during testing would be eliminated because the controller would not have to serve some the other devices. Also, the circuit and wiring should have to be able to withstand electromagnetic interference from the motor used to drive the engine.

REFERENCES

1. Philips, B.R., and Pavli, A.J.,"Resonance Tube Ignition of Hydrogen-Oxygen Mixtures." NASA Technical Note TN D6354.

2. Alderson, J.E.A., Hammerli, M., Murphy, J.R.B., and Taylor, J.B., "Program Overview Hydrogen and Energy Storage: 1979 to 1985", NRCC No. 26487.

3. Williams, L.O.,"Hydrogen Power, An Introduction to Hydrogen energy and its Applications", Permagon Press, New York, 1980.

4. Homan, H.S., De Boer, P.C.T., McLean, W.J., " The Effect of Fuel Injection on NO_x Emissions and Undesirable Combustion for Hydrogen-Fuelled Piston Engines. (Appendix 1)", Int. Journal of Hydrogen Energy, Vol. 8, No. 2, 1983, pp. 131-146.

5. Hama, J.et al., "Hydrogen-Powered Vehicle with Metal. Hydride Storage and D.I.S. Engine System" ,SAE PAPER No. 880036, 1988.

6. Davidson, D., Foirlie; M., Stuart A.E. "Development of a Hydrogen-Fuelled Farm Tractor", Academic Research Associates Paper.

7. Furuhama, s. and Kobayashi, Y., "A Liquid Hydrogen Car with a Two-Stroke Direct Injection Engine and LH2-Pump.", Int. Journal of Hydrogen Energy. Volume 9, No. 3, 1984, pp 205-213.

8. STROBL, W., and Peschka, W., "Liquid Hydrogen as a Fuel of the Future for Individual Transport", BMW AG PRESSE. from the Proceedings of the 6th World Hydrogen Energy Conference, Vienna, Austria, July 1986

9. Krepec, T., Miele, D., Lisio, C., "Improved Concept of Hydrogen on Board Storage and Supply for Automotive Applications." Int. Journal of Hydrogen Energy; Vol 15, No. 1, 1990, pp. 27-32.

10. Krepec, T. Lisio, C., Miele, D., "Problems Related to Gaseous Fuel Injection in Diesel Engines and Some Possible Solutions.", Proceedings of Workshop on Alternative Fuels for Transportation: Canadian Research Needs, May 1988, pp 221 - 239.

11. Furuhama, S., Yamane, K., Yamaguchi, I., "Combustion Improvement in a Hydrogen Fuelled Engine.", Int Journal of Hydrogen Energy Vol. 2, 1977, pp. 29

12. Ikegami, M., Miwa, K., and Shioji, M., "A Study of Hydrogen- Fuelled Compression Ignition Engines", Int. Journal of Hydrogen Energy, Vol. 7, No. 4, 1982, pp. 341-353.

13. Giannacopoulos, T., "A Feasibility Study on an Electronically Controlled Hydrogen Gas Injector", Master's Thesis, Department of Mechanical Engineering, Concordia University, Montreal ,June 1986.

14. Furuhama, S., and Kobayashi, Y., "Development of a Hot-Surface-Ignition Hydrogen Injection, Two-Stroke Engine." Int. Journal of Hydrogen Energy, Vol. 9, No.3, pp. 205-213.

15. Hartmann, J., "Om en ey Motode til Frenbrigelse af Lydsvinger", Dan. Mat. Fys. Medd, 1919.

16. Sprenger, H.S., "Uber Thermische Effekte bei Rezonanzrohren", Mitteilungen aus den Institute für Aerodynamik an der ETH, Zurich, Nr. 21, 1954, pp18-35.

17. Thompson P.A., "Jet Driven Resonance Tubes", AIAA Journal, Vol. 2, No. 7, July 1964.

18. Kang, S.W.,"Resonance Tubes," Ph.D. Thesis, 1964, Rensalaer Polytechnic Institute, Troy N.Y.

19. Brocher, E., "On the Maximum Attainable Temperature in Hartmann-Springer Tubes", Shock Tubes and Shock Waves Proceedings of the 12th Int. Symposium on Shock Tubes and Waves, 1979, pp. 161-168.

20. Conrad, W. E., Pavli, A.J., "A Resonance-Tube Igniter [illegible] Hydrogen Oxygen Rocket Engines", NASA TM X-1460.

21. Marchese, V.P., Rakowsky, E.L., and Bement, L.J., "A Fluidic Sounding Rocket Motor Ignition System", Journal of Spacecraft, Vol. 10, No. 11, November 1973.

22. Wu et J.H.T., Neemeh R.A., Ostrowski, P.P., Lee, P., "Experimental Investigation of a Cylinderical Resonator", AIAA. Journal. Vol. 12, No. 8, August 74, pp. 1076-1078.

23. McAlery, R.F., Pavlak, A., "Tapered Resonance Tubes: Some Experiments", AIAA Journal, Vol.8, No. 3, MArch 1970.

24. Brocher, E., Kawahashi, M., "Wave and Thermal Phenomena in Hartmann-Sprenger Tubes with an Area Construction", Shock Waves, Shock Tubes-Preceding of the 15th International Symposium on Shock Waves and Shock Tubes, 1985.

25. Neemeh, R. A., Ostrowski, P.P., Wv, J.H.I., "Thermal Performance of a Logarithmic Spiral Resonance Tubes", AIAA Journal, Vol.22, No. 12, December 1984.

26. Sakurai, A.,"Auto Ignition of Hydrogen by a Shock Compression Oxidizer",

27. Ishii, Y., Higashino, F., Sakurai, A., "Ignition of Spurting Hydrogen Jets Behind Reflected Shock Waves", JMES, No. 85-08807, November 1986.

28. Rudinger, G. "Non-Steady Duct Flow: Wave Diagram Analysis", D. Von Nostrand Company Inc., New York, 1955.

29. Wu, J.H.T., Neemeh, R.A., Ostrowski, P.P., "Subsonic Jet-Driven Resonance Tube",C.A.S.I. Transactions, Vol 8, No. 1, March 1975.

30. Miele, D.P., "Investigation on a Multi-Point Direct Injection and Control System for Gaseous Fuels in a Diesel Engine", Master's Thesis, Department of Mechanical Engineering, Concordia University, Montreal, Dec. 1990 (pending).

31. Heywood, J.B., "Internal Combustion Engine Fundementals", McGraw-Hill Publishers, New York, 1988.

32. Awad, S.A. "Experimental and Theoretical Investigations of Fluidic Ignitors by Use of a Shock Tube.", Technical Report, Faculty of Engineering and Computer Science, Concordia University, Montreal, September 1980.

APPENDIX A

Control Software

```
/* PROGRAM SOLENOID                                                    */

/* Used to operate the injector alone without external */
/* triggering.                                                         */
/*                                                                     */
/* The duration of injection, the time between         */
/* injections and the number of injections are         */
/* operator defined.                                                   */

# include <stdio.h>
# include <dos.h>
# include "labhead.h"

main()
{
     unsigned int   nopen13,nopen11,nclose1,count1,
                    i = 60,j = 10,  count  = 5;

     char                    kk;
     clrscr();
     outp(ATOD  ,0x80); outp(PIO   ,0x80);
start:
     printf("delay     time = %3u msec",i);
     printf("injection time =  %2u msec",j);
     printf("number of injections = %2u",count);
     printf("enter 'q' to quit");
     printf("      'r' to run as is");
     printf("      'x' to alter parameters");
     printf("enter character : ");
     kk = getch();
     if (kk == 'x' || kk == 'X') goto alter;
     if (kk == 'q' || kk == 'Q') goto end;
     printf("Strike a key to commence control program...");
     count1 = count;
     while ( !kbhit() ) {;} getch();
     nopen11 = 0x04;      /* open transistor 1 of inj #1  */
     nopen13 = 0x0c;      /* open transistor 3 of inj #1  */
     nclose1 = 0x08;      /* close injector # 1           */
     printf("Strike a key to halt program.....");
     outp(INJ1,nclose1); outp(INJ1,0x09);
     delay(8000);sound(800);delay(2000);nosound();
     while ( !kbhit()) {
              outp(INJ1,nopen11);
             delay(j);
             outp(INJ1,nclose1);
             outp(INJ1,nopen13);
             outp(INJ1,nclose1);
             delay(i-j);
             count--;
             if (count == 0) goto answer;
```

```
                    }
     getch();
answer:
     count = count1;
     printf("program ended ..............................");
     outp(INJ1,nclose1); outp(INJ1,0x09);
     clrscr();
     goto start;
alter:
     clrscr();
     printf("delay time i is set to :%3u",i);
     printf("enter delay     time i : ");
     scanf("%u",&i);
     printf("injection time set to  :%3u",j);
     printf("enter injection time j : ");
     scanf("%u",&j);
     printf("enter number of injections : ");
     scanf("%u",&count);
     goto start;
end:
}
```

```
/*  File: INJECT3C.T */

/* Note:  All reference and use of the lab master timer
have been removed and the piston position sensor is
triggering the IRQ2 interrupt directly. */

/* ------------------------------------------------------*/
/*                                                       */
/*  This program performs two functions required to      */
/*  control two injectors of a gaseous fuelled           */
/*  diesel engine.  It interrupts every second revolution*/
/*  to inject the required fuel dose.  The fuel dose     */
/*  is  a function of engine speed and load.  It reads   */
/*  the speed to set the required timing of the          */
/*  injectors and the metering valve position and reads  */
/*  an interrupt signal to ensure proper timing.         */
/*   The two signals are taken from a magnetic           */
/*  pick-up and an optical pick-up located on the        */
/*  engine crankshaft.  One pick-up signal is speed      */
/*   and the other is piston position of the first       */
/*  engine cylinder.                                     */
/*                                                       */
/*  Developed by:  Carmine Lisio & Domenico P. Miele     */
/*  Dated : April 20, 1988                               */
/*  Modified  by:  Daniel J. Quinz & Carmine Lisio       */
/*  Feb 4, 1989                                          */

/* ------------------------------------------------------*/

#include  <stdio.h>
#include  <dos.h>
#include  <conio.h>
#include  <labhead.h>

#define IRQ2   10              /* IRQ2  vector number     */
#define CYCLES 2               /* Cycle skip count        */

/*  ------------------------------------------------  */
/*                global variables                    */
/*  ------------------------------------------------  */

volatile int cycle_count = CYCLES;  /* cycle skip count  */

volatile unsigned int flag;  /*Interrupt termination flag*/

void interrupt inject();

/*  ------------------------------------------------  */
/*                     main program                   */
/*  ------------------------------------------------  */
```

```
main()
     {
          int low,high;
          void interrupt
          (*old_vec)();
          unsigned int intvec,zero,dspeed,speed;
          unsigned int nopen11,nopen13,nclose1,time2,time3;

          nopen11 = 0x04; /* open transistor 1 of inj #1 */
          nopen13 = 0x0c; /* open transistor 3 of inj #1 */
          nclose1 = 0x08; /* close injector # 1          */

          time2   = time3 = flag = zero = 0;

          printf("program is  about  to  commence ......");
     outp(ATOD,0x90);  /* output control byte to ATOD   */
     outp(PIO,0x80) ;  /* output control byte to PIO    */

     intvec  =  IRQ2;  /* get interrupt number          */
     old_vec =  getvect(intvec); /* save old IRQ vector */
     setvect(intvec,inject);     /* install new isr     */

     disable();                  /* disable interrupts  */
     outp(0x21,inp(0x21) & 0xfb);/* Enable irq2         */
     enable();                   /* enable interrupts   */

     printf("Strike a key to commence control program");

     while   ( !kbhit()  );      /* Wait for key press  */

     getch();                     /* Clear  keypress     */

     flag = zero;    /* Clear interrupt termination flag */

     printf(" Strike a key to halt program.............");

     while ( !kbhit() )
         {
                if ( flag == 1 )
             {
               flag = 0;          /* reset injection flag*/
               delay(time2);      /* # of times to
                                        repeat loop      */
               outp(INJ1,nopen11);/* open injector # 1   */
               delay (time3);     /* # of times to
                                     repeat loop         */

               disable();
               outp(INJ1,nclose1);/* close injector # 1  */
               outp(INJ1,nopen13);/* reverse current flow*/
```

```
                outp(INJ1,nclose1);/* close  injector # 1 */
                enable();
            }
        outp(ATOD+1,0X00);     /* output channel to convert  */
        outp(ATOD+2,0x00);     /* start conversion           */

        while (inp(ATOD) < 128);/* wait to end conversion    */
        low  = inp(ATOD+1);     /* lsb of conversion         */
        high = inp(ATOD+2);     /* msb of conversion         */
        speed = (high << 8)   | low;

        speed =  (unsigned  int)  dspeed*772.2*0.00488;
        if  (speed > 2000 || speed < 400)
            {
                speed  = zero;
                time2  = zero;
                time3  = zero;
            }
        if   (speed  !=  zero)
            {
                time3 = 10;
                time2 = 15000/speed;
                time2 = (time3);
            }
        }

        getch();
        puts("cycle  complete: program   ended.");

        disable();                          /* disable interrupts */
        outp(0x21,inp(0x21) | 0x04);  /* disable irq2         */
        enable();                           /* enable interrupts  */
        setvect(intvec,old_vec);      /* reset previous status
                                                    of irq2 */
        }
/*  ------------------------------------------------  */
/*              interrupt service routine             */
/*  ------------------------------------------------  */
void interrupt inject(void)
        {
            char  far *en  =  (char  far  *)  0xb0000000L;
            (*en)++;
            if  ( !(--cycle_count))
               {
                  cycle_count = CYCLES;/*  Reset cycle
                                           skip count     */
                  flag  =  1;          /* flag set to inject*/
               }
            outp(0x20,0x20);           /*Send EOI to 8259 pic*/
        }
```

```
/*  ------------------------------------------------  */
/*                LABHEAD.H file                      */
/*  ------------------------------------------------  */
#define DTOA 0x710
#define ATOD 0x714
#define INT 7
#define TIMER 0x718
#define PIO 0x71f
#define DAMAX 0x7ff
#define TIMERC   0x719
#define INJ1     0x71c
#define INJ2     0x71c
#define METER    0x71d
```

APPENDIX B

Instrument Calibration

This thesis consists of a multitude of experimental tests using a wide range of instrumentation consists of a linear variable differential transformer (LVDT), and two types of piezoelectric pressure transducers. The frequency to voltage integrated circuit must also be calibrated so that the analog voltage from the I.C. be interrupted correctly by the computer.

A.2.1 Calibration of LVDT

This transducer is used to measure the needle lift in the injector. The LVDT is an AVL type 421 model 103 inductive nozzle needle lift transducer. The signal from the LVDT is amplified through 02 carries amplifier. The signal from the carries amplifier is then recorded on a digital oscilloscope.

The method of calibration was o vary the lift of the solenoid and record the change in voltage. The change in lift was done by placing spaces to reduce the lift. From the calibration curve a trend was drawn and the slope of the curve describes the calibration as

$$k_{LVDT} = 3.645 \text{ V/mm}$$

The calibration curve is shown in Figure A1 and a sample lift vs. time curve shown in Figure A2.

LVDT CALIBRATION

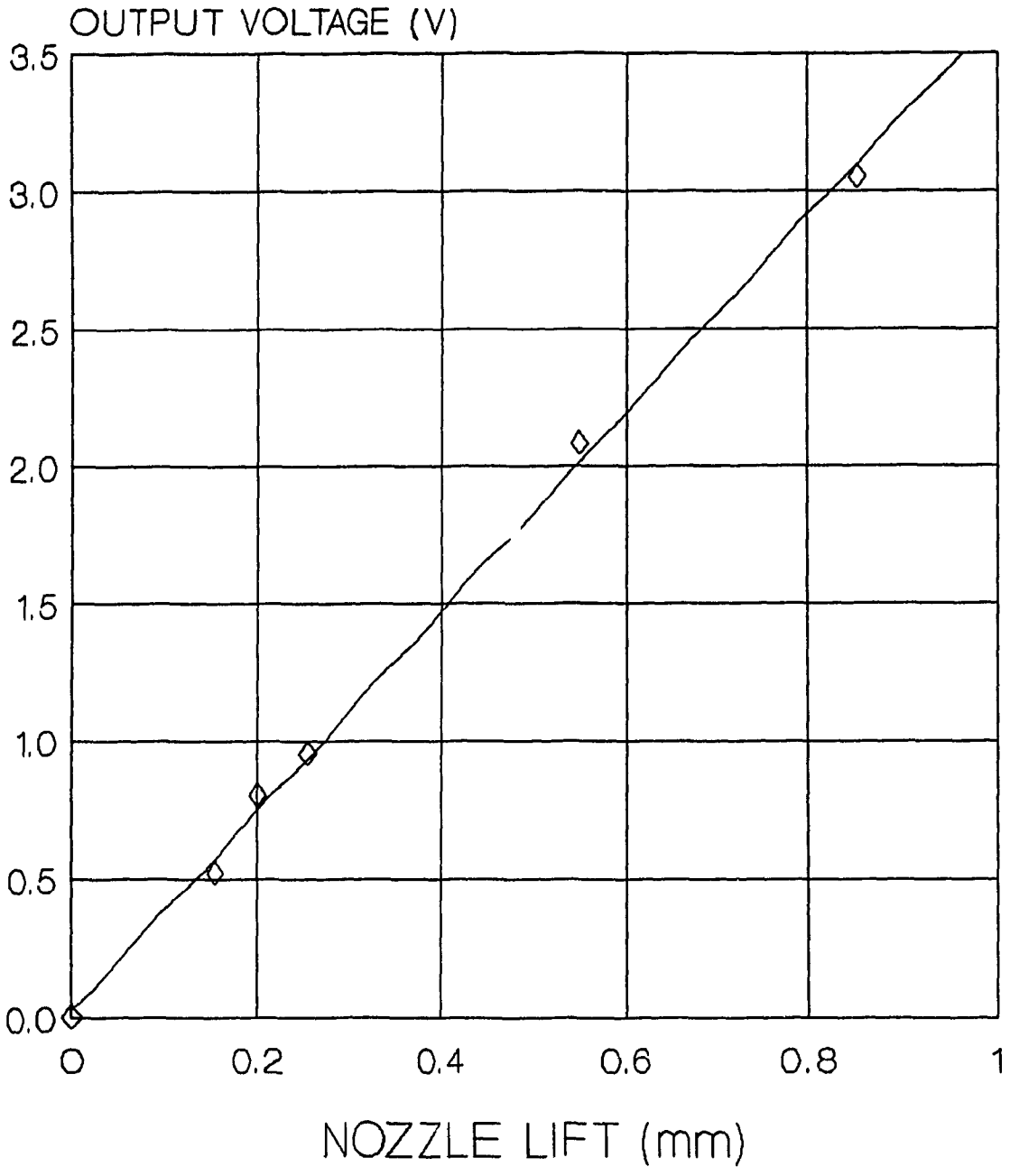

Figure A.1. LVDT Calibration Curve

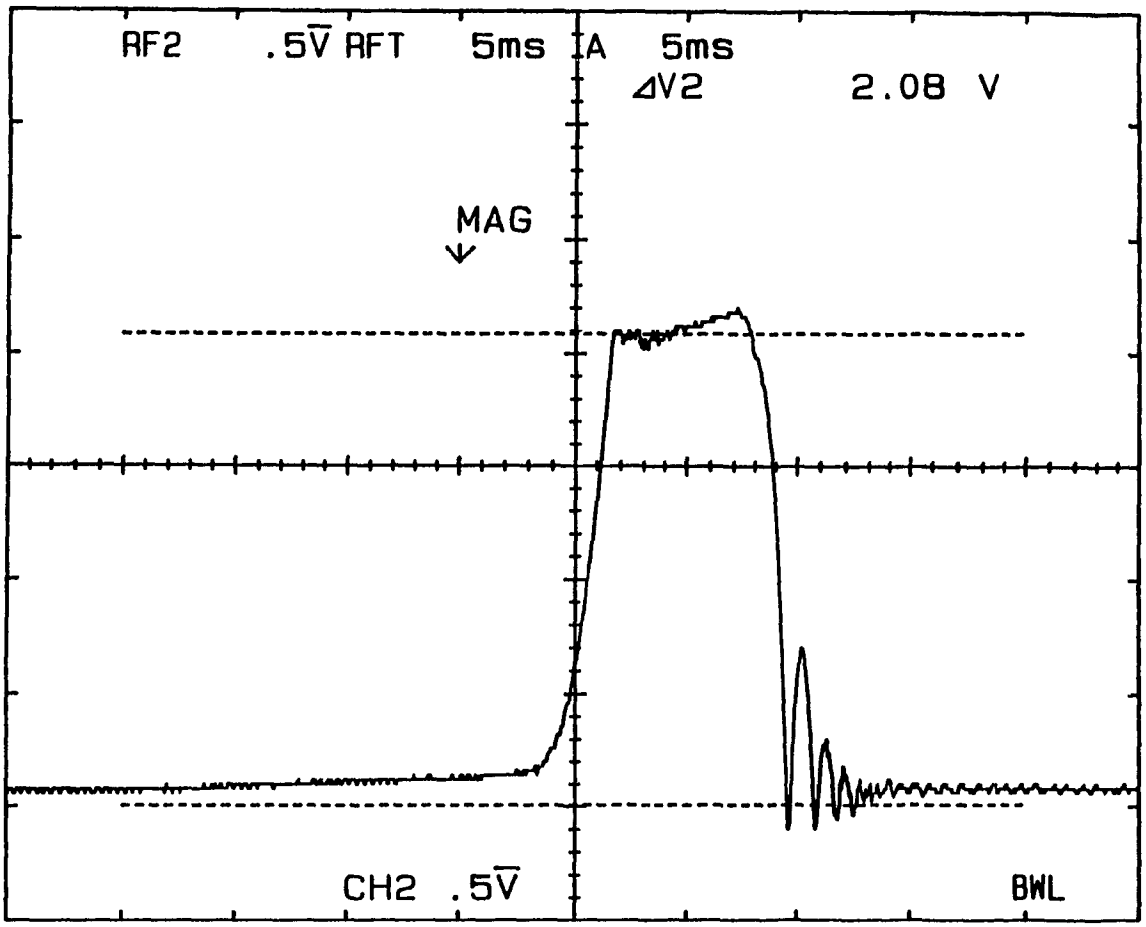

Figure A.2. Sample Injector Lift vs. Time Curve

A.2.2 Calibration of Pressure Transducers

There are two different types of pressure transducers and four transducers by Kistler Inc. The first of the transducers is used to measure the pressure in the combustion chamber. It is a Kistler Model 603B2 SIN 5002 and its signal is amplified using a Kistler Dual Mode amplifier Model 504E.

The method of calibration was by first locking the flywheel of the engine, there by fixing the piston position at TDC. With the intake and exhaust valves closed. Then the air was induced through the supercharging port and reading were taken. The calibration curve is shown in Figure A.3 and the sensitivity of the transducers and amplifier is:

$$K_{CHAMb} = 764.0 \frac{kPa}{V} \left(110.76 \frac{psi}{V} \right)$$

The second Kistler pressure transducer is used to measure the inlet gas pressure into the injector. It is a Kistler Model 603B2 S/N C10864 using a Kistler Dual Model Amplifier 5004. The calibration procedure was done by increasing the pressure in the injector as the needle remained closed and the output voltage was recorded. The calibration curve is shown in Figure A.4 and its sensitivity is

$$K_{PINJ} = 1322.4 \frac{kPa}{V} \left(191.72 \frac{psi}{V} \right)$$

Pressure Transducer Calibration
Cylinder head transducer

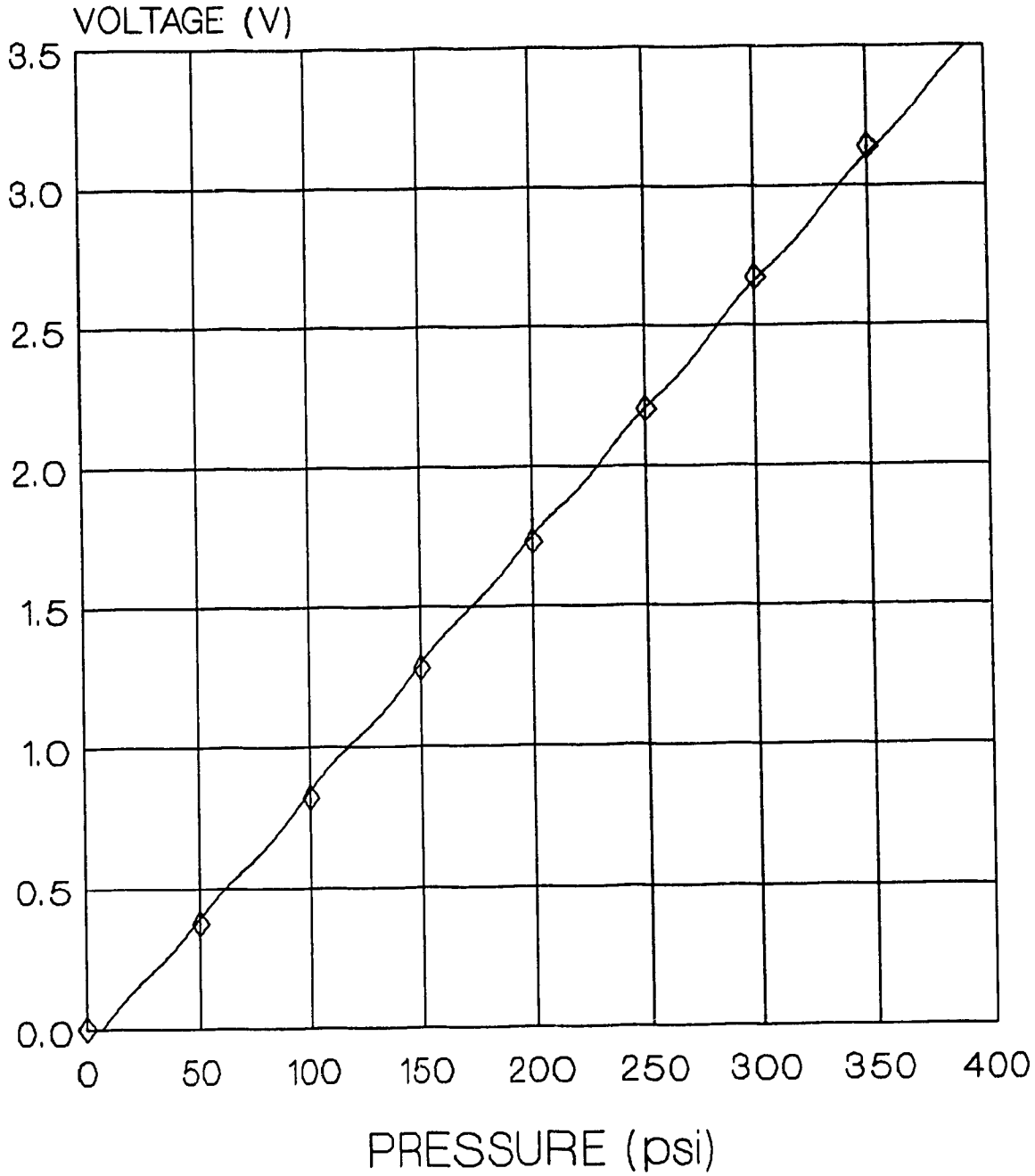

Figure A.3.Combustion Chamber Pressure Transducer Calibration

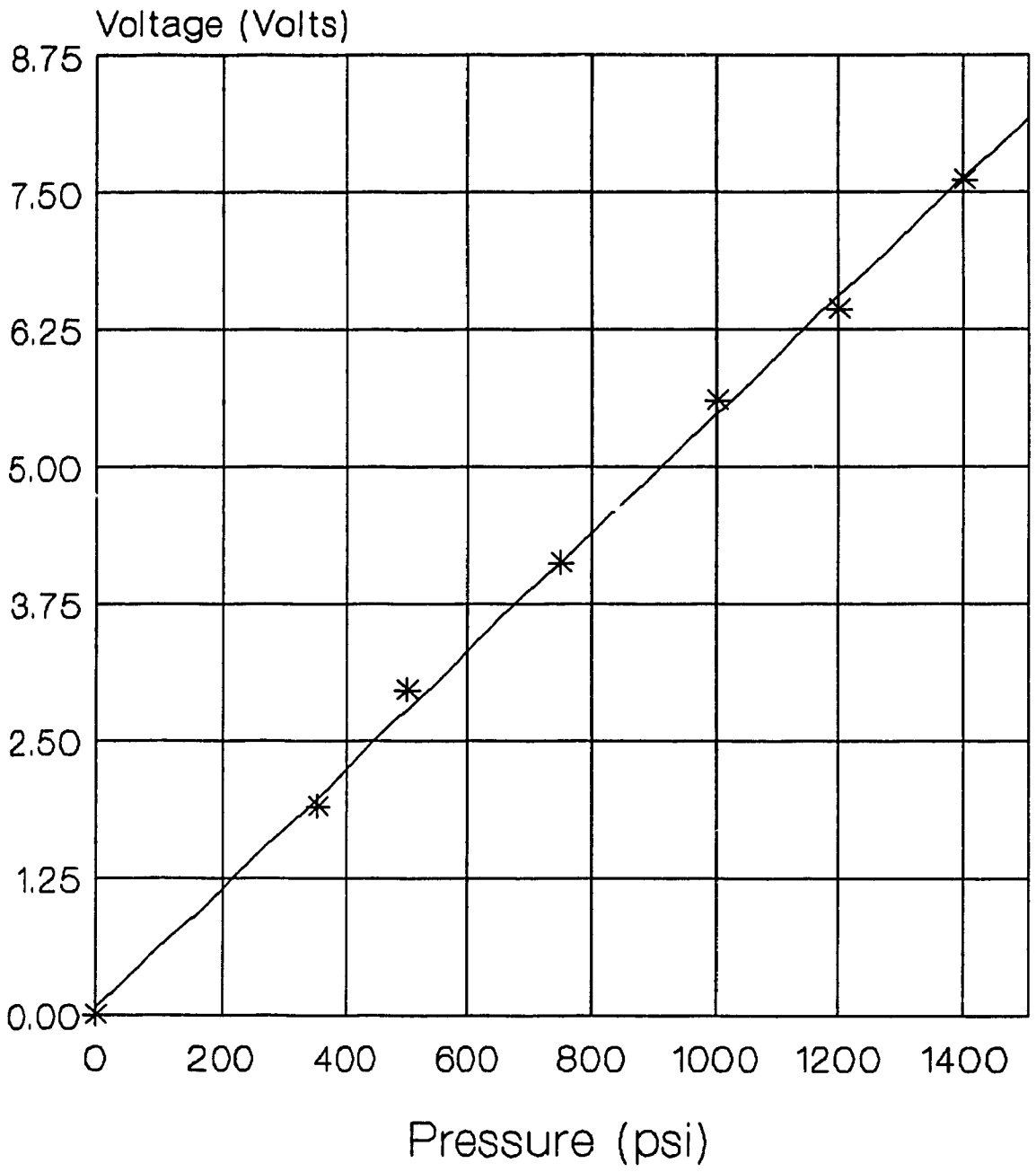

Figure A.4. Injector Pressure Transducer Calibration

The next type of piezoelectric pressure transducers are built by PCB. They are miniature transducers and are used to measure resonating pressure waves at the back wall of the resonance tubes. These transducers have a built in amplifier so only an external power supply is required. The first transducer is a PCB Model 105A03,, it has a range of 0 to 100 psi, and its sensitivity is:

$$k_{ptube} = 545.67 \frac{kPa}{V} \left(79.11 \frac{psi}{V} . \right)$$

The calibration curve was supplied by the vendor and is shown in Figure A.5. This transducer is used in the long tube gas inflow tests.

The second PCB transducer is a PCB Model 105A13, which has a range of 0 to 1000 psi and its sensitivity is:

$$k_{pres} = 1250 \frac{kPa}{V} \left(181.1 \frac{psi}{V} . \right)$$

Again the calibration curve is supplied by the vendor and is shown in Figure A.6.This pressure transducer is placed to form the end wall of the resonance tube and measures the pressure of the resonating waves at the back wall of the resonance tube.

PRESSURE TRANSDUCER CALIBRATION
PCB 105A03

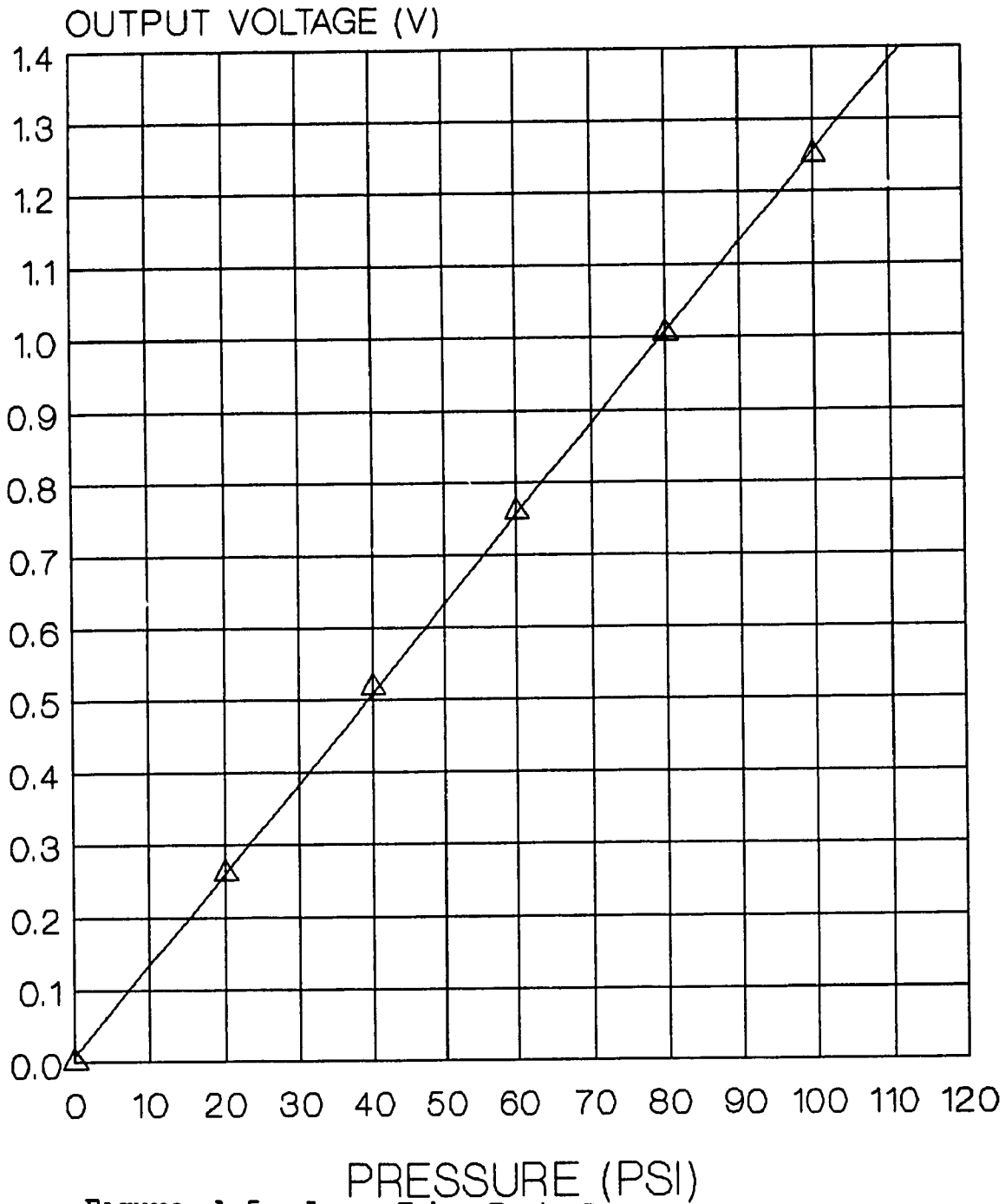

Figure A.5. Long Tube Test Pressure Transducer PCB 105A03

PRESSURE TRANSDUCER CALIBRATION
PCB 105A13

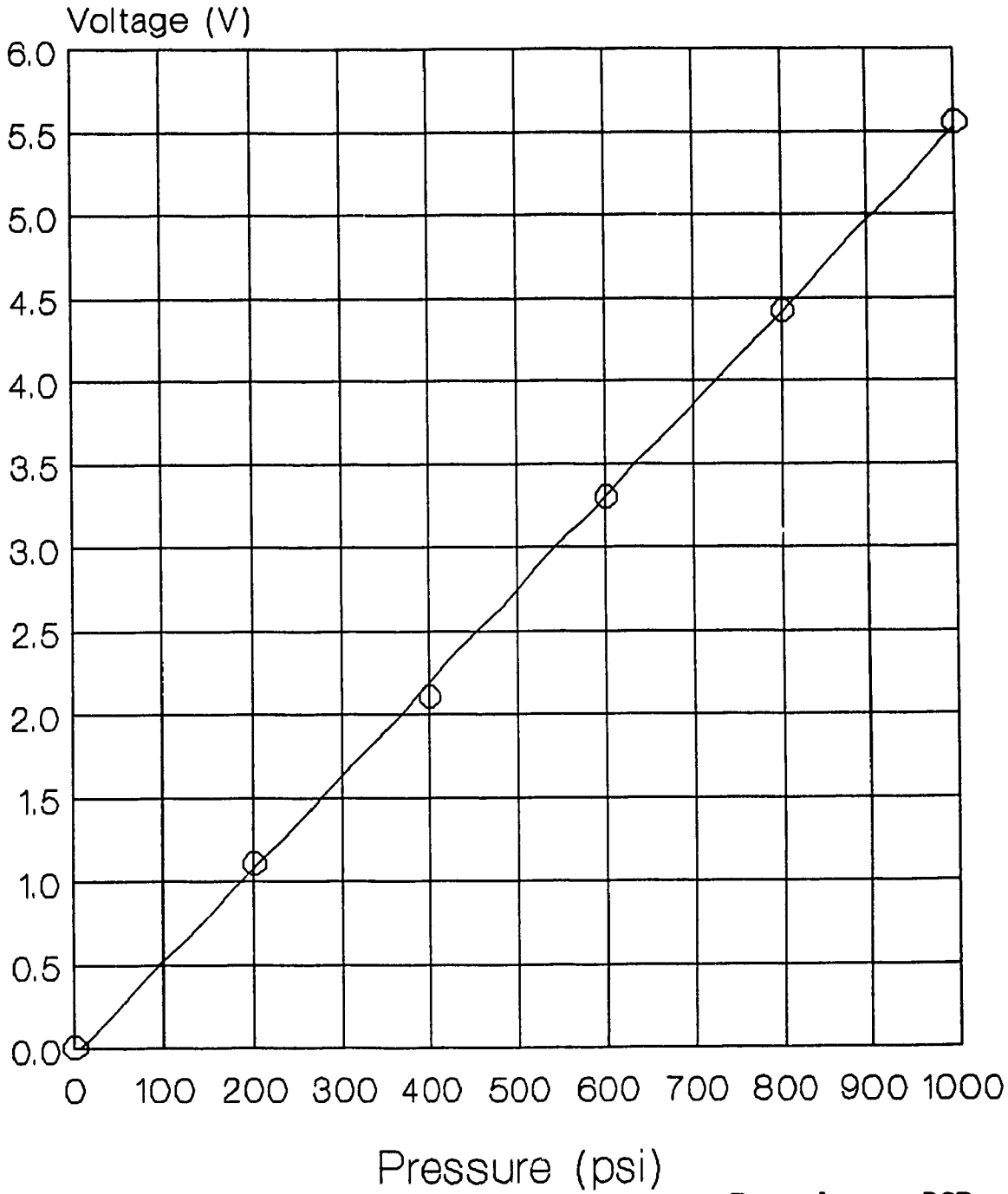

Figure A.6. Resonance Tube Pressure Transducer PCB 105A13

A.2.3 Calibration of FIV Integrated Circuit

The frequency to voltage circuit is set up to determine the rotational speed of the test engine. A magnetic pick-up sensor is coupled with a 30 tooth gear placed on the output shaft of the engine. These magnetic pulses are received by the F/V circuit and transformed into an analog voltage.

The calibration procedure consisted of inputting a sine wave from a Brienelle Instruments Model 3030 function generator with a peak to peak voltage of ±2V. The L:N2907 IC converts this signal and the voltage is read on a multimeter.

The frequency is converted to rotational speed using the following equations.

$$Y\ [\text{rpm}] = X\left[\frac{\text{cycles}}{\text{sec}}\right] * 60\ \frac{\text{sec}}{\text{min}} * 1\ \frac{\text{tooth}}{\text{cycle}} * 1\ \frac{\text{rev}}{30\ \text{teeth}}$$

$$Y\ [\text{rpm}] = 2X$$

The rotational speed vs. output voltage output calibration curve is shown in Figure A.7. The LN2907 saturates at 4.21V. Varying the output is done by changing the resistor and capacitor in the circuit shown in Chapter 5.

Voltage vs. Rotational Speed
LM2907 Frequency/Voltage IC

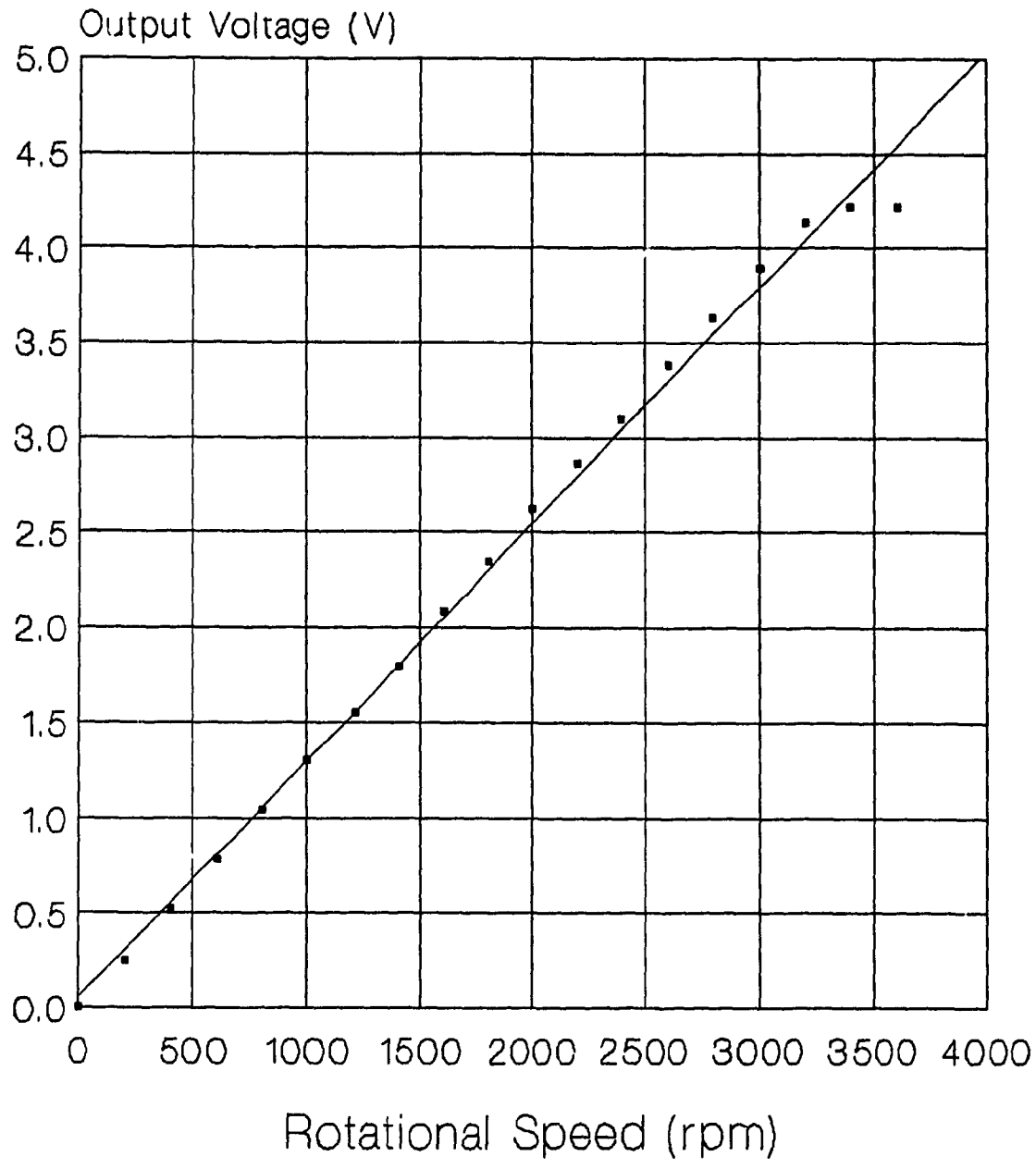

Figure A.7. Frequency to Voltage Converter Calibration

APPENDIX C

Derivation of Metering Valve Flow Area

The metering valve is a gas inflow throttling device which reduces the pressure in the injector during injection. This occurs because the inflow into the injector is smaller than the out flow during injection. There are several benefits to having this valve in the supply line; in allows for quicker closing of the injector thereby reducing gas lost during any post injection, in give a second method of metering the fuel dose,and it has been discovered to help reduce the "saddle effect" which occurs under certain conditions in resonance tube testing.

The valve is a HOKE 316SST model 2355F4Y. It has a 1.25 mm (0.0625 in.) diameter orifice and a 1^0 taper on the stem. A micrometer head is included to give accurate adjustment of the metering valve opening.

The flow area through the orifice can be derived using Figure A.8. The flow area vs. metering valve turns is giver in Figure A.9

Using Guldin's Rule for areas the flow area through the valve is given by:

$$A_{FLOW} = \pi \, D_{avr} \, (\overline{ab})$$

Where the height h is given by the segment $\overline{cb}$ we can solve for D_{avr}.

$$D_{avr} = D_{hole} - h \cos(\beta) \sin(\beta)$$

The segment $\overline{ab}$ is given by:

$$ab = h \sin(\beta)$$

With this specific metering valve $\beta = 1^0$, and D_{HOLE} = 0.001588 m, and also for 10 turns of the micrometer head results in a lift of 5mm. The flow area vs. area relationship is given by:

$$A_{FLOW} = 0.000087\ h - 0.000957\ h^2$$

and the the flow area vs.turns relation is:

$$A_{FLOW} = 0.0000435\ t - 0.000239\ t^2$$

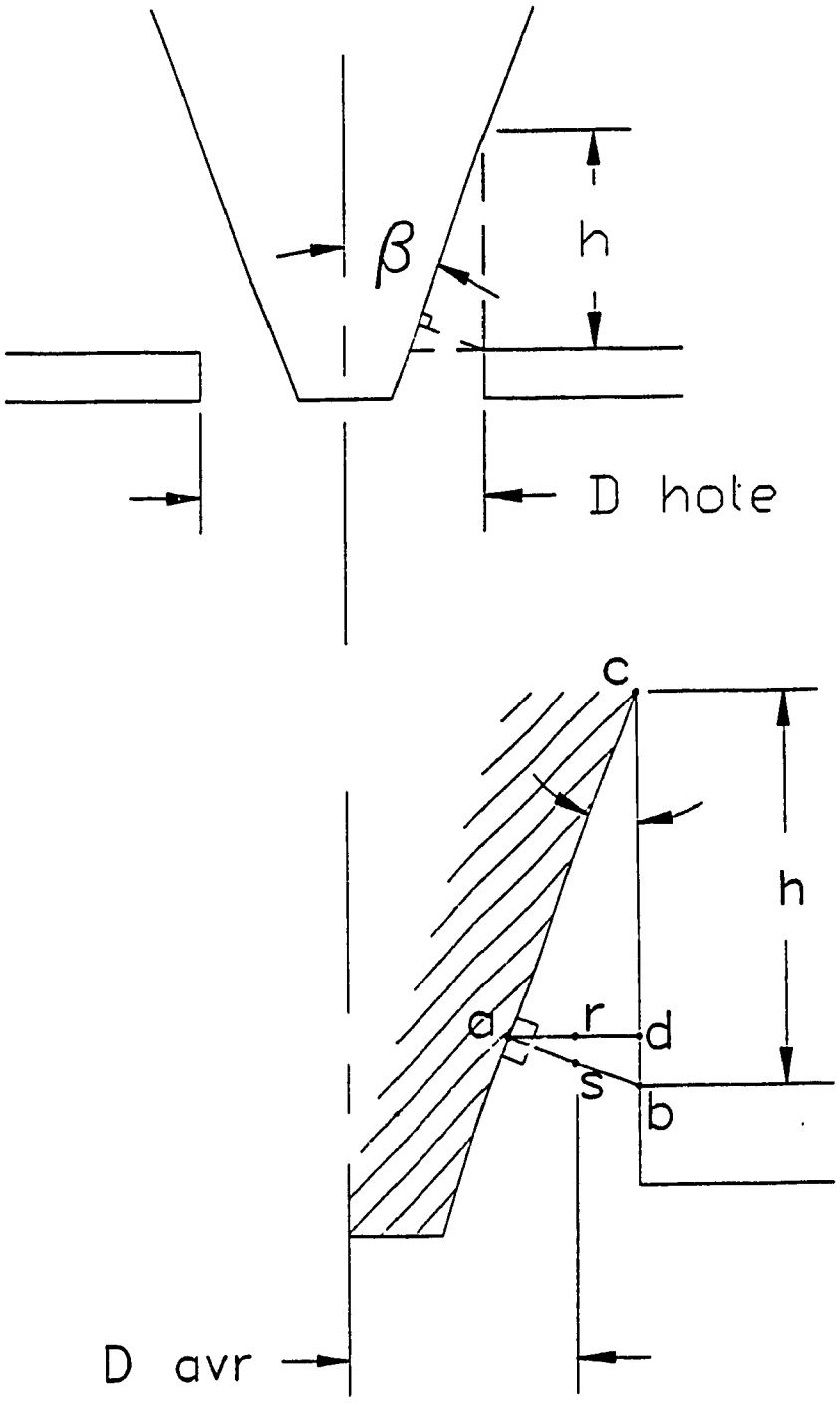

Figure A.8 Metering Valve Flow Area Derivation Schematic

METERING VALVE AREA
Hoke 316SST 2355F4Y

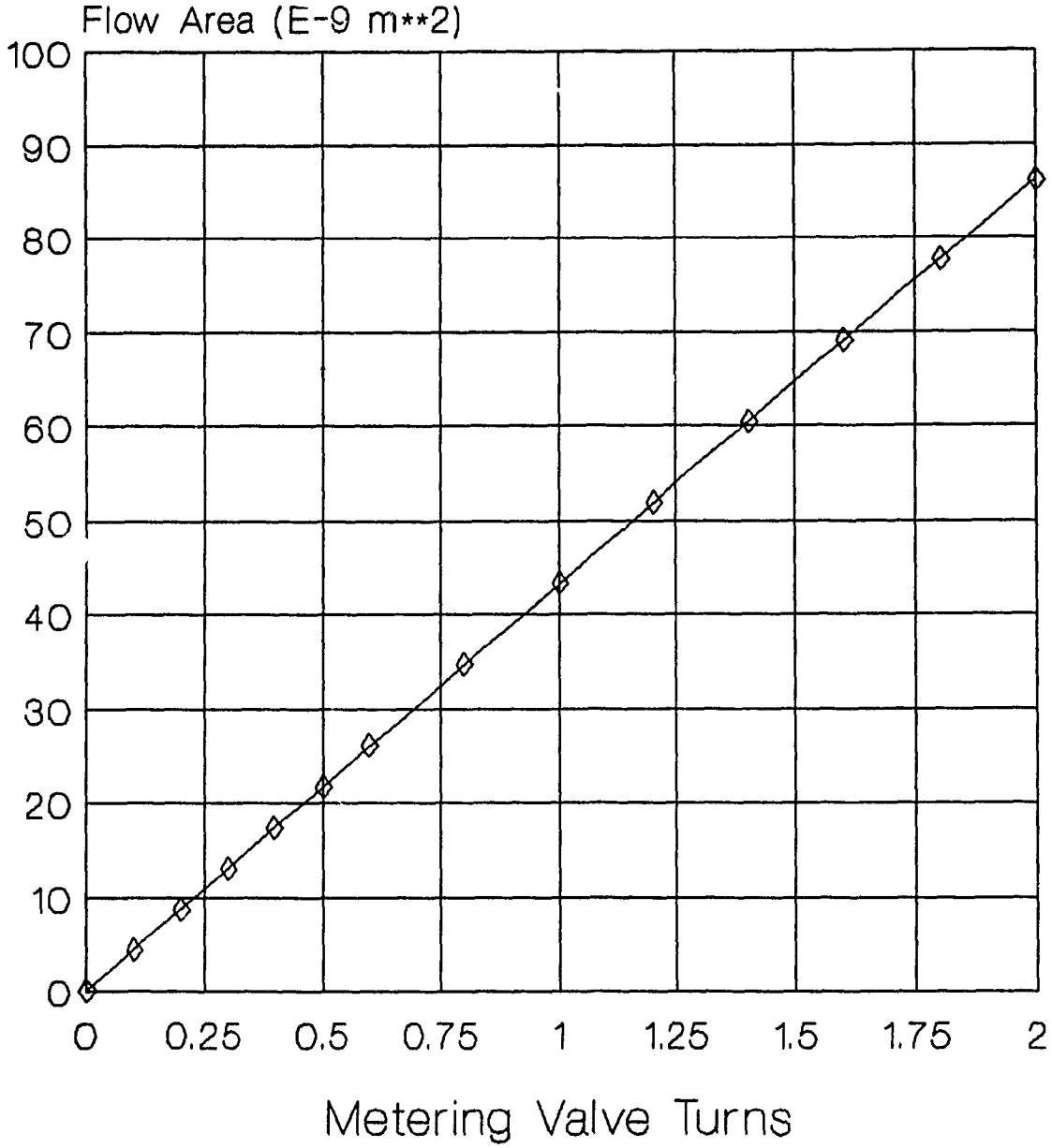

Figure A.9 Metering Valve Flow Area vs. Turns Calibration

APPENDIX D

Cylinder Head Redesign Drawings and Photos of the Main Test Rig

The cylinder head was totally rebuilt from a block of aluminium. The design drawings for the redesign of the cylider head are shown in Figure A.10 and A.11. The main test rig is shown in Figure A.12 and Figure A.13.

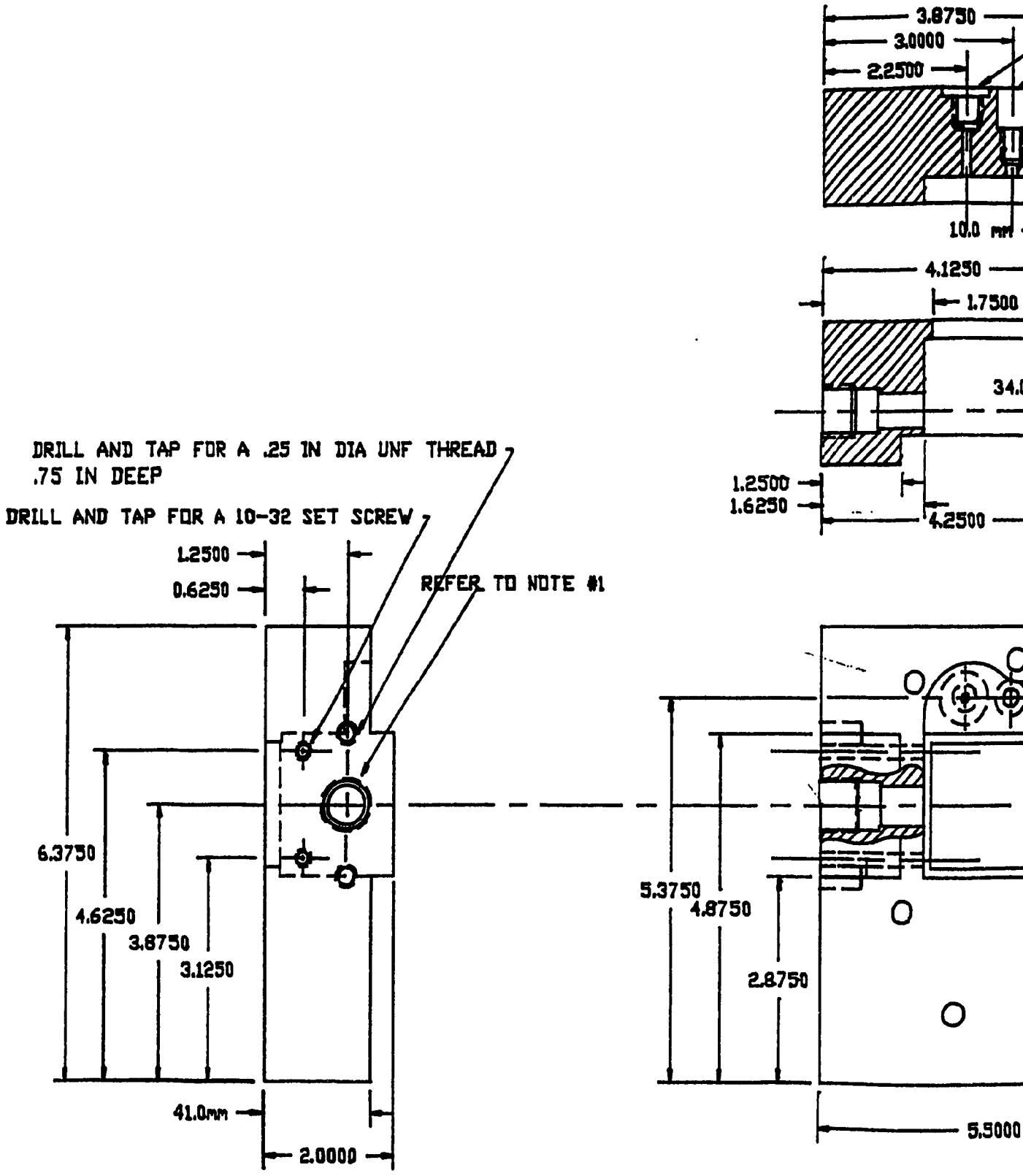

Figure 8.10 Cylinder Head Main Design Drawing

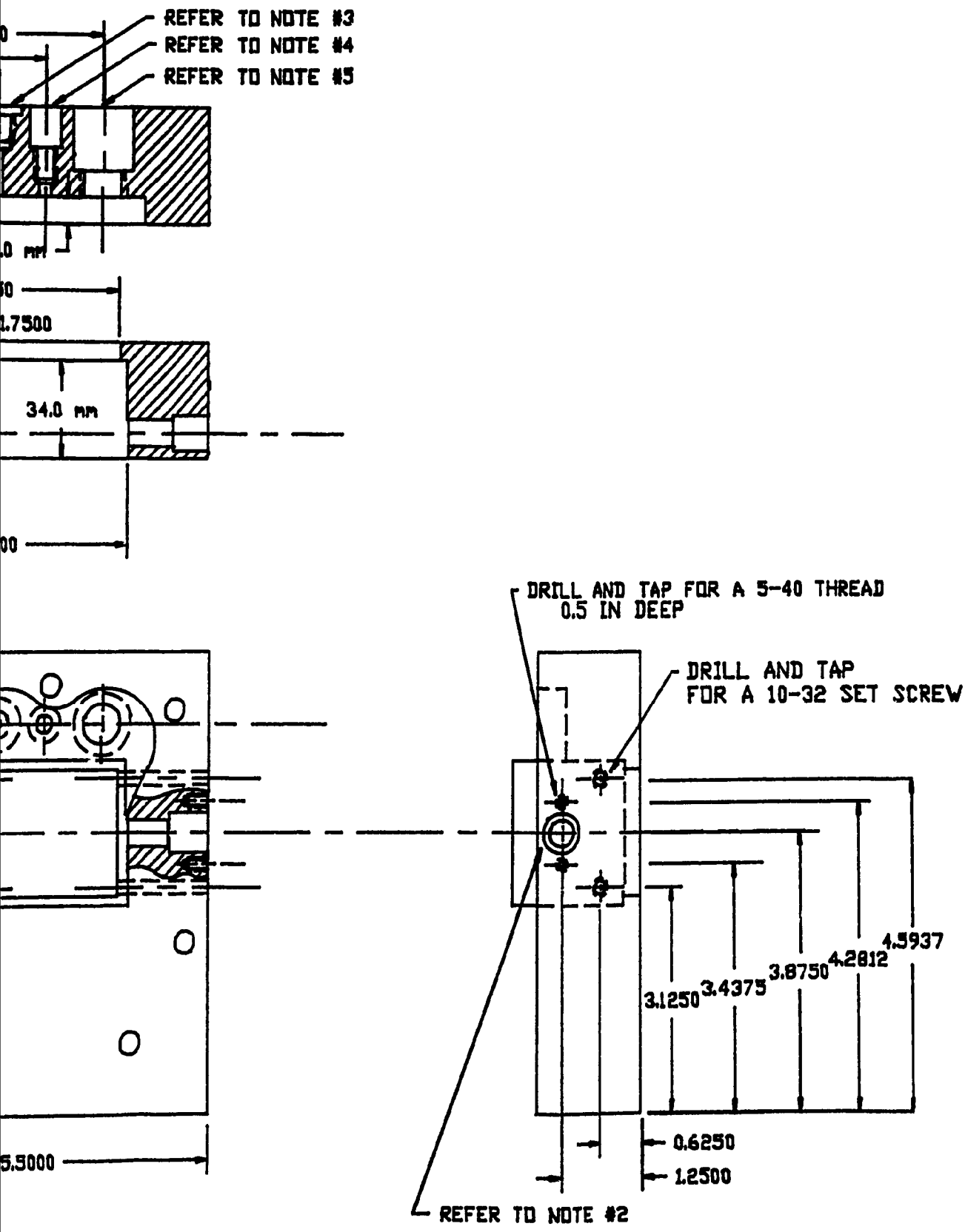
REFER TO NOTE #3
REFER TO NOTE #4
REFER TO NOTE #5
34.0 mm
DRILL AND TAP FOR A 5-40 THREAD
0.5 IN DEEP
DRILL AND TAP
FOR A 10-32 SET SCREW
3.1250
3.4375
3.8750
4.2812
4.5937
0.6250
1.2500
REFER TO NOTE #2

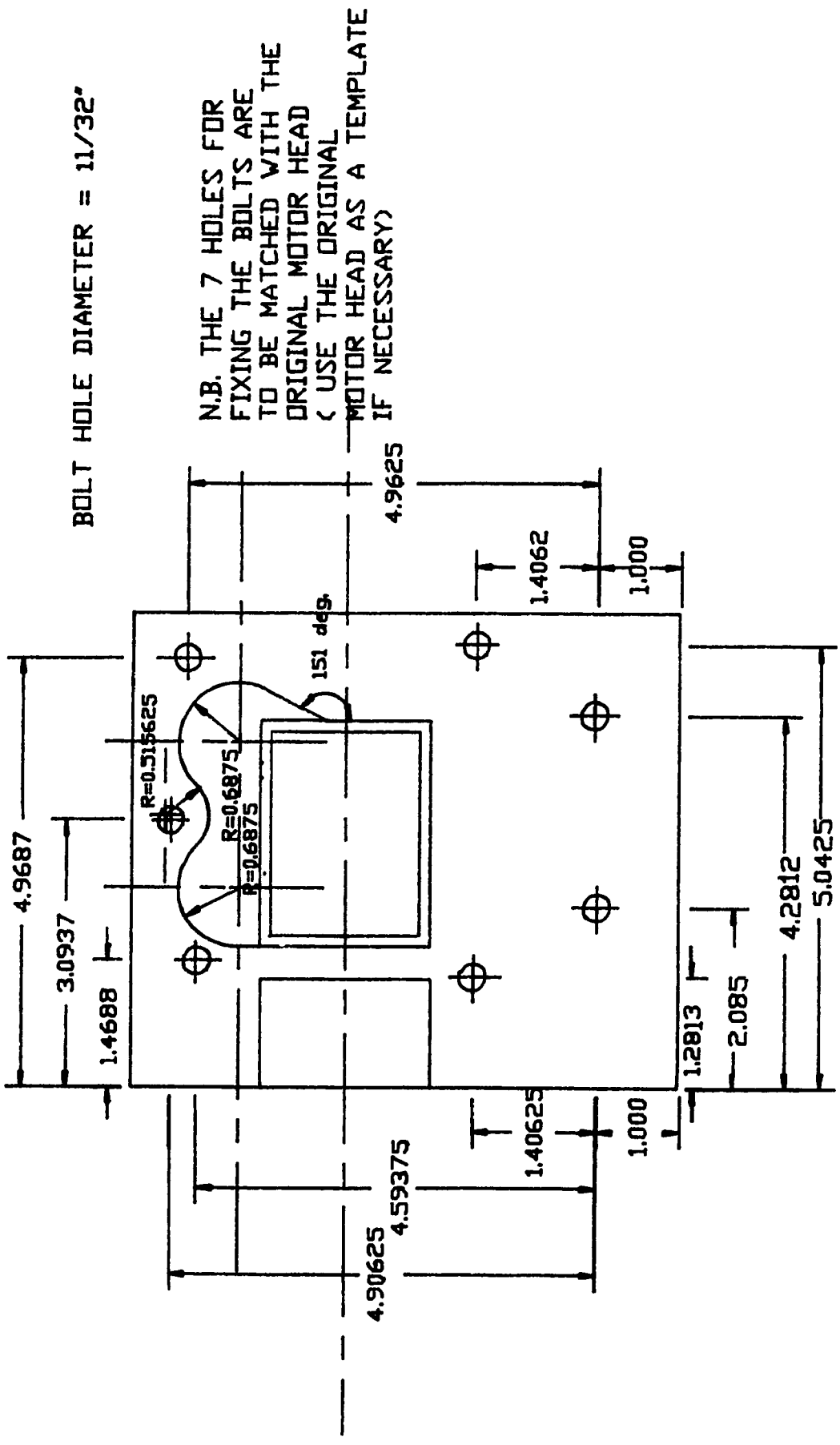

Figure A.11 Cylinder Head Bolt Hole Location Drawing

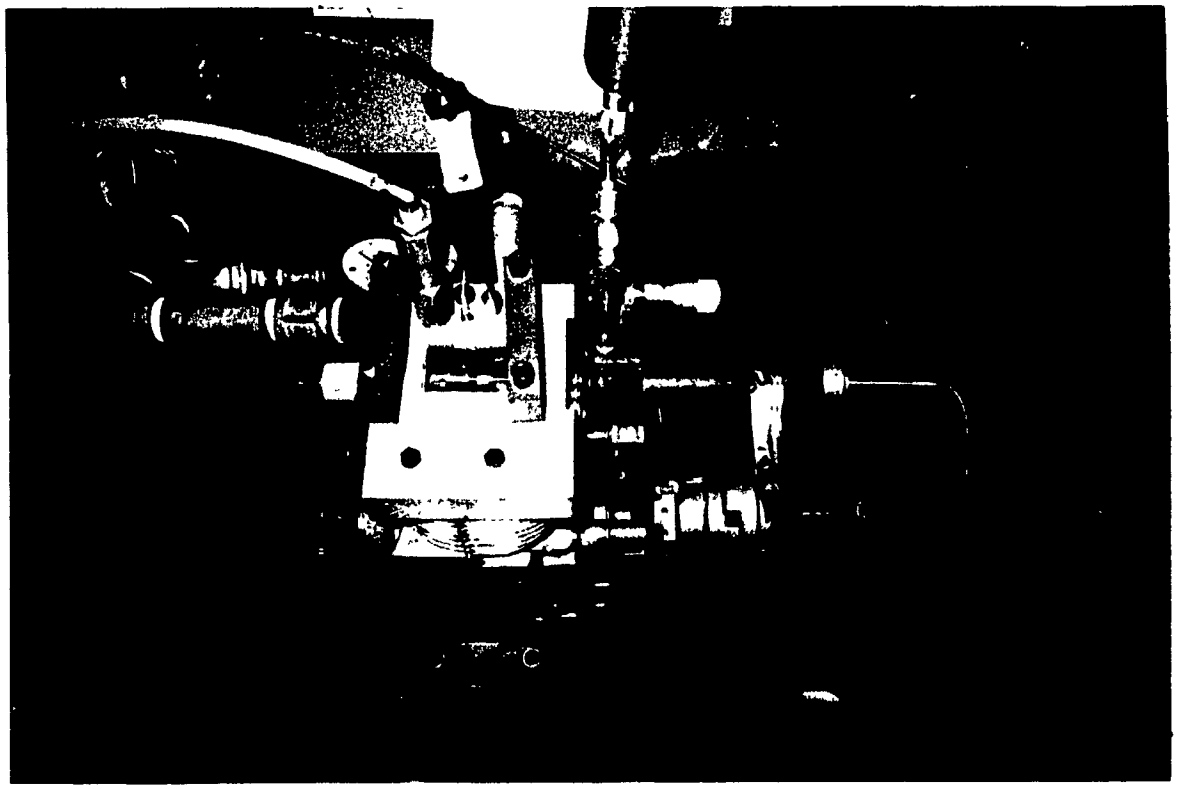

Figure A.12 Test Rig Photograph #1